DEPARTAMENTO DE ASTROFISICA

Universidad de La Laguna

Chemical abundances of volatile and refractory elements in stars with and without exoplanets

Memoria que presenta
D[a]. Lucía Suárez Andrés
para optar al grado de
Doctor en Ciencias Físicas.

Trabajo dirigido por el
D. Garik Israelian y el
D. Jonay I. González Hernández.

INSTITUTO Ð ASTROFISICA Ð CANARIAS
abril de 2017

Examination date: May, 2017
Thesis supervisor: Garik Israelian and Jonay I. González Hernández

ISBN: xx-xxx-xxxx-x
Depósito legal: TF-xxxx/2017
Some of the figures included in this document have been already published in *Astronomy & Astrophysics*.

Two road diverge in a wood, and I-,
I took the one less travelled by,
and that has made all the difference.
Robert Frost

Agradecimientos

Esta tesis es la culminación de muchos años de trabajo y esfuerzo. Ha sido necesaria mucha gente para poder llegar aquí. No hay espacio ni tiempo suficiente para poder agradeceros a todos, pero no por eso dejo de ser consciente de que sola no hubiera llegado hasta aquí.

En primer lugar quisiera agradecer a mis directores de tesis, Garik Israelian y Jonay González por vuestra guía y enseñanzas durante esta tesis. Gracias por transmitirme vuestros conocimientos. Gracias también por esos momentos de apoyo, en los que me transmitisteis la fuerza para seguir y no bajar los brazos.

Quisiera agradecer al Instituto de Astrofísica de Canarias por darme, primero con la beca necesaria para este proyecto, y luego durante la misma, la oportunidad de poder trabajar en unos de los mejores centros de investigación, con grandes personas trabajando en él. También por los medios puestos a mi alcance para que esta tesis haya sido posible.

Gracias a mis compañeros de despacho, tanto del corralón como del corralín. Gracias por los descansos de la tarde, los cafés de la mañana y en general, cualquier momento de apoyo durante esta etapa.

Por supuesto agradecer también a las amistades encontradas y conservadas entre esas paredes que forman el Instituto. Grandes personas que trabajan día a día entregando lo mejor de sí mismos en su puesto, ya sea de doctorandos, de postdoc o de administrativos. Gracias por apoyarme, por facilitarme las cosas y por infinidad de cosas más.

Gracias a Hristo, sabes que esta tesis tiene un pedazo de ti en ella. Por cuidarme y ayudarme tanto estos últimos meses, cuando el cansancio era

superior a todo. Ahora se cambian las tornas.

Por último, pero el agradecimiento más importante, a mi familia. Por estar ahí desde el minuto uno de esta tesis, que no comenzó hace cuatro años, sino hace más de dos décadas, cuando aún era muy pequeña. Era una niña y lo único que tenía claro era que quería estar donde estoy hoy. Gracias por todo vuestro apoyo para poder cumplir mi sueño.

La Laguna, 29 de Mayo de 2017

Resumen

Desde 1995 con el descubrimiento del primer exoplaneta orbitando una estrella de tipo solar (Mayor & Queloz 1995), el número de éstos ha crecido exponencialmente. A día de hoy, hay más de 4500 planetas detectados (más de 3200 confirmados). Además, el tamaño de estos planetas es muy diverso: desde planetas gigantes tipo Júpiter (los primeros en descubrirse) hasta planetas tipo Tierra (en auge gracias a la mejora en los métodos de detección). Para caracterizar los sistemas planetarios es necesario conocer la composición química de la estrella a la que orbitan.

En esta tesis presentamos un estudio uniforme de elementos volátiles y refractarios, con un total de 14 elementos distintos analizados.

En el caso de los elementos volátiles, se han analizado abundancias químicas de nitrógeno y carbono en una muestra de 74 y 1110 estrellas, respectivamente. En ambos casos se han utilizado bandas moleculares situadas en el ultravioleta cercano y óptico. Ésto es debido a que, en el caso del nitrógeno, no existen líneas atómicas en el óptico que se puedan estudiar. La única línea disponible de nitrógeno atómico se encuentra en 7468Å, en muchas ocasiones fuera del rango espectral de la instrumentación actualmente disponible. En el caso del carbono, existen líneas atómicas en 5380Å y 5052Å, pero que han presentado dificultades en su estudio. Por ello, abrimos una puerta a usar las bandas moleculares como método fiable del estudio de abundancias químicas. Para ello, hemos desarrollado un método de ajuste a puntos del continuo de la fotosfera estelar que nos permite normalizar el espectro de forma fiable. Ésto es necesario especialmente en el caso del nitrógeno, donde casi no es posible encontrar puntos de flujo del continuo de la fotosfera estelar.

Hemos analizado tanto estrellas con planetas como sin planetas, para buscar diferencias en su composición química. En el caso del nitrógeno y carbono, no hemos encontrado diferencias significativas entre las muestras.

Usando las abundancias de carbono obtenidas y datos de oxígeno, mag-

nesio y silicio de la bibliografía pertenecientes a nuestro grupo, hemos calculado los cocientes C/O y Mg/Si. Estos ratios son de gran importancia a la hora de caracterizar los planetas que orbitan las estrellas, ya que, en el caso del Mg/Si, éstos serán similares en el planeta y en la estrella. Para el C/O, éste depende de las líneas de hielo, o en otras palabras, de la distancia a la estrella a la que se forme el planeta. Las medidas de C/O obtenidas sirven de estimación para las que se podrán encontrar en los planetas.

En el caso de los elementos refractarios, se han estudiado 12 elementos diferentes: Na, Mg, Al, Si, Ca, Sc (ScI y ScII), Ti (TiI, TiII), V, Cr (CrI, CrII), Mn, Co y Ni. Hemos centrado nuestro estudio en las estrellas pobres en metales, dado el gran interés de estos objetos. Hemos encontrado sobre-abundancias de elementos α (Mg, Si y Ca) en nuestra muestra, confirmando resultados anteriores. Además se han obtenido resultados que apoyan la teoría de que esta sobre-abundancia está relacionada con las características químicas del disco protoplanetario de formación y no de la pertenencia a una población estelar u otra.

Abstract

Since the 1995 discovery of the first exoplanet orbiting a solar-type star (Mayor & Queloz 1995), the number of these has grown exponentially. To date, more than 4,500 planets have been detected (more than 3,200 confirmed). In addition, the size of these planets is very diverse, from giant Jupiter-type planets (the first to be discovered) to Earth-like planets (the number of which is booming, thanks to improved detection methods). To characterize a planetary system, it is necessary to know the chemical composition of its host star.

In this thesis, we present a uniform study of volatile and refractory elements, with a total of 14 different elements analysed.

In the case of volatile elements, chemical abundances of nitrogen and carbon were analysed in a sample of 74 and 1,110 stars, respectively. In both cases, molecular bands in the near ultraviolet and optical were used. This is because in the case of nitrogen, there are no atomic lines in the optical that can be studied; the only available line of atomic nitrogen is at 7,468Å, often outside the spectral range of currently available instrumentation. In the case of carbon, there are lines at 5,380Å and 5,052Å, but they are difficult to study. Therefore, we opened a door to use molecular bands as a reliable method to study chemical abundances. To do this, we developed a continuous tuning method of the stellar photosphere that allows us to normalize the spectrum reliably. This is especially necessary in the case of nitrogen, where the points of the continuum are practically non-existent.

We analysed stars with and without planets, to look for differences in their chemical composition. In the case of nitrogen and carbon, we found no significant differences between the samples.

Using the carbon abundances obtained and oxygen, magnesium, and silicon data from the literature belonging to our group, we calculated the C/O and Mg/Si ratios. These ratios are especially important in charac-

terizing the planets orbiting the stars because in the case of Mg/Si, these will be similar on the planet and in the star. For the C/O, this depends on the stars ice lines, the distance to the star where the planet formed. C/O measurements obtained are estimates for those that can be found on the planets.

In the case of refractory elements, 12 different elements have been studied: Na, Mg, Al, Si, Ca, Sc (ScI and ScII), Ti (TiI, TiII), V, Cr (CrI, CrII) Co, Mn, and Ni. We focused our study in metal-poor stars, given the great interest of these objects. We found overabundances of α elements (Mg, Si and Ca) in our sample, confirming previous results. In addition, we obtained results that support the theory that this overabundance is related to the chemical characteristics of the protoplanetary disk and not to the membership of a certain stellar population.

Contents

List of Figures

List of Tables

1

Introduction

Everything is theoretically impossible,
until it is done.
Robert A. Heinlein

1.1 Exoplanet detection techniques

Mankind has long wondered whether there was another world around the billions of stars in our galaxy, but it was not until 1992 that the first confirmed detection of an extrasolar planet occurred when two bodies were found to be orbiting the millisecond pulsar PSR 1257+12 (Wolszczan & Frail 1992; Backer et al. 1992)

The first detection of an extrasolar planet orbiting a solar-type star occurred three years later with the announcement of a planetary body orbiting 51 Pegasi (Mayor & Queloz 1995). Since then, only 22 years later, the number of confirmed exoplanets has risen to more than 3,500. As of the cut-off date for this thesis, 3,559 exoplanets were known, with more than 600 multiple systems.

Exoplanets are being discovered daily around different kinds of stars. Host stars like the Sun (main sequence stars) are not the only kind of hosts, as exoplanets can be found around very low-mass stars, low-metallicity stars, giant stars, and other advanced evolutionary stages, such as white dwarfs and pulsars. Their internal structure and composition vary widely, too.

Several methods for detecting exoplanets have been developed: Doppler

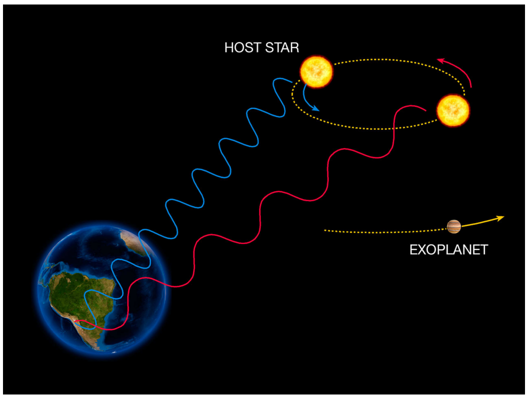

FIGURE 1.1— The radial velocity method. Credit: ESO

measurements, transit observations, microlensing, astrometry, pulsar timing, and direct imaging. Except for direct imaging, all are indirect detection methods.

- *Doppler measurements.* The radial velocity method, also known as Doppler spectroscopy, is one of the most effective methods to locate extrasolar planets with the existing technology. It relies on the fact that a star does not remain completely stationary when it is orbited by a planet. As the star moves in the small orbit resulting from the pull of the planet, it will move toward the planet and then away from it as it completes an orbit. The stars velocity along the planets line of sight is its radial velocity (see Fig. 1.1). The periodic changes in the star's radial velocity due to the mass and the inclination of the planet's orbit can be measured using high-precision spectroscopy. Using this method, Mayor & Queloz (1995) detected and confirmed 51 Pegasi b. Since then, more than 500 planets have been discovered using this method, which was the primary technique of finding exoplanets until the arrival of the *Kepler* space observatory.

- *Transit observations.* A planetary transit is the pass of a planet across its host star (as viewed from Earth), blocking a fraction of the star's light. Using photometric techniques, we can measure the periodic drop-off in the star's flux caused by these transits. Using this technique, we can also study the composition of the planet's atmosphere, as the light from the star would pass through its atmo-

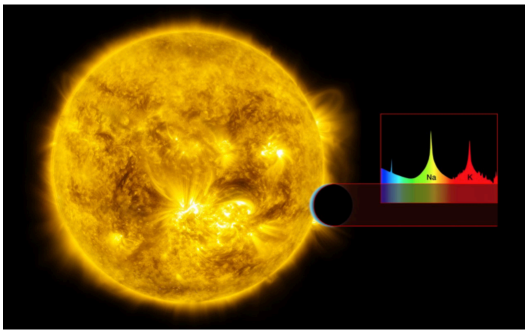

FIGURE 1.2— Chemical spectra of a transiting exoplanet. Credit: ESO

sphere. The light would be absorbed differently depending on the elements that form the planetary atmosphere, allowing us to identify its composition (see Fig. 1.2). Most exoplanets (more than 2,000) have been discovered by *Kepler* using this method.

- *Direct imaging.* This is the hardest way to detect an exoplanet, because of the extreme contrast between the light emitted by the host star and the planet, on the order of one-billionth. Coronography techniques to physically block the inner parts of the star, leaving only the corona and allowing any nearby planets to shine through, can be very useful, but they are difficult to apply. Another way is to use photometric observations in the infrared, since the contrast between the star and the planet drop off to a factor of thousandths. This is particularly useful in the case of very young planets, which are still contracting and thus emitting heat.

1.2 Chemical characterization of the host star

The properties of stars are derived from a combination of astrometric, photometric, and spectroscopic observations, interpreted primarily within the context of stellar evolutionary models. Chemical abundance analysis, using high-resolution and high-signal-to-noise spectroscopy, provides a fundamental diagnostic of star properties.

The composition of the star is determined not only by the epoch (the sooner they were formed, the less metallic they are) or their birthplace (thick or thin disk), but also the possible companions they may have.

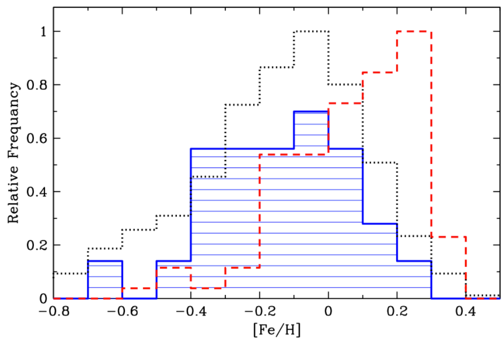

FIGURE 1.3— [Fe/H] distributions for stars with (high-mass planets in red and low-mass planets in blue) and without planets (black dotted line). Credit: Adibekyan et al. (2012b)

A known fact since the very first studies is that stars with high-mass planets[1]have significantly higher metal content than the average solar-type star in the solar neighbourhood (Gonzalez 1997; Santos et al. 2001). While the Sun and other nearby solar-type dwarfs have on average [Fe/H] ~ 0 (Reid & Cruz 2002), typical giant-exoplanet host stars have [Fe/H] $\gtrsim$ 0.15. Values of [Fe/H] = 0.45 for two early discoveries, 55 Cnc and 14 Her, placed them among the most metal-rich stars in the solar neighbourhood (Gonzalez & Laws 2000). Although planets have also been discovered around very low metallicity stars (BD+20 2457, with [Fe/H] = −1.0, by Niedzielski et al. 2009), an overall correlation between metallicity and giant-planet occurrence has been confirmed by subsequent works, using different samples and analysis procedures. (See Fig. 1.3 and Gonzalez et al. 2001a; Laws et al. 2003; Santos et al. 2003, 2004, 2005; Fischer & Valenti 2005; Gonzalez 2006; Adibekyan et al. 2012b)

Two hypotheses have been suggested to explain this anomaly:

- *Self-enrichment:* This scenario should be triggered by the action of hot Jupiters migrating from outside the protoplanetary disk. During this migration, planetesimals from the disk are accreted onto the star. This mechanism would be efficient only during the first 20–30 Myr when the surface convection layers of the star attain their minimum size configuration (Chavero et al. 2010). Israelian et al.

[1]We consider high-mass those planets with $M_P > 30M_\oplus$ and low-mass those with $M_P \leq 30M_\oplus$

(2001, 2003) found, in HD 82943, evidence of pollution, suggesting the infall of a planet (See also Mandell et al. 2004; Ghezzi et al. 2009)

The self-enrichment scenario could lead to a relative overabundance of refractories, such as Si, Mg, Ca, Ti, and the iron-group elements, compared with volatiles such as C, N, O, S, and Zn. The accretion of small planets may affect the composition of the convective layer of the stars (See Théado & Vauclair 2012, and references therein.) To how great an extent this affects the accretion of volatiles such as C, N, and O remains unanswered. (See González Hernández et al. 2013)

- *Primordial cloud:* Santos et al. (2001, 2002, 2003) proposed that the overabundance of metals is likely caused by a metal-rich primordial cloud. They claimed that the observed abundances are representative of the primordial cloud where the star was formed. According to this model, planets form a very short time after their host stars form the protoplanetary disk. This disk consists of the remnants of the collapsing cloud from which the star itself formed and continues to feed its material to the star. In the disk, dust grains may form. Those grains, made of rock and ice, are the seeds of planetesimals. If the disk contains enough material, and if the object's orbit around the host star is not obstructed, those planetesimals will continue to accrete mass and eventually form planets. Those processes are thought to take place on timescales of some 100 million years. In case of a successful planet formation, the material locked up in the planets will not end up in the stellar interior as long as the planetary orbit is stable and the planet does not eventually fall into the host star.

  This idea is supported by models of planet formation and evolution based on the core-accretion process (e.g. Ida & Lin 2004; Mordasini et al. 2012).

Later studies have confirmed the primordial cloud as the most likely reason for the metal-rich nature of stars with giant planets (Santos et al. 2004, 2005; Fischer & Valenti 2005; Sousa et al. 2008, 2011b; Buchhave et al. 2012)

The formation of rocky planets takes place in the inner part of the protoplanetary disk, where temperatures are high enough to prevent water and other volatile elements from condensing, so purely rocky material is allowed to consolidate and later form planetesimals. Following this theory, rocky planets are formed without the inclusion of water or any other volatile elements. Those materials are thought to have arrived on the terrestrial planets in a later phase through meteorite or planetesimal impacts. This model can also explain why gas giants are thought to have a composition very similar to their host stars, since they are formed in the outer regions of the protoplanetary disk, where temperatures are low enough for all elements to condensate and form dust grains.

1.2.1 Spectroscopy

Chemical abundance analysis, using high-resolution and high-signal-to-noise spectroscopy, provides a fundamental diagnostic of host-star properties. Spectroscopic analysis provides robust estimates of a number of basic stellar quantities. In most recent works (e.g., Tsantaki et al. 2013; Andreasen et al. 2017), the measured equivalent widths of 137 Fe I and Fe II absorption lines are used to estimate the four basic stellar parameters that influence the relative line strengths and line profiles: effective temperature ($T_{\rm eff}$), surface gravity ($\log g$), microturbulence velocity (ξ_T), and metallicity ([Fe/H]). These analyses make use of atmospheric models, typically assuming a plane-parallel geometry (e.g., Kurucz 1993) under the assumption of local thermodynamic equilibrium (LTE), along with basic atomic data and, most critically, the line oscillator strengths.

Once the main stellar parameters have been estimated, the abundances of chemical elements are derived from individual spectral lines using either measured equivalent widths or comparisons with synthetic spectra. Light elements such as Li, C, N, O, Na, Al, Mg, and S have relatively few spectral lines in solar-type stars, and high-quality spectra are required for reliable abundances. Also, some of these features are found either in the near-UV or in the near-IR (e.g., nitrogen, with molecular bands located at 3,360Å and an atomic line at 7,468 Å)

Abundance ratios also allow us to identify two main populations in the galactic disk of the Milky Way: an old, thick disk that formed within a relatively short period of time (about 1 Gyr) and a younger thin disk that took somewhat longer to form. The disks differ not only in galactic velocity components, by which they are usually defined, but also in their chemical composition (Adibekyan et al. 2011, 2012b). Also, for the galactic halo, two separate populations seem to exist that differ in their [α/Fe] ratio and seem to originate in different places (Nissen & Schuster 2010, 2011). Accordingly, most of the stars in the solar neighbourhood are thin disk stars ($\sim$ 95%); thick disk and halo stars have a share of only about 5%.

An important topic that is examined with the means of spectroscopic abundance analysis is galactic chemical evolution (GCE). Edvardsson et al. (1993) have shown that even in nearby solar-type stars, chemical evolution has taken place. That means the abundance ratios in younger stars differ from those in older ones.

Recently, the study of volatile and refractory elements (see Section 1.3) in solar-type stars has shown a strong correlation between stellar ages and the slope of [X/Fe] ratios versus condensation temperature (Tc): Old stars show steeper slope i.e., less refractory elements relative to volatiles (Adibekyan et al. 2014; Nissen 2015). These authors also found evidence that the Tc slopes also correlate with the mean galactocentric distance of the stars; this suggest that stars that probably originated in the inner Galaxy (small Rmean) have steeper slopes. The result fits well in the recent evolutionary picture of the Milky Way, showing that some fraction of old stars in the solar neighbourhood might have originated in the inner disk (e.g., Minchev et al. 2013).

1.2.2 Comparison stars

Consistent agreement in determining effective temperatures and metallicities has proven notoriously difficult. To establish statistical differences between stars with and without planets at the level of 0.1-0.2 dex, a reliable sample of comparison stars is required. The comparison sample should be demonstrably companion-free (given the definition of a "single" star in planet-search surveys), and analysis for both samples should be based on the same sets of spectroscopic lines and analysed in the same way. Santos et al. (2001) first presented a spectroscopic study of a volume-defined set of 43 F8-M1 stars within 50 pc included in the CORALIE program, and for which constant radial velocities over a long time interval provided evidence that the comparison stars do not host giant planets.

A more complete star sample was created following the work of the CORALIE program using the HARPS spectrograph (La Silla, ESO, Chile) under three different programs: HARPS-1 (Mayor et al. 2003), HARPS-2 (Lo Curto et al. 2010), and HARPS-4 (Santos et al. 2011). All observed stars were suitable for radial velocity measurements, as they are slow rotators and show little chromospheric activity. Stellar parameters for this new sample were published by Sousa et al. (2008, 2011a,b).

A selection of 1,111 stars from this sample was deeply studied by Adibekyan et al. (2012b), with 135 known planet-host stars. They obtained chemical abundances for 12 different elements, setting a reliable base for future chemical-abundance-related studies.

1.3 Refractory and volatile elements

Planet formation involves condensation, the change from gas into the liquid or solid phase of the same element or chemical species. This involves the loss of kinetic energy by collision, or by adsorption onto an existing, colder, condensation centre. In planetary science, elements and compounds with high equilibrium condensation temperatures are called refractory, while those with low condensation temperatures are called volatile. Refractory elements that have been most studied in the context of planet host stars include Al, Ca, Ti, and V (with condensation temperatures $T_C \sim 1400$ K); those with intermediate condensation temperatures include Co, Fe, Mg, Ni, and Si (with $T_C \sim 1300$ K). Volatile elements include C, N, O (with low $T_C \sim 300$ K), S, Zn (with $T_C \sim 700$ K) and Na, Cu, and Mn (with $T_C \sim 1100$ K).

1.3.1 Refractory elements

Studies of the relative abundances of refractory elements have conveyed a less clear-cut picture than for [Fe/H] when comparing values of [X/Fe] for planet hosts with those of comparison stars of the same [Fe/H].

A comparison study for 77 single stars and 42 planet-hosts from the CORALIE sample was made by Bodaghee et al. (2003). They reported that both samples have a similar behaviour when studying [X/Fe] vs. [Fe/H]. More recent studies using the high-quality HARPS spectra confirm that no important differences in [X/Fe] vs. [Fe/H] can be found for refractory elements (Neves et al. 2009; González Hernández et al. 2010, 2013; Delgado Mena et al. 2010).

The accepted conclusion is that planet-hosting stars are largely indistinguishable from other Population I stars when studying refractory-element abundances. One implication of this result is that no extraordinary chemical events, such as a nearby supernova, are necessary to stimulate planet formation.

On the other hand, studies by Haywood (2008, 2009) and Neves et al. (2009); Adibekyan et al. (2012a,b) found evidence of α-element enhancement in stars with planets, shown in Fig. 1.4 (Adibekyan et al. 2012b). These results support the core-accretion model of planet formation (See Pollack et al. 1996) In particular, Adibekyan et al. (2012b) found that planet-host stars show significant enhancement of α-elements at metallic-

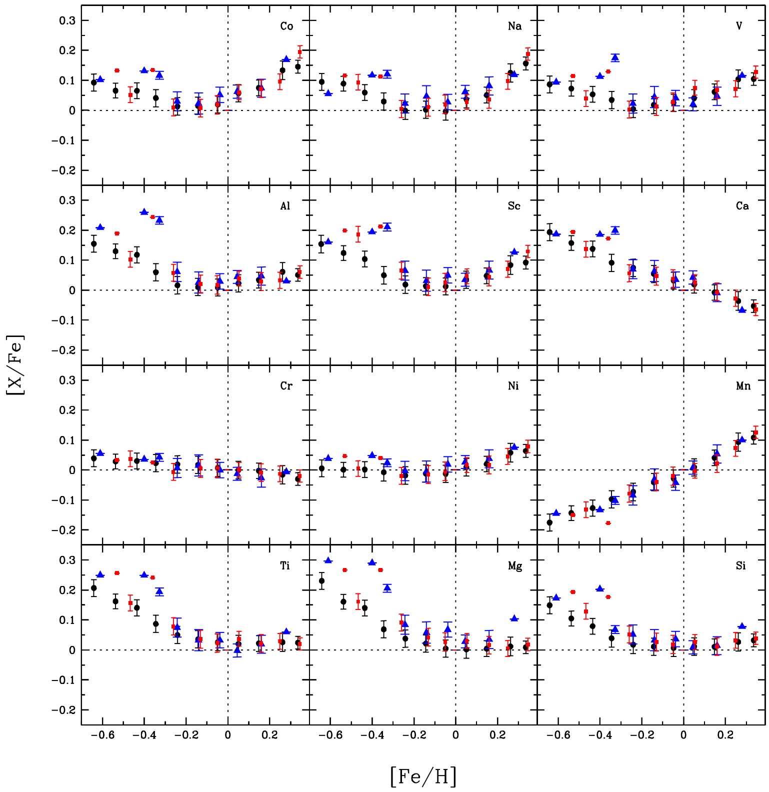

FIGURE 1.4— [X/Fe] abundance ratios against [Fe/H] for stars with and without planets. The symbols and error bars indicate the average and standard deviation, respectively, of each bin (0.1 dex). The red squares and blue triangles represent stars with Jupiter-mass and Neptunian/super-Earth mass planets, respectively. The black circles refer to stars without a planetary companion. The black dashes target the solar value. Credit: Adibekyan et al. (2012b)

ities slightly below solar and that they chemically belong to the Galactic thick disk.

1.3.2 Volatile elements

C and O are significant opacity sources in stars and are important in the chemistry of protoplanetary disks. Their forbidden lines are preferentially used as abundance indicators, but they are weak and blended and demand

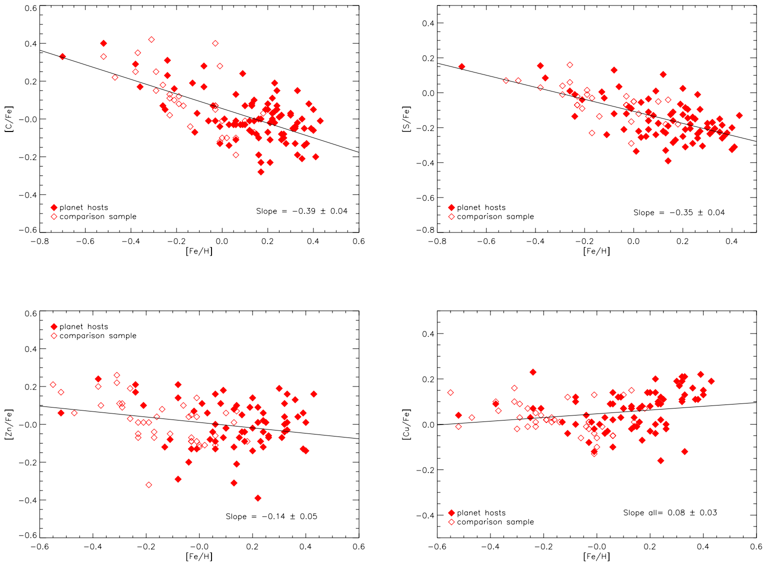

FIGURE 1.5— [X/Fe] vs. [Fe/H] for stars with and without planets. Credit: Ecuvillon et al. (2004a)

high-quality spectroscopy.

Santos et al. (2000) and Laws et al. (2003) reported sub-solar values for [C/Fe] and [Na/Fe] in planet-host stars, while subsequent investigations using inhomogeneous comparison samples gave a more uncertain picture of the trends for [C/Fe], [O/Fe], and [N/Fe] (Gonzalez et al. 2001a; Takeda et al. 2001; Sadakane et al. 2002; Takeda & Honda 2005)

Several studies tried to derive abundances of N, C, S, Zn, Cu, and O using a homogeneous sample derived from the HARPS and CORALIE programs (Ecuvillon et al. 2004a,b, 2006a,b; Delgado Mena et al. 2010; Da Silva et al. 2015). While most elements show a decreasing trend of [X/Fe] with increasing [Fe/H], the overall conclusion, again, is that the abundance trends of planet-host stars for the volatile elements are largely identical to those for the comparison stars at the corresponding (high) values of [Fe/H].

1.3.3 Implications for planet formation

The composition of planets is important to understand the planet formation and evolution processes, as well as their structure. If stellar abundances reflect planetary abundances, spectroscopic studies of host stars may also represent a step in identifying terrestrial planet composition and evolution. While the composition of giant gas planets can be inferred from transiting spectroscopic measurements of the planets atmosphere, the composition of the atmosphere of rocky planets can be difficult to estimate. To estimate the composition of these planets, two hypotheses have been proposed:

- Assume that the solid formed in equilibrium in the solar nebula so that equilibrium chemistry can help constrain the model (Elser et al. 2012; Madhusudhan et al. 2012; Thiabaud et al. 2014).
- Assume that elemental ratios Fe/Si and Mg/Si have stellar values in order to model the planetary formation (Valencia et al. 2010; Wang et al. 2013).

Gonzalez et al. (2001b) estimated that a metallicity at least half of that of the Sun is required to build a habitable terrestrial planet, as dictated by heat loss, volatile element inventory, and atmospheric loss. A key issue is the formation of planets that sustain plate tectonics, a recycling process that provides feedback to stabilize atmospheric temperatures on planets with oceans and atmospheres. Also likely important are the relative abundances of Si and Mg to Fe, which affects the mass of the core relative to the mantle in a terrestrial planet.

Elemental ratios are key features since they govern the formation and distribution of chemical species in the protoplanetary disk. Stars with different Mg/Si ratios may have terrestrial planets with differing compositions of the pyroxene-silicate mineral series $MgFeSiO_3$, or of the olivine series $MgFe_2SiO_4$, which might affect the volcanism of the planet, for example.

While Mg/Si governs the silicates, C/O governs the amount of carbides and also the silicates. For $C/O > 0.8$, Si will combine with C to form SiC, a carbide. On the other hand, if $C/O < 0.8$, Si will combine with O to form silicates, as SiO.

However, C and O, being volatile elements, are sensitive to environmental changes, such as temperature or pressure. The C/O ratio in planets can deviate significantly from the C/O found in the star, affecting the planetary formation. As presented in Brewer et al. (2016b) for hot Jupiter hosts, the average planet C/O ratio is super-stellar, but their large uncertainties do not exclude the possibility of the 1:1 relation for the stellar and planetary C/O ratios.

In the last few years, several studies have tried to understand the formation and evolution of planets using theoretical models. Bond et al. (2010a,b); Carter-Bond et al. (2012) computed planet formation with different initial composition, but they did not do a detailed study of the output volatile species. Elser et al. (2012) tried to study planetary formation by adding the formation of solids, but they could not reproduce some features present in the Solar System, like high abundance of Fe in Mercury.

Recently, Thiabaud et al. (2014); Marboeuf et al. (2014) made a complete theoretical study, presenting models not only including refractory species, but also volatiles. Thiabaud et al. (2015a) presented a complete study, taking into account the accretion of several compounds omitted in previous works such as He, H_2, H_2O, CO, CO_2, CH_3OH, CH_4, NH_3, N_2, and H_2S. Also, they investigated the importance of volatile elements in protoplanetary disks and their implications for planetary formation (Thiabaud et al. 2015b).

Although several works have studied either C/O (Nissen et al. 2014; Teske et al. 2014; Brewer & Fischer 2016; Brewer et al. 2016b) or Mg/Si (Carter-Bond et al. 2012; Brewer & Fischer 2016), only Delgado Mena et al. (2010) made a complete study on C/O vs. Mg/Si elemental ratios, in order to determine and investigate the nature of the possible terrestrial planets that could have formed in those planetary systems.

They obtained mineralogical ratios quite different from those of the Sun, showing there is a wide variety of planetary systems that are not similar to the Solar System. Many planet-host stars present a Mg/Si value lower than 1, so their planets would have a high Si content to form species such as $MgSiO_3$. This type of composition can have important implications for planetary processes like plate tectonics, atmospheric composition or volcanism (See Fig. 1.6.)

1.4 Organization and objectives of the thesis

This Ph.D. thesis is focused on the study of the chemical abundances of stars with and without known exoplanets. In particular, we have looked for chemical differences for nitrogen, carbon, and α-elements. The thesis is mainly composed by four articles, three of them already published and the last one in preparation (to be updated in the very last moment). The

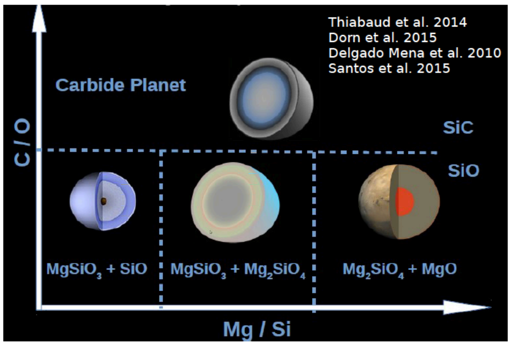

FIGURE 1.6— C/O versus Mg/Si ratios can help determine the composition of planetary companions. Reference: Thiabaud et al. (2014); Dorn et al. (2015); Delgado Mena et al. (2010); Santos et al. (2015)

thesis is organized as follows:

- In Chapter 2 we review the observations, data reduction and methodology used to obtain the presented results.
- In Chapter 3 we present nitrogen abundances for a sample of 74 solar-type stars making use of the molecular NH band at 3360Å, in the near-UV. We discuss a new method for normalising the continuum, along with a chemical with a detailed comparison of chemical abundances between stars with and without exoplanets. This chapter is based on Suárez-Andrés et al. 2016, A&A, 591, A69.
- In Chapter 4 we present carbon abundances for a sample of 1,110 solar-type stars making use of the molecular CH band at 4,300Å, in the optical. We present a chemical comparative between stars with and without exoplanets, never done for molecular carbon for such a wide sample. This chapter is based on Suárez-Andrés et al. 2017, A&A, 599, A96.
- In Chapter 5 we present a study of the implication of C/O and Mg/Si ratios in planetary formation, using the available O, Mg, and Si measurements, along with our C abundances. The sample consists of 499 solar-type stars selected from the 1,110 solar-type star sample studied in the previous chapter. This chapter is based on Suárez-Andrés et al. 2017, A&A, submitted.

- In Chapter 6 we present refractory element abundances for a sample of 21 solar-type metal-poor stars. Making use of the newly developed code by Andreasen et al. (2017) to obtain precise stellar parameters, we present chemical abundances in 21 metal-poor host stars in order to study a refractory element enhancement. This chapter is based on Suárez-Andrés et al. 2017, A&A, in preparation.
- In Chapter 7 we present our conclusions.
- In Chapter 8 we present collaborations and other works in which we participated.
- In Chapter 9 we explore future work.
- To conclude this manuscript, we present four appendices with the results obtained in the previous chapters.

2

Observations, data reduction and methodology

In this chapter we describe the spectroscopic data and the observations performed during this thesis at the Roque de los Muchachos Observatory (ORM, La Palma). Then we explain the procedures followed to reduce the data. Finally, we make a brief introduction of the available methods to determine chemical abundances and the tools used.

2.1 Observations and data reduction

For all the targets in our sample we used high-resolution spectra (R $\gtrsim$ 60000), with medium to high signal-to-noise (70-200) obtained with four different instruments: UVES at VLT (ESO, Paranal, Chile), HARPS at 3.6-m telescope (ESO, La Silla, Chile), FIES at NOT (Nordic Optical Telescope, ORM, Spain). For UVES, HARPS and FEROS we used already reduced data obtained under programs 092.C-0695, 094.C-0367, 2014B/020 and HARPS GTO.

2.1.1 UVES

UVES, an acronym for Ultraviolet and Visual Èchelle Spectrograph, is the high-resolution optical spectrograph of the VLT located at the Nasmyth B focus of UT2. It is a cross-dispersed échelle spectrograph designed to operate with high efficiency from the atmospheric cut-off at 3000Å until ∼110,00Å. To this aim, the light beam from the telescope is split in two arms (UV to Blue, and Visual to Red) within the instrument. The two arms can be operated separately, or in parallel via a dichroic beam splitter. The resolving power is about 40000 when a 1-arcsec slit is used. The maximum (two-pixel) resolution is 80,000 and 110,000 in the Blue and the Red Arm, respectively.

2.1.2 HARPS

HARPS, an acronym for High Accuracy Radial velocity Planet Searcher, is a high-precision échelle planet finding spectrograph installed in 2002 on the ESO's 3.6-m telescope Cassegrain focus (La Silla, Chile). The first light was achieved in February 2003. HARPS has discovered over 130 exoplanets to date, with the first one in 2004, making it the most successful planet-finder after the *Kepler* space observatory. It is a second-generation radial-velocity spectrograph, based on experience with the ELODIE and CORALIE instruments.

The instrument is built to obtain very high long-term radial velocity accuracy (at about 1 m/s). To achieve this goal, HARPS is designed as an échelle spectrograph fed by a pair of fibres and optimised for mechanical stability. It is contained in a vacuum vessel to avoid spectral drift due to temperature and air pressure variations. One of the two fibres collects the star light, while the second is used to either record simultaneously a Th-Ar reference spectrum or the background sky. Both fibres have an aperture on the sky of 1 arc-second, what transforms in a power resolution of ∼115,000.

It covers a spectral range from 3780-6910Å, distributed in 72 orders. The detector consists of a 2 CCD mosaic (4k x 4k with 15 micron-size pixels), with a wavelength gap from 5300-5330Å.

These characteristics make HARPS one of the best instruments to find extrasolar planets using the RV method.

2.1.3 FEROS

FEROS, an acronym for Fiber-fed, Extended Range, échelle Spectrograph, is a bench-mounted prism-crossdispersed èchelle spectrograph mounted at the 2.2-m telescope in La Silla (Chile). It is designed to be a high-resolution (R∼48,000), high-efficiency (20%), versatile spectrograph providing in a single spectrogram almost complete spectral coverage from ∼3500Å to ∼9200Å. This spectral range is found in 39 orders, with a CCD EEV detector of 2k x 4k.

Although it has not been specially designed for high-RV measurements, it can obtain precision up to 25 m/s.

2.1.4 FIES

FIES, an acronym for FIbre-fed Èchelle Spectrograph, is a cross-dispersed high-resolution èchelle spectrograph installed in 1999 on the Nordic Optical Telescope (NOT) (ORM, La Palma, Spain). The current installed fibre bundle allows a maximum spectral resolution of R = 67000. This bundle also provides a medium-resolution fibre, allowing a spectral resolution of R = 48000. The entire spectral range 3700-7300Å[1] is covered without gapdf in a single, fixed setting. To isolate it from sources of thermal and mechanical instability, FIES is mounted in a heavily insulated building separate from and adjacent to the NOT dome since 2006.

2.1.4 Observational Campaigns

Several campaigns took place at the NOT with FIES to observe the metal-poor sample used in Chapter 6. Details on dates can be found in Table 2.1.

Observations were conducted with both the high-resolution and medium-resolution fibres, depending on the brightness of the target: for those targets fainter than $V \sim 10$, the medium-resolution fibre was used, in order to maintain a S/N homogeneity for all the sample above 100. No binning was applied, using the standard 1x1 configuration. An arc was taken after every exposure.

2.1.4 Data reduction

FIES comes with a dedicated reduction software (FIEStool), which provides a fully reduced spectrum for quick-look analysis after the end of each exposure, using library calibrations. The same software is also available to observers for final analysis of the data using the nightly calibration frames.

For the normalization of continuum, we applied a 5th degree polynomial using the CONTINUUM task of IRAF[2]. RV corrections were applied using the *fxcor* and *dopcor* tasks, also in IRAF. The first task allows us to compare our spectra with a similar one used as a template (in our case, the Sun). This task looks for the shift in the spectra by performing a correlation between them. Once this shift has been determined, we apply them

[1]Since October 2016, a new CCD has been installed, offering a spectral coverage of 3700 to 9100Å for the high-resolution fibre

[2]IRAF is distributed by the National Optical Astronomy Observatory, which is operated by the Association of Universities for Research in Astronomy (AURA) under a cooperative agreement with the National Science Foundation.

Table 2.1— Observing dates for the FIES campaigns

Campaign	Observing dates
52-209	8-9 October 2015, 19-21 February 2016
	17-18 March 2016
53-202	12-13 April 2016, 29-30 May 2016,
	1 June 2016, 10-12 July 2016,
	19 September 2016

to our targets using *dopcor*. If more than one spectra was available for each target, they were combined using the task *scombine* after correcting for RV.

2.2 Methods for abundance determination

The methods by which the abundance analysis can be undertaken are reviewed in this section. The chemical abundances of stellar atmospheres may be calculated from the equivalent width (EW) of the observed spectral lines or, alternatively, from the comparison between the synthetic and observed spectra.

2.2.1 Equivalent widths

The equivalent width is a convenient measure of the strength of an absorption line. What all instruments record is the convolution of the intrinsic line shape with the instrumental broadening function; if the latter is broader than the intrinsic width of the absorption line recorded, much of the information encoded in the line profile itself is lost. However, the equivalent width is invariant to the convolution and it is a conserved quantity. Some stellar parameters of interest can be deduced from measurements of the line equivalent widths, particularly the relative fractions of atoms and ions in different excitation and ionisation stages and the relative abundances of different elements.

We define the equivalent width W of an absorption line as the width, in wavelength units, of a rectangular strip of a spectrum having the same area (see Fig 2.1).

The EW of a spectral line is defined as:

$$W_\lambda = \int_{-\infty}^{\infty} \frac{(I_{\lambda,0} - I_\lambda)d\lambda}{I_{\lambda,0}} \tag{2.1}$$

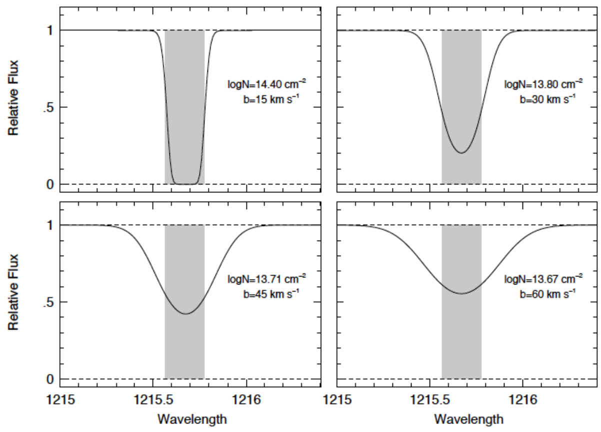

FIGURE 2.1— Four absorption lines with the same equivalent width (represented by the shaded grey area) but different widths, as measured by the value of b (kms^{-1}). N (cm^{-2}) is column density, defined as the number of absorbers in a column of unit cross-sectional area.

where $I_{\lambda,0}$ is the intensity at its starting point within the star's interior. In flux units,

$$W = \int_0^\infty \frac{(F_C - F_\nu)d\nu}{F_C}, \tag{2.2}$$

where F_C and F_ν are the fluxes in the continuum and the line, respectively. W stands for the width of line flux normalised to the continuum flux. To represent the variations of W versus the abundance, we use the curve of growth.

Integration of Eq. 2.2 then gives the sought-after relationship between the equivalent width (EW) of an absorption line and the column density N of absorbing atoms. This relationship, which is illustrated in Fig. 2.2, is known as the Curve of Growth (CoG), because it describes how W grows with increasing N.

The CoG technique consists on determining the theoretical CoG for a given spectral line and to obtain the chemical abundance (A) by comparing the observational measurement of W with that theoretical one.

The radiative transfer equation for a stationary plane-parallel is:

$$\frac{dI_\nu}{\kappa_\nu \rho dz} = -I_\nu + S_\nu \tag{2.3}$$

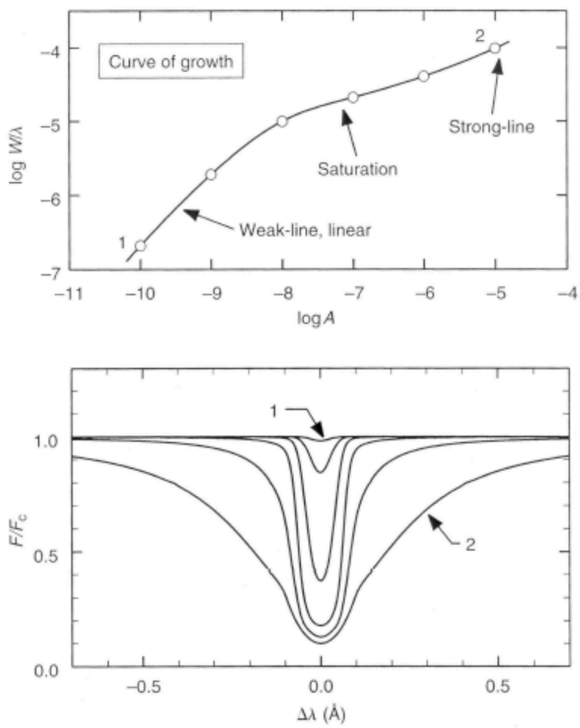

FIGURE 2.2— Both the *EW* (top) and the profile (bottom) change with chemical abundances of the absorbing species. The dots in the CoG relate with the dots in the profiles below. Models have $S_0 = 0.87$ and $logg = 4.0$ dex. Based on Gray (1992)

where κ_ν, ρ and S_ν are the absorption coefficient, density and the source function, respectively. Under the plane-parallel assumption, considering local thermodynamic equilibrium (LTE), flux can be expressed as:

$$F_\nu = 2\pi \int_{-\infty}^{\infty} B_\nu(T) E_2(\tau_\nu) \frac{l_\nu + \kappa_\nu}{\kappa_0} \tau_0 \frac{dlog\tau_0}{loge}, \quad (2.4)$$

where τ_ν is the optical depth, l_ν is the line absorption coefficient and $E_2(\tau_\nu)$ an extinction factor.

If we only consider the case of a weak line in the LTE regime, F_ν will come from a certain optical depth and B_ν=l_ν, so it can be simplified to:

$$\frac{(F_C - F_\nu)}{F_C} \approx B \frac{l_\nu}{\kappa_\nu} \quad (2.5)$$

where B is a constant. If we substitute in Eq. 2.1 and taking into account Eqs. 2.5 and 2.6, W transforms into:

$$l_\nu \rho = N\alpha \quad (2.6)$$

$$\alpha = f \frac{\pi e^2}{mc} \frac{\lambda^2}{c} \quad (2.7)$$

$$W = \frac{B}{\kappa_\nu} \int_0^\infty l_\nu d_\nu = B \frac{\pi e^2}{mc} \frac{\lambda^2}{c} f \frac{N}{\kappa_\nu} \quad (2.8)$$

Introducing the number abundance relative to hydrogen, $A = N_E/N_H$, and the fraction of the r-th stage of ionization, N_r/N_E given by Boltzmann's equation, N can be written as:

$$N = A \frac{N_r}{N_E} N_H \frac{g}{u(T)} exp(\frac{-\chi}{\kappa T}) \quad (2.9)$$

Finally obtaining:

$$log(\frac{W}{\lambda}) = log \frac{\pi e^2 N_H/N_H}{mc^2 u(T)} + logA + loggf\lambda - (5040/T)_\chi - log\kappa_\nu \quad (2.10)$$

where $gf\lambda$ is the statistical weight of the oscillator strength and χ is the excitation potential.

The MOOG code (Sneden 1973) has several EW and spectral synthesis tools. The routine *abfind* is the one used to obtain chemical abundances using the equivalent width.

Moreover, for the EW measurements it is important to define the profile function used for the line fit and the corresponding strength calculation of each lines. The Gaussian profile is widely used and is considered to be an almost perfect approximation for weak absorption lines. However, some caution should be taken when measuring strong lines (typically EW > 120 mÅ). In this case the Gaussian profile cannot perfectly fit the wings of the line and in these cases several authors prefer to use the Lorentzian profile.

2.2.2 Synthesis

The synthesis method is the computation of a complete spectral interval in which all of the observed lines are included. Synthesis works best when all the spectral lines can be identified and have known atomic parameters. This technique stresses on the computational strength of the analysis. It can be simplified to a trial-and-error method in which the abundances, often the f-values and the line-broadening parameters, are adjusted until the shape of the spectrum is reproduced. In case of severe blending of the lines, as in the case of molecular features (see Fig. 2.3), the synthesis method is one of the few methods available to obtain reliable chemical abundances.

The MOOG code (Sneden 1973) have spectral synthesis routines within their tools. The routine *synth* is the one used to obtain abundances using synthetic spectra.

The FITTING programme, developed by González Hernández et al. (2011) creates the following input data, required by MOOG: the atmospheric model, the line list, the range of abundances of the grid of synthetic spectra, and the wavelength at which we want to analyse these abundances. We use a χ^2 comparison for the observed and synthetic spectra, and we define $\chi^2=\sum_{i=1}^{N}(F_i-S_i)^2/N$, where F_i and S_i are the observed and synthetic fluxes respectively at wavelength point i.

Due to the spectral regions chosen to study in this thesis, measuring the EW of stars in long spectral ranges was impossible. In this work, we focus on deriving precise and accurate chemical abundances for several elements using the spectral synthesis technique, due to the characteristics of the studied features.

2.2.3 Atmosphere models

In this thesis, we have made use of the atmosphere models ATLAS9, developed by Kurucz (1993). They consist of a grid of mono-dimensional models under the assumption of plane-paralel, LTE atmospheres. Avail-

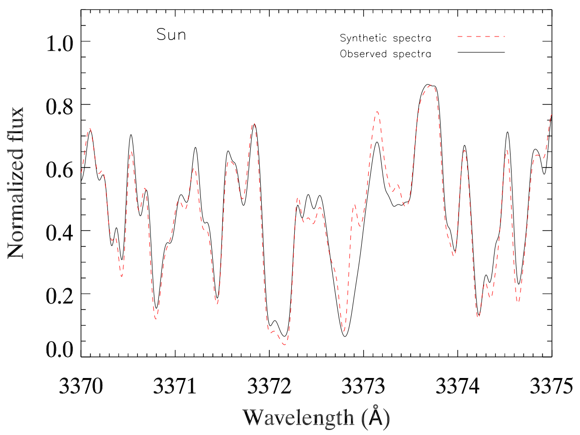

FIGURE 2.3— A solar spectral range showing a studied molecular feature of nitrogen.

able T_{eff} range from 3500K until 50000K, with $\log g$ from 0.0 dex to 5.0 dex and metallicities [Fe/H] from -3.0 dex to +1.0 dex. These models faces convection with overshooting, through the mixing length theory.

3

Nitrogen abundances: the 3360Å band

This chapter is based on Suárez-Andrés et al. (2016), A&A, 591, A69

ABSTRACT – We present a detailed spectroscopic analysis of 74 solar-type stars, 42 of which are known to harbour planets. We determine the nitrogen abundances of these stars and investigate a possible connection between N and the presence of planetary companions. We have used VLT/UVES to obtain high-resolution near-UV spectra of our targets. We identify several spectral windows from which accurate N abundance can be obtained. We discuss the behaviour of [N/Fe] and [N/H] with stellar parameters and the important of this element in stars with planetary companions.

THE study of C, N, and O in stars is crucial because they are the most abundant elements after H and He. These elements play an important role in stellar interiors because they generate energy through the CNO cycle, thereby affecting the lifetime of the stars (Liang et al. 2001)

Nitrogen is created in a different nucleosynthetic process from that giving rise to carbon and oxygen. Whereas for carbon and oxygen the dominant production modes are the α-chain reactions, for nitrogen the dominant production mode lies in the re-arrangement of nuclei during the CNO cycle (see Maeder 2009). One important question regarding N is its origin. Since N needs C and O to be formed, if it is formed from pre-existing C and O in the star, it is called "secondary". If, instead, the carbon and oxygen are produced in the star itself and then used to produce nitrogen, then the nitrogen is called "primary". Several studies have proved that production of nitrogen at low metallicities comes from primary rather than secondary sources (Pagel & Edmunds 1981; Bessell & Norris 1982; Carbon et al. 1987; Henry et al. 2000; Israelian et al. 2004). At higher metallicities, secondary processes dominate. Two main sources for primary production have been proposed:

- Rotating massive stars, implying detached N and Fe abundances and overabundance of N regarding Fe (Maeder & Meynet 2000).

- Intermediate-mass stars (4-8 $M_{\odot}$) during their thermally pulsing AGB phase through CNO processing in the convective envelope (Marigo 2001; van den Hoek & Groenewegen 1997). The contribution by massive stars is negligible (Liang et al. 2001; Pettini et al. 2002), so dominant contributors are intermediate- and low-mass stars (ILMS). These ILMSs are also a source for secondary production.

Gonzalez et al. (2001a) and Santos et al. (2001) discovered that, on average, planet hosts are more metal-rich than “single” stars (stars with no known companion planet; from now on designated as single stars).

Interestingly, recent studies suggest that specific element abundances may have a particularly relevant role in the planet formation process (Adibekyan et al. 2014, 2015a) or in its composition (Santos et al. 2015). The abundances of volatiles (such as C, N, and O) may be particularly relevant in this respect. This consideration prompted the study of specific chemical abundances in the planet hosts. There are very few studies of nitrogen in solar-type stars owing to the lack of strong atomic lines. Ecuvillon et al. (2004a) studied the abundance of nitrogen of 91 solar type stars. Using both the NH molecular band at 3360Å and the NI atomic line at 7468Å, they rejected the self-enrichment scenario as a formation source on the grounds that they could find no under-abundances of volatiles compared to refractory elements. They showed that the [N/H] abundance scales perfectly with metallicity for both planet-host and comparison samples. They also found no difference for nitrogen in the [N/Fe] abundance ratios when comparing stars with and without planets.

More recently, Da Silva et al. (2015), using the CN band at 4215Å, have studied the abundance of nitrogen in 140 dwarf stars. They found a steeper slope for the [N/Fe] versus [Fe/H] abundance ratios than Ecuvillon et al. (2004a).

The main problem in studying nitrogen abundances is the lack of strong nitrogen lines in the red part of the spectrum so that near-UV measurements are required. We are forced to study the very crowded molecular band at 3360Å, where continuum determination is not straightforward.

The purpose of this study is to extend the sample of Ecuvillon et al. (2004a) and investigate in detail nitrogen abundances using the 3360Å NH molecular band. We have performed a systematic study of nitrogen abundances in dwarf stars with a wide range of stellar parameters. The strategy and methodology followed in this study is the same as that stated in Ecuvillon et al. (2004a), but with a larger sample and higher-quality spectra.

We have also determined the kinematic properties of our sample. Then using the kinematic and chemical properties of the stars, we separated them into different stellar populations to investigate the N abundances within a Galactic context.

This work is the first step in comparing CNO abundances of planet-host stars with the CNO abundances of their planets (through transmission spectroscopy or direct spectroscopy, as in the case of *Spitzer*). Testing and improving planetary formation models will play a key role in future studies of habitability, CNO being key elements for life.

3.1 Analysis

3.1.1 Stellar parameters and chemical abundances

The stellar parameters used in this study were taken from Sousa et al. (2008, 2011a,b); Tsantaki et al. (2013); González Hernández et al. (2010, 2013). All stellar parameters used were derived by measuring equivalent widths of Fe I and Fe II lines using the code ARES (Sousa et al. 2007). Also, chemical abundances of elements other than N were adapted in targets with more recent stellar parameters (derived by our group with the same technique). To do this, the uncertainties presented in their original source were followed so systematic effects in the chemical abundances or the stellar parameters are negligible, not affecting the consistency of our results.

Chemical abundances of the elements with spectral lines present in the NH band were obtained from Adibekyan et al. (2012b) and González Hernández et al. (2010, 2013). These elements are Ca, Ti, Mn, and Si (note that the abundances of these elements were simply scaled with iron in Ecuvillon et al. 2004a). The N abundance is also affected by C and O molecular equilibrium. The C and O abundances were obtained from Suárez-Andrés et al. (2017) and Bertran de Lis et al. (2015), respectively. However, there are 26 stars with no previous measurements of O. We have decided to use the aforementioned results to interpolate for a given set of stellar parameters and use these new O abundances to calculate the molecular equilibrium. Our tests show that N abundances are unaffected by changes of the order of ±0.2 dex in C and O.

Nitrogen abundances were determined using a standard local thermodynamic equilibrium (LTE) analysis with the spectral synthesis code MOOG (Sneden 1973, 2013 version) and a grid of Kurucz (1993) ATLAS9 atmospheres. All the atmospheric parameters, $T_{\rm eff}$, $logg$, ξ_t and [Fe/H] were taken, as already mentioned, from Sousa et al. (2008, 2011a,b); Tsantaki et al. (2013); González Hernández et al. (2010, 2013). The adopted solar abundances for nitrogen and iron were $\log\epsilon(\rm N)_\odot$=8.05 dex and $\log\epsilon(\rm Fe)_\odot = 7.47$ (Santos et al. 2004).

3.1.2 NH band

The NH band is the strongest feature observed in the $\lambda\lambda 3345 - 3375$Å spectral region. We determined N abundances by fitting synthetic spectra to the data in this wavelength range. The dissociation potential used for NH spectra is $D_o = 3.37$ eV, as recommended in Grevesse et al. (1990). The complete line list used in this study was obtained from Ecuvillon et al. (2004a), which was calibrated with the KURUCZ ATLAS spectrum (Kurucz et al. 1984) using the abundance $\log\epsilon(\rm N)_\odot$=8.05 dex.

The number and the strength of the atomic lines of different elements in the spectral region of the NH band increases with metallicity. The presence of many blended lines and numerous strong molecular bands make the placement of the continuum level very difficult. The high-resolution solar atlas (Kurucz et al. 1984) can help to achieve a reliable continuum placement for solar-type stars (e.g. Ecuvillon et al. 2004a). However, large variations of metallicity and effective temperature among the stars in our sample do not allow us to use the solar spectrum as a reference. To account for this effect, we have generated a grid of synthetic spectra for all the stars in our sample. Synthetic spectra are calculated for a given set of stellar parameters and variations of nitrogen abundances [N/H] between −0.7 and 0.5. Our reference points for the continuum placement are those for which the flux variation (for a given $T_{\rm eff}$) due to the N abundance changes from [N/Fe] = −0.7 to +0.5, is less than 1%. This strategy is demonstrated in Fig. 3.2 for two stars with different atmospheric parameters. Rotational broadening was set as a free parameter (it was fixed in Ecuvillon et al. 2004a) with $v \sin i$ varying between 0.0 and 14.0 with a step of 1 km/s. Macroturbulence was not taken into account. In order to find the best fit abundance value for each star, we used the FITTING program (González Hernández et al. 2011) and the MOOG synthesis code in its 2013 version. The best fit was obtained using a χ^2 minimization procedure by comparing each synthetic spectrum with the observed one in the following spectral regions: 3344.0 − 3344.3Å, 3346.2 − 3346.7Å, 3347.0 − 3347.8Å, 3353.8 − 3354.4Å, 3357.4 − 3358.0Å, 3358.5 − 3359.7Å, 3360.3 − 3362.0Å, 3364.1 − 3364.8Å, 3370.8 − 3371.8Å, 3374.9 − 3375.4Å. These spectral regions were chosen because of the presence of relatively strong NH features that allow reliable abundance measurements. We use a χ^2 comparison for the observed and synthetic spectra.Best-fit nitrogen abundances are extracted from each spectral range and the final nitrogen abundance for each star is then computed as the average of these values.

The FITTING program creates the following input data, required by MOOG: the atmospheric model, the line list, the range of nitrogen abundance of the grid of synthetic spectra, and the wavelength at which we want to analyse these abundances. To obtain the final abundance value, we analysed ten different ranges but use only those that have abundance values within 1σ.

In Fig. 3.1 and 3.2 we show the observed and synthetic spectra for the Sun and two stars that are depicted for different temperatures and metallicities within our sample. For these two stars, three different nitrogen abundances are also shown.

To examine how variations in the atmospheric parameters affect the NH abundances, we test [N/H] sensitivity in stars with very different parameter values, given the wide range of stellar parameters. For each set of stars we tested the nitrogen-abundance sensitivity to changes in the atmospheric parameter (± 100K for $T_{\rm eff}$, ± 0.2 dex in $logg$, ± 0.2 in metallicity). The results are shown in Table 3.1. The effect of microturbulence was not taken into account because an increase of 0.3 kms^{-1} produced an average decrease of 0.002 dex in nitrogen abundance, which is negligible in comparison with the effects of other parameters. The error due to continuum placement of 0.1 dex was considered for all stars. All effects were added quadratically to obtain the final uncertainties in nitrogen abundances using the following relation:

$$\Delta[\mathrm{N/H}] = (\Delta^2_\sigma + \Delta^2_{T_{\rm eff}} + \Delta^2_{\log g} + \Delta^2_{\rm met} + \Delta^2_{\rm cont})^{1/2}$$

3.2 Results

We analysed near-UV high-resolution spectra of 42 planet host stars and 32 comparison stars. We aim to explore possible differences in nitrogen

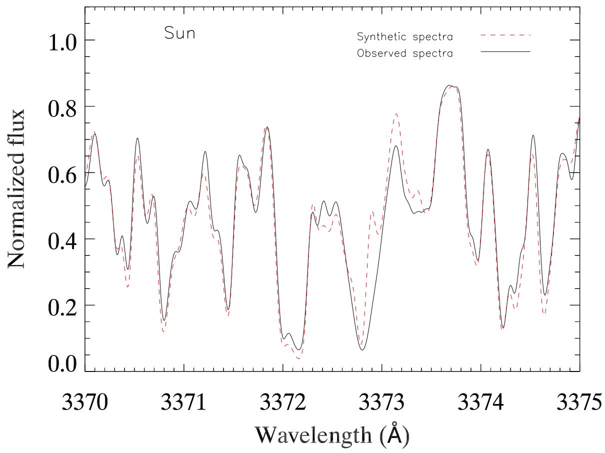

FIGURE 3.1— Solar observed (solid line) and synthetic (dotted line) spectra in the spectral region 3370-3375Å.

TABLE 3.1— Sensitivity of the nitrogen abundance derived from the NH band at 3360Å. Changes of 100 K in $T_{\rm eff}$, 0.2 dex in gravity, and 0.2 in [Fe/H] were applied.

	Star ($T_{\rm eff}$; $\log g$; [Fe/H])		
	HD 93083 (5048; 4.32; 0.04)	HD 222582 (5779; 4.32; -0.01)	HD 39091 (6003; 4.42; 0.09)
$\Delta T_{\rm eff} = \pm$ 100K	±0.05	±0.08	±0.10
	HD 11964A (5332; 3.90; 0.10)	HD 93083 (5105; 4.43; 0.09)	HD 1237 (5514; 4.50; 0.07)
Δlogg = ± 0.2 dex	∓0.01	∓0.05	∓0.03
	HD 4208 (5599; 4.44; -0.28)	HD 69830 (5402; 4.40; -0.06)	HD 73256 (5526; 4.42; 0.23)
Δ([Fe/H]) = ± 0.2 dex	∓0.16	∓0.01	∓0.08

abundances between the two samples. Our results for planet-host are presented in Appendix C.

In Fig. 3.3 we show the [N/Fe] abundance ratio as a function of $T_{\rm eff}$. Stars with effective temperatures below 5000 K were excluded from the

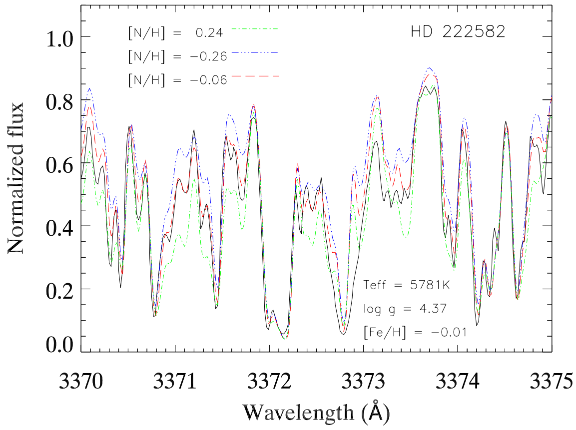

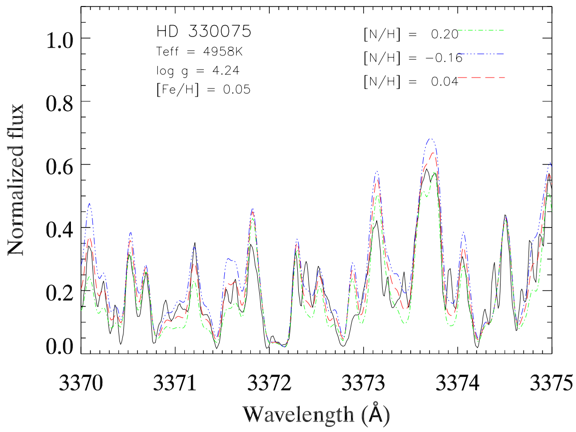

FIGURE 3.2— Observed (solid) and synthetic spectra (green-dotted lined, red-dashed and blue-dashed dotted) of HD 222582 (top) and HD 330075 (bottom).

analysis because of uncertainties in the behaviour of those cool stars: we find no explanation for the decrease in nitrogen abundance as we move

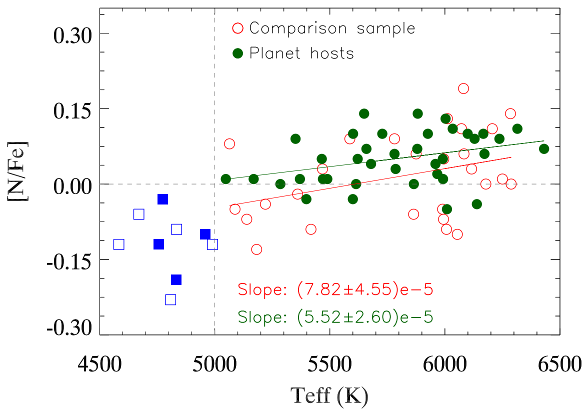

FIGURE 3.3— [N/Fe] abundance ratio of the stars in this study plotted against effective temperature, $T_{\rm eff}$. Filled green circles represent planet hosts and open red circles the comparison sample. Filled blue squares represent cool planet hosts while open blue squares represent single stars. The vertical dashed line at 5000 K separates the cool stars from the studied sample.

to lower temperatures. We do not study the cool stars as their behaviour differs from what it is expected possibly due to unknown blends or known blends with non-accurate atomic parameters, so a revision of their stellar parameters may be required. The vertical dashed line at 5000 K separates the cool stars from the sample studied. From now on in this paper, all results and conclusions will refer to stars with $T_{\rm eff} > 5000$ K (65 stars). Because of the high dispersion, we did not find any clear trend of [N/Fe] with $T_{\rm eff}$. However, it can be seen that most of the planet-host stars have [N/Fe] > 0.

We have also looked for distinguishable trends between these samples by representing [N/Fe] and [N/H] abundance ratios as functions of [Fe/H] for both samples (see Fig. 3.4). These plots indicate that both samples behave approximately similarly. However, there seems to be a steeper trend in [N/H] vs [Fe/H] for stars with planets, whereas stars without planets almost maintain the 1:1 relation. We note the same behaviour in the upper panel of Fig. 3.4, where the stars with planets below and above solar metallicity have values of [N/Fe] lower and higher than zero respectively. Unfortunately, owing to the metal-rich nature of giant-planet hosts, the number of stars with giant planets at metallicities below solar is too small for us to be able to confirm this behaviour. The observed trend may simply be related to Galactic chemical evolution.

In the upper panel of Fig. 3.5 we show the [N/H] abundance distributions for both samples. As can be seen, there is an offset between the samples, which is expected because planet-host stars are metal rich as compared with single stars. We expect this result because, if nitrogen scales with iron, then we can expect higher [N/H] because giant-planet host stars are enhanced in Fe. In the lower panel of Fig. 3.5 we show the [N/Fe] abundance distribution. We see that most of the stars with planets have [N/Fe] $\geq$0 ($\sim$ 90%), as opposed to the single-star sample, more spread than the stars with planets sample. In this case, only $\sim$60% of the stars have [N/Fe] $\geq$ 0. A Kolmogorov-Smirnov (K-S) test predicts the $\sim$0.06 probability (P_{KS}) that stars with and without planets come from the same distribution. The distribution of abundance ratios [N/Fe] vs [Fe/H] of stars without planets shows a weak linear increasing trend, although the slope is consistent with zero (see Fig. **??**). The number of points may not be sufficient to really confirm this increasing trend. Thus, we may conclude that stars with planets are, on average, nitrogen rich when compared to single stars, but it may be due to the metal-rich nature of the planet host stars.

If we extend the study of nitrogen abundance to metal-poor stars (Israelian et al. 2004), we will ensure that the behaviour seen in Figure 3.6 is part of the same trend observed in these metal-poor stars down to metallicites ~ -2.0 dex. In Fig. 3.6 we can see how these two sets, (Israelian et al. (2004) and this study) follow the same trend down to metallicities of -2.0 dex because nitrogen behaves like a secondary production element in this range of metallicities. At metallicities lower than -2.0 dex, we see a signature of primary N.

3.3 Galactic evolution of N: dependence on age

Interpretation of chemical abundances in terms of stellar ages can be helpful to constrain the effects of Galactic chemical evolution.

Stellar ages for our sample were estimated applying stellar evolutionary models from the Padova group (Bressan et al. 2012), using the web interface [1](see Sousa et al. 2011a, for more details)

Nissen (2015) performed a detailed study of abundance ratios of several

[1]http://stev.oapd.inaf.it/cgi-bin/cmd

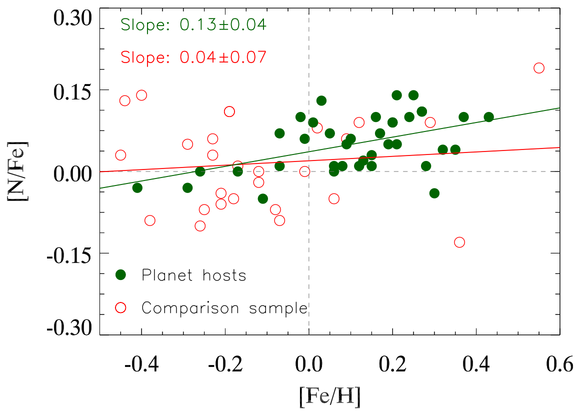

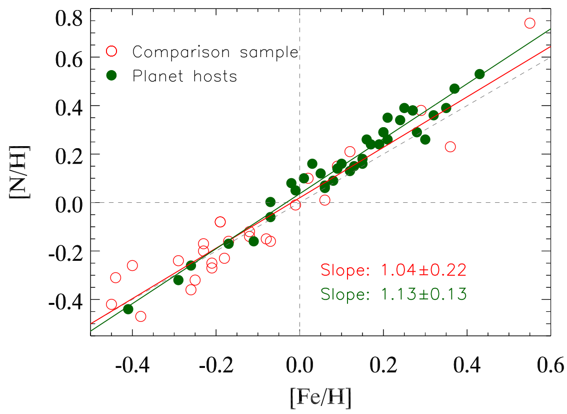

FIGURE 3.4— [N/H] and [N/Fe] abundance ratios of our sample stars versus metallicity, [Fe/H]. Filled green circles represent planet hosts and open red circles, the comparison sample. Dashed lines stand for solar values.

elements, such as C, O and Si, as a function of the stellar age. They conclude that each element behaves in a different way regarding the stellar

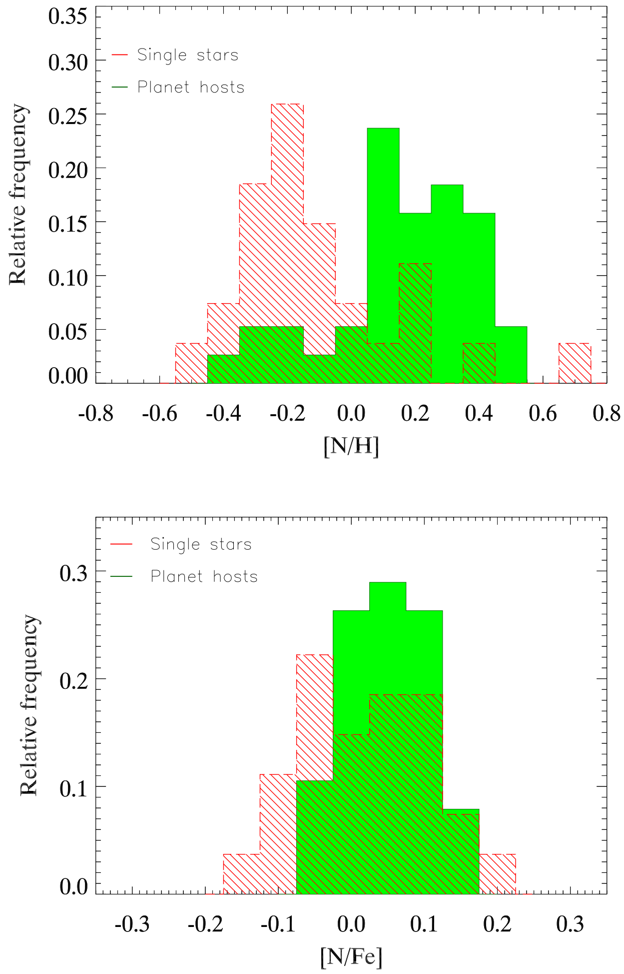

FIGURE 3.5— [N/H] and [N/Fe] abundance distributions.

age, suggesting that more variables such an evolving initial mass function and asymptotic giant branch stars should also be considered. Although that work is only for solar twin stars, we try to extend this result to solar type stars and for nitrogen, an element not studied in that work.

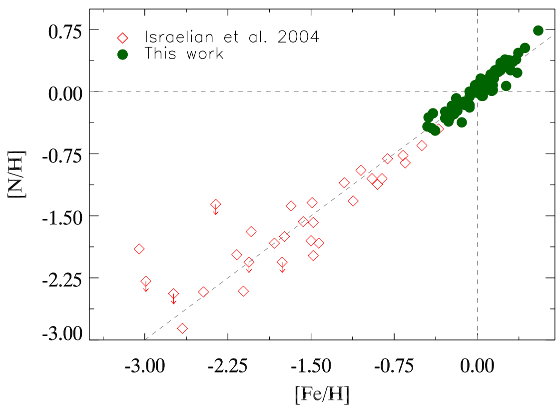

FIGURE 3.6— [N/H] plotted against [Fe/H] for metal-poor stars from Israelian et al. (2004) indicated by red squares and stars from this study indicated by green circles.

In Fig. 3.7 we show [N/Fe] abundances as a function of stellar age for the thin disk stars. There seem to be a weak trend in the behaviour of nitrogen, as its abundance decreases with age. Although single stars appear to show a steeper decreasing trend towards older stars than planet hosts stars, probably due to the low number of points and the high dispersion of the abundance measurements,the slopes of these two trends are consistent within their error bars.

3.4 Kinematic properties

To study the kinematic properties of the sample stars and which stellar populations they belong to, we applied both purely chemical (e.g. Adibekyan et al. 2011; Recio-Blanco et al. 2014) and kinematic approaches (e.g. Bensby et al. 2003; Reddy et al. 2006). The Galactic space velocity components of the stars were calculated as in Adibekyan et al. (2012b) using the astrometric [2] and radial velocity data of the stars. The average errors in the U, V, and W velocities are approximately 2–3 km s^{-1}.

To assess the likelihood of the stars being members of different stellar

[2]The SIMBAD Astronomical Database (http://simbad.u-strasbg.fr/simbad/) was used.

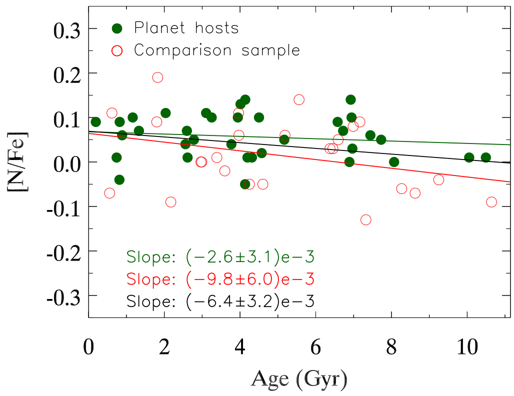

FIGURE 3.7— Abundance ratio of [N/Fe] as a function of stellar age for the stars belonging to the thin disk. Linear fit is provided for the whole sample (black line) and each sub-sample (red and green lines).

populations we followed Reddy et al. (2006), and adopted the results of Bensby et al. (2003) for the population fractions. According to this separation, among the 65 stars, we have 58 (89%) stars from the thin disc, four from the thick disc, and three transition stars that do not belong to any group.

The separation of the Galactic stellar components based only on stellar abundances is probably superior to that based on kinematics alone (e.g. Navarro et al. 2011; Adibekyan et al. 2011) because chemistry is a relatively more stable property of sunlike stars than spatial positions and kinematics. We used the position of the stars in the [α/Fe]–[Fe/H] plane (here α refers to the average abundance of Si and Ti) to separate the thin- and thick-disc stellar components. We adopt the boundary (separation line) between the stellar populations from Adibekyan et al. (2011). According to our separation, 53 stars (≈82%) are not enhanced in α-elements and belong to the thin-disc population. The [α/Fe] versus [Fe/H] plot for the sample stars is shown in the bottom panel of Figure 3.8.

In the top plot of Fig. 3.8 we show the dependence of [N/α] on the metallicity. The figure shows that the [N/α] abundance ratio correlates with the metallicity. This trend is expected if the N abundance scales

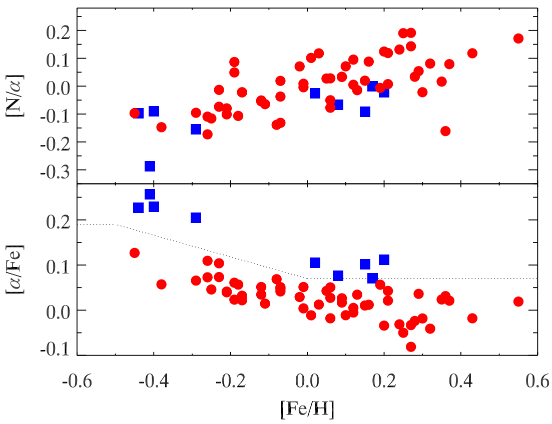

FIGURE 3.8— [N/α] plotted against [Fe/H] (top) and [α/Fe] plotted against [Fe/H] (bottom) for the sample. Stars that are enhanced in α-elements are shown in blue squares and the thin-disc stars (non-α-enhanced) are represented by red filled circles.

with the iron abundance, as was suggested above.

3.5 The star–planet connection

The increasing number of exoplanets discovered via different methods has led to a wide diversity of parameters (masses, radii, eccentricity, orbital period, etc.) being known for these planets. Many studies have suggested that the formation of giant planets correlates with the metallicities of stellar hosts (Santos et al. 2001, 2004; Fischer & Valenti 2005; Sousa et al. 2011a; Mortier et al. 2013). Moreover, it has been shown that the formation of planets (of both high and low masses) at low metallicities is favoured by enhanced α-elements (Adibekyan et al. 2012b,c)

Models of planet formation require precise stellar abundances. Chemical abundances of planet hosts are useful when studying the properties of the planetary companion (Sousa et al. 2015). The relationship between [N/Fe] and the mass of the planet is shown in Figure 3.9. In those stars which host many planets, the most massive planet was considered in the plot. As we can see, the masses of the planets are between 0.015 and 10.3 M_J, but most stars have planets with less than 4 M_J orbiting around them. To remove this bias, which is due to the lack of planets with higher

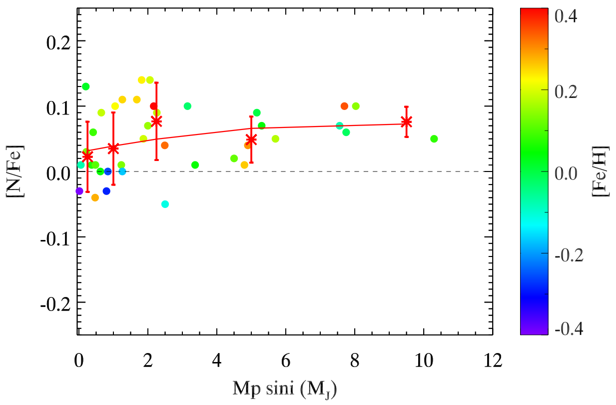

FIGURE 3.9— [N/Fe] plotted against $M_p \sin i$, with [Fe/H] in the auxiliary axis. Dots represent the whole sample and red asterisks represent binned values. We also represent in red a second-degree polynomial fit for those binned values.

masses, we created bins with increasing steps, with sizes of 0.5, 1, 1.5 M_J and two bins of 4 M_J. Error bars indicate the standard deviation of each bin. Although the results are biased because of the lack of data in the highest-mass part, we cannot obtain a clear relationship between [N/Fe] and the planetary mass (covariance $s_{x,y} = 0.031$; where $x = M_J$ and $y = [N/Fe]$). We see an increase of the [N/Fe] ratio in the first mass bins followed by constant [N/Fe] value for the more massive planets. Even so, the number of stars is not statistically significant to confirm this.

3.6 Conclusions

We present nitrogen abundances for 74 solar-type stars observed with the UVES spectrograph at the VLT/UT2 Kueyen telescope (Paranal Observatory, ESO, Chile). In our sample, 42 of the 74 are planet-hosts and 32 stars do not have any known planetary companion. All targets have been studied using spectral synthesis in the NH band at 3360Å. The stars in our sample have effective temperatures between 4583 K and 6431 K, metallicities from −0.45 to 0.55 dex, and surface gravities from 3.69 to 4.82 dex. We performed a detailed analysis of this sample to obtain precise nitrogen abundances and investigate possible differences between the stars with planets and the single stars. Nitrogen abundances of both samples behave in a similar way regarding T_{eff}, $\log g$, and [Fe/H].

We extended our results to the metal-poor regime, comparing our results with previous work by Israelian et al. (2004). Both results can be accommodated under a common fit in an [N/H] versus [Fe/H] plot until metallicities down to -2.0 *dex* (where the production of nitrogen has a secondary origin), suggesting that both metal-poor stars and solar-like stars follow the same behaviour.

The correlation between the presence of planets and nitrogen abundances is expected: The large amount of nitrogen in a protoplanetary disc would favour the formation of massive giant planets through the core accretion scenario.

We searched for correlations between planet mass and [N/Fe] abundance ratio, but did not find any significant correlation.

4

Carbon abundances: the 4300Å band

This chapter is based on Suárez-Andrés et al. (2017), A&A, 599, A96

ABSTRACT – We present a detailed spectroscopic analysis of 1110 solar-type stars, 143 of which are known to have planetary companions. We have determined the carbon abundances of these stars and investigate a possible connection between C and the presence of planetary companions. We used the HARPS spectrograph to obtain high-resolution optical spectra of our targets. We discuss the behaviour of [N/Fe] and [N/H] with stellar parameters and the important of this element in stars with planetary companions

Carbon is created through a different process from nitrogen and oxygen. In this case, α-chain Carbon reactions are the dominant processes. Both massive ($M_\star > 8M_\odot$) and low- to intermediate-mass stars contribute to carbon production, but the relative importance of each type of star has not been clarified owing to uncertainties in the metallicity-dependent mass loss (Meynet & Maeder 2002; van den Hoek & Groenewegen 1997).

The analysis of the HARPS stellar sample done by Adibekyan et al. (2012b) shows that this chemical overabundance found in stars with planets is not exclusive to iron. Using a sample of 1111 FGK stars they show that stars hosting a giant planet in their systems show an over-abundance in 12 refractory elements. They find that, at metallicities below −0.3 dex, about 76% of the planet hosts are enhanced in α elements at a given metallicity. This proves that planet formation requires a certain amount of metals, even for low-mass planets Adibekyan et al. (2012c).

There are several studies of carbon in solar-type stars, but hardly any of these use CH molecular features (see Clegg et al. 1981) Instead, the most commonly used features are the C_2 Swan (5128Å and 5165Å), the CN molecular band (4215Å), and two atomic lines (5380.3Å and 5052.2Å). This last feature becomes very weak for cool stars ($T_{eff} < 5100K$).

Previous studies by Delgado Mena et al. (2010) and Da Silva et al. (2011, 2015) using some of the above-mentioned carbon features show that there is no difference in behaviour regarding carbon between stars with and without any known planetary companion. The enrichment found was attributed to Galactic chemical evolution.

In this chapter we study the volatile C element using the CH band and derive C abundances for 1110 HARPS FGK stars, thereby complementing the Adibekyan et al. (2012b) study of refractory elements. We propose that CH molecular features are a good alternative to atomic lines. We also investigate whether the presence of a (giant) planetary companion affects the carbon abundance of the planet host stars.

4.1 Sample description

The high-resolution spectra analysed in this work were obtained with the HARPS spectrograph at La Silla Observatory (ESO, Chile) during the HARPS GTO programme (see Mayor & Queloz 1995; Lo Curto et al. 2010; Santos et al. 2011). The spectra had already been used previously in the analysis of stellar parameters, as well as the derivation of precise chemical abundances (see Sousa et al. 2008, 2011a,b; Tsantaki et al. 2013; Adibekyan et al. 2012b)

The high spectral resolving power ($R = 115,000$) of HARPS and a good signal-to-noise ratio (S/N) are an optimal combination for properly analysing the CH band at 4300Å. About 41% of the stars within our sample, at 4300Å, have S/N>150, 18% have S/N in the range 100–150, and 30% have S/N below 100. Only 4% of our sample have S/N lower than 40.

The sample consists of 1110 FGK solar-type stars with effective temperatures between 4400 K and 7212 K, metallicities from −1.39 to 0.55 dex, and surface gravities from 3.59 to 4.96 dex. 143 out of 1110 are planet hosts,[1] whereas the other 967 are comparison sample or comparison stars (stars with no known planetary companion).

[1]Data from www.exoplanet.eu.

4.2 Analysis

4.2.1 Stellar parameters and chemical abundances

The stellar parameters used in this study were taken from Sousa et al. (2008, 2011a,b) and Tsantaki et al. (2013), who used the same spectra as we did for this study. All the stellar parameters were derived by measuring equivalent widths of FeI and FeII lines using the ARES and ARES2 code (Sousa et al. 2007, 2015b). Chemical abundances of elements with spectral lines present in the features studied were obtained from Adibekyan et al. (2012b). These elements are Ca, Si, Sc, and Ti. Also, chemical abundances of elements other than carbon were adapted in targets with more recent stellar parameters (also obtained by our group using the aforementioned technique, see Tsantaki et al. 2013) following uncertainties presented in their original sources, so systematic effects in the chemical abundances or the stellar parameters are negligible and do not affect the consistency of our results.

Carbon abundances were determined using a standard local thermodynamic equilibrium (LTE) analysis with the MOOG spectral synthesis code (2013 version, Sneden 1973) and a grid of Kurucz (1993) ATLAS9 atmospheres. All atmospheric parameters, $T_{\rm eff}$, $\log g$, ξ_t, and [Fe/H] were taken, as mentioned above, from Sousa et al. (2008, 2011a,b) and Tsantaki et al. (2013). Adopted solar abundances for carbon and iron were $\log\epsilon(\mathrm{C})_{\odot} = 8.50$ dex and $\log\epsilon(\mathrm{Fe})_{\odot} = 7.52$ (Caffau et al. 2010, 2011) For oxygen, we adopt $\log\epsilon(\mathrm{O})_{\odot} = 8.71$ dex (Bertran de Lis et al. 2015).

As molecular carbon abundances are affected by molecular equilibrium, we need to consider oxygen and nitrogen. Oxygen, being an α-element, does not keep pace with [Fe/H] as nitrogen does (see Bertran de Lis et al. 2015; Suárez-Andrés et al. 2016). However, there were 575 stars with no previous measurements of O and 1054 stars with no previous measurements of N. We decided to use the available oxygen 6158Å results and perform an interpolation for these 575 stars with no oxygen measurements (see Section 4.3.1). We obtained individual O and N abundances for the available targets from Bertran de Lis et al. (2015) and Suárez-Andrés et al. (2016), respectively. As nitrogen re-scales with [Fe/H], we obtained carbon abundances, thus providing individual values of oxygen and scaling nitrogen with the metallicity.

We did not consider NLTE effects because these features are probably immune to such effects at these metallicities, although little computational work has been done in this area (Asplund 2005; Schuler et al. 2008).

4.2.2 CH band

The CH band is the strongest feature observed in the spectral region 4300Å. We determined carbon abundances by fitting synthetic spectra to data in this wavelength range. The dissociation potential used for CH spectra is $D_o = 3.464$ eV, as recommended in Grevesse et al. (1990). The complete line list used in this work was obtained from VALD3 (Ryabchikova et al. 2015). We slightly modified log gf values of the strongest lines in order to fit the solar spectrum.

The continuum was normalized locally with a 5th-degree polynomial using the CONTINUUM task of IRAF.

In order to find the best fit abundance value for each star, we used the FITTING program González Hernández et al. (2011) and the synthesis MOOG code in its 2013 version. The best fit was obtained using a χ^2 minimization procedure, by comparing each synthetic spectrum with the observed one in the following spectral regions: $4276.8-4282.2$Å, $4292.8-4293.4$Å, $4294.5-4298.3$Å, $4301.5-4303.7$Å, $4307.1-4310.7$Å, $4322.6-4324.6$Å, $4360.1-4360.6$Å, $4362.3-4367.0$Å, $4377.0-4377.4$Å, $4387.2-4387.7$Å. These regions were chosen for the presence of relatively strong CH features that allow reliable abundance measurements. We use a χ^2 comparison between observed and synthetic spectra. Best-fit carbon abundances are extracted from every spectral range and then the final carbon abundance for each star is computed as the average of these values. All the atmospheric parameters, $T_{\rm eff}$, $logg$, ξ_t and [Fe/H] were fixed, as well as all the chemical abundances used in the determination of C (see Section 4.2.1 and 4.3) Rotational broadening was set as a free parameter with v sin$i$ varying between 0.0 and 14.0 km/s with a step of 1 km/s (For more information about the procedure followed, see Suárez-Andrés et al. 2016).

In Figs. 4.1 and 4.2 we show the observed and synthetic spectra for the Sun and two stars that are depicted for different temperature and metallicity within our sample. For these two stars, best fit and two other different carbon abundances are also shown.

To examine how variations in the atmospheric parameters affect carbon abundances, we tested the [C/H] sensitivity in stars with widely differing parameters, given the wide range of stellar parameters in our sample. For each set of stars, we tested the carbon abundance to changes in the stellar parameters (± 50 K for $T_{\rm eff}$ and ± 0.1 dex in $\log g$ and metallicity). Results are shown in Table 4.1. The effect of microturbulence was not taken into account because an increase of 0.1 km s^{-1} produced an average decrease of 0.0005 dex in carbon abundances, which is negligible with regard to the

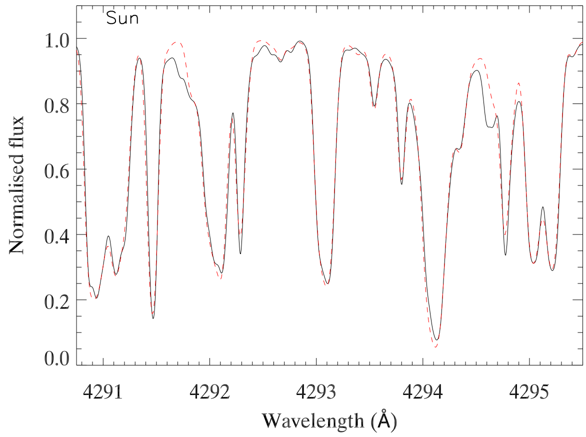

FIGURE 4.1— Observed solar spectrum (solid) and synthetic spectra (red-dashed lined).

effects of other parameters. An error due to a continuum placement was considered for all stars of 0.05 in those stars with higher S/N and 0.1 for those with lower S/N, thereby increasing the considered continuum error with decreasing S/N. All effects were added quadratically to obtain the final uncertainties in carbon abundances following this expression:

$$\Delta[\mathrm{C/H}] = (\Delta^2_\sigma + \Delta^2_{T_\mathrm{eff}} + \Delta^2_{\log g} + \Delta^2_{[\mathrm{Fe/H}]} + \Delta^2_\mathrm{cont} + \Delta^2_\mathrm{interp})^{1/2}$$

Where Δ_σ refers to the error due to the χ^2-fitting. Δ^2_interp is added only for those stars with interpolated oxygen values.

4.3 Results

4.3.1 Carbon abundances

In 2015, Bertrán de Lis et al. (using the same spectra used in this work) obtained oxygen abundances for 698 stars by studying two atomic features: 6158Å and 6300Å. We do not use 6300Å results, owing to the uncertainties of that feature caused by the presence of a blended nickel line. In order to obtain oxygen values for all our sample, we performed an interpolation of

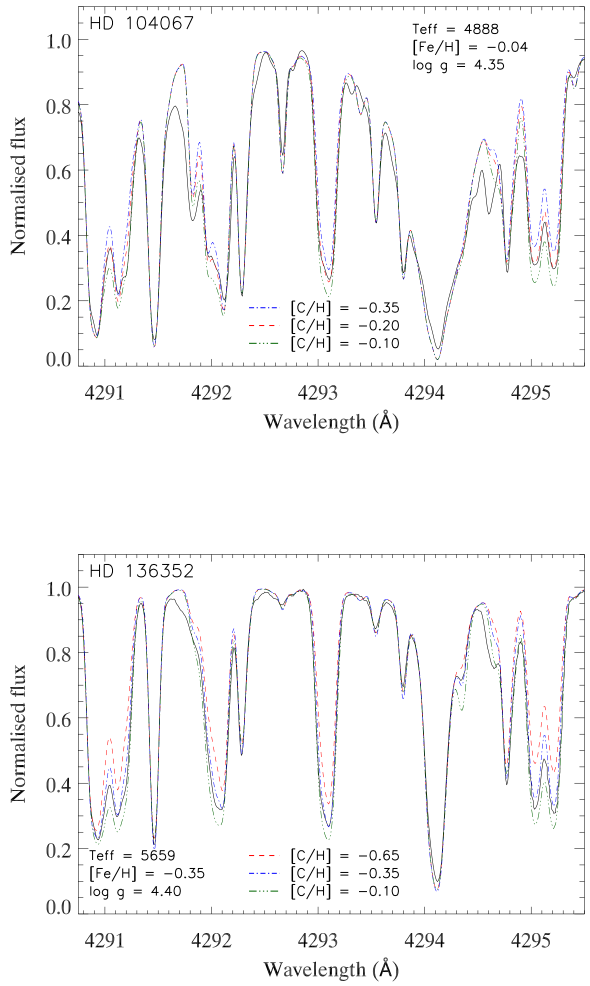

FIGURE 4.2— Observed (solid) and synthetic spectra (green-dotted lined, red-dashed, and blue-dashed dotted) of HD 104067 (top) and HD 136352 (bottom).

TABLE 4.1— Sensitivity of the carbon abundance derived from the CH band at 4300Å. Changes of 50K in T_{eff}, 0.1 dex in gravity and 0.1 in [Fe/H] were applied.

	Star (T_{eff}; *logg*; [Fe/H])			
	HD 103720 (5017; 4.43; -0.02)	HD 222595 (5618; 4.43; -0.01)	HD 75881 (6239; 4.44; 0.07)	HD 66740 (6666; 4.49; 0.04)
$\Delta T_{eff} = \pm$ 50K	±0.03	±0.03	±0.06	±0.04
	HD 159868 (5552; 3.91; -0.09)	HD 168746 (5561; 4.31; -0.11)	HD 290327 (5505; 4.41; -0.14)	HD 41087 (5562; 4.52; -0.13)
Δlogg = ± 0.1 dex	∓0.02	∓0.01	±0.00	±0.00
	HD 68089 (5597; 4.53; -0.77)	HD 161098 (5574; 4.49; -0.26)	HD 206163 (5506; 4.42; 0.02)	HD 203384 (5564; 4.42; 0.26)
Δ([Fe/H]) = ± 0.1 dex	∓0.13	∓0.02	∓0.02	∓0.02

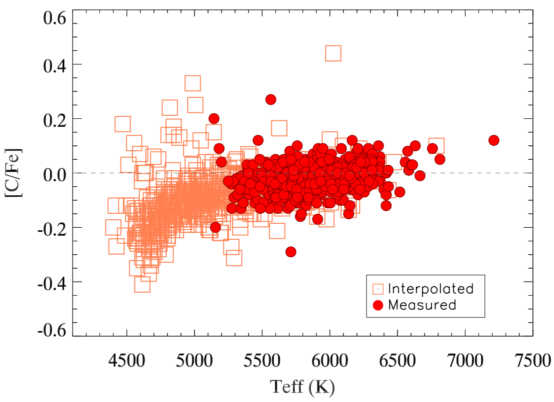

FIGURE 4.3— [C/Fe] as a function of T_{eff}. Filled red circles indicate those stars with available oxygen information, and open red squares indicate those stars with interpolated oxygen values.

their [O/Fe] vs [Fe/H] results only for the 6158Å feature. The interpolation consist of a 3^{rd} degree polynomial (ax^3+bx^2+cx+d), where the coefficients are: $a = 0.33$,$b = 0.75$, $c = -0.36$, $d = 0.03$). All the interpolations are consistent with an [O/H] vs [Fe/H] plot with previous measurements González Hernández et al. (2013). We obtained oxygen abundances for 575 stars in order to complete the sample of 1110 stars.

In Fig. 4.3 we see carbon abundances as a function of $T_{\rm eff}$. We can see that for $T_{\rm eff} > 4800$ K, both sets of data, those using real data and those using interpolated data, follow the same increasing trend for $T_{\rm eff}$ with similar dispersion (all stars from 4400 K to 5144 K have interpolated oxygen data). For those stars with $T_{\rm eff} < 4800$ K we find a steep decrease in [C/Fe] abundance ratios with temperature. A similar effect can also be found for other α-elements (Adibekyan et al. 2012b), as well as for nitrogen (Suárez-Andrés et al. 2016).

Stars with effective temperatures below 4800 K were excluded from the analysis because of uncertainties in the behaviour of those cool stars: we find no explanation for the decrease in carbon abundance as we move to lower temperatures.

4.3.2 Comparison with literature

A few studies can be found using the CH band at 4300Å, as opposed to C atomic lines. Delgado Mena et al. (2010) studied, among other elements, the carbon abundances of 451 stars of the HARPS sample, using the same spectra that we did. They used two atomic lines: 5380.3Å and 5052.2Å. To confirm the validity of our study, we will compare our results of stars in common. In Fig. 4.4, top panel, we can see the molecular [C/H] results of these stars as a function of atomic [C/H]. Representing the 1:1 relation with a dashed line, we can see how the results show good agreement between themselves for effective temperatures above 5200 K, whereas for cooler stars the results show some disagreements. Thus, we have decided to continue only with the analysis of stars with effective temperatures above 5200 K. In the bottom panel of Fig. 4.4 we show two sets: stars with $T_{\rm eff} > 5200$ K in common with Delgado Mena et al. (2010; filled circle) and stars with $T_{\rm eff} > 5200$ K in common with Nissen et al. (2014, open squares). Carbon abundances from Nissen et al. (2014) were obtained by studying the same atomic lines as in Delgado Mena et al. (2010). The slope of the fit, with its standard deviation, is provided for each set. As can be seen in Fig. 4.4, bottom panel, all sets data from this work, Delgado Mena et al. (2010) and Nissen et al. (2014) show good agreement

4.4 Carbon abundances in stars with and without planets

We analysed optical high-resolution spectra of 112 planet host stars and 639 comparison stars. We aim to explore possible differences in carbon abundances between both samples. Our results can be found in Appendix D.

To test for a possible relation between carbon abundances and the masses of planetary companions, we separated the planet population into two groups: low-mass planets (LMP; with masses less than or equal to 30 $M_{\oplus}$) and high-mass planets (HMP; with masses greater than 30 $M_{\oplus}$). In those stars which host several planets, the most massive planet was considered in our study. Our sample consist of 23 low-mass and 89 high-mass planet hosts.

We also look for distinguishable trends between these samples by representing [C/Fe] as a function of $T_{\rm eff}$ (see Fig. 4.5). As mentioned, we find a increasing trend of the [C/Fe] abundances on $T_{\rm eff}$ (for both planet and non-planet-hosts). However, the spread of [C/Fe] abundance values with $T_{\rm eff}$ amounts to about 0.1 dex from 5200 K to 6200 K, with $\sim$65% of our sample with [C/Fe] $<$ 0.0. Statistics for these relations are provided in Table 4.2. In Fig. 4.5 we can see a dashed line at 4800 and 5200 K separating the cool stars from the sample studied.

We look for distinguishable trends between the host and non-planet host samples by representing [C/Fe] and [C/H] abundance ratios as functions of [Fe/H] (see Fig. 4.6). In Fig. 4.6 top panel, [C/H] vs. [Fe/H] is represented. We can see how all the samples behave in the same way, and that no difference between them can be found. If we look at the slopes of each sample, we find very similar values, thus confirming that stars with and without planets follow the same trend.

In the bottom panel of Fig. 4.6, we find that [C/Fe] follows the same trend found in other α-elements. As presented in Da Silva et al. (2015), a decreasing trend can be found for metallicity values below solar, whereas for super-solar values, this trend has a positive slope. We can see in Fig. 4.6 how the slope for planets and the comparison sample at high metallicities follows the same behaviour, whereas for the low iron abundances the planet-host trend is steeper than for the comparison sample (for comparison sample only those stars with [Fe/H] $>$ -0.74 are taken (the minimum metallicity found for a planet host star in our sample)).

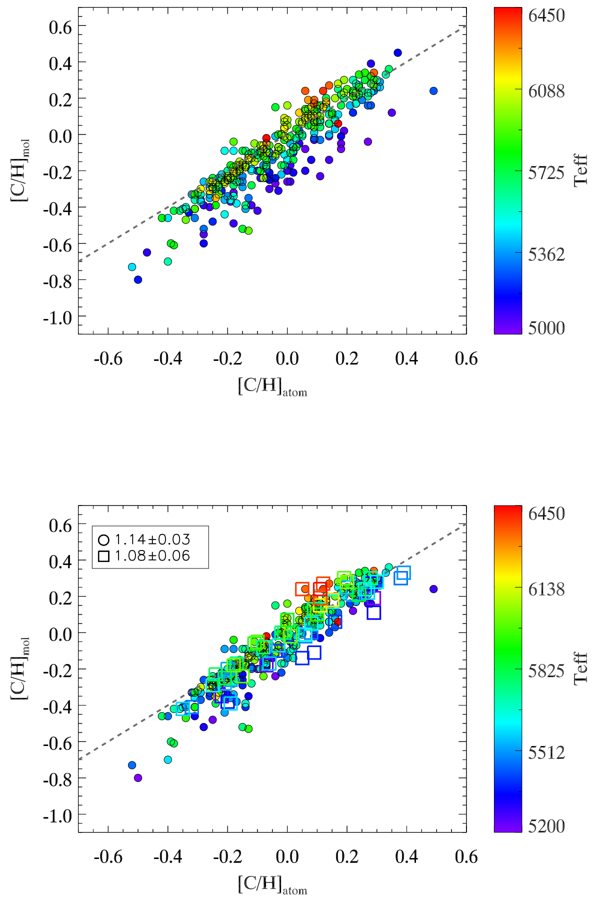

FIGURE 4.4— Top panel: molecular [C/H] results from this work as a function of atomic [C/H] extracted from Delgado Mena et al. (2010). The dashed line represents a 1:1 relation. Bottom panel: comparison for common stars with the works of Delgado Mena et al. (2010, filled circle) and Nissen et al. (2014, open squares) for stars with $T_{eff} > 5200K$.

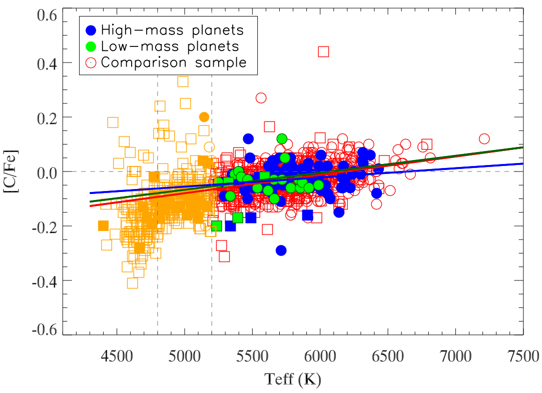

FIGURE 4.5— [C/Fe] vs. T_{eff}. Filled circles represent planet hosts and open circles, the comparison sample. Squares represent interpolated oxygen values.

This behaviour stands for stars with both low- and high-mass planetary companions. Statistics for these relations are also provided in Table 4.3.

To evaluate the significance of the correlations we performed a simple bootstrapped Monte Carlo test. For more details on the test we refer the reader to Figueira et al. (2013) and Adibekyan et al. (2014).

4.4.1 The star–planet connection

Since the discovery of the first exoplanet around a main-sequence star back in 1995 Mayor & Queloz (1995), the number of known exoplanets has increased exponentially. These discoveries have been made for a wide diversity of stars. Many studies of the hosts stars have proved that the formation of high-mass planets correlates with the metal content of the star (see Santos et al. 2001, 2004; Fischer & Valenti 2005; Sousa et al. 2011a; Mortier et al. 2013; Buchhave et al. 2012). Moreover, it has been shown that the formation of planets at low metallicities is favoured by enhanced α-elements (Adibekyan et al. 2012b,c).

In Figs. 4.7 and 4.8 we can see the relative frequency of the planetary samples compared with the comparison sample (NP).[2] In the top panel we show the [C/Fe] distributions for all the samples and find no differences

[2]Undetected low-mass planets might be present in the comparison sample

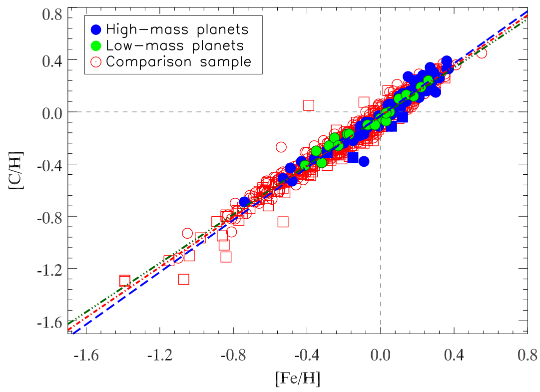

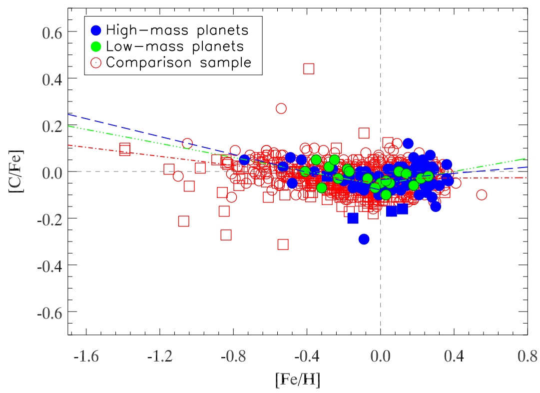

FIGURE 4.6— [C/H] and [C/Fe] vs. [Fe/H] plots. Filled circles represent planet hosts and the open circle, the comparison sample. Dotted lines represent solar values. Squares stand for interpolated oxygen values.

Table 4.2— Statistics for the comparison sample - NP, low-mass planets - LMP, high-mass planets - HMP) for [C/H] vs [Fe/H] and [C/Fe] vs $T_{\rm eff}$ and [Fe/H] (see Figs. 4.5 and 4.6).

	[C/Fe] vs $T_{\rm eff}$			
	Slope	$\rm Slope_{err}$	R	σ_R
NP	6.74E-05	7.13E-06	0.35	8.7
LMP	6.24E-05	3.95E-05	0.33	1.5
HMP	3.38E-05	2.16E-05	0.17	1.6
	[C/H] vs [Fe/H]			
	Slope	$\rm Slope_{err}$	R	σ_R
NP	0.97	8.02E-03	0.98	24.5
LMP	0.93	4.06E-2	0.98	4.6
HMP	1.00	2.90E-02	0.97	9.0
	[C/Fe] vs [Fe/H] (for [Fe/H] $<$ 0.0)			
	Slope	$\rm Slope_{err}$	R	σ_R
NP	-0.10	1.57E-02	-0.31	6.1
LMP	-0.15	8.24E-02	-0.46	1.7
HMP	-0.20	8.31E-02	-0.49	2.5
	[C/Fe] vs [Fe/H] (for [Fe/H] $>$ 0.0)			
	Slope	$\rm Slope_{err}$	R	σ_R
NP	0.00	3.46E-02	0.01	0.1
LMP	0.14	1.10E-1	0.44	1.2
HMP	0.07	7.50E-02	0.12	0.9

among them. In the middle panel, we show [C/H] distributions for the same samples. There is a slight offset between the samples, especially between the comparison and the high-mass planet sample. We can confirm that the high-mass planet offset found for [C/H] is due to the metal-rich nature of their host stars, as no carbon enhancement is found (see Fig. 4.6, bottom). We found a completely different behaviour for the low-mass planetary sample, which do not seem to be preferentially metal-rich (Sousa et al. 2008, 2011b; Ghezzi et al. 2009; Mayor et al. 2011; Buchhave et al. 2012; Buchhave & Latham 2015). In the bottom panel, we show [C/H] but

TABLE 4.3— Statistics for the three samples studied (comparison sample - NP, low-mass planets - LMP, high-mass planets - HMP) for [C/H] and [C/Fe] abundances. Also, [C/H] abundances for those stars considered as solar analogues ($T_{eff} = T_{eff,\odot} \pm 300$ K) are provided.

	[C/Fe]				
	Mean	SD	Median	Minimum	Maximum
NP	-0.03	0.06	-0.02	-0.31	0.44
LMP	-0.03	0.04	-0.03	-0.11	0.05
HMP	-0.03	0.06	-0.02	-0.29	0.12
	[C/H]				
	Mean	SD	Median	Minimum	Maximum
NP	-0.17	0.29	-0.14	-1.30	0.45
LMP	-0.13	0.21	-0.17	-0.62	0.24
HMP	0.03	0.23	0.10	-0.69	0.39
	$[C/H]_{analogs}$				
	Mean	SD	Median	Minimum	Maximum
NP	-0.03	0.06	-0.02	-0.31	0.44
LMP	-0.03	0.04	-0.03	-0.11	0.05
HMP	-0.03	0.06	-0.02	-0.29	0.12

for solar analogue (stars with $T_{eff} = T_{eff,\odot} \pm 300$ K, but not necessarily solar gravity or metallicity). Statistics for these results are provided in Table 4.3.

To see if there is any resemblance between each sub-sample of planet host with the non-planet host sample we performed a Kuiper test (also known as invariant Kolmogorov–Smirnov (K–S) test), instead of the usual K–S test. Although K–S is suitable in our case, its sensitivity is higher around the median value, neglecting the tails. The Kuiper test compares two cumulative distribution functions and obtains the sum of the maximum distances above and below $S_N(x)$, where $S_N(x)$ is the cumulative distribution function of the probability distribution from which a dataset with N events is drawn. In our study, a zero value of the K–S test refers to datasets with no similarities among them. Unity refers to the maximum similarity that can be found for the compared datasets (Press et al. 1992; Kirkman, T.W. 1996).

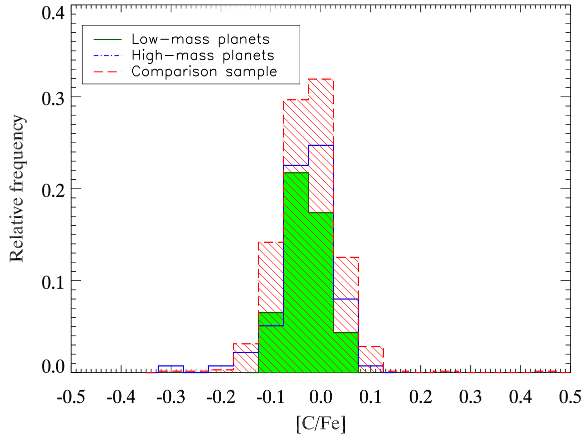

FIGURE 4.7— [C/Fe] distributions of three different samples: stars without planets (NP, in red), low-mass planets (LMP, in green), and high-mass planets (HMP, in blue).

In Fig. 4.9 we can see the cumulative fraction for both [C/H] and [C/Fe] for the three cases: stars with high-mass planets (HMP: blue, dashed dotted line), stars with low-mass planets (LMP: green, dashed line), and the comparison sample (NP: red, full line). In the top panel, we can see how all samples behave in a similar way. If we apply a Kuiper test to these samples, as shown in Table 4.4, we can see that all the samples share similarities: when taking [C/Fe] into account, the high-mass planetary sample behaves like the non-planet hosts and low-mass samples, as there is a probability of similarity between them. The planetary samples, however, separate from each other in [C/H]. Whereas the small-planet sample is more in agreement with the non-planet host sample, the high-mass planet sample detaches itself completely from this behaviour. These results are consistent with the results represented in Figs. 4.7 and 4.8.

We looked deeper into the relation between [C/Fe] and the mass of the planet, as shown in the top panel of Fig. 4.10. The masses of the planets range between 0.0097 and 47 $M_{\rm J}$[3], but most stars have planets with less than 1 $M_{\rm J}$ orbiting around them. To remove this bias due to

[3]Only one star has a companion of 47 $M_{\rm J}$, which can be considered a brown dwarf, according to the standard definition of brown dwarf.

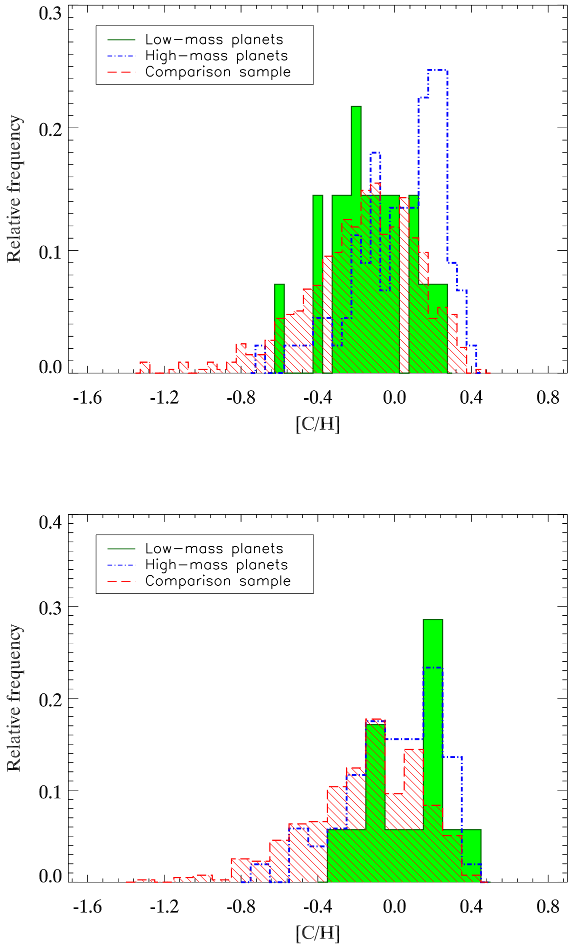

FIGURE 4.8— Top panel: [C/H] distributions of three different samples: stars without planets (NP, in red), low-mass planets (LMP, in green), and high-mass planets (HMP, in blue). Bottom panel: [C/H] distributions for the same three groups, but considering only solar analogues ($T_{eff} = T_{eff,\odot} \pm 300$ K)

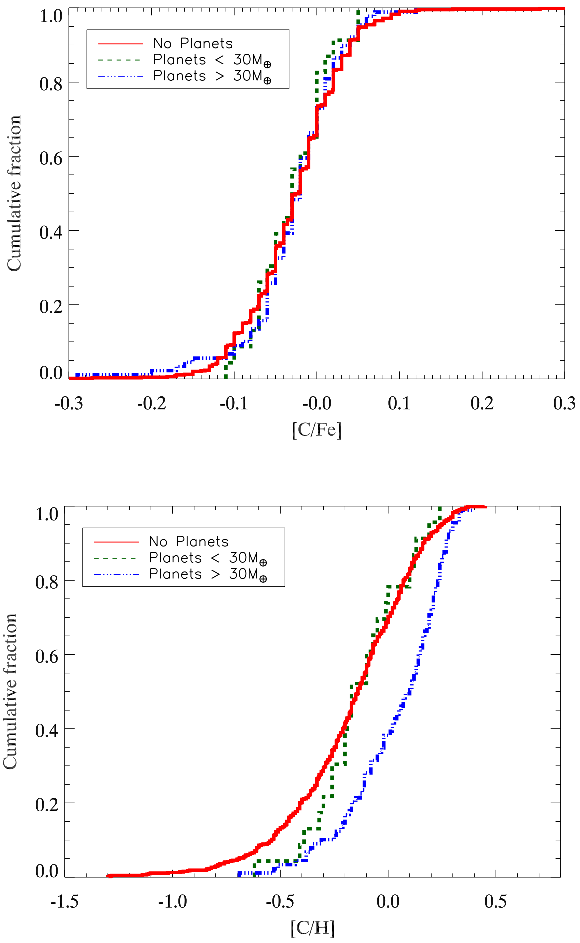

FIGURE 4.9— Top: Cumulative functions for the three different samples (LMP, HMP, and NP) for [C/H] abundances. Bottom: Cumulative functions for the three different samples (LMP, HMP, and NP) for [C/Fe] abundances.

TABLE 4.4— Kuiper test for the sample. We tested the relation between the low-mass planets (LMP) sample, the high-mass planets sample (HMP) and the comparison sample (NP) sample, for both [C/Fe] and [C/H]. Zero represents no similarity between the samples while unity represents the maximum similarity.

Sample	[C/Fe]	[C/H]
LMP - NP	0.54	0.72
HMP - NP	0.65	2.19e-08
LMP - HMP	0.85	3.78-03

the lack of planets with higher masses, we created bins with increasing steps, with bin sizes of 0.03, 0.07, 0.2, 0.3, 0.4, 2.0, 3.0, 5.0, 10.0, and 27.0 $M_{\rm J}$. Error bars indicate the standard deviation of each bin. We can see how the [C/Fe] ratio shows a flat tendency for all masses because the deviation is negligible. We tested a possible relation between [C/Fe] and the planetary mass and obtained a covariance $s_{x,y} = 0.001$, where $x = M_{\rm J}$ and $y =$ [C/Fe]. In Fig. 4.10 bottom, we reduce the sample to solar analogues. In our case, we considered as solar analogues those stars with $T_{\rm eff} = T_{\rm eff,\odot} \pm 300$ K. We obtained a covariance $s_{x,y} = 0.003$.

4.5 Kinematics properties and stellar populations

To study the kinematic properties of the sample stars and the stellar populations they belong to, we took the classification obtained by Adibekyan et al. (2012b), who applied both purely chemical (e.g. Adibekyan et al. 2011, 2013; Recio-Blanco et al. 2014) and kinematic approaches (e.g. Bensby et al. 2003; Reddy et al. 2006) to classify their stars. The Galactic space velocity components of the stars were calculated in Adibekyan et al. (2012b) using the astrometric [4] and radial velocity data of the stars. The average errors in the U, V, and W velocities are about 2–3 km s^{-1}. The main source of the parallaxes and proper motions was the updated version of the Hipparcos catalog (van Leeuwen 2007). Data for eight stars with unavailable Hipparcos information were taken from the TYCHO Reference Catalog (Hog et al. 1998).

The separation of the Galactic stellar components based only on stellar

[4]The SIMBAD Astronomical Database (http://simbad.u-strasbg.fr/simbad/) was used (Wenger et al. 2000).

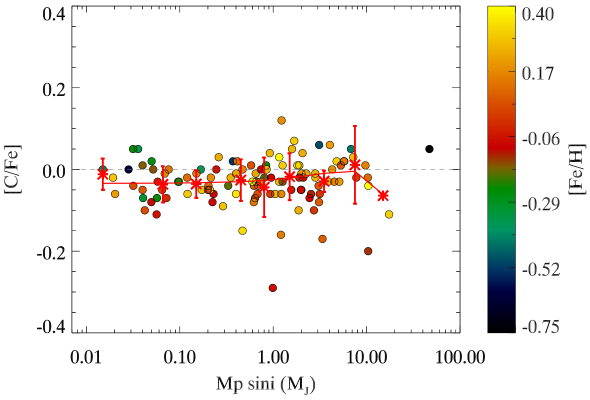

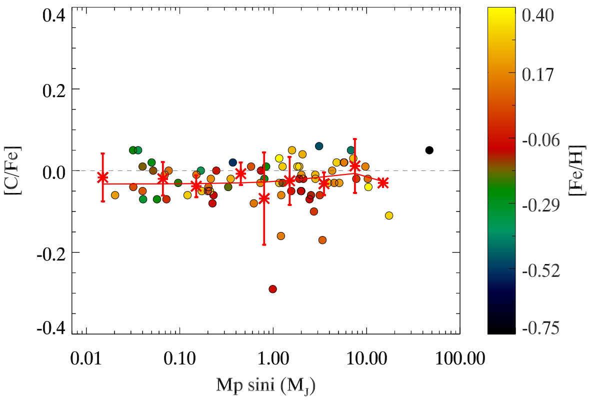

FIGURE 4.10— [C/Fe] versus $M_{\rm p} sini$ plot. Filled circles represent the whole sample, whereas red asterisks represent binned values. Hotter colours represent metallicities above solar while cooler colours represent metallicies below solar. Also in red, the fit for these binned values. In the top panel, for all the studied sample, in the bottom, for solar analogues ($T_{\rm eff} = T_{\rm eff,\odot} \pm 300$ K)

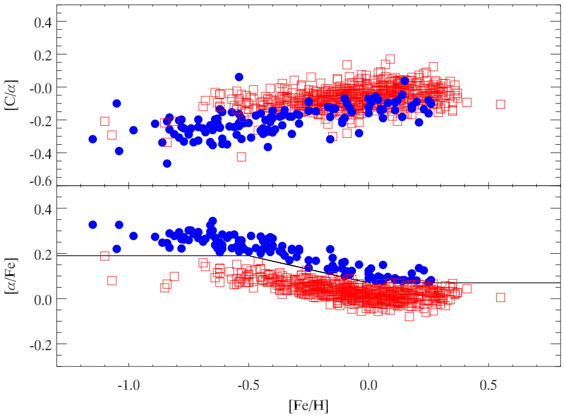

FIGURE 4.11— [C/α] and [α/Fe] vs. [Fe/H]] and [α/Fe] vs. [Fe/H]. Stars that are enhanced in α-elements are shown as blue squares and non-α-enhanced stars are represented by red squares.

abundances is probably superior to that based on kinematics alone (e.g. Navarro et al. 2011; Adibekyan et al. 2011) because chemistry is a relatively more stable property of sun-like stars than their spatial positions and kinematics. We used the position of the stars in the [α/Fe]–[Fe/H] plane (here α refers to the average abundance of Si, Mg, Ti) to separate the thin- and thick-disc stellar components. We recall that Ca was not included in the α index, because at super-solar metallicities the [Ca/Fe] trend differs from that of other α-elements Adibekyan et al. (2012b). We adopt the boundary (separation line) between the stellar populations from Adibekyan et al. (2011). According to our separation, 640 stars ($\approx$85 per cent) are not enhanced in α-elements and belong to the thin-disc population. The [α/Fe] versus [Fe/H] plot for the sample stars is shown in the bottom panel of Figure 4.11.

At the top panel of Fig. 4.11 we show the dependence of [C/α] on the metallicity. This trend is expected if the C abundance scales with the iron abundance, as was suggested above. It is interesting to note that at super-solar metallicities, [C/α] remains almost constant for both samples.

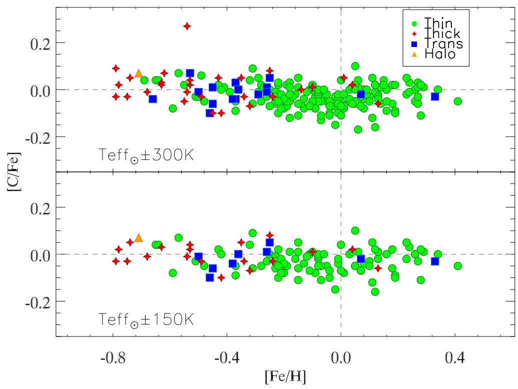

FIGURE 4.12— [C/Fe] versus [Fe/H] for solar analogues with S/N $\geq$ 200. Filled green dots refer to to the thin-disc population, filled blue squares to transition objects, orange triangles to halo stars, and red stars to thick-disc stars.

In Fig. 4.12 we present [C/Fe] against [Fe/H] for the sample of solar analogues. The selected stars have $T_{eff} = T_{eff,\odot} \pm 300$ K in the top panel and $T_{eff} = T_{eff,\odot} \pm 150$ K in the bottom panel. These solar analogues also have S/N > 200 to ensure optimal accuracy in our conclusions.

Figure 4.12 shows that, opposite to the chemical separation (using Ti, Mg, and Si for the α abundances), the thin and thick discs are not chemically different for C. In Adibekyan et al. (2012b), it was suggested that several α-elements show different trends with metallicity.

4.6 Summary and conclusions

We present carbon abundances for 1110 solar-type stars observed with HARPS. In our sample, 143 of the 1110 are planet-hosts and 967 stars have no known planetary companion. All the targets have been studied using spectral synthesis of the CH band at 4300Å. All the stars within our sample have effective temperatures between 4400 K and 7212 K, metallicities from −1.39 to 0.55 dex, and surface gravities from 3.59 to 4.96 dex.

We have performed a detailed spectral analysis of this sample to obtain precise carbon abundances and investigate possible differences between stars with planets and the comparison sample. We confirm that both samples, planet host stars and comparison stars, show no different behaviour when we study their carbon abundances as a function of different stellar parameters such as T_{eff} and [Fe/H].

We have compared our results with similar work Delgado Mena et al. (2012), as seen in Fig 4.4. When comparing stars common to both works, we get agreement between the atomic and the molecular results, thus ensuring that molecular abundances from the CH 4300Å band can be a reliable alternative to atomic values.

We searched for a correlation between the presence of planets and carbon abundances. We found that both planet-hosts and non-planet-hosts usually have [C/Fe] $\leq$ 0.0 ($\sim$65% of the sample). We searched for a correlation between the carbon abundance and the planetary masses but found a flat trend for all the masses.

We looked for similarities between the three samples studied: the non-planet host samples and the low- and high-mass planetary sample. We found that both low- and high-mass planet hosts are not different from the comparison sample. No sample shows signs of carbon enhancement.

We performed a chemical and kinematic separation for our sample and obtained a clear separation between the thin and the thick disc populations based on a dependence of [C/α] with metallicity. However, no differences in carbon abundances can be found for the different stellar populations.

We conclude that the molecular CH band located at 4300Å can be used to obtain reliable and accurate carbon abundances and therefore provide an accurate measurement of C/O ratios that can be used to investigate the mineralogy of exoplanets (Suárez-Andrés et al. 2016, in prep).

5

C/O vs Mg/Si ratios in solar type stars: The HARPS sample

This chapter is based on Suárez-Andrés et al. (2017), A&A, submitted

ABSTRACT – We present a detailed study of the Mg/Si and C/O ratios and their importance in determining the mineralogy of planetary companions. Using 499 solar-like stars from the HARPS sample, we determine these ratios and study the nature of the possible planets formed. We find a diversity of mineralogical ratios that reveal the different kinds of planetary systems that can be formed, most of them dissimilar to our solar system. The different values of the Mg/Si and C/O ratios can determine different composition of planets formed.

THE determination of the chemical composition of extrasolar planets has been the subject of numerous studies in recent years. One of the keystones has been the fact that stars hosting giant planets are considered to be metal-rich when compared with single stars (Gonzalez 1997; Santos et al. 2001, 2004; Fischer & Valenti 2005; Gonzalez 2006). Stars hosting low mass planets (with masses below 30 $M_{\oplus}$) do not seem to be preferentially metal-rich (e.g. Sousa et al. 2008, 2011a)

Recent studies of chemical abundances in stars with and without planets have shown no important differences in [X/Fe] versus [Fe/H] trends between both groups of stars for refractory (González Hernández et al. 2010; Delgado Mena et al. 2012) and volatile elements (Suárez-Andrés et al. 2016; Suárez-Andrés et al. 2017). On the other hand, studies by Haywood (2008, 2009) and Adibekyan et al. (2012a) found evidence of α-elements enhancement in stars with planets.

As both planetesimals and planets are formed within the same enviroment, their composition is expected to be the same as that of their host star. This assumption might be true for refractory species, but not for the volatile ones (Lodders 2003; Thiabaud et al. 2014). Although this fact does not affect the Mg/Si ratio for rocky planets, it can affect the C/O ratio (Dorn et al. 2015; Thiabaud et al. 2015b)

Variations in C/O ratios can also be found among planetary atmospheres and host stars (Madhusudhan et al. 2012; Konopacky et al. 2013; Moses et al. 2013; Brewer et al. 2016b) and among planets in the same planetary system. This is due to different parameters (temperature, pressure, etc.) and processes at work during the planet formation stage, including possible migrations of planets from their birthplace (Öberg et al. 2011; Ali-Dib et al. 2014; Madhusudhan et al. 2012; Thiabaud et al. 2015a,b; Brewer et al. 2016b)

In the last few years, several studies have tried to understand the formation and evolution of planets using theoretical models. Bond et al. (2010a,b), Carter-Bond et al. (2012) studied planet formation scenarios with different initial composition, but they didn't do a detailed study of the output volatile species. Elser et al. (2012) tried to study this planet formation model by adding the formation of solids, but they were unable to reproduce some features present in the solar system, such as high Fe on Mercury.

Recently, Thiabaud et al. (2014); Marboeuf et al. (2014) made a complete study, presenting models not only for refractory species, but for volatiles as well. Thiabaud et al. (2015a) presented a complete study, taking into account the accretion of several compounds omitted in previous works such as He, H_2, H_2O, CO, CO_2, CH_3OH, CH_4, NH_3, N_2, and H_2S. Also, they computed the importance of volatile elements in protoplanetary discs and their implications in planetary formation (Thiabaud et al. 2015b). Their models show that the condensation of volatile species as a function of radial distance allows for C/O enrichment in specific parts of the protoplanetary disc of up to four times the solar value. This could lead to the formation of planets that can be enriched in C/O in their envelope up to three times the solar value. Their models are consistent with recent observations of hot-Jupiter atmospheres (Brewer et al. 2016b).

The amount of carbides and silicates formed in planets is controlled by the C/O ratio (e.g. Bond et al. 2010a)

- if C/O < 0.8: Si will form solid SiO_4^{4-} and SiO_2, serving as seeds for Mg silicates for which the exact composition will be determined by the Mg/Si ratio.

- if C/O $>$ 0.8: Si will be solid as SiC. Also, graphite and TiC will be formed.

Silicates are an important ingredient in the formation of rocky planets, as they are the most abundant compounds in the mantle and crust of these planets (Morgan & Anders 1980). Silicate distribution is ruled by the Mg/Si ratio of the planet host star. Concerning the Mg/Si ratio, the principal components could be, as proposed by Bond et al. (2010b):

- if Mg/Si $<$ 1, Mg forms orthopyroxene ($MgSiO_3$) and the remaining Si forms other minerals, such as feldspar ($CaAl_2Si_2O_8$, $NaAlSiO_8$) or olivine(Mg_2SiO_4)
- if 1 $<$ Mg/Si $<$ 2, Mg is distributed equally between pyroxene and olivine.
- if Mg/Si $>$ 2, Si forms olivine and the remaining Mg forms other oxides like MgO.

Testing and improving planetary formation models is key in to future studies of habitability, as these ratios are essential elements in defining the structure of the planet.

In this chapter we present a study of C/O and Mg/Si ratios in solar-type stars and their implications for possible terrestrial planetary formation.

5.1 Sample description

The high-resolution spectra analysed in this chapter were obtained with the HARPS spectrograph at La Silla Observatory(ESO, Chile) during the HARPS GTO programme (see Mayor et al. 2003; Lo Curto et al. 2010; Santos et al. 2011, for more information about the program.). The spectra have been already used previously in the analysis of stellar parameters, as well as the derivation of precise chemical abundances (see e.g. Sousa et al. 2008, 2011a,b; Adibekyan et al. 2012b; Tsantaki et al. 2013; Bertran de Lis et al. 2015; Suárez-Andrés et al. 2017).

The studied sample is part of the 1111 stars sample presented by Adibekyan et al. (2012b) for which the abundance of volatiles were measured (Bertran de Lis et al. 2015; Suárez-Andrés et al. 2017). We limited our metallicity sample for stars with [Fe/H] $>$ -0.6, which is the lower

[Fe/H] for the planet hosts sample. 499 FGK solar-type stars were studied, with effective temperatures between 5250 K and 6666 K, metallicities from −0.59 to 0.55 dex, and surface gravities from 3.81 to 4.82 dex.

Of 499 stars, 99 are planet hosts[1], whereas the other 400 are single stars (stars with no known planetary companion, also known as comparison stars).

5.2 Chemical abundances

To obtain the carbon-to-oxygen (C/O) and magnesium-to-silicon (Mg/Si) elemental ratios we used chemical abundances from Adibekyan et al. (2012b); Bertran de Lis et al. (2015) and Suárez-Andrés et al. (2017) for Mg and Si, O, and C, respectively. All these chemical abundances were obtained using the same high-resolution high-quality HARPS spectra and the same stellar parameters, allowing us to obtain precise elemental ratios. For carbon we used the CH molecular band located at 4300 Å (see Suárez-Andrés et al. 2017), whereas for the rest of the elements atomic features were used. Recent studies on molecular CH features (Suárez-Andrés et al. 2017) have demostrated that they are as reliable as atomic ones, and provide consistent results. Adopted solar abundances for all elements are $\log \epsilon(\mathrm{C})_\odot = 8.50$ dex (Caffau et al. 2010), $\log \epsilon(\mathrm{O})_\odot = 8.71$ (Caffau et al. 2008) and $\log \epsilon(\mathrm{Mg})_\odot = 7.58$ dex and $\log \epsilon(\mathrm{Si})_\odot = 7.55$ from (Anders & Grevesse 1989).

5.3 [C/O] and Galactic chemical evolution

[C/O] and [Mg/Si] ratios can help us to understand how the planets are formed. In order to study the effects of Galactic Chemical Evolution (GCE) (and how this can help to understand the formation of planets) we will first study the solar ratios [C/O] and [Mg/Si]. As presented in Adibekyan et al. (2015a) for a sample of 589 stars, the results inferred about planetary companions from [Mg/Si] are affected by GCE. They suggest a dependence of the planetary structure on GCE (i.e., low-mass planets that were formed at different times and places in the Galaxy may tend to have different structures and evolutions).

To test for possible relations between [C/O] ratio and the masses of planetary companions, we separated the planet population into two groups: low-mass planets (LMP; with masses less than or equal to 30

[1] Data from www.exoplanet.eu and the SWEET-CAT catalog (www.astro.up.pt/resources/sweet-cat/)

$M_\oplus$) and high-mass planets (HMP; with masses greater than 30 $M_\oplus$). In those stars which host several planets, the most massive planet was considered in our study. Our sample consist of 19 low-mass and 80 high-mass planet hosts. We obtained [C/O] ratios to study if GCE also plays a role in planetary formation. In Fig. 5.1 we show the dependence of [C/O] on the metallicity for stars with and without detected planets. To remove the trend of [C/O] with GCE we fitted all our data points (all stars with and without detected planets) with a quadratic dependence on metallicity and then subtracted the fit. Mean squared deviation for the fit is 0.06.[2] $[C/O]_{corr}$ represents the [C/O] after substracting this GCE trend. [C/O] distributions for all the presented sub-samples are shown in Fig.

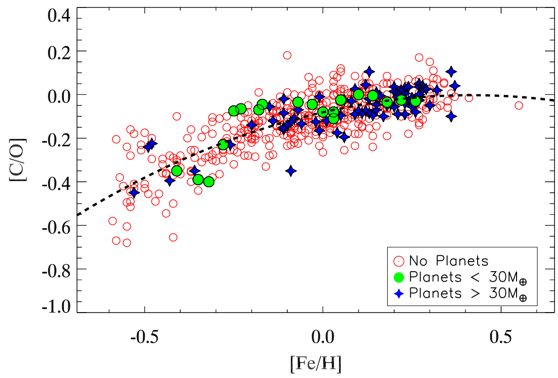

FIGURE 5.1— [C/O] as a function of [Fe/H] for stars with and without detected companions. Trend line provides a linear fit to all the data points.

5.2. A slight difference can be found between the centres of each gaussian fitting, but they are within a 0.07 difference (see Table 5.1). To obtain a clearer picture, we tested the sample using a two Kolmogorov-Smirnov (K–S) test (see Table 5.2 and Fig. 5.3). By comparing the obtained results for [C/O] and for $[C/O]_{corr}$, we found that the difference between the low-mass sample and the single stars dissapears. The low-mass sample shows a significant similarity with the comparison one, as the high-mass sample did with for [Mg/Si] (see Adibekyan et al. 2017). Although the

[2] $[C/O]=-0.45*[Fe/H]^2+0.38*[Fe/H]-0.08$

TABLE 5.1— Statistics for the fitted histograms presented in Figures 5.2, 5.5 and 5.9. The low-mass planets (LMP) and the high-mass planets sample (HMP)

	Sample	Center-fit	FWHM
C/O	Single stars	0.45	0.29
	Planets: LMP	0.52	0.10
	Planets: HMP	0.52	0.21
Mg/Si	Single stars	1.11	0.24
	Planets: LMP	1.07	0.26
	Planets: HMP	1.12	0.16
$[C/O]_{corr}$	Single stars	-0.11	0.25
	Planets: LMP	-0.01	0.11
	Planets: HMP	-0.03	0.17

TABLE 5.2— K–S test for GCE and non-GCE corrected samples. Zero represents no similarity between the samples, and unity represents the maximum similarity.

Sample	[C/O]	$[C/O]_{corr}$
LMP - NP	0.07	0.17
HMP - NP	4.09E-05	0.38

similarity seems to increase for the high-mass sample, it is still too low. This result confirms that both [Mg/Si] and [C/O] ratios are affected by stellar metallicity. Also, that the [C/O] ratio might play an important role in the formation of giant planets, as the [Mg/Si] ratio does for the small ones.

5.4 Elemental ratios

Theoretical studies suggest that C/O and Mg/Si are very important in determining the mineralogy of terrestrial planets.

Elemental ratios were calculated using the following equation:

$$A/B = N_A/N_B = 10^{log\epsilon(A)}/10^{log\epsilon(B)} \tag{5.1}$$

where $\log\epsilon(A)$ and $\log\epsilon(B)$ are absolute abundances. Errors were estimated by evaluating an increase or decrease in the $log\epsilon(A) - log\epsilon(B)$ abundance ratio, due to the relative errors (For more details, see Delgado Mena et al. 2012). Average errors are represented in all figures.

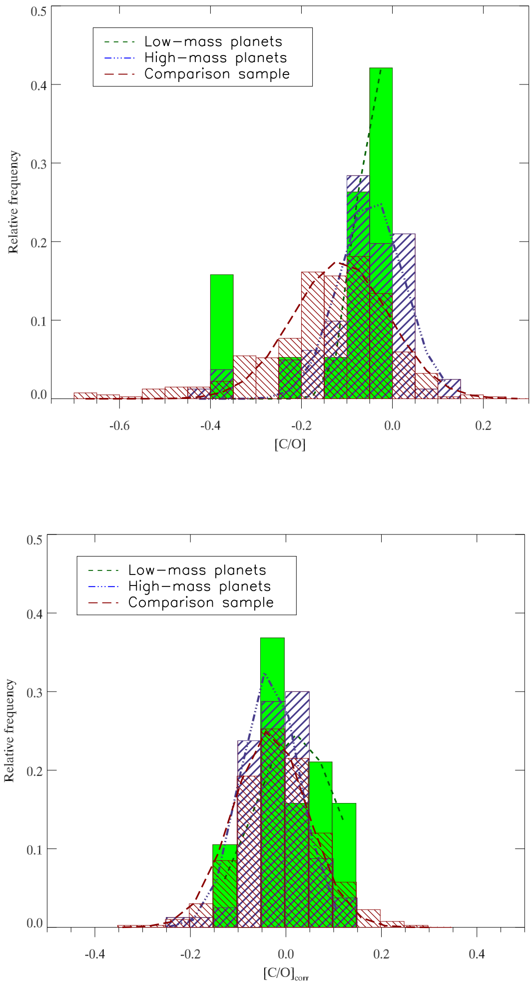

FIGURE 5.2— [C/O] distributions before (upper panel) and after (lower panel) correcting for the Galactic chemical evolution (GCE) effects.

5.4.1 C/O

The carbon-to-oxygen ratio (C/O) in planet-host stars can provide key in-

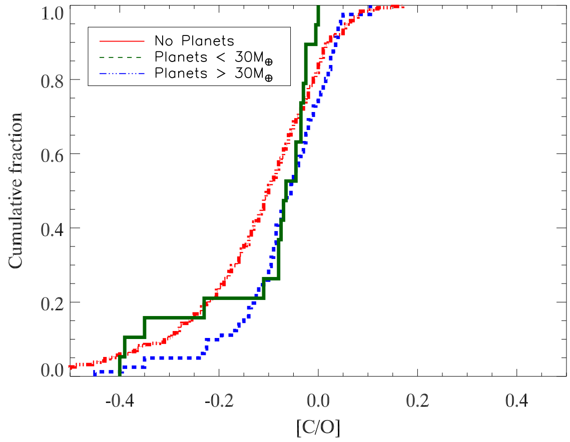

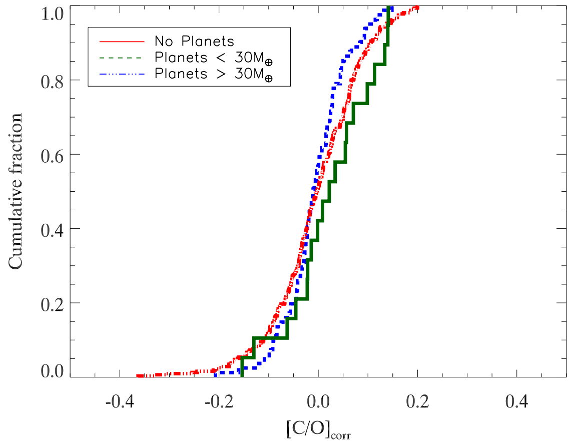

FIGURE 5.3— Cumulative distributions for [C/O], before (upper panel) and after (lower panel) the GCE correction.

formation about the protoplanetary disc in which the planet was formed. The dependence on the distance for volatile elements will affect the C/O ratios expected in exoplanetary atmospheres, as volatiles are heavily affected by different distances (or different ice line positions) during the early lifetime of the nebula while planets accrete (Öberg et al. 2011; Ali-Dib et al. 2014; Brewer et al. 2016b). Since mineralogy of planets is commonly studied in terms of absolute ratios, we will use them instead of solar ones.

Figure 5.4 shows the C/O ratios derived in this paper as a function of [Fe/H] for these samples, stars with and without planets. We obtain a linear fit for both samples, with very little differences between them. We can see a dependence of C/O on metallicity, in agreement with other works, such as Nissen et al. (2014), Teske et al. (2014) and Brewer & Fischer (2016).

To test for possible relations between C/O and Mg/Si ratios and the masses of planetary companions, we separated the planet population into two groups: low-mass planets and high-mass planets. If we take a closer look at the C/O distribution for the studied samples in Fig. 5.5, we can see that they exhibit almost the same behaviour, with an small offset of 0.05 dex. In our sample, 100% of stars with planets have C/O values lower than 0.8. These results are in contrast with the work by Delgado Mena et al. (2012) on part of this sample due to a most precise derivation of oxygen abundances (which were underestimated in some cases, leading to very high C/O ratios). Also, the use of the 6158Å unblended oxygen line improves the results when compared to those that used the 6300Å one.

We can see in Fig. 5.5 the C/O distributions for single stars and both planetary samples. Both low and high-mass planets cover a wide range of C/O centred at C/O$\sim$0.5 (see detailed statistics in Table 5.1). A cumulative histogram (Fig. 5.6) shows us that each sample behaves in a different way.

We performed a K–S test to confirm these behaviours. A low similarity can be found among the low-mass planets sample and the single one (only 5%), whereas no significant similarity can be found among the high-mass sample and the comparison one.

Several authors have studied the C/O ratios in stars with planets (e.g. Delgado Mena et al. 2012; Petigura & Marcy 2011; Nissen 2013; Nissen et al. 2014; Teske et al. 2014). In Fig. 5.7 we can see our results compared with the work of Nissen et al. (2014), Teske et al. (2014), and González Hernández et al. (2013). To make this comparison possible, we scaled carbon and oxygen abundances presented by these authors to our reference values (log$N_\odot$(O) = 8.71 and log$N_\odot$(C) = 8.50). We can see a good fit at all metallicities.

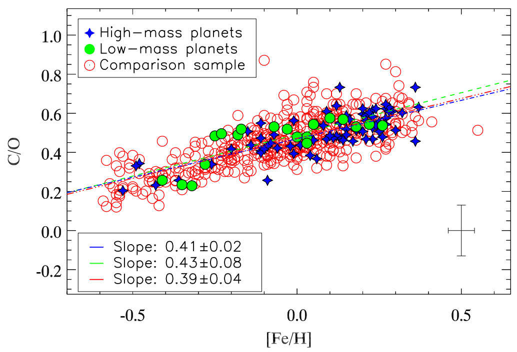

FIGURE 5.4— C/O versus [Fe/H]. Red open circles refer to single stars while green dots refer to low-mass planet host stars and blue diamonds to high-mass planet-hosts.

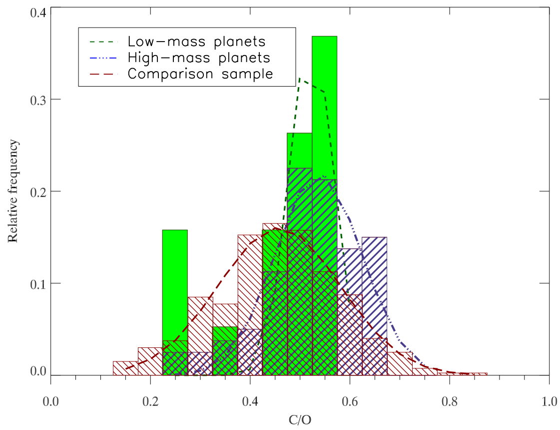

FIGURE 5.5— C/O distributions for stars harbouring low-mass (green) and high-mass (blue) planets. Stars without planets are shown in red.

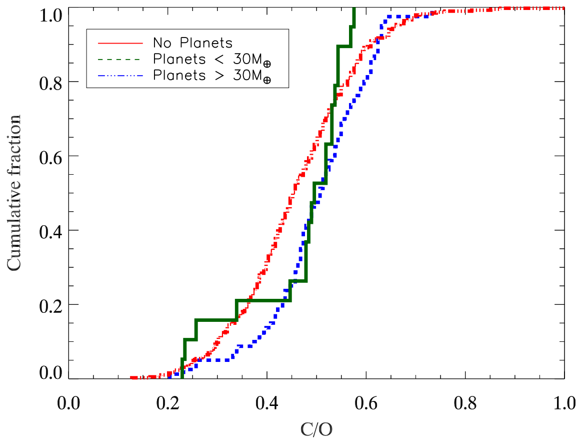

FIGURE 5.6— Cumulative C/O distributions for single stars (red) and stars with planets(low-mass in green and high-mass planets in blue)

TABLE 5.3— K–S test for all the samples. Zero represents no similarity between the samples, and unity represents the maximum similarity.

Sample	C/O	Mg/Si
LMP - NP	0.052	0.018
HMP - NP	3.237E-04	0.004

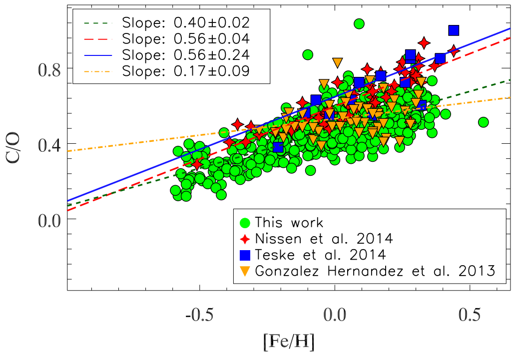

FIGURE 5.7— Comparative C/O versus [Fe/H]. In red stars, data from Nissen et al. (2014); in green circles, stars from this study; in blue squares, data from Teske et al. (2014), and in orange triangles, data from González Hernández et al. (2013).

5.4.2 Mg/Si

The magnesium and silicon elemental ratio, Mg/Si, controls the exact composition of silicates (Dorn et al. 2015) that can be found in the planetary companion, as this ratio, along with Fe/Si, does not depend so strongly on the distance to the star as the C/O ratio does (Thiabaud et al. 2015a,b).

In Fig. 5.8 top panel we show Mg/Si ratios as a function of metallicity. As expected, the Mg/Si ratio decreases with [Fe/H]. We also find a relation between Mg/Si ratios and T_{eff}, as shown in Fig. 5.8 bottom panel. We have estimated the slopes of the Mg/Si ratios as a function of effective temperature for T_{eff} greater than 6100K. There seems to be a different behaviour and the slopes of these trends for these two T_{eff} ranges (see Table 5.4). NLTE effects are the most plausible explanation for this behaviour Zhao & Gehren (2000a,b), as mentioned by Adibekyan et al. (2017). We will study, from now on, only the sample with $T_{eff} < 6100$K.

Mg/Si distributions for both planet-host stars and the comparison sample are shown in Figure 5.9. We can see that all samples exhibit the same behaviour. All samples are concentrated around Mg/Si$\sim$1.07, our solar reference. Statistics for these histograms are shown in Table 5.1. The

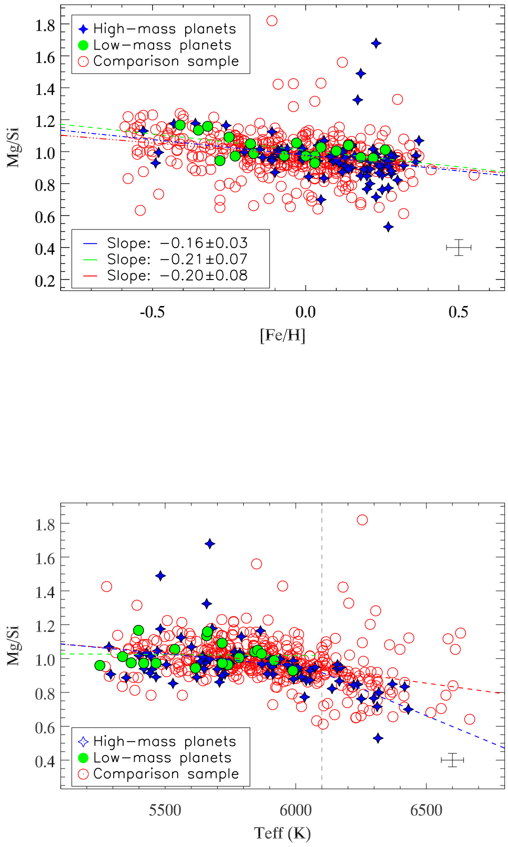

FIGURE 5.8— Mg/Si ratios as a function of [Fe/H] (top panel) and T_{eff} (bottom panel). Red open circles refer to single stars while green dots refer to low-mass planet host stars and blue diamonds to high-mass planet-hosts.

TABLE 5.4— Statistics for the three groups studied (Comparison sample, low-mass planets and high-mass planets) for Mg/Si vs T_{eff} (see Fig. 5.8, bottom panel).

	Mg/Si vs. T_{eff} (for T_{eff} < 6100)	
	Slope	$Slope_{err}$
NP	-1.39E-04	0.32E-04
LMP	-1.21E-05	8.98E-05
HMP	-1.63E-04	0.90E-04
	Mg/Si vs T_{eff} (for T_{eff} > 6100)	
	Slope	$Slope_{err}$
NP	-2.37E-04	2.54E-04
LMP	-	-
HMP	-7.17E04	2.97E-04

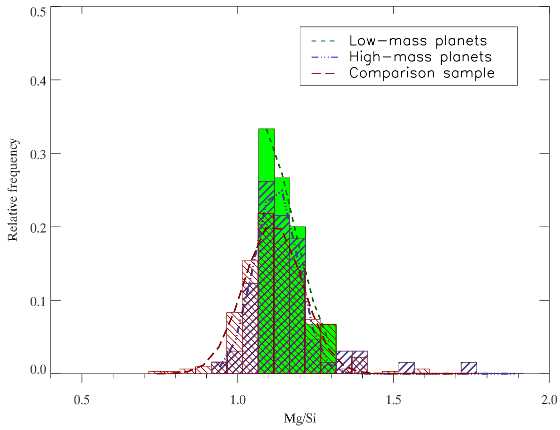

FIGURE 5.9— Mg/Si distributions for stars harbouring low-mass (green) and high-mass (blue) planets. Stars without planets are shown in red.

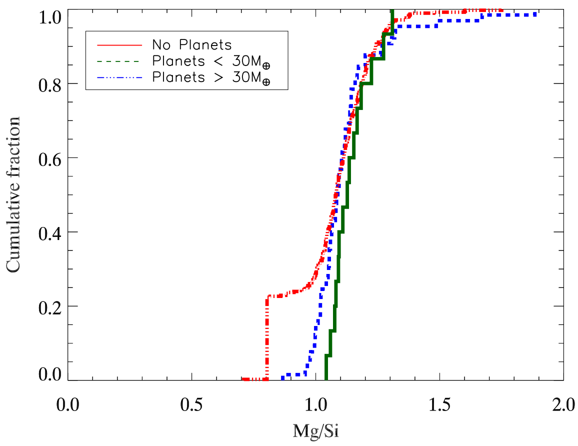

FIGURE 5.10— Cumulative Mg/Si distributions for single stars (red) and stars with planets (low-mass (green) and high-mass planets (blue)).

high-mass sample has a broader distribution than the low-mass one, but the limited number of the last does not allow us to inferred any different result than the similarity between the samples. A similar result can be found in Brewer et al. (2016b). In our sample 100% of the low-mass sample have an Mg/Si value of between 1.0 and 2.0 while 85% of the high-mass sample exhibit this behaviour. We also find that none of the low-mass planet hosts have Mg/Si values below 1.0, but 15% of the high-mass sample does. No stars with Mg/Si values greater than 2.0 were found.

A cumulative histogram (Fig. 5.10) shows the behaviour of each sample. We performed a K–S test to confirm the different kinds of behaviour in the samples. If zero indicates no similarity and the unity the maximum similarity, we can see in Table 5.3 that no significant similarities can be found between the samples. These results agree with those obtained by Adibekyan et al. (2015a).

5.5 C/O vs Mg/Si ratios: Implications on planet formation

We studied C/O ratios as a function of the Mg/Si ratios as a way to study the possible scenario for the formation of planets. In Fig. 5.11 we can see how stars with and without planets are distributed in a C/O against Mg/Si plot. As can be seen, stars with planets, both low-mass and high-mass, are concentrated at C/O values of 0.5-0.6 and Mg/Si values of $\sim$ 1.1. The solar values of $C/O_{\odot} = 0.61$ and $Mg/Si_{\odot} = 1.07$, derived from the adopted solar values for oxygen, carbon, magnesium, and silicon, are also represented.

As presented in Section 5.4, 100% of the sample with low-mass companions have an Mg/Si value of between 1.0 and 2.0, while 85% of the high-mass companion sample does, which means that Mg is equally distributed between pyroxene and olivine. We also find 15% of high-mass planet hosts with Mg/Si values below 1.0, so Mg will be found in only orthopyroxene form, whereas Si will take several forms, such as feldspars or olivine. No stars with Mg/Si values greater than 2.0 were found. As it can be seen, the high-mass planetary sample can be found preferably with lower Mg/Si ratios. We highlight the fact that stars with low-mass companions present Mg/Si > 1.

Regarding C/O, 100% of stars with planets have C/O values lower than 0.8, meaning that Si will take solid form as SiO_4^{4-} and SiO_2. Only 12% of our sample has C/O > 0.4 (8 stars). The exact composition will be ruled by the Mg/Si ratio.

Recent models by Carter-Bond et al. (2012); Marboeuf et al. (2014); Thiabaud et al. (2014, 2015a) and Thiabaud et al. (2015b) suggest that elemental ratios may suffer great variations when studied in planet host stars and in planetary atmospheres. They suggest that migration plays a key role when forming elemental ratios in planetary atmospheres and the location of planet formation, as the total C/O ratios are governed by ices. Öberg et al. (2011) studied the influence of different snowlines of oxygen and carbon-rich species. They suggest a common region between the H_2O and CO snowlines with giant planetary formation. These snowlines and the migration from the original birthplace can affect the abundance of volatiles, but not the abundance of refractory elements, such as Mg, Si, and Fe. Thiabaud et al. (2015b) proposed that elemental ratios such as Mg/Si and Fe/Si would show similar values in both planet hosts and planetary atmospheres. As for the C/O ratio, they proposed large differences between the star and the planets (see Öberg et al. 2011). This

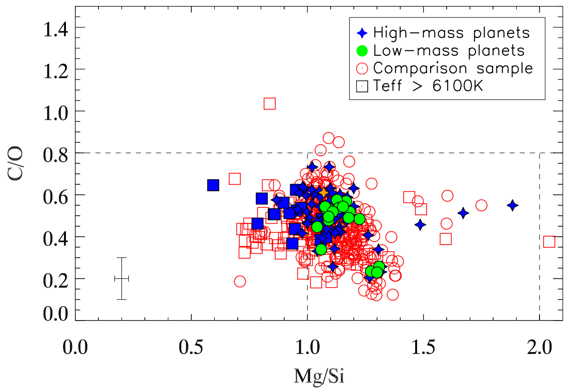

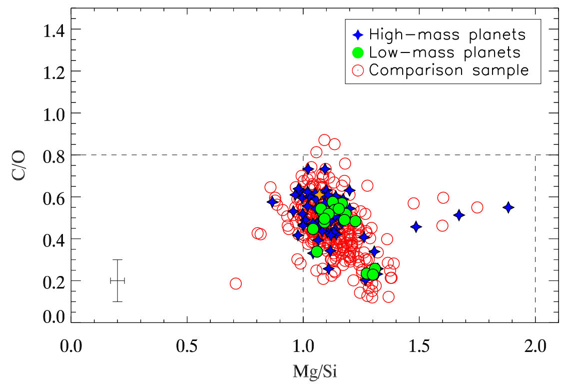

FIGURE 5.11— Top panel: C/O vs. Mg/Si. The red circles refer to single stars (400 stars), and green dots refer to stars harbouring planets (99 stars). Bottom panel: the same as the top panel but only for stars with T_{eff} < 6100K (312 single stars, 19 low-mass planet hosts and 65 high-mass planet hosts). An orange star represents solar values.

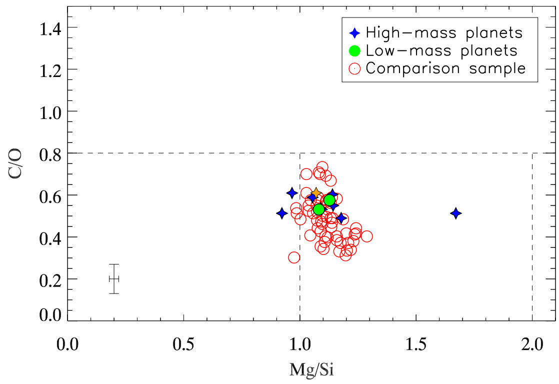

FIGURE 5.12— C/O vs. Mg/Si for solar analogues, with $T_{\rm eff} = T_{\rm eff,\odot} \pm 300$ K, logg = logg$_\odot$ $\pm$ 0.2 dex and [Fe/H] = [Fe/H]$_\odot$ $\pm$ 0.2 K (58 single stars, 2 low-mass planet hosts and 9 high-mass planet hosts). An orange star represents solar values.

assumption was confirmed for hot-Jupiter hosts by Brewer et al. (2016b), where they show that the average planet C/O ratio is super-stellar, but their large uncertainties do not exclude the possibility of the 1:1 relation for the stellar and planetary C/O ratios.

5.5.1 C/O, Mg/Si and masses

We studied C/O and Mg/Si ratios as a function of mass of planetary companion (the most massive planet in case of multiple planets). In Fig. 5.13 we see no clear dependence on the planetary mass, as the range of planetary masses is too wide in comparison with the slopes (-0.04 for Mg/Si and 0.04 for C/O).

As proposed by Thiabaud et al. (2015b), Mg/Si ratios in stars will give a direct information about the composition of the planet, as no differences are expected between them. Our stellar Mg/Si ratios can be translated as planetary Mg/Si ratios (see Santos et al. 2015; Dorn et al. 2015)

Regarding C/O, and given the indirect relation between the star and the planet, our results are an estimation of the C/O that could be found in the planet. For example, WASP-12b shows a high C/O ratio, above 1 (Kreidberg et al. 2015), while its host star shows C/O = 0.48 (Teske et al. 2014). Brewer et al. (2016b) have proposed that planetary C/O will be super-stellar (while O/H could be sub-stellar) in hot-Jupiters.

5.6 Summary and conclusions

We present a detailed study of the C/O and Mg/Si elemental ratios for 499 solar-type stars observed with the HARPS high-resolution spectrograph. In our sample, 99 of 499 are planet-hosts and 400 stars have no known planetary companion. All the stars within our sample have effective temperatures between 5250 K and 6666 K, metallicities from −0.59 to 0.55 dex and surface gravities from 3.81 to 4.82 dex.

We searched for any correlation between the presence of planets and these elemental ratios. We found an increasing trend for C/O with [Fe/H], found by previous authors and expected by GCE models. We looked for similarities between the three samples studied: the single star samples and the low- and high- mass planetary sample. We find no similarities between the samples.

We also studied a plausible relation between [C/O] ratios and GCE. [C/O] ratios are not only affected by GCE, they also play an important role in the formation of high-mass planets, as [Mg/Si] does with the low-mass ones.

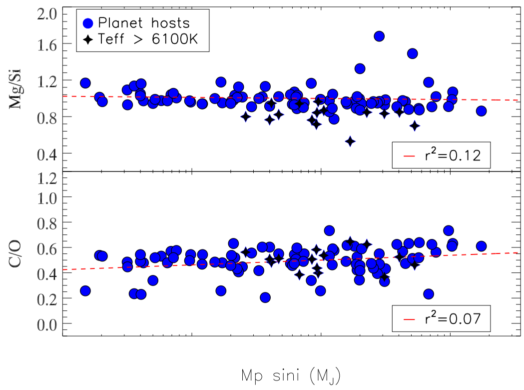

FIGURE 5.13— Mg/Si and C/O elemental ratios as a function of the planetary mass. Full circles represent stars with T_{eff} < 6100K, and crosses represent stars with T_{eff} > 6100K. A correlation for T_{eff} < 6100K is provided for both sets, C/O and Mg/Si (in this case, after removing the 3 outliers with Mg/Si > 1.3).

We followed the same procedure for Mg/Si and obtained a decreasing trend for Mg/Si as a function of [Fe/H], while two different trends were found when studying Mg/Si as a function of T_{eff}: an increasing trend for T_{eff} < 6100 K and a decreasing trend for T_{eff} > 6100 K. This behaviour applies to both single stars and planetary samples.

We looked for a possible correlation between the presence of planets and these elemental ratios, and separating the planetary sample in low- and high- mass planets found that a ∼5% similarity can be found between the low-mass planets and the single stars, whereas this last sample bears no similarity with the high-mass sample.

Overall, 99% of our sample present C/O < 0.8, while all our confirmed planet host stars present C/O values below 0.8, suggesting that the composition of the bulk of the planets should be graphite, TiC and solid Si in SiC form. 12% of our sample has C/O < 0.4. Regarding Mg/Si, 12% of our planet host sample present Mg/Si values lower than 1, suggesting a composition of pyroxene and feldspars. The other 88% present Mg/Si values between 1 and 2, so an equal proportion of olivine and pyroxene is expected. These results agree (within the errors and taking into account different solar reference values) with recent studies of C/O and Mg/Si ratios in the solar neighbourhood (Brewer & Fischer 2016) as they obtained peaks for distributions at ∼0.5 for C/O and ∼1.1 for Mg/Si.

In the last few years, several models have suggested that C/O in planet host stars and planetary atmospheres is not the same, owing to migrations and snowlines, although more observations of atmospheres in transiting exoplanets are required to confirm these models.

These ratios give a hint of possible planetary abundances. As there is a direct relation between host star and planet abundances for Mg/Si, we can confirm the silicate composition of the planets. For C/O, as the elements composing this ratio are sensitive to icelines, there is an indirect relation, but we can be sure that our results could be an estimation of those found in planetary atmospheres.

6

Refractory-elements in metal-poor stars

This chapter is based on Suárez-Andrés et al. (2017), A&A, in preparation

ABSTRACT – We present a detailed spectroscopic analysis for 21 solar-type planet host stars for 12 refractory elements. Two of these stars have low-mass companions while the other 18 are known to harbour high-mass planets. We aim to confirm previous results that suggested that metal-poor stars hosting planets are α-enhanced belong to the thick disk. We have used high resolution and high signal-to-noise optical spectra for all our targets. Spectral synthesis for each feature was performed with the codes MOOG and FITTING. Precise chemical abundances for Na, Mg, Al, Si, Ca, Sc, Ti, V, Cr, Mn, Co, and Ni have been analysed in a sample of planet-host and single stars where no planets have been detected so far. Metal-poor stars with both low-mass and high-mass planets in our sample seem to show on average higher abundances for Mg, Si, and Ti for stars by about 0.1 dex with respect to stars without detected planets. We studied population membership of our sample, when evaluating stars individually, we find that metal-poor stars hosting planets tend to be α-enhanced and chemically and kinematically belong to the thick disk as metallicity decreases below -0.25 dex down to about -0.55 dex. We also find, however, three stars with high-mass planets with metallicity in the range -0.550.70 dex that chemically and kinematically belong to the thin disk, thus showing no α-enhancement, something unexpected if especially at these low metallicities, the chemical environment is the most important factor in the formation of planets.

ENHANCEMENTS of alpha elements in metal-poor stars were first identified by Aller & Greenstein (1960) and established by Wallerstein (1962), who found excesses of Mg, Si, Ca, and Ti relative to Fe.

In the core-accretion scenario of planet formation, the amount of metals is important to the formation of both low- and high-mass planets, which require a lot of planetesimals for their core formation (Ida & Lin

2004; Mordasini et al. 2012). Although theoretical modeling suggests that metallicity is a key parameter of planet formation, Haywood (2008) suggested that the presence of high-mass planets is strongly related to the galactocentric radius, but not metallicity. Combined with the existing radial metallicity gradient, the presence of high-mass planets around metal-poor and metal-rich stars is explained.On the other hand, not so many metal-poor planet-host stars have been studied because of their limited number. More studies on these stars can help shed some light on the formation of their planetary companion and if chemical composition plays an important role in it. In this work, we have carried out a complete study on α and iron-peak elements of stars observed in the Northern Hemisphere. In this chapter, we present a complete and uniform study, together with previous works from Adibekyan et al. (2012b,c), on chemical abundances for metal-poor planet-host stars.

In this chapter we perform a detailed study of Na, Mg, Al, Ca, Sc, Ti, V, Cr, Mn, Co and Ni in a set of 21 planet-harbouring stars in the metallicity range $-0.66 \leq$ [Fe/H] ≤ -0.08.

This chapter is organized as follows: in Chapter 6.1, we briefly introduce the observations and physical properties of the stars in the sample. The method used for the analysis of the data is explained in Chapter 6.2. The study of the abundances of refractory elements relative to Fe in exoplanet-hosting stars can be found in Chapter 6.3. The kinematical properties of the exoplanet-hosting stars are presented in Chapter 6.4. Finally, in Chapter 6.5, we draw our main conclusions.

6.1 Observations and sample description

The sample used in this work consists of 21 FGK stars observed with FIES spectrograph (Frandsen & Lindberg 1999; Telting et al. 2014) at the 2.56m Nordic Optical Telescope (NOT) in La Palma, Spain, during several campaigns. (See Table 6.1.) FIES spectral resolving power ranges from 46,000 to 67,000, depending on the used fiber. Also, data from other instruments (UVES and FEROS) were added to the sample for completeness. The sample was selected using the SWEET-CAT catalog (Santos et al. 2013).

Our planet-host dwarf stars have effective temperatures between 5,111K and 6,853K, metallicities from -0.08 to -0.66 dex, and surface gravities from 3.83 to 4.91 dex.

Table 6.1— Observing logs for the FIES campaigns.

Campaign	Observing dates
52-209	8 October 2015, 17-18 March 2016
53-202	12-13 April 2016, 29-30-31 May 2016
	10-11-12 July 2016, 19 September 2016

6.2 Analysis

High spectral resolving power and high signal-to-noise ratio (S/N) are optimal to properly analyse these targets and the selected spectral lines. The average S/N of our sample in the studied regions is 150. Thirty-two percent of our sample has S/N above 200. The individual spectrum of each star was reduced using the FIEStool pipeline and then combined with IRAF after correcting for its radial velocity. Precise stellar parameters used were derived by measuring equivalent widths of Fe I and Fe II lines using the code FASMA (Andreasen et al. 2017). All stellar parameters for our sample were taken from Andreasen et al. (2017).

For dwarf stars with (spectroscopic) log g above 4.2 dex, we applied an asterosismology correction for an accurate measure, based on Mortier et al. (2014).

Elemental abundances for 12 elements (Na, Mg, Al, Si, Ca, Ti, Cr, Ni, Co, Sc, Mn, and V) were determined using a standard local thermodynamic equilibrium (LTE) analysis with the spectral synthesis code MOOG (Sneden 1973, 2013 version) and a grid of Kurucz (1993) ATLAS9 atmospheres. Chemical abundances were taken from Anders & Grevesse (1989). The line list used in this work was taken from Adibekyan et al. (2012b), based on Neves et al. (2009). To complete the line list, we made use of VALD3 data (See Ryabchikova et al. 2015).

Due to our high-quality spectra we normalized the continuum using the CONTINUUM task of IRAF.

To find the best fit abundance value for each star and each element, we used the FITTING program (González Hernández et al. 2011) and the MOOG synthesis code. The best fit was obtained using a χ^2 minimization procedure by comparing each synthetic spectrum with the observed one in each spectral feature.

Best-fit abundances are extracted from each spectral range and the final abundance for each star and each element is then computed as the average of these values. Individual lines for a given star and element

TABLE 6.2— Stellar parameters for our sample and mass of the most massive planet that they harbour.

Star	$T_{\rm eff}$ (K)	log g (dex)	[Fe/H] (dex)	$\xi_t (kms^{-1})$	Instrument	Planetary mass (M_J)
HD 114762	5879 ± 39	4.23 ± 0.04	-0.66 ± 0.03	1.16 ± 0.07	FIES	10.98
HD 155358	5906 ± 33	4.24 ± 0.03	-0.61 ± 0.02	1.30 ± 0.05	FIES	0.85
HD 154857	5584 ± 23	3.90 ± 0.04	-0.23 ± 0.02	1.18 ± 0.03	FIES	2.58
HD 197037	6233 ± 45	4.22 ± 0.04	-0.12 ± 0.03	1.22 ± 0.06	FIES	0.79
HD 220842	5999 ± 39	4.30 ± 0.06	-0.08 ± 0.03	1.21 ± 0.05	FIES	3.18
HD 37124	5460 ± 35	4.24 ± 0.04	-0.42 ± 0.03	0.61 ± 0.07	FIES	0.70
HD 70573	5889 ± 186	4.32 ± 0.27	-0.42 ± 0.13	1.14 ± 0.01	FIES	6.10
HD 97658	5219 ± 54	4.60 ± 0.10	-0.28 ± 0.04	0.78 ± 0.11	FIES	0.02
HIP 109384	5236 ± 43	4.44 ± 0.08	-0.24 ± 0.03	0.60 ± 0.10	FIES	1.56
KELT-6	6246 ± 88	4.22 ± 0.09	-0.22 ± 0.06	1.66 ± 0.13	FIES	3.71
Kepler 37	5378 ± 53	4.47 ± 0.12	-0.23 ± 0.04	0.58 ± 0.13	FIES	0.04
Kepler 444	5111 ± 43	4.50 ± 0.13	-0.51 ± 0.03	0.37 ± 0.15	FIES	-
WASP-21	5959 ± 49	4.43 ± 0.08	-0.23 ± 0.04	1.13 ± 0.07	FIES	0.30
WASP-37	5917 ± 72	4.25 ± 0.15	-0.23 ± 0.05	0.59 ± 0.13	FIES	1.80
WASP-58	6039 ± 55	4.23 ± 0.10	-0.09 ± 0.04	1.12 ± 0.08	FIES	0.89
HAT-P-24	6470 ± 181	4.33 ± 0.27	-0.41 ± 0.10	1.40 ± 0.03	UVES	0.69
HAT-P-39	6745 ± 236	4.39 ± 0.47	-0.21 ± 0.12	1.53 ± 0.04	UVES	0.60
WASP-61	6265 ± 168	4.21 ± 0.21	-0.38 ± 0.11	1.44 ± 0.02	UVES	2.06
WASP-100	6265 ± 168	4.21 ± 0.21	-0.38 ± 0.11	1.44 ± 0.02	UVES	2.03
HD 6434	6470 ± 181	4.33 ± 0.27	-0.41 ± 0.10	1.40 ± 0.03	FEROS	0.44
HD 13445	5114 ± 61	4.55 ± 0.13	-0.29 ± 0.04	0.66 ± 0.15	FEROS	3.90

with a line dispersion higher than 2-σ were excluded. All the atmospheric parameters, T_{eff}, $\log g$, ξ_t, [Fe/H] were fixed. Rotational broadening was set as a free parameter with v sin$i$ varying between 0.0 and 15.0 km/s with a step of 0.5 km/s. For more information about the followed procedure, see Suárez-Andrés et al. (2016).

In Fig. 6.1, we show the observed and synthetic spectra for the Sun and two stars that are depicted for different temperature and metallicity within our sample (HD 197037 and Kepler 444). For these two stars, the best fit and two different abundances are also shown.

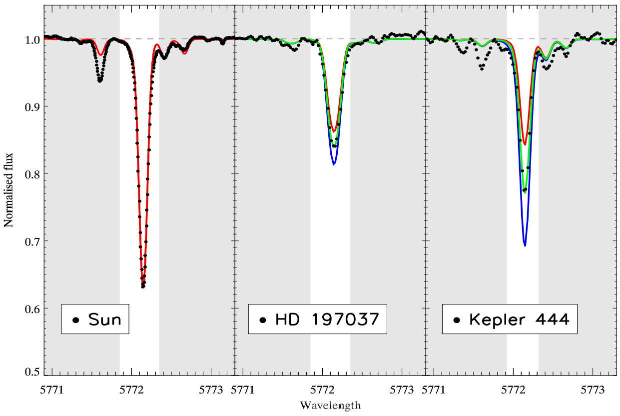

FIGURE 6.1— Synthesis of a spectral region for the Sun (left panels) and two dwarf stars with different stellar parameters, HD197037 (T_{eff}=6233K, log$g$=4.22 and [Fe/H]=-0.12) and Kepler 444 (T_{eff}=5111K, log$g$=4.50 and [Fe/H]=-0.51) is shown. Grey regions delimit the region analysed for the χ^2 best fit.

To examine how variations in the atmospheric parameters affect our abundances, we tested the [X/H] sensitivity in stars with widely differing parameters. For each set of stars, we tested the chemical abundance to changes in the stellar parameters ($\pm$50 K for $T_{\rm eff}$ and $\pm$0.1 dex in $\log g$, metallicity and ξ_t). Results are shown in Table 6.3. An error due to a continuum placement was considered for all stars of 0.005. All effects were added quadratically to obtain the final uncertainties following this expression:

$$\Delta[\mathrm{X/H}] = (\Delta_{\sigma}^2 + \Delta_{T_{\mathrm{eff}}}^2 + \Delta_{\log g}^2 + \Delta_{[\mathrm{Fe/H}]}^2 + \Delta_{\mathrm{cont}}^2 + \Delta_{\xi_{\mathrm{t}}}^2)^{1/2}$$

6.3 Results

To test for possible relations between the studied abundances and the masses of planetary companions, we separated the planet population into two groups: low-mass planets (LMP, with masses less than or equal to 30 $M_{\oplus}$) and high-mass planets (HMP, with masses greater than 30 $M_{\oplus}$). In stars that host several planets, the most massive planet was considered in our study. Our sample consists of four low-mass and 21 high-mass planet hosts.

We looked for distinguishable trends between these samples by representing [X/Fe] as a function of T_{eff}, as shown in Fig. 6.2. We plot underneath results from Adibekyan et al. (2012b), but limiting their sample to our metallicity range.

We also looked for trends between these samples by representing [X/Fe]

TABLE 6.3— The sensitivity of abundances on the model parameters for each element.

Star (T_{eff}, [Fe/H], log g, ξ_{t})	Na	Mg	Al	Si	Ca	ScI	ScII	TiI	TiII	V	CrI	CrII	Mn	Co	Ni
								T_{eff} ; ±50 K							
HD 13445 (5114, -0.29, 4.55, 0.66)	-0.05	+0.06	-0.12	+0.10	+0.10	+0.09	+0.08	-0.10	+0.12	+0.20	+0.07	+0.05	+0.08	-0.08	-0.08
Kepler 37 (5378, -0.23, 4.47, 0.13)	+0.08	+0.08	-0.08	+0.06	+0.08	+0.10	+0.08	+0.10	+0.04	-0.08	+0.07	+0.04	+0.12	-0.04	-0.04
WASP-21 (5959, -0.23, 4.43, 1.13)	+0.06	+0.06	+0.06	+0.04	+0.06	+0.04	+0.02	+0.10	+0.02	+0.10	+0.06	+0.02	+0.08	+0.04	+0.04
								[Fe/H] ; ±0.10 dex							
WASP-21 (5959, -0.23, 4.43, 1.13)	+0.00	-0.08	-0.03	+0.03	-0.03	-0.03	+0.02	+0.04	+0.04	+0.04	-0.03	+0.00	-0.02	+0.01	-0.01
HD 6434 (5704, -0.54, 4.23, 0.80)	-0.04	-0.04	-0.04	-0.02	+0.00	-0.03	-0.02	+0.04	-0.01	+0.00	-0.06	-0.04	-0.04	-0.04	-0.03
HD 114762 (5879, -0.66, 4.40, 1.16)	-0.02	-0.04	-0.04	-0.02	+0.04	+0.00	+0.01	+0.03	+0.06	+0.08	-0.05	-0.03	-0.01	-0.04	-0.04
								log g ; ±0.10 dex							
HD 154857 (5584, -0.23, 3.90, 1.18)	-0.01	-0.01	+0.00	+0.01	-0.02	+0.04	+0.04	-0.01	+0.04	-0.01	-0.02	+0.02	-0.01	+0.01	+0.01
HIP 109384 (5236, -0.24, 4.44, 0.60)	+0.00	+0.03	+0.04	+0.08	+0.05	+0.08	+0.08	+0.08	+0.09	+0.09	+0.03	+0.05	+0.08	+0.08	+0.10
HD 97658 (5219, -0.28, 4.60, 0.78)	+0.04	+0.04	+0.06	+0.08	+0.08	+0.06	+0.06	+0.08	+0.08	+0.08	+0.04	+0.08	+0.04	+0.08	+0.08
								ξ_t ; ±0.10 dex							
WASP-37 (5917, -0.23, 4.25, 0.59)	+0.02	+0.02	+0.01	+0.01	+0.03	+0.03	+0.02	+0.00	+0.01	+0.01	+0.00	+0.01	+0.00	+0.01	+0.01
HD 197037 (6233, -0.12, 4.22, 1.22)	-0.01	+0.01	+0.00	+0.00	+0.02	+0.00	-0.01	-0.02	-0.02	+0.02	+0.02	+0.02	+0.00	+0.02	+0.02
WASP-21 (5959, -0.23, 4.43, 1.13)	+0.06	+0.04	+0.05	++0.00	+0.07	-0.01	+0.11	-0.01	+0.12	+0.07	+0.10	+0.06	+0.04	-0.06	-0.06

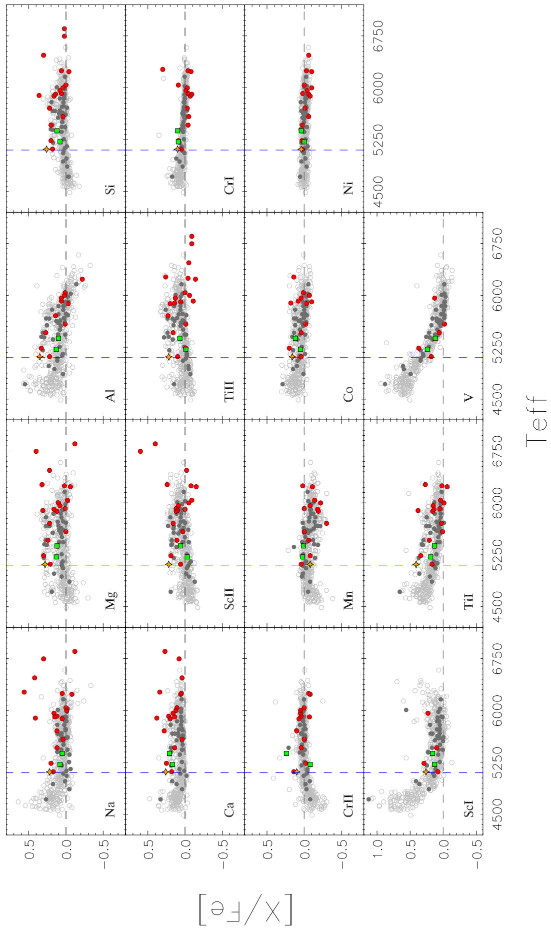

FIGURE 6.2— [X/Fe] abundance ratios as a function of T_{eff} for all the 12 studied elements. Open grey dots are single stars (Taken from Adibekyan et al. 2012b). Full dark-grey dots are stars with planets from the comparison sample. Coloured stars are our results (green squares for low-mass planets and red dots for high-mass companions).

Table 6.4— Sample of the obtained abundances

Star	...	[Mg/H]	[Si/H]	[Ca/H]	...	Population
HD 155358	...	-0.45±0.14	-0.47±0.03	-0.47±0.07	...	Thin
HD 37124	...	-0.18±0.06	-0.22±0.07	-0.28±0.08	...	Thin
HD 220842	...	-0.28±0.06	-0.34±0.09	-0.26±0.09	...	Thin
...	...	...	...	...	...	

as a function of the stellar metallicity (see Figs. 6.3, 6.4) for those selected stars. We plot underneath results of a limited sample taken from Adibekyan et al. (2012b).

[X/Fe] histograms of exoplanet-hosting stars can help us characterize the distribution of the individual elements relative to Fe. The [X/Fe] distributions are shown in Fig. 6.5. We can see the frequency distribution for [X/Fe] for the three cases: stars with high-mass planets (HMP: blue, dashed dotted line), stars with low-mass planets (LMP: green, dashed line), and the comparison sample (NP: red, full line). Note that we used the average of TiI & TiII for Ti, the average of CrI & CrII for Cr, and the average of ScI & ScII for Sc to increase the statistics. To also increase the statistics, we show in the bottom panel of Fig. 6.6 planetary data from both this work and Adibekyan et al. (2012b), doubling the available planetary sample. In Table 6.5, we can see the diference between the $<$ [X/Fe] $>$ for the planetary and non-planetary samples. It can be seen there is an overabundance for the planetary samples for α-elements.

There is a slight offset between the planetary samples, as it seems that the [X/Fe] distributions of low-mass planet hosts start at higher [X/Fe] values compared with the distributions of high-mass planet-host.

In Fig. 6.7 we can see the cumulative fraction for [X/Fe] for the three cases: stars with high-mass planets (HMP: blue, dashed dotted line), stars with low-mass planets (LMP: green, dashed line), and the comparison sample (NP: red, full line).

To see if there is any resemblance between each sub-sample of planet host and the non-planet host sample, we performed a Kolmogorov-Smirnov (K–S) test. To increase the validity of our statistics, we added the planetary sample taken from Adibekyan et al. (2012b). In our study, a zero value of the K–S test refers to datasets with no similarities among them. Unity refers to the maximum similarity that can be found for the compared datasets.

We have applied a K–S test to these samples, as shown in Table 6.6. To avoid unnecessary errors, we limited our comparison sample to -0.08

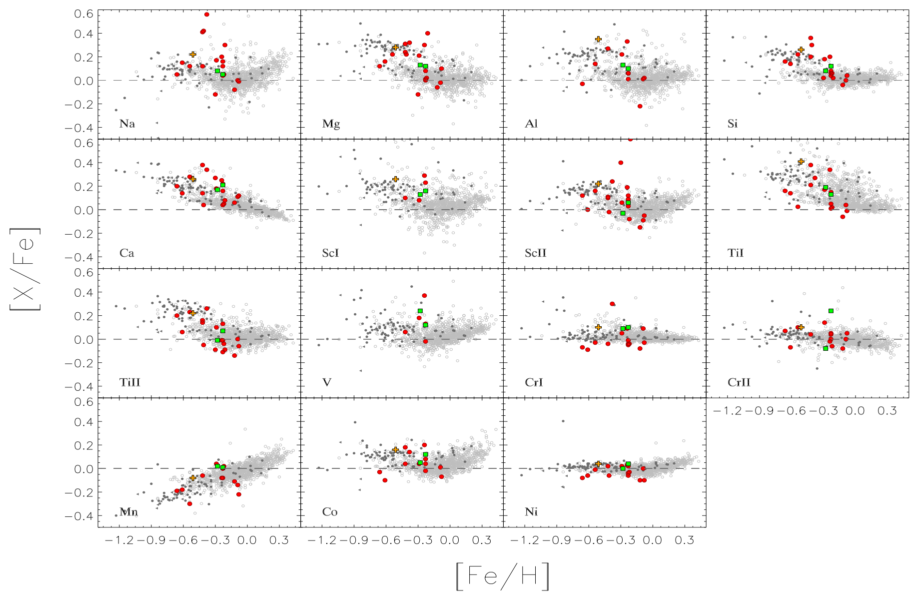

FIGURE 6.3— [X/Fe] abundance ratios as a function of [Fe/H] for all the 12 studied elements. Open grey dots single stars (Taken from Adibekyan et al. 2012b). Full dark-grey dots are stars with planets from the comparison sample. Coloured stars are our results (green squares for low-mass planets and red dots for high-mass companions).

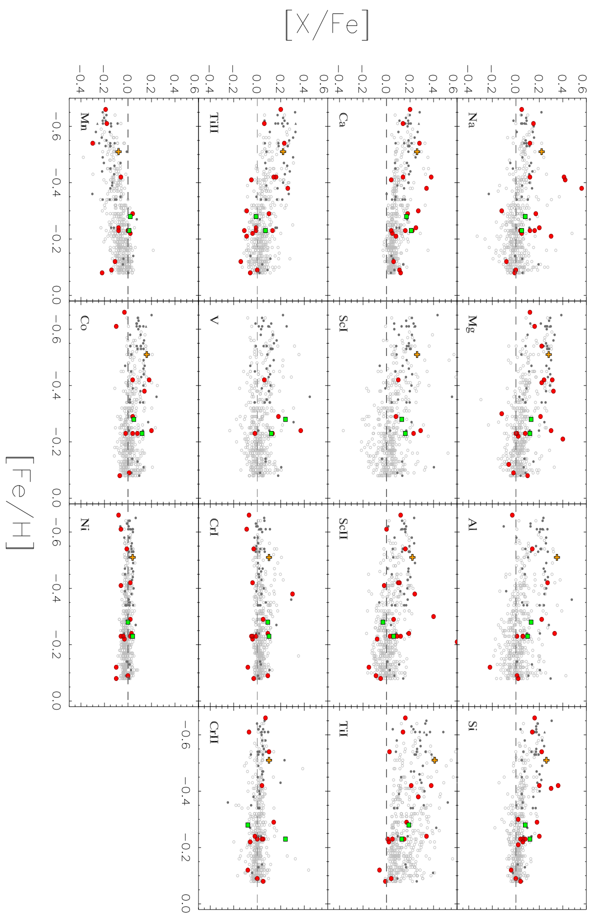

FIGURE 6.4— Same as previous figure. Stars from Adibekyan et al. (2012b) are limited in metallicity (-0.08 ≤ [Fe/H] ≤ -0.66)

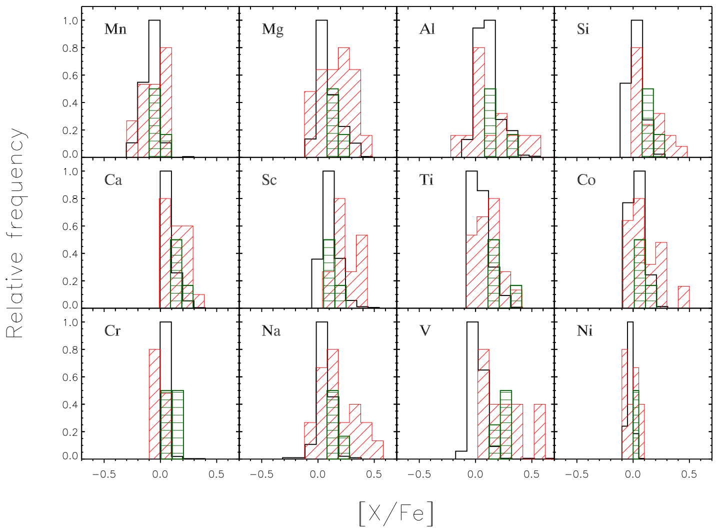

FIGURE 6.5— [X/Fe] distributions of the different elements. Stars without planets are represented in black (taken from Adibekyan et al. 2012b). Stars harbouring high-mass planets are shown in red while stars with low-mass planets are in dashed green. The sets were scaled to clarify the histograms at 1.0 (no planets), 0.8 (high-mass planets), and 0.5 (low-mass planets).

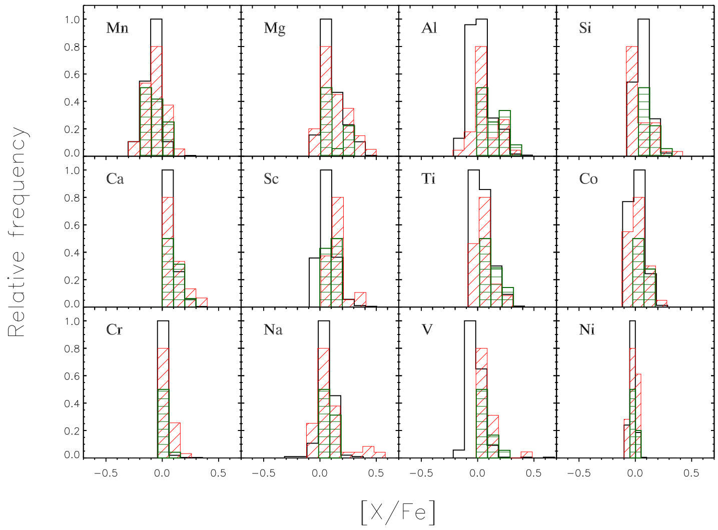

FIGURE 6.6— [X/Fe] distributions of the different elements. Stars without planets are represented in black (taken from Adibekyan et al. 2012b). Stars harbouring high-mass planets are shown in red while stars with low-mass planets are in dashed green. The sets were scaled to clarify the histograms at 1.0 (no planets), 0.8 (high-mass planets), and 0.5 (low-mass planets). Planetary samples include data from Adibekyan et al. (2012b).

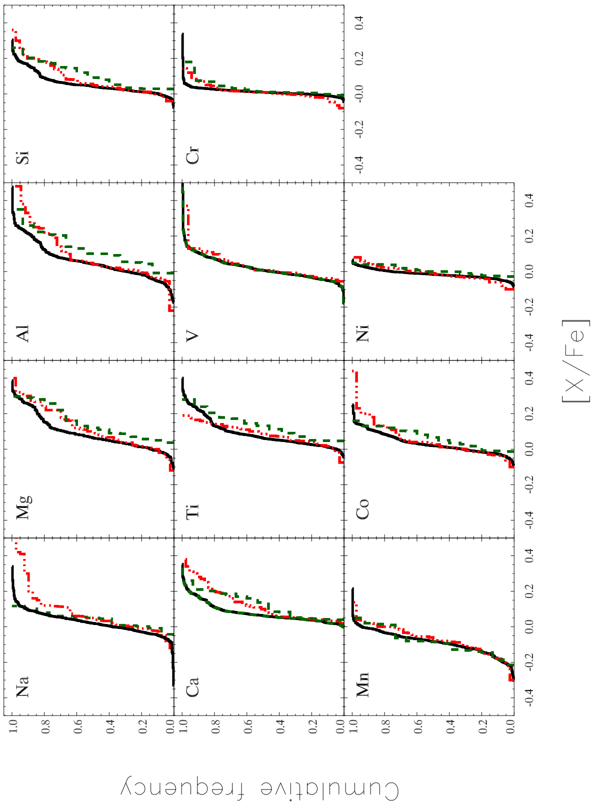

Figure 6.7— Cumulative distribution functions of [X/Fe]. The stars with high- and low-mass planets are represented by a red dash and a green solid line, respectively. The stars without planets are represented by a black dotted line.

TABLE 6.5— Average abundance ratios [X/Fe] for stars with and without planets and the difference of averages between low-mass and high-mass planet hosts and stars without planets.

Species X	Low-mass hosts <[X/Fe]>	High-mass hosts <[X/Fe]>	Without planets <[X/Fe]>	Difference of averages Low-mass - Non-hosts	High-mass - Non-hosts
Na	0.05	0.08	0.02	0.03	0.06
Mg	0.13	0.13	0.06	0.07	0.07
Al	0.11	0.08	0.05	0.06	0.03
Si	0.10	0.09	0.04	0.06	0.05
Ca	0.12	0.12	0.09	0.03	0.03
Sc	0.07	0.09	0.05	0.02	0.04
Ti	0.11	0.09	0.07	0.04	0.02
V	0.06	0.04	0.03	0.03	0.01
Cr	0.02	0.01	0.02	0.00	-0.01
Mn	-0.07	-0.08	-0.08	0.01	0.00
Co	0.05	0.04	0.03	0.02	0.01
Ni	0.01	-0.02	-0.01	0.02	-0.01

≤ [Fe/H] ≤ -0.66 and 5100K ≤ T_{eff} ≤ 6853K. Stars with high-mass companions share some similarities with single stars, especially for V. These results are consistent with the results represented in Fig. 6.7.

As presented in Adibekyan et al. (2012a), in the low-metallicity regime almost all planet-hosts have high [α/Fe] values, typical for stars belonging to the thick disk. Stars without planets with low and high [α/Fe] values belong to the thin and thick disk, respectively.

6.3.1 Kepler 444

One interesting target in our sample is Kepler 444, a K-dwarf star with five confirmed transiting (hot) terrestrial planetary companions, all with sizes between Mercury and Venus (Campante et al. 2015). With an age of 11.2±1.0 Gyr, Kepler 444 is the oldest known system of terrestrial-size planets, as it formed when the universe was less than 20% of its current age.

Given its age, Kepler 444 is an object of a great interest, as it shows that exoplanets have been forming since a very early time. We did a complete chemical study on this old star, given its great important in understanding planetary formation. For its stellar parameters, we obtained $T_{eff} = 5111 \pm 43$, logg $= 4.50 \pm 0.13$ and [Fe/H] $= -0.51 \pm 0.03$, in agreement with Campante et al. (2015).

We performed a detailed abundance study of this target, obtaining chemical abundances for all 12 elements. Our results on [Ti/Fe] and [Si/Fe]

Table 6.6— K-S probabilities for the sample. We tested the relation between the high- and low-mass planet samples (HMP, LMP) and the comparison sample (NP) for all [X/Fe] abundances.

Element	NP-LMP	NP-HMP
Na	0.26	0.01
Mg	0.05	0.12
Al	0.01	0.47
Si	0.03	0.19
Ca	0.02	0.00
Sc	0.04	0.06
Ti	0.06	0.23
V	0.06	0.90
Cr	0.32	0.28
Mn	0.43	0.06
Co	0.12	0.39
Ni	0.01	0.08

agree, within errors, with those obtained in Campante et al. (2015). (See Table 6.7.)

We also obtained the targets probabilities of belonging to the thick or thin disk or the the halo. As we can see in Section 6.4.1, our results agree with those obtained by Campante et al. (2015). (See Fig. 6.8 and Table 6.8.) In Section 6.4.2, we study if this membership was maintained based on its chemistry. In Campante et al. (2015), the only α-element used to study the chemistry was Ti. We also obtained Mg and Si to confirm that Kepler 444 can be catalogued as a star from the thick disk based only on its chemistry, in agreement with Campante et al. (2015). (See Fig 6.9).

6.4 Kinematic properties and chemical separations

6.4.1 Kinematical properties

Kinematic studies on planet-host stars are an important way to understand planetary formation. The first papers did not find any significant kinematic peculiarity for them (Gonzalez 1999; Reid & Cruz 2002; Barbieri, M., & Gratton, R. G. 2002). Haywood (2008, 2009), combining the chemical and kinematic data, concluded that most metal-rich stars that host high-mass planets originate from the inner Galactic disk. On the other hand, Adibekyan et al. (2012a) proposed that chemical composi-

Table 6.7— Kepler 444 chemical abundances

Element	[X/Fe]
Na	0.22±0.11
Mg	0.28±0.11
Al	0.35±0.07
Si	0.26±0.04
Ca	0.26±0.09
Sc	0.24±0.09
Ti	0.32±0.10
Cr	0.10±0.06
Mn	-0.08±0.09
Co	0.16±0.07
Ni	0.04±0.04

tion of the planetary cloud and not Galactic birthplace was a key issue in planetary formation.

To separate different stellar populations by their kinematics, we computed Galactic space velocities for our targets. The space velocity components (U,V,W) were derived with respect to the local standard of rest (LSR), adopting the standard solar motion ($U_{\odot}$, $V_{\odot}$, $W_{\odot}$) = (11.1, 12.24, 7.25) kms^{-1} proposed by Schönrich et al. (2010). We obtained parallaxes and proper motions from the Gaia catalog (Lindegren et al. 2016). Three stars with no available data from Gaia were extracted from the Hipparcos catalog (van Leeuwen 2007). Radial velocities were obtained from the Geneva-Copenhagen Survey (Holmberg et al. 2009), Vogt et al. (2005); Kipping et al. (2010); Howard et al. (2011); Hellier et al. (2012, 2014); Damasso et al. (2015); Campante et al. (2015) and Hébrard et al. (2016). Five stars have no available data on parallaxes or proper motions.

To select a membership of our targets, we followed the method described in Reddy et al. (2006) to select memberships for our targets. We adopted all the demanded variables (asymmetric drift, dispersion, and population fractions) from this paper as well as from Bensby et al. (2003). To obtain the probability of membership to a certain population (thick disk, thin disk, or halo), the minimum probability that we required was 70%. All targets with probabilities below that level were included in the transition population. According to Bensby et al. (2003) criteria, 10 stars belong to the thin disk, four to the thick disk, and two are considered to be transition stars. Following Reddy et al. (2006) criteria, 11 stars belong to the thin disk, three to the thick disk, and two are transition stars. We

TABLE 6.8— Galactic space velocities and membership to stellar population probabilities. Bensby et al. (2003) and Reddy et al. (2006) criteria were followed to obtain membership.

				Bensby et al. (2003)				Reddy et al. (2006)			
Star	U	V	W	Pop_{thin}	Pop_{thick}	Pop_{halo}	group	Pop_{thin}	Pop_{thick}	Pop_{halo}	group
WASP-100	7	24	40	0.90	0.10	0.00	thin	0.93	0.07	0.00	thin
HAT-P-24	24	-5	23	0.99	0.01	0.00	thin	0.98	0.02	0.00	thin
HD 70573	10	4	-10	0.99	0.01	0.00	thin	0.99	0.01	0.00	thin
HD 155358	1	-21	39	0.93	0.07	0.00	thin	0.91	0.09	0.00	thin
HD 37124	44	-34	-36	0.87	0.13	0.00	thin	0.88	0.12	0.00	thin
WASP-61	-7	6	-2	0.99	0.01	0.00	thin	0.99	0.01	0.00	thin
HD 97658	0	13	2	0.99	0.01	0.00	thin	0.99	0.01	0.00	thin
HD 154857	31	4	-29	0.98	0.02	0.00	thin	0.97	0.03	0.00	thin
KELT-6	-4	24	8	0.99	0.01	0.00	thin	0.99	0.01	0.00	thin
HD 197037	46	16	-6	0.99	0.01	0.00	thin	0.99	0.01	0.00	thin
HD 114762	-68	-54	64	0.01	0.99	0.00	thick	0.03	0.97	0.00	thick
HD 6434	101	-58	6	0.38	0.62	0.00	trans	0.80	0.20	0.00	thin
Kepler-444	66	-114	-79	0.00	1.00	0.00	thick	0.00	1.00	0.00	thick
HD 13445	-89	-64	-22	0.23	0.77	0.00	thick	0.66	0.34	0.00	trans
HIP 109384	-7	-48	-63	0.07	0.93	0.00	thick	0.11	0.89	0.00	thick
HD 220842	29	-1	59	0.42	0.58	0.00	trans	0.44	0.56	0.00	trans

note that all transition stars, for both criteria, correspond to transition stars between the thin and thick disk. No star belonging to the halo was found.

The distribution of our sample in the Toomre diagram, following both Bensby et al. (2003) and Reddy et al. (2006) criteria, is shown in Fig. 6.8. A sample of the obtained probabilities, along with Galactic space velocity components, can be found in Table 6.8.

6.4.2 Chemical separation

Thin and thick disk stars are different not only based in their kinematics, but also on their chemistry (Navarro et al. 2011; Adibekyan et al. 2011). Adibekyan et al. (2011) showed that stars could be catalogued in terms of their [α/Fe] abundance, where α stands for the average of Mg, Si and Ti. In Fig. 6.9 we plot [α/Fe] vs. [Fe/H] for our sample, taking into account their kinematic membership. We also show single stars from Adibekyan et al. (2012b) separated by their population membership. Same symbols as for our sample are followed to distinguish between the thin and thick disk. It can be seen that both populations are mixed, with the presence of thin disk stars very close to the chemical separation line between thin and thick stars. We can also see that stars belonging to the thin disk show signs of enhancement compared with other stars from the same population, but without any companion.

Haywood (2008, 2009) reported that at low metallicities ([Fe/H] < -0.3 dex), most of stars harbouring planets will belong to the thick disk

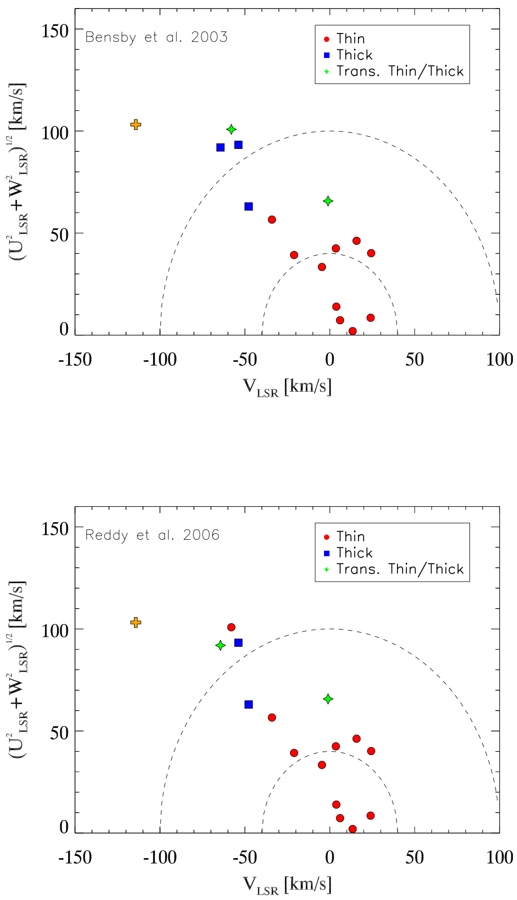

FIGURE 6.8— Toomre diagram for our sample, following the methods from Bensby et al. (2003) (top) and Reddy et al. (2006) (bottom). An orange cross represents Kepler 444.

rather than the thin disk. As opposed to models that suggest that metallicity plays a key role, they suggest there is a strong relation with the galactocentric radius. In Adibekyan et al. (2012a), it is proposed that chemical composition, and not Galactic birthplace, is the key factor for metal-poor planets to lie in the high-α/thick-disk region. It is based on two assumptions: the continuous increase from -0.2 to -0.3 dex for the planetary sample and the overabundance of α-elements in planet hosts. We see a hint of increasing trend for the aforementioned metallicities, but our limited sample does not allow us to confirm it. On the other hand, we can see that our planet hosts are overabundant in α-elements when compared to those stars without a planetary companion. Our results agree with those found in Adibekyan et al. (2012a) that rules out the membership scenario but suggests a dependence on the chemical environment where they are formed.

6.4.3 Planetary properties

We looked deeper into a plausible relation between [X/Fe] and some planetary properties[1], such as the mass of the planet or the period. As in previous sections, planetary companions were split in two sub-samples, depending on the mass.

In Fig. 6.10 we can see the [X/Fe] abundances as a function of the planetary mass. Masses range between 0.023 and 10.98 $M_{\rm Jup}$sini, with 15% of the sample belonging to the low-mass sub-sample. Again, no trends could be found regarding chemical abundances and planetary masses.

In Fig. 6.11 we can see the [X/Fe] abundances as a function of the planetary period. Periods range between 2.85 and 3,452.00 days, with 68% of the sample with a period less than 365 days. No trends could be found regarding chemical abundances and orbital periods.

6.5 Summary and conclusions

We presented a differential abundance analysis between 21 metal-poor stars with and without planets for 12 refractory elements (Na, Mg, Al, Si, Ca, Ti, Cr, Ni, Co, Sc, Mn, and V). Eighteen of these stars harbour high-mass planets ($M_{\rm pl} > 30 M_\oplus$), and two stars harbour low-mass planets ($M_{\rm pl} < 30 M_\oplus$). Stellar parameters were taken from Andreasen et al. (2017).

[1]Data from *www.exoplanet.eu* and *exoplanetarchive.ipac.caltech.edu/*

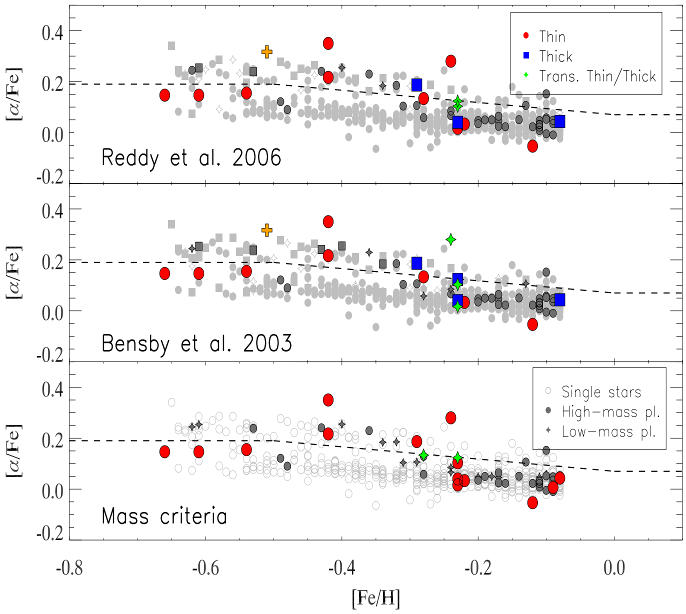

FIGURE 6.9— Top and middle panels: [α/Fe] as a function of [Fe/H] for our sample. Our kinematic results are shown with different symbols. Comparison stars and planetary sample, taken from Adibekyan et al. (2012b), are shown in light and dark grey, respectively. An orange cross represents Kepler 444. Bottom panel: [α/Fe] as a function of [Fe/H], separating between planetary samples.

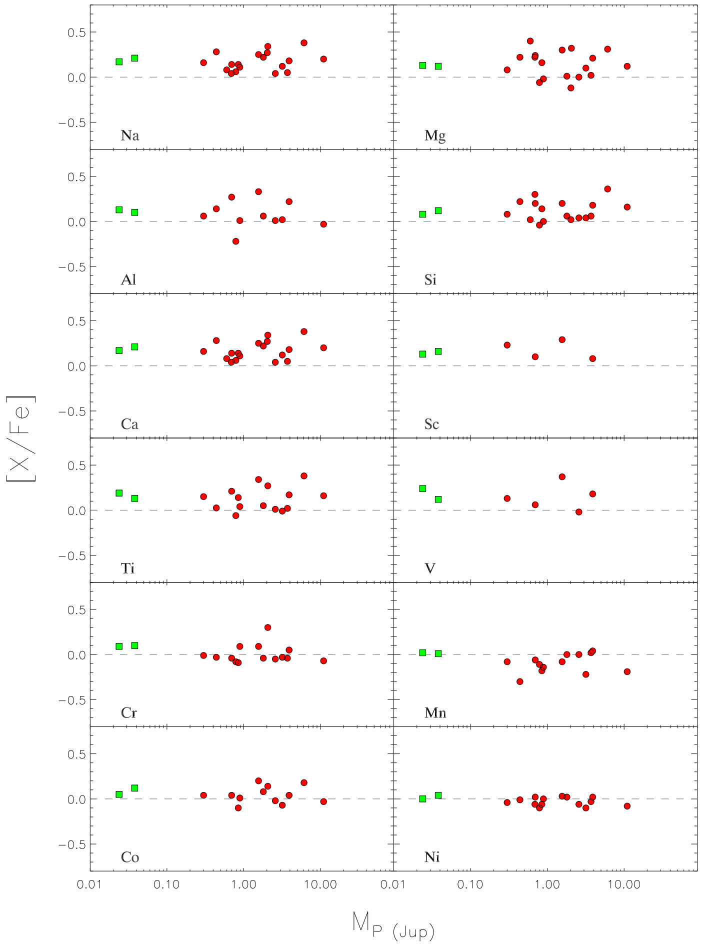

FIGURE 6.10— [X/Fe] as a function of planetary mass. Green squares refer to low-mass companions, while red dots refer to high-mass companions.

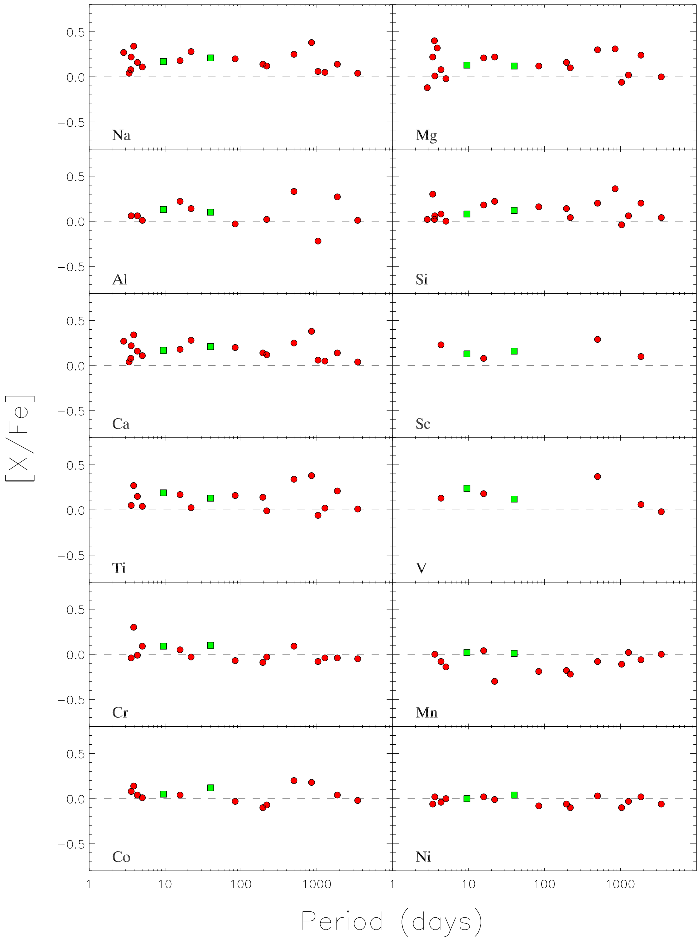

FIGURE 6.11— [X/Fe] as a function of the period of the planet. Green squares refer to low-mass companions, while red dots refer to high-mass companions.

Results from [X/Fe] histograms suggest that stars harbouring low-mass planets are completely different from single stars.

For high-mass companions, all [X/Fe] are different except for [V/Fe].

We also studied population membership for the sample, obtaining between 63% and 69% of stars belonging to the thin disk and between 25% and 19% to the thick disk, depending on the applied criteria (Bensby et al. (2003); Reddy et al. (2006), respectively). We found no chemical differences when comparing the thick and thin star sub-samples, suggesting that birthplace does not place an important role in the enhancement of some elements, but chemical composition of the formation environment does (as proposed by Adibekyan et al. (2012a).

We also looked for a relation between planetary mass and orbital period. We find no trends for any of these parameters, suggesting there is no relation between the refractory elements and those planetary parameters.

7

Conclusions

In this thesis, we studied the chemical abundances of stars with and without planets to look for chemical clues in planetary formation. Here is a summary of our main findings.

7.1 Volatile elements

We performed a detailed analysis of the NH band at 3,360Å for a sample of 74 stars, 42 of which are known to host a planetary companion. Since this band is located in the near UV, we developed a continuous tuning method that allows us to normalize the spectrum reliably and thereby obtain precise chemical abundances.

To obtain these abundances, we used a synthetic fitting method and a χ^2 comparison between the synthetic and observed spectra. Best-fit abundances were extracted for each spectral feature, and then the final abundance was computed as the average of these values.

We also performed a detailed analysis of the CH band at 4,300Å for a sample of 1,110 stars, 143 of which are planet-host stars. We looked for suitable spectral regions to obtain reliable chemical abundances, following the method applied to study nitrogen chemical abundances.

We studied both nitrogen and carbon abundances as a function of the stellar parameters of the host star, $T_{\rm eff}$, $\log g$, and [Fe/H]. Carbon and nitrogen abundances were indistinguishable when comparing single stars and planet-host stars (both low- and high-mass planets) sample.

We searched for correlations between the presence of planets and nitrogen and carbon abundances. There is no clear correlation between the presence of planets and nitrogen abundances, which was expected, as the large amount of nitrogen in a protoplanetary disk would favour the formation of giant planets through the core-accretion scenario. For carbon, we do not find a correlation either. That indicates that volatiles elements may not play an important role on giant planet formation with respect to low-mass planet formation.

We performed a kinematic and chemical separation study for nitrogen and only a chemical separation for carbon. Chemically, we obtained a clear separation between the thin and the thick disk populations based on a dependence of [N/α] and [C/α] with metallicity.

To separate different stellar populations by their kinematics, we computed Galactic space velocities for our targets. We obtained a clear separation between the different populations of the Galactic disk based not only on their chemistry, but also on their kinematics, finding a solid agreement between our results.

7.2 Elemental ratios

We performed C/O and Mg/Si studies in a sample of 499 stars from the HARPS GTO sample derived from our carbon studies. Studying these elemental ratios in planet host stars can help us infer some chemical characteristics of their companions.

For the Mg/Si ratio, 12% of our planet host sample present Mg/Si values lower than 1, suggesting a composition of pyroxene and feldspars. The other 88% present Mg/Si values between 1 and 2, so an equal proportion of olivine and pyroxene is expected. We highlight the fact that 100% of our low-mass sample has Mg/Si values above 1. Regarding C/O, 100% of stars with planets have C/O values lower than 0.8, meaning that Si will take solid form as SiO_4^{4-} and SiO_2. The exact composition will be ruled by the Mg/Si ratio.

These ratios hint at possible planetary abundances. Since there is a direct relation between host stars and planet abundances for Mg/Si, we can confirm the silicate composition of the planets. For C/O, since the elements comprising this ratio are sensitive to ice lines, there is an indirect relation, but we can be sure that our results could be an estimate of those found in planetary atmospheres.

7.3 Refractory elements

Refractory elements are also important to understand planetary formation. We presented a differential abundance analysis between metal-poor stars with and without planets for 12 refractory elements (Na, Mg, Al, Si, Ca, Ti, Cr, Ni, Co, Sc, Mn, and V).

Of our 21 available targets, 18 of these stars harbour high-mass planets ($M_{pl} > 30M_{\oplus}$) and three stars harbour low-mass planets ($M_{pl} < 30M_{\oplus}$).

Although we have a small sample of planet-host stars at low metallicities, the [X/Fe] histograms suggests that stars harbouring low- and high-mass planets are completely different from single stars. We found an over-abundance for α-elements for both planetary samples when compared with single stars, confirming that planet-host at low metallcities tends to belong to the thick disk. However, we also found three stars with high-mass planets with metallicity in the range -0.55 – -0.70 dex that chemically and kinematically belong to the thin disk, thus showing no α-enhancement, something unexpected if especially at these low metallicities, the chemical environment is the most important factor in the formation of planets.

We also studied population membership for the sample, obtaining between more than 60% of stars belonging to the thin disk and around 20% to the thick, depending on the applied criteria (Bensby et al. (2003); Reddy et al. (2006), respectively). We looked for a relation between chemical abundances and planetary mass and orbital period. We found that refractory element abundances are not affected by either the planetary mass or the orbital period of the planet.

We also found no chemical differences when comparing the thick and thin stars sub-samples, suggesting that birthplace does not place an important role in the enhancement of some elements, but chemical composition of the formation environment does (as proposed by Adibekyan et al. 2012a).

8

Future work

In this chapter we present our future work, a continuation of this thesis. We will continue to study chemical signatures in several planet-host stars.

- KIC 8462852:
  This star, also known as *Tabby's Star*, is one of the most intriguing stars ever found. It suffers from both long-time and short-time flux decreases. The causes of these decrements are still unknown. We have high-resolution data from FIES at NOT (ORM, La Palma) during a non-decrement phase. For the current semester, we have been granted a target of opportunity (ToO) time, also at NOT, to study this target if a flux-decrement event happens. We will be able to compare any chemical variation that might happen in the star with a high degree of confidence, given the excellent quality of the data.

- α-element abundances in stars with brown dwarf companions:
  We have high-resolution observations performed with HERMES at Mercator (ORM, La Palma). Following the work of Mata Sánchez et al. (2014), we will expand the number of sources with studied chemical abundances in order to obtain a better understanding of these systems.

- α-element abundances in evolved stars:
  Together with the dwarf sample presented in Chapter 6, we obtained high-resolution spectra with FIES at NOT (ORM, La Palma) of giant metal-poor stars with known companions. With the already-presented chemical study on this type of stars by Adibekyan et al.

(2015b), we will compare our results to find some chemical clues in the mechanism of planetary formation around evolved stars.

- Thorium studies:
  Thorium, along with europium, can be used as chronographs to estimate stellar age. With the available HARPS data (used in Chapter 4 to obtain carbon abundances), given its high signal-to-noise ratio and quality, we can obtain reliable Th measures. Europium will be taken from Delgado Mena et al. (2017, submitted) using the same sample and stellar parameters that we will use.

9

Collaborations and other works

Works using the tool FITTING:

- Suárez-Andrés, L., González Hernández, J.I., Israelian, G. et al., 2014, MNRAS, 447, 2261
  We present Utrecht Echelle Spectrograph@William Herschel Telescope high-resolution spectra of the low-mass X-ray binary (LMXB) Cygnus X-2. We have derived the stellar parameters of the secondary star using χ^s2 *minimization procedure, and taking into account any possible veiling from the accretion disc. We determine a metallicity higher than solar ([Fe/H] = 0.27* $\pm$ *0.19), as seen also in the neutron star X-ray binary Centaurus X-4. The high quality of the secondary's spectrum allows us to determine the chemical abundances of O, Mg, Si, Ca, S, Ti, Fe, and Ni. We found that some* α*-elements (Mg, Si, S, Ti) are enhanced, consistent with a scenario of contamination of the secondary star during the supernova event. Surprisingly oxygen appears to be under-abundant, whereas enhanced abundances of Fe and Ni are measured. Assuming that these abundances come from matter that has been processed in the SN and then captured by the secondary star, we explore different SN explosion scenarios with diverse geometries. A non-spherically symmetric SN explosion, with a low mass cut, seems to reproduce better the observed abundance pattern of the secondary star compared to the spherical case.*

Collaborations:

- Adibekyan, V., Figueira, P., Santos, N. C., et al. 2015, A&A, 583, A94
  Aims: The main goal of this work is to explore which elements carry the most information about the birth origin of stars and, as such, which are best suited for chemical tagging. Methods: We explored different techniques to minimize the effect of outlier value lines in the abundances by using Ni abundances derived for 1111 FGK-type stars. We evaluate how the limited number of spectral lines can affect the final chemical abundance. Then we make an efficient even footing comparison of the [X/Fe] scatter between the elements that have a different number of observable spectral lines in the studied spectra. Results: When several spectral lines are available, we find that the most efficient way of calculating the average abundance of elements is to use a weighted mean (WM), whereby we consider the distance from the median abundance as a weight. This method can be used effectively without removing suspected outlier lines. When the same number of lines are used to determine chemical abundances, we show that the [X/Fe] star-to-star scatter for iron group and -capture elements is almost the same. The largest scatter among the studied elements, was observed for Al and the smallest for Cr and Ni. Conclusions: We recommend caution when comparing [X/Fe] scatters among elements where a different number of spectral lines are available. A meaningful comparison is necessary to identify elements that show the largest intrinsic scatter, which can then be used for chemical tagging.

- Adibekyan, V., Delgado-Mena, E., Figueira, P., et al. 2016, A&A, 591, A34
  Context. Several studies have reported a correlation between the chemical abundances of stars and condensation temperature (known as Tc trend). Very recently, a strong Tc trend was reported for the ζ Reticuli binary system, which consists of two solar analogs. The observed trend in $\zeta 2$ Ret relative to its companion was explained by the presence of a debris disk around $\zeta 2$ Ret. Aims: Our goal is to re-evaluate the presence and variability of the Tc trend in the ζ Reticuli system and to understand the impact of the presence of the debris disk on a star. Methods: We used very high-quality spectra of the two stars retrieved from the HARPS archive to derive very precise

stellar parameters and chemical abundances. We derived the stellar parameters with the classical (non-differential) method, while we applied a differential line-by-line analysis to achieve the highest possible precision in abundances, which are fundamental to explore for very tiny differences in the abundances between the stars. Results: We confirm that the abundance difference between ζ^2 Ret and ζ^1 Ret shows a significant ($\sim 2\sigma$) correlation with Tc. However, we also find that the Tc trends depend on the individual spectrum used (even if always of very high quality). In particular, we find significant but varying differences in the abundances of the same star from different individual high-quality spectra. Conclusions: Our results for the ζ Reticuli system show, for example, that non-physical factors, such as the quality of spectra employed and errors that are not accounted for, can be at the root of the Tc trends for the case of individual spectra.

- Adibekyan, V., Delgado-Mena, E., Figueira, P., et al. 2016, A&A, 592, A87
Context. During the past decade, several studies reported a correlation between chemical abundances of stars and condensation temperature (also known as Tc trend). However, the real astrophysical nature of this correlation is still debated. Aims: The main goal of this work is to explore the possible dependence of the Tc trend on stellar Galactocentric distances, Rmean. Methods: We used high-quality spectra of about 40 stars observed with the HARPS and UVES spectrographs to derive precise stellar parameters, chemical abundances, and stellar ages. A differential line-by-line analysis was applied to achieve the highest possible precision in the chemical abundances. Results: We confirm previous results that [X/Fe] abundance ratios depend on stellar age and that for a given age, some elements also show a dependence on Rmean. When using the whole sample of stars, we observe a weak hint that the Tc trend depends on Rmean. The observed dependence is very complex and disappears when only stars with similar ages are considered. Conclusions: To conclude on the possible dependence of the Tc trend on the formation place of stars, a larger sample of stars with very similar atmospheric parameters and stellar ages observed at different Galactocentric distances is needed.

- González Hernández, J. I., Suárez-Andrés, L., et al. 2017, MNRAS, 465, L15

We present new medium-resolution spectroscopic observations of the black hole X-ray binary Nova Muscae 1991 taken with X-Shooter spectrograph installed at the 8.2m-VLT telescope. These observations allow us to measure the time of inferior conjunction of the secondary star with the black hole in this system that, together with previous measurements, yield an orbital period decay of $\dot{P} = -20.7 \pm 12.7$ *ms* yr^{-1} (-24.5 ± 15.1 μ*s per orbital cycle). This is significantly faster than those previously measured in the other black hole X-ray binaries A0620-00 and XTE J1118+480. No standard black hole X-ray binary evolutionary model is able to explain this extremely fast orbital decay. At this rate, the secondary star would reach the event horizon (as given by the Schwarzschild radius of about 32 km) in roughly 2.7 Myr. This result has dramatic implications on the evolution and lifetime of black hole X-ray binaries.*

- D. T. Andreasen, S. G. Sousa, M. Tsantaki, G.D.C. Teixeira et al. 2017, A&A, accepted.
  http://www.aanda.org/articles/aa/pdf/forth/aa29967-16.pdf
  Thanks to the importance that the star-planet relation has to our understanding of the planet formation process, the precise determination of stellar parameters for the ever increasing number of discovered extrasolar planets is of great relevance. Furthermore, precise stellar parameters are needed to fully characterize the planet properties. It is thus important to continue the efforts to determine, in the most uniform way possible, the parameters for stars with planets as new discoveries are announced. Aims. In this paper we present new precise atmospheric parameters for a sample of 50 stars with planets. The results are presented in the catalogue: SWEET-Cat. Methods. Stellar atmospheric parameters and masses for the 50 stars were derived assuming local thermodynamic equilibrium (LTE) and using high-resolution and high signal-to-noise spectra. The methodology used is based on the measurement of equivalent widths with ARES2 for a list of iron lines. The line abundances were derived using MOOG. We then used the curve of growth analysis to determine the parameters. We implemented a new minimization procedure which significantly improves the computational time. Results. The stellar parameters for the 50 stars are presented and compared with previously determined literature values. For SWEETCat, we compile values for the effective temperature, surface gravity, metallicity, and stellar mass for almost all the planet host stars listed

in the Extrasolar Planets Encyclopaedia. This data will be updated on a continuous basis. The data can be used for statistical studies of the star-planet correlation, and for the derivation of consistent properties for known planets.

- Delgado-Mena, E., et al. 2017, in preparation.

A

List of Acronyms

CoG	Curve of Growth
ESO	European Southern Observatory
EW	Equivalent width
FEROS	Fiber-Fed, Extended Range, èchelle Spectrograph
FIES	Fibre-Fed Èchelle Spectrograph
FWHM	Full-Width Half Maximum
GCE	Galact Chemical Evolution
HARPS	High Accuracy Radial velocity Planet Searcher
NOT	Nordic Optical Telescope
ORM	Observatorio Roque de los Muchachos
SD	Standard deviation
VLT	Very Large Telescope
UVES	Ultraviolet and Visual Èchelle Spectrograph

B

Nomenclature

c	Light velocity
κ_ν	Absorption coefficient
S_ν	Source function
ρ	Density
τ_ν	Optical depth
$E_2(\tau_\nu)$	Extintion factor
B_ν	Light velocity
l_ν	line absorption coefficient
α	Absorptance

C

Nitrogen abundances

Table C.1: Nitrogen abundances

Star	Teff	logg	Vtur	[Fe/H]	[N/H]	$\sigma_{[N/H]}$
HD 870	5360	4.4	0.79	-0.12	-0.14	0.10
HD 1581	5990	4.49	1.24	-0.18	-0.23	0.10
HD 3823	6054	4.37	1.44	-0.26	-0.36	0.12
HD 8326	4834	4.35	0.44	0.04	-0.05	0.10
HD 8389A	5182	4.33	0.81	0.36	0.23	0.11
HD 9796	5139	4.34	0.49	-0.25	-0.32	0.10
HD 15337	5088	4.36	0.51	0.06	0.01	0.10
HD 16270	4583	4.23	0.16	0.14	0.02	0.11
HD 20807	5875	4.5	1.15	-0.23	-0.17	0.10
HD 21019	5468	3.93	1.1	-0.45	-0.42	0.12
HD 33636	5994	4.71	1.79	-0.08	-0.15	0.11
HD 35854	4808	4.35	0.16	-0.14	-0.37	0.11
HD 37226	6178	4.16	1.61	-0.12	-0.12	0.10
HD 40105	5064	3.69	0.91	0.02	0.10	0.10
HD 44573	4990	4.42	0.61	-0.07	-0.19	0.11
HD 65907A	5995	4.62	1.18	-0.29	-0.24	0.10
HD 72769	5587	4.3	0.86	0.29	0.38	0.11
HD 73121	6083	4.27	1.33	0.09	0.15	0.11
HD 76151	5781	4.44	0.93	0.12	0.21	0.10
HD 103891	6072	4.05	1.5	-0.19	-0.08	0.11
HD 108063	6081	4.11	1.54	0.55	0.74	0.15
HD 119629	6250	4.17	1.73	-0.17	-0.16	0.11
HD 141597	6285	4.38	1.23	-0.4	-0.26	0.14
HD 191033	6206	4.47	1.35	-0.19	-0.08	0.13
HD 205536	5418	4.36	0.79	-0.07	-0.16	0.11
HD 208068	6007	4.64	1.17	-0.38	-0.47	0.13
HD 211415	5864	4.42	1.01	-0.21	-0.27	0.12
HD 213042	4670	4.22	0.35	0.14	0.08	0.11
HD 214094	6288	4.28	1.46	-0.01	-0.01	0.10
HD 220367	6116	4.45	1.44	-0.23	-0.20	0.11
HD 222335	5220	4.48	0.62	-0.21	-0.25	0.10
CD-436810	6011	4.41	1.09	-0.44	-0.31	0.11
HD 142	6431	4.82	2.1	0.05	0.12	0.10
HD 1237	5489	4.46	1.04	0.06	0.07	0.10
HD 2039	5990	4.56	1.24	0.34	0.36	0.10

Continued on next page

Table C.1 – continued from previous page

Star	Teff	logg	Vtur	[Fe/H]	[N/H]	$\sigma_{[N/H]}$
HD 2638	5169	4.41	0.66	0.12	0.13	0.11
HD 4203	5728	4.23	1.18	0.43	0.53	0.11
HD 4208	5600	4.41	0.88	-0.29	-0.32	0.12
HD 16141	5786	4.17	1.1	0.15	0.18	0.10
HD 17051	6237	4.46	1.31	0.2	0.29	0.13
HD 19994	6315	4.44	1.66	0.27	0.38	0.12
HD 20794	5398	4.41	0.7	-0.41	-0.44	0.11
HD 23079	6009	4.5	1.2	-0.11	-0.16	0.10
HD 27894	4833	4.3	0.33	0.26	0.07	0.13
HD 28185	5621	4.36	0.92	0.19	0.24	0.12
HD 30177	5601	4.34	0.89	0.37	0.47	0.14
HD 39091	5991	4.4	1.09	0.09	0.14	0.10
HD 50554	6129	4.41	1.11	0.01	0.10	0.12
HD 52265	6167	4.44	1.28	0.24	0.34	0.12
HD 65216	5614	4.46	0.81	-0.17	-0.17	0.10
HD 63454	4756	4.32	0.31	0.13	0.01	0.11
HD 69830	5370	4.38	0.67	-0.07	-0.06	0.10
HD 70642	5659	4.43	0.81	0.17	0.24	0.11
HD 72659	5926	4.24	1.13	-0.02	0.08	0.10
HD 73256	5465	4.36	1.0	0.21	0.26	0.10
HD 74156	6099	4.34	1.38	0.16	0.26	0.11
HD 75289	6139	4.35	1.22	0.3	0.26	0.12
HD 82943	5992	4.42	1.06	0.28	0.29	0.13
HD 93083	5048	4.32	0.81	0.08	0.09	0.10
HD 106252	5880	4.4	1.13	-0.07	0.00	-0.10
HD 114386	4774	4.37	0.01	-0.09	-0.12	0.10
HD 114729	5865	4.2	1.29	-0.26	-0.26	0.10
HD 117207	5649	4.31	0.95	0.21	0.35	0.10
HD 117618	6003	4.45	1.16	0.03	0.16	0.10
HD 11964A	5285	3.81	0.95	0.06	0.06	0.11
HD 208487	6172	4.54	1.22	0.1	0.16	0.11
HD 210277	5470	4.26	0.9	0.15	0.16	0.10
HD 213240	5967	4.28	1.22	0.13	0.15	0.10
HD 216435	6034	4.21	1.27	0.27	0.38	0.12
HD 216437	5882	4.25	1.25	0.25	0.39	0.11
HD 216770	5351	4.31	0.85	0.2	0.29	0.10
HD 217107	5679	4.32	1.15	0.35	0.39	0.10
HD 222582	5781	4.37	1.02	-0.01	0.05	0.10
HD 330075	4958	4.24	0.32	0.05	-0.05	0.10

D

Carbon abundances

Table D.1: Carbon abundances

Star	Teff	logg	Vtur	[Fe/H]	[C/H]	$\sigma_{[C/H]}$
BD+062932	5272	4.43	0.06	-0.84	-1.11	0.12
BD+063077	6136	4.95	1.07	-0.36	-0.33	0.15
BD+083095	5728	4.12	0.85	-0.77	-0.76	0.20
BD-002387	4833	4.47	0.85	0.03	-0.18	0.13
BD-010184	4728	4.34	0.40	-0.34	-0.42	0.13
BD-012505	4741	4.51	0.44	-0.11	-0.37	0.16
BD-033746	4732	4.63	0.15	-0.90	-0.85	0.17
BD-034797	4622	4.21	0.30	0.06	-0.20	0.22
BD-044138	4604	4.39	0.38	-0.11	-0.33	0.24
BD-050484	4674	4.42	0.21	-0.39	-0.55	0.16
BD-050578	5470	4.39	0.79	0.09	0.04	0.13
BD-053176	4758	4.39	0.82	-0.09	-0.30	0.14
BD-053596	4594	4.32	0.27	-0.34	-0.56	0.20
BD-054065	4895	4.41	0.42	-0.29	-0.36	0.12
BD-060904	5066	4.46	0.46	-0.17	-0.23	0.12
BD-063481	4815	4.36	0.41	-0.14	-0.24	0.13
BD-064196	4688	4.30	0.42	-0.03	-0.22	0.14
BD-064756	4646	4.54	0.70	-0.23	-0.49	0.21
BD-082534	5405	4.43	0.41	-0.78	-0.76	0.12
BD-082823	4816	4.43	0.81	-0.06	-0.23	0.14
BD-084501	6216	4.81	2.36	-1.39	-1.30	0.15
BD-090872	4660	4.35	0.77	-0.19	-0.41	0.14
BD-091261	4717	4.69	0.92	-0.75	-0.88	0.18
BD-092670	4806	4.46	0.51	-0.08	-0.20	0.13
BD-094191	4804	4.44	0.63	-0.32	-0.49	0.14
BD-112763	4911	4.44	0.38	-0.26	-0.34	0.13
BD-120327	4680	4.35	0.57	-0.34	-0.54	0.16
BD-123458	4803	4.86	0.43	-0.83	-1.06	0.15
BD-130116	4615	4.33	0.61	-0.49	-0.80	0.18
BD-130321	4772	4.41	0.78	0.02	-0.21	0.16
BD-131161	5389	4.37	0.68	0.09	0.12	0.12
BD-140184	4714	4.32	0.76	-0.38	-0.52	0.18
BD-145003	4640	4.41	0.35	-0.51	-0.51	0.21
BD-160308	5183	4.48	0.51	-0.41	-0.40	0.13
BD-160931	4840	4.38	0.46	-0.11	-0.24	0.13
BD-170063	4665	4.19	0.57	0.01	-0.27	0.14

Continued on next page

Table D.1 – continued from previous page

Star	Teff	logg	Vtur	[Fe/H]	[C/H]	$\sigma_{[C/H]}$
BD-173242	4627	4.48	0.31	-0.29	-0.57	0.21
BD-195953	4775	4.51	0.71	-0.14	-0.26	0.15
BD-213153	4622	4.38	0.76	-0.17	-0.40	0.18
BD-223528	4747	4.28	0.63	-0.17	-0.33	0.13
CD-2310879	6788	4.67	1.82	-0.24	-0.14	0.16
CD-436810	6011	4.41	1.09	-0.44	-0.47	0.12
CD-4512460	5960	4.42	0.75	-0.86	-0.95	0.14
CD-452997	5312	4.39	0.24	-0.84	-0.79	0.12
CD-571633	5975	4.46	1.14	-0.85	-1.02	0.12
HD 10002	5230	4.28	0.72	0.13	0.12	0.12
HD 100289	5483	4.42	0.70	0.03	-0.02	0.12
HD 100508	5384	4.39	0.86	0.35	0.29	0.12
HD 100777	5530	4.31	0.81	0.25	0.22	0.12
HD 101339	5731	4.48	0.88	-0.10	-0.13	0.12
HD 101367	5615	4.38	0.91	0.29	0.16	0.12
HD 101581	4615	4.40	0.11	-0.51	-0.51	0.23
HD 101612	6281	4.41	1.17	-0.36	-0.40	0.14
HD 101644	5678	4.58	0.72	-0.56	-0.61	0.13
HD 101650	4626	4.29	0.11	-0.45	-0.69	0.28
HD 10166	5187	4.44	0.57	-0.39	-0.43	0.12
HD 10180	5898	4.39	1.11	0.08	0.04	0.11
HD 101930	5083	4.35	0.58	0.16	0.02	0.13
HD 102117	5620	4.28	0.99	0.26	0.21	0.11
HD 102136	5349	4.43	0.75	-0.09	-0.15	0.12
HD 102200	6185	4.59	1.52	-1.10	-1.12	0.13
HD 102300	5987	4.23	1.14	-0.31	-0.34	0.13
HD 102365	5616	4.40	0.91	-0.28	-0.26	0.12
HD 102438	5562	4.43	0.84	-0.29	-0.30	0.12
HD 102843	5432	4.35	0.79	0.16	0.12	0.12
HD 103197	5250	4.45	0.84	0.22	0.19	0.13
HD 103720	5017	4.43	0.90	-0.02	-0.18	0.12
HD 103891	6072	4.05	1.50	-0.19	-0.17	0.13
HD 103949	4774	4.49	0.43	-0.07	-0.14	0.12
HD 104006	5046	4.58	0.28	-0.78	-0.66	0.12
HD 104067	4888	4.35	0.66	-0.04	-0.16	0.13
HD 104263	5456	4.35	0.81	0.01	0.01	0.12
HD 104760A	5953	4.43	1.02	0.12	0.10	0.12
HD 104800	5697	4.47	0.87	-0.79	-0.82	0.12
HD 104982	5682	4.42	0.91	-0.20	-0.28	0.11
HD 105004	5756	4.33	0.80	-0.81	-0.92	0.11
HD 105671	4571	4.41	0.23	0.09	-0.11	0.24
HD 105779	5792	4.51	0.91	-0.25	-0.27	0.12
HD 105837	5932	4.60	1.14	-0.50	-0.53	0.12
HD 105938	6208	4.27	1.60	0.03	-0.05	0.12
HD 106116	5656	4.35	0.91	0.13	0.07	0.11
HD 106275	4978	4.33	0.59	-0.13	-0.20	0.12
HD 106290	6012	4.55	1.03	0.13	0.14	0.12
HD 10647	6222	4.63	1.22	0.01	-0.05	0.12
HD 106589	5597	4.37	0.67	-0.23	-0.20	0.12
HD 10700	5322	4.46	0.56	-0.52	-0.52	0.11
HD 107094	5562	4.54	0.74	-0.51	-0.53	0.11
HD 107148	5744	4.30	0.93	0.28	0.23	0.11
HD 108063	6081	4.11	1.54	0.55	0.45	0.13
HD 108147	6318	4.53	1.30	0.21	0.24	0.12
HD 108309	5781	4.24	1.08	0.13	0.11	0.12
HD 108341	5122	4.45	0.64	0.04	-0.08	0.12
HD 108564	4818	4.67	0.26	-0.97	-0.73	0.13
HD 108768	5633	4.45	0.86	0.14	0.10	0.12

Continued on next page

Table D.1 – continued from previous page

Star	Teff	logg	Vtur	[Fe/H]	[C/H]	$\sigma_{[C/H]}$
HD 108935	4724	4.30	0.55	0.02	-0.19	0.16
HD 10895	5685	4.52	0.78	-0.27	-0.32	0.12
HD 109098	5888	4.14	1.24	0.06	0.07	0.12
HD 109200	5056	4.37	0.56	-0.35	-0.37	0.12
HD 109271	5783	4.28	0.97	0.10	0.10	0.12
HD 109310	5922	4.55	1.15	-0.51	-0.51	0.12
HD 109368	4651	4.36	0.67	-0.23	-0.43	0.21
HD 109409	5833	4.11	1.24	0.31	0.33	0.12
HD 109423	5040	4.39	0.63	-0.06	-0.20	0.12
HD 109684	5992	4.38	1.22	-0.34	-0.36	0.12
HD 109723	5647	4.47	0.88	-0.04	-0.17	0.12
HD 109988	5193	4.46	0.81	0.14	0.07	0.12
HD 110291	5480	4.38	0.69	-0.02	-0.08	0.12
HD 110557	5267	4.36	0.71	-0.06	-0.15	0.12
HD 110619	5615	4.52	0.91	-0.41	-0.40	0.12
HD 110668	5850	4.45	0.98	0.17	0.18	0.12
HD 111031	5749	4.30	1.05	0.26	0.26	0.11
HD 111232	5482	4.46	0.62	-0.43	-0.38	0.11
HD 111515	5398	4.47	0.71	-0.61	-0.54	0.12
HD 111564	6004	4.37	1.13	0.07	0.05	0.12
HD 111777	5666	4.46	0.82	-0.68	-0.69	0.11
HD 112100	5081	4.44	0.50	-0.16	-0.21	0.13
HD 11226	6112	4.35	1.28	0.05	0.10	0.11
HD 112283	6433	4.84	1.86	-0.13	-0.19	0.13
HD 112540	5523	4.48	0.80	-0.17	-0.24	0.12
HD 113101	5456	4.37	0.66	-0.07	-0.10	0.12
HD 113513	5751	4.54	0.94	0.17	0.06	0.13
HD 113569	4994	4.41	0.41	-0.22	-0.28	0.12
HD 113679	5768	4.26	1.08	-0.61	-0.64	0.11
HD 11397	5564	4.46	0.75	-0.54	-0.27	0.13
HD 114076	5069	4.32	0.04	-0.47	-0.52	0.13
HD 114386	4774	4.37	0.01	-0.09	-0.11	0.11
HD 114561	5829	4.50	0.88	-0.07	-0.08	0.13
HD 114613	5712	3.94	1.18	0.18	0.20	0.12
HD 114729	5865	4.20	1.23	-0.26	-0.25	0.11
HD 114747	5086	4.40	0.87	0.21	0.12	0.13
HD 114783	5060	4.37	0.76	0.03	-0.05	0.12
HD 114853	5698	4.43	0.92	-0.23	-0.29	0.11
HD 11505	5757	4.39	0.99	-0.22	-0.20	0.12
HD 115341	6058	4.55	1.10	-0.01	-0.01	0.12
HD 115499	5542	4.45	0.95	0.07	-0.02	0.12
HD 115585	5683	4.19	1.14	0.36	0.36	0.11
HD 115617	5537	4.38	0.81	-0.03	-0.10	0.12
HD 115674	5633	4.43	0.85	-0.18	-0.25	0.11
HD 115773	6312	4.23	1.57	-0.08	-0.09	0.12
HD 115902	5705	4.39	0.86	-0.01	-0.11	0.12
HD 11608	4959	4.32	0.56	0.22	0.10	0.16
HD 116259	5700	4.21	0.99	0.11	0.10	0.12
HD 116284	5213	3.87	0.83	-0.01	-0.06	0.12
HD 116410	5939	4.43	1.07	0.23	0.20	0.12
HD 11683	4957	4.35	0.71	-0.27	-0.44	0.12
HD 116858	4913	4.45	0.54	-0.22	-0.32	0.12
HD 116883	4902	4.36	0.52	-0.20	-0.34	0.13
HD 116920	4928	4.37	0.48	-0.25	-0.34	0.11
HD 116963	4735	4.43	0.51	-0.06	-0.28	0.14
HD 1171	5293	4.47	0.48	-0.53	-0.84	0.12
HD 117105	5912	4.44	1.13	-0.28	-0.33	0.12
HD 117207	5649	4.31	1.01	0.21	0.25	0.11

Continued on next page

Table D.1 – continued from previous page

Star	Teff	logg	Vtur	[Fe/H]	[C/H]	$\sigma_{[C/H]}$
HD 117359	5246	4.43	0.68	-0.13	-0.21	0.13
HD 117618	6003	4.45	1.13	0.03	-0.02	0.11
HD 117938	4738	4.27	0.36	-0.13	-0.36	0.13
HD 118466	5049	4.34	0.49	0.20	0.07	0.14
HD 118563	5477	4.45	0.68	-0.04	-0.14	0.12
HD 119173	5779	4.26	0.52	-0.62	-0.66	0.12
HD 119291	4611	4.22	0.59	-0.10	-0.32	0.22
HD 11938	4703	4.25	0.76	0.01	-0.22	0.14
HD 119503	4885	4.40	0.83	-0.04	-0.21	0.12
HD 119629	6250	4.17	1.73	-0.17	-0.15	0.12
HD 119638	6111	4.48	1.22	-0.13	-0.13	0.11
HD 11964A	5285	3.81	0.99	0.06	0.02	0.11
HD 119782	5120	4.41	0.60	-0.07	-0.20	0.11
HD 119949	6359	4.47	1.65	-0.41	-0.31	0.12
HD 120344	5623	4.42	0.65	-0.19	-0.23	0.12
HD 120362	5517	4.51	1.05	0.10	-0.05	0.12
HD 120491	4680	4.49	0.40	-0.34	-0.50	0.15
HD 121004	5687	4.48	0.76	-0.71	-0.74	0.11
HD 121504	6022	4.52	1.12	0.14	0.08	0.11
HD 122308	5253	4.44	0.59	-0.32	-0.36	0.12
HD 122474	5716	4.37	0.88	0.13	0.02	0.12
HD 122862	6009	4.25	1.29	-0.10	-0.08	0.11
HD 123265	5311	4.31	0.85	0.18	0.16	0.12
HD 123319	5619	4.56	0.67	-0.52	-0.62	0.12
HD 12345	5386	4.42	0.70	-0.22	-0.29	0.12
HD 123517	6082	4.08	1.53	0.09	0.06	0.11
HD 123619	6166	4.45	1.38	-0.32	-0.31	0.13
HD 123651	5926	4.55	1.05	-0.48	-0.48	0.12
HD 1237	5489	4.46	1.04	0.06	-0.11	0.12
HD 12387	5704	4.42	0.93	-0.25	-0.17	0.11
HD 124106	5067	4.48	0.61	-0.17	-0.32	0.12
HD 124292	5426	4.37	0.77	-0.14	-0.17	0.12
HD 124364	5601	4.49	0.83	-0.27	-0.36	0.12
HD 124785	5867	4.20	1.29	-0.56	-0.52	0.12
HD 125072	4794	4.27	0.53	0.24	0.15	0.13
HD 125184	5660	4.11	1.13	0.27	0.22	0.12
HD 125271	4779	4.33	0.36	-0.22	-0.30	0.12
HD 125455	5095	4.40	0.56	-0.21	-0.30	0.12
HD 125522	4839	4.45	0.40	-0.46	-0.45	0.12
HD 125595	4691	4.17	0.32	0.08	-0.05	0.16
HD 125612	5913	4.43	1.02	0.24	0.27	0.12
HD 125881	6046	4.49	1.10	0.07	0.04	0.11
HD 12617	4766	4.31	0.19	0.14	0.00	0.12
HD 126525	5645	4.40	0.90	-0.09	-0.17	0.12
HD 126681	5570	4.70	0.82	-1.15	-1.14	0.12
HD 126793	5904	4.43	1.22	-0.71	-0.66	0.12
HD 126803	5470	4.48	0.56	-0.61	-0.72	0.12
HD 126829	4726	4.51	0.82	-0.14	-0.37	0.14
HD 127124	5079	4.43	0.82	-0.04	-0.21	0.13
HD 128113	4922	4.28	0.35	-0.17	-0.23	0.12
HD 128340	6259	4.64	1.42	-0.55	-0.51	0.12
HD 128431	5429	4.43	0.61	-0.34	-0.36	0.13
HD 128571	6159	4.40	1.23	-0.37	-0.41	0.13
HD 128674	5571	4.50	0.80	-0.37	-0.41	0.12
HD 129191	5832	4.39	0.99	0.24	0.14	0.12
HD 129229	5872	3.89	1.37	-0.42	-0.42	0.11
HD 129642	4919	4.35	0.53	-0.09	-0.22	0.12
HD 129829	6196	4.66	1.30	-0.16	-0.19	0.13

Continued on next page

Table D.1 – continued from previous page

Star	Teff	logg	Vtur	[Fe/H]	[C/H]	$\sigma_{[C/H]}$
HD 130322	5341	4.40	0.81	-0.03	-0.14	0.11
HD 13060	5189	4.31	0.69	0.01	-0.21	0.12
HD 130930	4963	4.39	0.44	-0.01	-0.14	0.12
HD 130989	6414	4.27	1.85	-0.23	-0.23	0.13
HD 130992	4712	4.37	0.31	-0.13	-0.23	0.13
HD 131183	5670	4.24	0.97	0.09	0.13	0.12
HD 131218	5797	4.55	0.96	-0.06	-0.10	0.12
HD 131565	5612	4.47	0.72	-0.16	-0.20	0.13
HD 131653	5324	4.54	0.35	-0.66	-0.67	0.12
HD 131664	5901	4.50	1.04	0.31	0.25	0.12
HD 1320	5699	4.55	0.89	-0.26	-0.29	0.12
HD 132411	4673	4.32	0.31	-0.29	-0.41	0.12
HD 13252	5358	4.33	0.59	-0.25	-0.26	0.12
HD 132569	5026	4.49	0.59	-0.26	-0.38	0.12
HD 132648	5419	4.49	0.76	-0.38	-0.41	0.12
HD 133633	5571	4.48	0.69	-0.45	-0.45	0.12
HD 134060	5940	4.42	1.10	0.12	0.11	0.12
HD 134088	5675	4.46	0.86	-0.75	-0.78	0.12
HD 134113	5782	4.25	1.27	-0.74	-0.69	0.12
HD 134440	4987	4.80	1.03	-1.32	-0.99	0.12
HD 134606	5614	4.30	1.00	0.27	0.21	0.12
HD 134664	5823	4.46	0.99	0.07	0.00	0.11
HD 134702	5782	4.50	0.74	-0.04	-0.20	0.13
HD 134929B	5330	4.36	0.79	0.07	0.02	0.13
HD 134985	5096	4.44	0.09	-0.61	-0.74	0.12
HD 134987	5700	4.22	1.08	0.23	0.28	0.12
HD 135468	6417	4.25	1.82	-0.02	-0.02	0.13
HD 135625	6003	4.32	1.16	0.12	0.10	0.12
HD 13578	5842	4.18	1.12	-0.03	-0.03	0.12
HD 136352	5659	4.40	0.90	-0.35	-0.30	0.11
HD 136713	4911	4.32	0.69	0.08	0.01	0.12
HD 136894	5402	4.37	0.75	-0.11	-0.19	0.12
HD 137010	4797	4.41	0.48	-0.22	-0.36	0.15
HD 13724	5824	4.42	1.02	0.21	0.15	0.11
HD 137303	4632	4.38	0.17	-0.35	-0.35	0.16
HD 137388	5144	4.35	0.93	0.19	0.39	0.12
HD 137676	5253	3.93	0.74	-0.53	-0.59	0.12
HD 13789	4667	4.29	0.30	-0.01	-0.28	0.14
HD 13808	5033	4.36	0.63	-0.21	-0.31	0.12
HD 138549	5552	4.40	0.87	-0.01	-0.09	0.11
HD 138799	5224	4.36	0.71	0.02	-0.07	0.13
HD 1388	5970	4.42	1.13	0.00	-0.05	0.12
HD 138914	4983	4.38	0.66	-0.12	-0.25	0.13
HD 139189	5075	4.41	0.78	0.02	-0.08	0.12
HD 139332	4899	4.30	0.04	0.00	-0.16	0.13
HD 139536	5209	4.71	1.13	-0.04	-0.22	0.14
HD 139590	6200	4.49	1.31	0.13	0.14	0.12
HD 139710	5123	4.41	0.90	-0.08	-0.20	0.12
HD 139879	6203	4.61	1.25	0.30	0.30	0.12
HD 140785	5756	4.12	1.09	-0.05	-0.11	0.12
HD 140901	5584	4.40	0.90	0.08	0.00	0.11
HD 141128	6758	4.67	1.65	0.07	0.16	0.14
HD 141597	6285	4.38	1.23	-0.40	-0.31	0.13
HD 141598	5593	4.37	0.75	-0.10	-0.07	0.13
HD 141624	5871	4.40	1.01	-0.38	-0.44	0.12
HD 141937	5892	4.46	1.00	0.13	0.14	0.11
HD 142	6431	4.82	1.74	0.05	0.06	0.15
HD 142022A	5482	4.35	0.83	0.18	0.15	0.12

Continued on next page

Table D.1 – continued from previous page

Star	Teff	logg	Vtur	[Fe/H]	[C/H]	$\sigma_{[C/H]}$
HD 142709	4536	4.21	0.35	-0.31	-0.43	0.17
HD 142879	5707	4.51	0.74	-0.39	-0.48	0.12
HD 143114	5811	4.46	0.92	-0.41	-0.39	0.12
HD 143295	4940	4.40	0.64	-0.01	-0.20	0.11
HD 143638	5954	4.48	1.04	-0.27	-0.27	0.12
HD 14374	5375	4.42	0.78	-0.07	-0.18	0.12
HD 143790	6557	4.11	2.05	-0.06	-0.02	0.14
HD 144342	5403	4.47	0.90	0.07	-0.04	0.12
HD 144411	4839	4.45	0.23	-0.32	-0.39	0.12
HD 144497	4953	4.52	0.61	-0.11	-0.24	0.12
HD 14452	5313	4.50	0.85	-0.16	-0.26	0.12
HD 144585	5880	4.32	1.15	0.32	0.25	0.11
HD 144589	6372	4.28	1.72	-0.05	-0.08	0.12
HD 144628	5022	4.43	0.43	-0.45	-0.46	0.12
HD 144846	6102	4.52	1.11	0.13	0.15	0.11
HD 144880	6152	4.38	1.33	-0.30	-0.33	0.12
HD 145344	6143	4.39	1.48	-0.68	-0.62	0.12
HD 145377	6054	4.53	1.11	0.12	0.14	0.12
HD 145417	5006	4.82	0.65	-1.23	-0.98	0.12
HD 145598	5465	4.59	0.63	-0.75	-0.73	0.12
HD 145666	5984	4.56	1.04	-0.02	-0.05	0.12
HD 145809	5778	4.15	1.14	-0.25	-0.25	0.12
HD 145927	5819	4.41	0.93	-0.03	0.00	0.12
HD 1461	5740	4.36	0.97	0.18	0.12	0.11
HD 146233	5810	4.46	1.00	0.05	0.00	0.12
HD 14635	4685	4.27	0.51	0.00	-0.22	0.13
HD 14680	4913	4.33	0.48	-0.18	-0.28	0.12
HD 147147	4856	4.51	0.71	-0.17	-0.33	0.12
HD 147195	5557	4.48	0.68	-0.05	-0.12	0.12
HD 14744	4871	4.38	0.51	-0.17	-0.30	0.12
HD 14745	6290	4.72	1.46	-0.14	-0.17	0.13
HD 14747	5547	4.46	0.72	-0.37	-0.34	0.12
HD 147512	5515	4.40	0.81	-0.09	-0.12	0.11
HD 147513	5907	4.58	1.39	0.12	-0.04	0.13
HD 147518	5626	4.40	0.67	-0.63	-0.61	0.16
HD 148156	6251	4.51	1.36	0.25	0.25	0.12
HD 148211	5948	4.36	1.40	-0.62	-0.55	0.12
HD 148303	4829	4.44	0.55	-0.03	-0.17	0.12
HD 148577	5713	4.29	0.95	-0.09	-0.07	0.12
HD 14868	5864	4.44	0.90	0.02	-0.11	0.12
HD 148816	5908	4.39	1.36	-0.71	-0.64	0.12
HD 149200	6416	4.64	1.74	0.15	0.03	0.13
HD 149396	5657	4.47	0.91	0.19	0.10	0.12
HD 149724	5747	4.24	1.08	0.37	0.36	0.13
HD 149747	5823	3.95	1.28	-0.34	-0.32	0.12
HD 150139	5968	4.29	1.29	-0.51	-0.53	0.12
HD 150177	6216	4.18	1.76	-0.58	-0.50	0.11
HD 150433	5680	4.48	0.88	-0.36	-0.36	0.12
HD 150437	5826	4.29	1.09	0.30	0.30	0.12
HD 150474	5425	4.01	0.96	0.01	-0.01	0.13
HD 151504	5431	4.35	0.87	0.06	0.00	0.13
HD 151692	4737	4.40	0.55	-0.07	-0.27	0.14
HD 151772	6631	4.81	2.27	-0.36	-0.26	0.13
HD 151933	5849	4.29	1.03	-0.21	-0.23	0.12
HD 152433	6144	4.49	1.19	-0.10	-0.15	0.12
HD 152533	4822	4.36	0.40	-0.04	-0.17	0.14
HD 153276	6000	4.48	1.12	0.04	0.16	0.13
HD 15337	5088	4.36	0.51	0.06	-0.03	0.12

Continued on next page

Table D.1 – continued from previous page

Star	Teff	logg	Vtur	[Fe/H]	[C/H]	$\sigma_{[C/H]}$
HD 153851	5015	4.43	0.81	-0.28	-0.38	0.12
HD 153950	6074	4.39	1.23	-0.01	-0.11	0.12
HD 154088	5337	4.35	0.85	0.26	0.24	0.11
HD 154195A	5961	4.48	1.01	-0.19	-0.25	0.13
HD 154363	4581	4.17	0.14	-0.62	-0.88	0.22
HD 154387	4719	4.50	0.08	-0.25	-0.47	0.14
HD 154577	4847	4.48	0.31	-0.73	-0.59	0.11
HD 154962	5778	4.12	1.22	0.30	0.32	0.12
HD 155717	4949	4.48	0.76	-0.13	-0.29	0.12
HD 155968	5790	4.42	0.92	0.16	0.15	0.13
HD 156079	5892	4.24	1.16	0.28	0.23	0.12
HD 156098	6517	4.20	2.06	0.18	0.11	0.13
HD 15612	5256	4.49	0.87	-0.11	-0.24	0.12
HD 156411	5910	3.99	1.31	-0.11	-0.11	0.12
HD 156423	5184	4.46	0.21	-0.43	-0.47	0.13
HD 156517	5013	4.45	0.81	0.03	-0.09	0.12
HD 156991	5934	4.57	0.99	-0.07	-0.09	0.12
HD 157172	5419	4.32	0.77	0.09	0.07	0.12
HD 157338	6037	4.49	1.17	-0.07	-0.10	0.11
HD 157347	5667	4.38	0.91	0.01	-0.07	0.11
HD 157668	5195	4.49	0.65	-0.23	-0.27	0.13
HD 157830	5549	4.50	0.80	-0.24	-0.32	0.12
HD 1581	5990	4.49	1.12	-0.18	-0.23	0.11
HD 15906	4884	4.49	0.65	-0.01	-0.15	0.13
HD 159868	5552	3.91	1.05	-0.09	-0.11	0.12
HD 16008	5712	4.42	0.78	-0.09	-0.38	0.13
HD 160089	6312	4.78	1.60	0.11	0.12	0.13
HD 160691	5750	4.19	1.09	0.29	0.30	0.12
HD 160836	4791	4.49	0.92	-0.16	-0.36	0.14
HD 161098	5574	4.49	0.81	-0.26	-0.33	0.11
HD 161256	5652	4.27	0.93	0.14	0.17	0.13
HD 16141	5786	4.17	1.11	0.15	0.13	0.11
HD 161555	5850	4.15	1.23	0.12	0.12	0.13
HD 161566	6230	4.20	1.67	-0.28	-0.24	0.12
HD 161612	5594	4.42	0.88	0.16	0.07	0.11
HD 162020	4723	4.31	0.51	-0.10	-0.27	0.11
HD 162236	5336	4.42	0.82	-0.12	-0.18	0.12
HD 162396	6121	4.33	1.43	-0.34	-0.31	0.12
HD 16270	4583	4.23	0.16	0.14	0.00	0.14
HD 16280	4754	4.39	0.56	-0.19	-0.36	0.13
HD 16297	5379	4.44	0.78	-0.03	-0.17	0.12
HD 163102	6433	4.64	1.94	0.00	-0.05	0.13
HD 163436	5030	4.43	0.45	-0.07	-0.26	0.12
HD 16382	5953	4.50	1.04	0.03	0.02	0.12
HD 16417	5843	4.16	1.18	0.14	0.13	0.11
HD 165131	5870	4.45	0.99	0.06	0.06	0.12
HD 16536	5282	4.39	0.70	-0.08	-0.17	0.13
HD 16548	5690	3.96	1.15	0.15	0.02	0.12
HD 165920	5286	4.36	0.79	0.27	0.24	0.13
HD 166724	5099	4.43	0.64	-0.09	-0.26	0.12
HD 166745	5621	4.31	0.98	0.25	0.24	0.12
HD 16714	5541	4.45	0.74	-0.18	-0.18	0.12
HD 167300	5837	4.30	1.05	-0.45	-0.41	0.11
HD 167359	5357	4.46	0.72	-0.20	-0.29	0.12
HD 167677	5474	4.43	0.65	-0.29	-0.30	0.12
HD 16784	5837	4.34	1.14	-0.65	-0.66	0.11
HD 168159	4618	4.33	0.54	-0.12	-0.28	0.21
HD 168746	5561	4.31	0.81	-0.11	-0.17	0.11

Continued on next page

Table D.1 – continued from previous page

Star	Teff	logg	Vtur	[Fe/H]	[C/H]	$\sigma_{[C/H]}$
HD 168769	5361	4.45	0.87	-0.01	-0.13	0.12
HD 168863	4905	4.40	0.56	0.16	0.03	0.15
HD 168870	5325	4.43	0.67	-0.32	-0.37	0.13
HD 168871	5986	4.44	1.17	-0.09	-0.10	0.11
HD 16905	4867	4.35	0.51	0.15	0.01	0.14
HD 169830	6370	4.20	1.56	0.18	0.24	0.11
HD 170493	4658	4.29	0.07	0.22	0.08	0.15
HD 17051	6237	4.46	1.29	0.20	0.19	0.12
HD 170958	5599	4.83	1.38	-0.04	-0.16	0.12
HD 171028	5671	3.84	1.24	-0.48	-0.53	0.11
HD 171587	5412	4.59	0.76	-0.64	-0.58	0.12
HD 171665	5652	4.44	0.89	-0.05	-0.10	0.12
HD 171825	4908	4.48	0.39	-0.12	-0.29	0.12
HD 171942	5615	4.42	0.72	-0.10	-0.18	0.12
HD 171990	6048	4.15	1.40	0.06	0.10	0.12
HD 172513	5487	4.46	0.79	-0.07	-0.20	0.12
HD 172568	5728	4.58	0.78	-0.37	-0.36	0.12
HD 172643	5645	4.50	0.73	-0.15	-0.17	0.12
HD 173885	6264	4.37	1.61	-0.20	-0.15	0.12
HD 174153	6196	4.49	1.34	-0.08	-0.08	0.12
HD 17439	5721	4.44	0.87	0.08	0.03	0.12
HD 174545	5199	4.40	0.88	0.22	0.26	0.13
HD 175179	5764	4.46	0.88	-0.66	-0.61	0.12
HD 17548	6011	4.44	1.18	-0.53	-0.46	0.12
HD 175607	5392	4.51	0.60	-0.62	-0.62	0.12
HD 176157	5170	4.36	0.69	-0.15	-0.25	0.13
HD 176354	5271	3.84	1.07	0.27	0.23	0.13
HD 176535	4727	4.36	0.54	-0.15	-0.27	0.13
HD 176666	6103	4.63	1.18	-0.37	-0.43	0.12
HD 176986	4931	4.44	0.56	0.03	-0.07	0.12
HD 177033	4918	4.50	0.45	-0.13	-0.24	0.12
HD 177122	6021	4.52	1.03	-0.10	-0.14	0.12
HD 177409	5896	4.51	0.99	-0.04	-0.14	0.11
HD 177565	5614	4.39	0.91	0.08	0.08	0.11
HD 177758	5933	4.51	1.11	-0.54	-0.47	0.12
HD 17865	5877	4.32	1.16	-0.57	-0.50	0.12
HD 178904	5727	4.41	0.98	0.09	0.11	0.12
HD 179346	6229	4.76	1.35	-0.03	0.01	0.12
HD 17970	5038	4.39	0.20	-0.45	-0.48	0.12
HD 179949	6312	4.56	1.36	0.23	0.27	0.12
HD 18001	5772	4.44	0.80	-0.07	-0.18	0.12
HD 180409	6031	4.51	1.16	-0.15	-0.16	0.12
HD 18083	6144	4.70	1.33	0.03	0.02	0.13
HD 181249	4906	4.25	0.24	-0.13	-0.26	0.12
HD 181428	6151	4.45	1.29	0.06	0.06	0.12
HD 181433	4879	4.40	0.50	0.36	0.27	0.18
HD 181720	5792	4.25	1.16	-0.53	-0.51	0.12
HD 183658	5809	4.40	1.00	0.03	0.03	0.12
HD 183783	4547	4.27	0.22	-0.21	-0.36	0.16
HD 18386	5446	4.37	0.92	0.14	0.03	0.12
HD 183870	4961	4.41	0.65	-0.09	-0.21	0.13
HD 185283	4848	4.37	0.27	-0.06	-0.15	0.15
HD 185615	5555	4.33	0.84	0.08	0.08	0.12
HD 186061	4916	4.36	0.42	-0.05	-0.18	0.12
HD 186302	5662	4.44	0.78	-0.03	-0.07	0.12
HD 18719	5211	4.39	0.80	-0.09	-0.24	0.12
HD 187456	4739	4.20	0.00	0.06	-0.10	0.14
HD 187760	4618	4.45	0.23	-0.32	-0.45	0.17

Continued on next page

Table D.1 – continued from previous page

Star	Teff	logg	Vtur	[Fe/H]	[C/H]	$\sigma_{[C/H]}$
HD 18777	5058	4.39	0.57	0.01	-0.07	0.13
HD 188091	5120	4.32	0.87	0.08	0.00	0.13
HD 18822	5272	4.43	0.87	-0.07	-0.16	0.13
HD 18838	5500	4.48	0.64	-0.17	-0.17	0.12
HD 188559	4693	4.34	0.08	-0.03	-0.18	0.14
HD 188748	5616	4.45	0.83	-0.13	-0.21	0.12
HD 188815	6217	4.34	1.31	-0.53	-0.55	0.14
HD 189004	5094	4.36	0.67	-0.07	-0.22	0.12
HD 189242	4891	4.44	0.51	-0.38	-0.47	0.11
HD 189567	5718	4.39	0.95	-0.25	-0.20	0.12
HD 189625	5848	4.43	1.03	0.19	0.09	0.12
HD 189987	4746	4.25	0.09	-0.06	-0.18	0.13
HD 190204	5476	4.63	1.14	-0.02	-0.12	0.13
HD 190248	5566	4.24	0.99	0.32	0.30	0.12
HD 19034	5526	4.49	0.71	-0.45	-0.44	0.12
HD 190524	5825	4.50	0.85	-0.13	-0.08	0.12
HD 190613	5776	4.33	0.95	0.00	-0.05	0.12
HD 190647	5636	4.18	0.99	0.23	0.24	0.11
HD 190954	5430	4.44	0.74	-0.43	-0.47	0.12
HD 190984	6007	4.02	1.58	-0.49	-0.43	0.11
HD 191033	6206	4.47	1.35	-0.19	-0.22	0.12
HD 191285	4634	4.41	0.38	-0.28	-0.45	0.20
HD 191797	5061	4.50	0.86	-0.06	-0.22	0.12
HD 191847	5020	4.39	0.55	-0.16	-0.20	0.12
HD 191902	4691	4.25	0.31	-0.18	-0.37	0.13
HD 192031	5212	4.46	0.21	-0.83	-0.80	0.12
HD 192117	5433	4.42	0.74	-0.07	-0.22	0.12
HD 19230	5254	4.63	0.46	-0.57	-0.56	0.13
HD 192310	5099	4.43	0.73	-0.03	-0.14	0.12
HD 192865	6307	4.44	1.59	0.13	0.16	0.12
HD 192961	4418	4.23	0.02	-0.30	-0.42	0.18
HD 193193	5979	4.40	1.15	-0.05	-0.07	0.11
HD 193406	4728	4.50	0.54	-0.34	-0.47	0.14
HD 193844	4933	4.38	0.48	-0.34	-0.40	0.11
HD 193901	5611	4.41	0.54	-1.07	-1.28	0.12
HD 19423	5752	4.23	0.96	-0.09	-0.10	0.12
HD 19467	5718	4.29	0.96	-0.15	-0.14	0.11
HD 194717	5247	4.26	0.33	-0.28	-0.33	0.13
HD 195145	5625	4.41	0.82	0.17	0.10	0.12
HD 195200	6201	4.44	1.25	-0.08	-0.10	0.12
HD 195302	5039	4.42	0.56	0.03	-0.10	0.12
HD 195564	5663	4.02	1.11	0.05	0.00	0.11
HD 195633	6154	4.25	1.47	-0.51	-0.46	0.12
HD 196050	5871	4.26	1.21	0.23	0.21	0.11
HD 196384	6611	4.79	1.78	-0.13	-0.10	0.14
HD 196397	5378	4.33	0.68	0.29	0.28	0.13
HD 19641	5806	4.39	0.94	-0.01	-0.05	0.12
HD 196761	5414	4.46	0.76	-0.31	-0.35	0.12
HD 196800	6007	4.40	1.17	0.18	0.20	0.11
HD 196892	6072	4.50	1.21	-0.89	-0.84	0.12
HD 197083	5735	4.50	0.90	-0.45	-0.51	0.11
HD 197197	5812	4.20	1.25	-0.46	-0.56	0.11
HD 197210	5563	4.42	0.81	-0.04	-0.09	0.11
HD 197300	6022	4.69	1.21	0.02	-0.04	0.12
HD 197536	6105	4.39	1.34	-0.41	-0.43	0.11
HD 197823	5344	4.37	0.82	0.10	-0.03	0.12
HD 1979	5626	4.52	0.74	-0.09	0.07	0.12
HD 197921	4913	4.36	0.34	0.13	-0.03	0.13

Continued on next page

Table D.1 – continued from previous page

Star	Teff	logg	Vtur	[Fe/H]	[C/H]	$\sigma_{[C/H]}$
HD 198075	5842	4.55	0.95	-0.24	-0.33	0.11
HD 199086	6149	4.65	1.21	0.18	0.06	0.12
HD 199190	5937	4.27	1.14	0.15	0.19	0.12
HD 199288	5776	4.51	0.93	-0.63	-0.60	0.12
HD 199289	5928	4.64	1.30	-0.98	-0.97	0.12
HD 199604	5817	4.34	1.04	-0.62	-0.62	0.11
HD 199847	5763	4.22	1.04	-0.54	-0.50	0.12
HD 199868	6152	4.45	1.26	-0.13	-0.16	0.12
HD 199933	4608	4.29	0.32	-0.11	-0.28	0.15
HD 19994	6315	4.44	1.72	0.27	0.34	0.13
HD 199960	5928	4.42	1.13	0.27	0.23	0.12
HD 20003	5465	4.37	0.83	0.03	-0.07	0.12
HD 200083	4828	4.42	0.42	-0.09	-0.21	0.14
HD 200143	5112	4.46	0.96	0.02	-0.19	0.12
HD 200349	4844	4.50	0.59	-0.26	-0.38	0.13
HD 200505	5035	4.45	0.80	-0.46	-0.55	0.12
HD 200538	6042	4.38	1.22	0.10	0.07	0.12
HD 200633	5853	4.51	1.01	0.05	0.01	0.12
HD 201161	4884	4.36	0.63	-0.04	-0.15	0.13
HD 2014	5054	4.37	0.64	-0.07	-0.13	0.12
HD 201422	5841	4.63	0.98	-0.16	-0.26	0.12
HD 201496	5974	4.44	1.12	-0.04	0.01	0.12
HD 202206	5708	4.38	1.01	0.28	0.17	0.11
HD 202209	6009	4.68	1.19	-0.01	-0.05	0.12
HD 202389	4732	4.43	0.49	-0.25	-0.43	0.14
HD 2025	4851	4.49	0.51	-0.37	-0.42	0.12
HD 202605	5637	4.47	1.02	0.18	0.08	0.12
HD 202819	4737	4.40	0.59	-0.26	-0.46	0.15
HD 202871	6055	4.54	1.04	-0.09	-0.17	0.12
HD 203335	6306	4.56	1.44	-0.04	0.01	0.13
HD 203384	5564	4.42	0.90	0.26	0.28	0.12
HD 203413	4668	4.36	0.18	0.08	-0.15	0.13
HD 203432	5591	4.29	0.98	0.27	0.30	0.12
HD 203771	4963	4.43	0.50	0.13	0.08	0.14
HD 203850	4808	4.45	0.13	-0.71	-0.57	0.12
HD 203897	5184	4.42	0.65	-0.18	-0.28	0.12
HD 20407	5885	4.52	1.09	-0.43	-0.41	0.12
HD 204287	5743	4.15	1.10	-0.04	-0.11	0.12
HD 204313	5732	4.33	1.00	0.16	0.16	0.11
HD 204385	6048	4.45	1.15	0.08	0.06	0.11
HD 20492	4770	4.30	0.59	0.02	-0.14	0.15
HD 204941	4997	4.36	0.44	-0.20	-0.28	0.12
HD 205294	6370	4.30	1.71	-0.25	-0.21	0.13
HD 205536	5418	4.36	0.79	-0.07	-0.10	0.12
HD 205591	6575	4.75	1.85	-0.08	0.00	0.13
HD 206116	6231	4.57	1.36	0.24	0.27	0.12
HD 206163	5506	4.42	0.94	0.02	-0.09	0.11
HD 206172	5626	4.53	0.82	-0.23	-0.28	0.12
HD 20619	5716	4.51	0.92	-0.21	-0.26	0.12
HD 206630	4853	4.48	0.06	-0.41	-0.43	0.14
HD 206998	5822	4.24	1.13	-0.69	-0.69	0.13
HD 2071	5729	4.49	0.95	-0.08	-0.10	0.11
HD 207129	5946	4.48	1.06	0.01	-0.06	0.11
HD 207190	6178	4.33	1.51	-0.42	-0.43	0.12
HD 207583	5525	4.42	0.93	0.02	-0.09	0.11
HD 207699	4874	4.36	0.63	-0.12	-0.24	0.13
HD 207700	5660	4.26	0.98	0.04	0.06	0.13
HD 20781	5236	4.31	0.77	-0.12	-0.20	0.12

Continued on next page

Table D.1 – continued from previous page

Star	Teff	logg	Vtur	[Fe/H]	[C/H]	$\sigma_{[C/H]}$
HD 20782	5770	4.35	1.00	-0.06	-0.08	0.11
HD 207832	5718	4.45	0.86	0.15	0.12	0.12
HD 207869	5527	4.50	0.73	-0.45	-0.45	0.12
HD 20794	5398	4.41	0.67	-0.41	-0.41	0.12
HD 207970	5524	4.36	0.80	0.05	-0.01	0.12
HD 208	5914	4.47	1.05	-0.31	-0.22	0.12
HD 208068	6007	4.64	1.17	-0.38	-0.49	0.12
HD 20807	5875	4.50	1.04	-0.23	-0.24	0.12
HD 208272	5167	4.41	0.78	-0.07	-0.21	0.13
HD 208487	6172	4.54	1.24	0.10	0.12	0.12
HD 20852	6813	4.76	2.34	-0.35	-0.30	0.23
HD 208573	4744	4.25	0.28	0.05	-0.07	0.12
HD 208672	5986	4.61	1.07	0.13	0.095	0.12
HD 20868	4802	4.26	0.55	0.05	-0.12	0.15
HD 208704	5835	4.38	1.04	-0.08	-0.09	0.11
HD 209100	4649	4.44	0.28	-0.13	-0.22	0.15
HD 209449	5854	4.16	1.19	0.41	0.36	0.12
HD 209458	6182	4.58	1.25	0.06	0.02	0.11
HD 209566	5500	4.38	0.75	0.12	0.11	0.12
HD 209742	5054	4.37	0.47	-0.17	-0.27	0.12
HD 21019	5468	3.93	1.05	-0.45	-0.46	0.12
HD 210272	5713	4.13	1.16	-0.22	-0.19	0.12
HD 210277	5470	4.26	0.86	0.15	0.27	0.12
HD 210320	5597	4.31	0.87	0.11	0.06	0.12
HD 210329	4965	4.40	0.45	-0.18	-0.25	0.13
HD 210507	4998	4.42	0.69	0.07	-0.07	0.12
HD 210573	4918	4.48	0.68	-0.07	-0.21	0.13
HD 210752	5970	4.52	1.20	-0.55	-0.60	0.12
HD 210918	5747	4.35	0.99	-0.10	-0.09	0.12
HD 210975	4678	4.25	0.36	-0.45	-0.55	0.14
HD 211038	4974	3.67	0.78	-0.27	-0.35	0.12
HD 211188	5053	4.41	0.42	-0.12	-0.18	0.12
HD 211317	5965	4.30	1.21	0.27	0.29	0.12
HD 21132	6243	4.60	1.44	-0.37	-0.40	0.12
HD 211369	4868	4.41	0.29	0.07	-0.07	0.12
HD 211415	5864	4.42	0.99	-0.21	-0.25	0.11
HD 211534	5032	4.43	0.14	-0.31	-0.33	0.12
HD 211583	4761	4.39	0.26	0.05	-0.12	0.15
HD 21161	5923	4.24	1.14	0.09	0.11	0.12
HD 212036	5687	4.41	0.80	-0.01	-0.07	0.12
HD 21209A	4612	4.28	0.33	-0.39	-0.42	0.16
HD 212231	5762	4.20	1.01	-0.30	-0.28	0.12
HD 212301	6299	4.58	1.29	0.20	0.19	0.12
HD 21251	4920	4.41	0.68	-0.09	-0.24	0.12
HD 212563	4954	4.45	0.69	-0.03	-0.22	0.11
HD 212580	5099	4.38	0.61	-0.10	-0.17	0.12
HD 212708	5644	4.31	0.99	0.26	0.26	0.11
HD 212918	5051	4.48	0.41	-0.21	-0.29	0.13
HD 213042	4670	4.22	0.35	0.14	-0.02	0.14
HD 213240	5967	4.28	1.25	0.13	0.10	0.11
HD 213575	5676	4.22	1.02	-0.15	-0.10	0.12
HD 213628	5517	4.40	0.83	-0.01	-0.07	0.14
HD 213852	4943	4.24	0.40	0.15	0.09	0.13
HD 213941	5565	4.45	0.72	-0.44	-0.47	0.12
HD 214094	6288	4.28	1.46	-0.01	0.06	0.11
HD 21411	5458	4.51	0.81	-0.27	-0.37	0.12
HD 214383	4876	4.47	0.59	-0.16	-0.27	0.11
HD 214385	5679	4.47	0.81	-0.33	-0.33	0.12

Continued on next page

Table D.1 – continued from previous page

Star	Teff	logg	Vtur	[Fe/H]	[C/H]	$\sigma_{[C/H]}$
HD 214759	5397	4.27	0.85	0.15	0.14	0.12
HD 214867	5807	4.66	1.23	0.01	-0.11	0.12
HD 214954	5738	4.48	0.99	0.14	0.16	0.13
HD 214998	4847	4.37	0.77	0.06	-0.11	0.13
HD 215152	4803	4.26	0.28	-0.08	-0.19	0.18
HD 215257	6052	4.46	1.40	-0.63	-0.61	0.12
HD 215456	5798	4.14	1.19	-0.08	-0.08	0.12
HD 215497	5110	4.40	0.90	0.20	0.09	0.13
HD 215625	6282	4.58	1.35	0.10	0.05	0.12
HD 215722	4728	4.40	0.71	-0.10	-0.32	0.16
HD 215902	5454	4.46	0.53	-0.25	-0.32	0.12
HD 215906	6259	4.56	1.55	-0.28	-0.30	0.13
HD 216008	5773	4.38	0.91	-0.04	-0.15	0.12
HD 216215	5220	4.45	0.58	-0.20	-0.24	0.13
HD 216435	6034	4.21	1.34	0.27	0.28	0.12
HD 216770	5351	4.31	0.91	0.20	0.19	0.11
HD 216777	5654	4.56	0.88	-0.37	-0.42	0.12
HD 21693	5418	4.38	0.76	0.00	-0.05	0.12
HD 217221	5184	4.45	0.77	0.01	-0.10	0.13
HD 217395	5916	4.52	0.95	-0.13	-0.14	0.12
HD 21749	4562	4.24	0.28	0.02	-0.22	0.18
HD 21759	5142	4.49	0.43	-0.61	-0.46	0.13
HD 217786	5966	4.35	1.12	-0.14	-0.12	0.12
HD 217958	5970	4.45	1.29	0.28	0.32	0.13
HD 218249	4956	4.41	0.33	-0.43	-0.44	0.13
HD 218340	5889	4.42	0.97	0.09	0.05	0.12
HD 218379	5938	4.11	1.24	0.15	0.21	0.12
HD 218504	5962	4.34	1.21	-0.55	-0.53	0.12
HD 218511	4424	4.52	0.26	-0.05	-0.32	0.18
HD 218572	4697	4.41	0.33	-0.58	-0.52	0.12
HD 218750	5166	4.39	0.57	0.08	0.00	0.12
HD 218885	5763	4.46	0.80	-0.28	-0.35	0.12
HD 219077	5338	3.92	0.97	-0.15	-0.35	0.12
HD 219249	5494	4.51	0.79	-0.39	-0.40	0.12
HD 21938	5800	4.41	0.99	-0.47	-0.42	0.12
HD 219495	4787	4.40	0.93	0.13	-0.17	0.17
HD 21977	5930	4.45	1.03	0.10	0.14	0.12
HD 220256	5090	4.32	0.53	-0.14	-0.23	0.12
HD 220339	4938	4.42	0.50	-0.37	-0.40	0.12
HD 220367	6116	4.45	1.34	-0.23	-0.21	0.12
HD 220456	5887	4.50	1.01	-0.02	-0.12	0.12
HD 22049	5049	4.45	0.83	-0.15	-0.26	0.11
HD 220507	5676	4.30	1.01	0.00	0.04	0.12
HD 220894	6282	4.60	1.35	0.02	0.02	0.13
HD 221146	5899	4.36	1.09	0.10	0.07	0.11
HD 221287	6417	4.60	1.29	0.06	-0.02	0.12
HD 221343	5848	4.54	0.99	0.11	0.15	0.12
HD 221356	6100	4.51	1.12	-0.20	-0.30	0.12
HD 221420	5838	3.98	1.28	0.34	0.34	0.11
HD 221638	6360	4.53	1.43	-0.21	-0.24	0.13
HD 22177	5666	4.26	1.02	0.20	0.20	0.12
HD 221974	5170	4.30	0.74	0.30	0.24	0.14
HD 222237	4722	4.34	0.13	-0.39	-0.44	0.12
HD 222335	5220	4.48	0.62	-0.21	-0.31	0.12
HD 222422	5435	4.43	0.77	-0.15	-0.26	0.12
HD 22249	5773	4.63	0.96	-0.06	-0.14	0.12
HD 222582	5781	4.37	1.00	-0.01	-0.03	0.11
HD 222595	5618	4.43	0.88	-0.01	-0.07	0.12

Continued on next page

Table D.1 – continued from previous page

Star	Teff	logg	Vtur	[Fe/H]	[C/H]	$\sigma_{[C/H]}$
HD 222669	5898	4.44	1.01	0.06	0.07	0.11
HD 222721	5361	4.43	0.52	-0.31	-0.36	0.13
HD 22282	5433	4.32	0.77	0.12	0.11	0.12
HD 223121	4958	4.28	0.43	0.06	-0.06	0.12
HD 223171	5830	4.16	1.12	0.11	0.16	0.11
HD 223272	5118	4.41	0.58	0.13	0.09	0.13
HD 223282	5343	4.50	0.63	-0.41	-0.46	0.12
HD 223315	5650	4.44	0.89	0.30	0.22	0.12
HD 223854	6080	4.08	1.60	-0.54	-0.54	0.12
HD 224047	5167	4.43	0.62	-0.23	-0.28	0.12
HD 224063	5591	4.27	0.84	0.14	0.04	0.12
HD 224230	4944	4.47	0.56	-0.10	-0.20	0.14
HD 224287	5330	4.38	0.59	-0.29	-0.37	0.12
HD 224347	6092	4.27	1.31	-0.42	-0.44	0.12
HD 224393	5792	4.54	0.96	-0.37	-0.46	0.12
HD 224432	4828	4.38	0.58	-0.06	-0.22	0.12
HD 224433	5527	4.42	0.72	0.09	0.13	0.12
HD 224578	6158	4.67	1.13	-0.01	-0.03	0.12
HD 224619	5425	4.40	0.79	-0.20	-0.24	0.12
HD 224685	5504	4.47	0.76	-0.40	-0.40	0.13
HD 224789	5150	4.40	0.93	-0.04	-0.20	0.12
HD 224817	5894	4.36	1.13	-0.53	-0.49	0.11
HD 225297	6181	4.55	1.24	-0.09	-0.12	0.12
HD 22610	4981	4.41	0.64	-0.22	-0.33	0.12
HD 22879	5949	4.68	1.20	-0.79	-0.70	0.12
HD 22897	4837	4.44	0.69	-0.25	-0.41	0.14
HD 22918	4924	3.61	0.73	0.02	-0.16	0.13
HD 23030	5951	4.37	1.22	0.20	0.25	0.12
HD 23079	6009	4.50	1.12	-0.11	-0.18	0.11
HD 23249	5027	3.66	0.93	0.07	-0.01	0.13
HD 23356	4919	4.45	0.52	-0.15	-0.27	0.12
HD 23456	6190	4.61	1.38	-0.31	-0.35	0.12
HD 23472	4813	4.38	0.43	-0.19	-0.38	0.14
HD 23901	5264	3.93	0.84	-0.40	-0.41	0.13
HD 24062	6107	4.62	1.34	0.28	0.24	0.12
HD 24085	6065	4.47	1.22	0.17	0.16	0.12
HD 24112	6175	4.35	1.26	0.16	0.19	0.12
HD 24331	4948	4.56	0.46	-0.30	-0.32	0.12
HD 24558	5274	4.40	0.67	-0.47	-0.47	0.12
HD 24633	5276	4.36	0.59	-0.04	-0.17	0.12
HD 24892	5360	3.99	0.88	-0.33	-0.34	0.12
HD 25061	5243	4.42	0.80	0.07	-0.001	0.13
HD 25105	5306	4.42	0.74	-0.15	-0.20	0.12
HD 25120	5104	4.37	0.85	-0.21	-0.24	0.12
HD 25171	6160	4.43	1.22	-0.11	-0.13	0.12
HD 25357	5117	4.72	1.02	-0.03	-0.24	0.14
HD 25565	5145	4.41	0.73	0.00	-0.10	0.12
HD 25587	6258	4.61	1.78	-0.12	-0.13	0.12
HD 2567	6038	4.44	1.19	0.22	0.19	0.13
HD 25673	5116	4.45	0.48	-0.51	-0.49	0.13
HD 25704	5942	4.52	1.37	-0.83	-0.79	0.12
HD 25912	5900	4.52	0.99	0.12	0.02	0.12
HD 2638	5169	4.41	0.66	0.12	-0.01	0.13
HD 26430	4948	4.37	0.55	-0.26	-0.30	0.12
HD 26729	5718	4.17	1.13	0.31	0.30	0.12
HD 26887	6016	4.46	1.00	-0.35	-0.38	0.12
HD 26965A	5098	4.35	0.42	-0.36	-0.39	0.12
HD 27063	5759	4.44	0.94	0.05	0.15	0.12

Continued on next page

Table D.1 – continued from previous page

Star	Teff	logg	Vtur	[Fe/H]	[C/H]	$\sigma_{[C/H]}$
HD 27471	5871	4.25	1.13	0.11	0.11	0.12
HD 2768	5548	4.40	0.81	-0.03	-0.12	0.12
HD 27894	4833	4.30	0.33	0.26	0.12	0.18
HD 28185	5621	4.36	0.94	0.19	0.21	0.12
HD 28254	5653	4.15	1.08	0.36	0.39	0.12
HD 283	5135	4.49	0.47	-0.55	-0.65	0.12
HD 28471	5727	4.36	0.95	-0.07	-0.14	0.12
HD 28701	5718	4.47	0.95	-0.32	-0.28	0.12
HD 28807	6602	4.67	1.89	0.06	0.09	0.13
HD 28821	5663	4.37	0.88	-0.12	-0.13	0.12
HD 28969	6255	4.68	1.47	-0.01	-0.01	0.12
HD 290038	5006	4.42	0.56	0.01	-0.10	0.12
HD 290327	5505	4.41	0.73	-0.14	-0.20	0.12
HD 29137	5768	4.28	1.10	0.30	0.33	0.12
HD 291763	4987	4.50	0.12	-0.61	-0.58	0.12
HD 29263	5780	4.35	0.94	0.03	0.04	0.12
HD 29303	5819	4.52	0.93	-0.12	-0.18	0.12
HD 29428	5743	4.48	0.82	-0.06	-0.11	0.12
HD 297396	4717	4.30	0.46	0.06	-0.18	0.15
HD 29980	6019	4.71	1.57	0.12	0.08	0.13
HD 29985	4678	4.39	0.65	-0.22	-0.56	0.15
HD 30053	6139	4.51	1.20	-0.22	-0.33	0.12
HD 30177	5601	4.34	0.89	0.37	0.33	0.12
HD 30278	5374	4.37	0.72	-0.19	-0.26	0.12
HD 30306	5520	4.32	0.89	0.18	0.06	0.12
HD 30523	4662	4.57	0.79	-0.16	-0.53	0.14
HD 30669	5400	4.37	0.55	0.13	0.13	0.12
HD 30858	5182	4.45	0.88	-0.13	-0.28	0.13
HD 309701	4814	4.39	0.00	-0.30	-0.36	0.12
HD 31103	6078	4.49	1.08	0.09	0.05	0.12
HD 31128	6096	4.90	3.02	-1.39	-1.29	0.12
HD 31527	5917	4.47	1.09	-0.17	-0.17	0.11
HD 31532	5896	4.07	1.33	-0.08	-0.13	0.12
HD 31560	4655	4.36	0.08	0.00	-0.16	0.12
HD 31822	6061	4.61	1.15	-0.19	-0.26	0.11
HD 3220	5846	4.51	0.87	-0.22	-0.32	0.12
HD 3229	6583	4.14	1.80	-0.09	-0.08	0.13
HD 323631	4984	4.44	0.38	-0.28	-0.30	0.13
HD 324492	4962	4.15	0.52	-0.27	-0.39	0.15
HD 326267	4719	4.31	0.45	-0.26	-0.45	0.15
HD 32724	5834	4.28	1.14	-0.16	-0.18	0.11
HD 32804	5910	4.53	1.08	0.06	-0.11	0.12
HD 329788	5151	4.35	0.19	-0.08	-0.14	0.13
HD 330075	4958	4.24	0.32	0.05	-0.08	0.12
HD 33081	6399	4.56	2.47	-0.16	-0.22	0.14
HD 33473A	5740	3.97	1.20	-0.13	-0.15	0.12
HD 33725	5240	4.35	0.63	-0.19	-0.26	0.12
HD 33811	5554	4.39	0.78	0.30	0.17	0.12
HD 33822	5726	4.29	0.98	0.26	0.26	0.12
HD 34327	5883	4.20	1.19	-0.06	-0.07	0.12
HD 34449	5861	4.45	0.92	-0.09	-0.13	0.11
HD 34688	5104	4.34	0.54	-0.22	-0.42	0.12
HD 3569	5093	4.43	0.39	-0.34	-0.40	0.12
HD 35854	4808	4.35	0.16	-0.14	-0.23	0.12
HD 36003	4568	4.34	0.24	-0.13	-0.32	0.16
HD 36051	6118	4.63	1.21	-0.08	-0.08	0.12
HD 361	5888	4.54	1.00	-0.13	-0.17	0.11
HD 36108	5924	4.36	1.21	-0.20	-0.24	0.11

Continued on next page

Table D.1 – continued from previous page

Star	Teff	logg	Vtur	[Fe/H]	[C/H]	$\sigma_{[C/H]}$
HD 36179	5327	4.45	0.69	-0.08	-0.20	0.12
HD 36379	6039	4.35	1.29	-0.18	-0.15	0.11
HD 37226	6178	4.16	1.61	-0.12	-0.07	0.12
HD 37548	5950	4.26	1.19	-0.04	0.01	0.12
HD 37962	5732	4.47	0.88	-0.19	-0.24	0.12
HD 37986	5479	4.29	0.92	0.24	0.23	0.12
HD 37990	6215	4.56	1.15	0.00	-0.04	0.12
HD 38078	5651	4.47	0.62	-0.29	-0.34	0.13
HD 3808	5572	4.46	0.82	-0.17	-0.21	0.12
HD 3823	6054	4.37	1.39	-0.26	-0.27	0.11
HD 38265	5549	4.43	0.72	-0.14	-0.17	0.12
HD 38277	5882	4.35	1.10	-0.06	-0.06	0.12
HD 38355	5314	4.35	0.75	0.09	0.07	0.12
HD 38382	6110	4.46	1.18	0.04	0.03	0.11
HD 38385	7212	4.61	2.87	0.09	0.21	0.27
HD 38510	5914	4.32	1.30	-0.81	-0.82	0.12
HD 38772	6106	4.37	1.16	-0.23	-0.23	0.12
HD 38858	5719	4.49	0.94	-0.23	-0.26	0.11
HD 38973	6015	4.43	1.14	0.05	0.07	0.11
HD 39091	5991	4.40	1.12	0.09	0.07	0.12
HD 39194	5173	4.51	0.39	-0.63	-0.60	0.12
HD 39427	5682	4.52	0.86	-0.18	-0.20	0.12
HD 3964	5729	4.50	0.85	0.05	0.05	0.12
HD 40105	5064	3.69	0.91	0.02	-0.08	0.12
HD 4021	5831	4.71	1.32	0.02	-0.09	0.13
HD 40307	4774	4.42	0.10	-0.36	-0.45	0.12
HD 40397	5498	4.35	0.83	-0.14	-0.14	0.12
HD 40483	6371	4.39	1.80	-0.06	-0.04	0.13
HD 40503	4953	4.29	0.81	-0.03	-0.14	0.12
HD 40865	5719	4.50	0.87	-0.38	-0.42	0.12
HD 41087	5562	4.52	0.85	-0.13	-0.20	0.12
HD 41248	5713	4.49	0.84	-0.37	-0.32	0.14
HD 41323	5756	4.56	0.84	-0.31	-0.37	0.12
HD 4208	5600	4.41	0.88	-0.29	-0.31	0.12
HD 42505	4738	4.40	0.61	-0.22	-0.40	0.14
HD 4307	5840	4.13	1.22	-0.21	-0.23	0.12
HD 4308	5662	4.44	0.90	-0.32	-0.39	0.12
HD 43197	5449	4.30	0.83	0.36	0.33	0.12
HD 44120	6059	4.25	1.31	0.14	0.15	0.11
HD 44219	5766	4.20	1.06	0.04	0.05	0.12
HD 44420	5772	4.30	1.06	0.28	0.30	0.11
HD 44447	6004	4.41	1.26	-0.22	-0.19	0.12
HD 4457	5015	4.53	0.65	-0.37	-0.36	0.13
HD 44573	4990	4.42	0.61	-0.07	-0.21	0.12
HD 44594	5828	4.37	1.06	0.15	0.11	0.11
HD 44804	5366	4.48	0.97	0.03	-0.096	0.12
HD 45184	5869	4.47	1.03	0.05	0.00	0.12
HD 45289	5731	4.34	0.99	0.00	-0.07	0.12
HD 45364	5428	4.37	0.71	-0.18	-0.21	0.12
HD 457	6089	4.43	1.17	0.34	0.37	0.12
HD 4597	6025	4.43	1.11	-0.39	0.05	0.11
HD 45977	4689	4.30	0.52	0.03	-0.28	0.17
HD 47186	5643	4.34	0.93	0.22	0.20	0.11
HD 48115	5825	4.48	0.89	-0.19	-0.31	0.12
HD 4838	4704	4.63	0.76	-0.21	-0.50	0.14
HD 48611	5330	4.48	0.60	-0.36	-0.41	0.13
HD 49035	5640	4.35	1.01	0.24	0.20	0.12
HD 4915	5660	4.50	0.90	-0.21	-0.29	0.12

Continued on next page

Table D.1 – continued from previous page

Star	Teff	logg	Vtur	[Fe/H]	[C/H]	$\sigma_{[C/H]}$
HD 50590	4760	4.33	0.09	-0.21	-0.33	0.13
HD 50806	5598	4.10	1.03	0.01	0.06	0.12
HD 51608	5323	4.36	0.68	-0.08	-0.19	0.12
HD 51754	5848	4.49	1.05	-0.55	-0.61	0.12
HD 52265	6167	4.44	1.32	0.24	0.18	0.12
HD 52449	6362	4.55	1.29	0.12	0.13	0.12
HD 52919	4628	4.43	0.26	-0.09	-0.24	0.17
HD 5349	5092	3.88	1.00	0.43	0.32	0.14
HD 5388	6311	4.24	1.65	-0.28	-0.23	0.13
HD 54521	5973	4.54	1.02	-0.01	-0.03	0.12
HD 55	4554	4.54	0.06	-0.67	-0.56	0.16
HD 55693	5908	4.38	1.07	0.35	0.27	0.12
HD 56274	5734	4.51	0.94	-0.54	-0.55	0.11
HD 56380	5317	4.35	0.53	-0.42	-0.46	0.12
HD 564	5902	4.53	0.95	-0.20	-0.24	0.12
HD 57568	4821	4.51	0.38	-0.47	-0.55	0.12
HD 58489	4800	4.33	0.59	0.10	-0.14	0.15
HD 58676	5104	4.37	0.75	-0.02	-0.10	0.12
HD 59468	5582	4.36	0.88	0.01	-0.01	0.12
HD 59711A	5741	4.44	0.86	-0.12	-0.17	0.12
HD 59984	5962	4.18	1.45	-0.69	-0.65	0.11
HD 61051	5363	4.37	0.70	-0.10	-0.13	0.12
HD 61383	5716	4.20	1.12	-0.49	-0.52	0.12
HD 61447	5637	4.37	0.89	0.17	0.20	0.13
HD 61902	6209	4.38	1.58	-0.62	-0.53	0.11
HD 61986	5725	4.48	0.85	-0.34	-0.34	0.12
HD 62128	5828	4.22	1.16	0.33	0.30	0.12
HD 62364	6255	4.47	1.42	-0.11	-0.18	0.12
HD 62847	5362	4.48	0.67	-0.25	-0.29	0.12
HD 62849	5338	3.59	1.04	-0.17	-0.34	0.12
HD 63454	4756	4.32	0.31	0.13	-0.06	0.12
HD 6348	5080	4.47	0.33	-0.59	-0.55	0.13
HD 63685	5497	4.05	0.94	0.00	0.00	0.12
HD 63754	6200	4.21	1.57	0.21	0.29	0.12
HD 63765	5445	4.41	0.82	-0.15	-0.22	0.11
HD 64640	5174	4.31	0.77	0.18	0.09	0.12
HD 65216	5614	4.46	0.81	-0.17	-0.20	0.11
HD 65277	4701	4.30	0.30	-0.30	-0.38	0.12
HD 65562	5018	4.35	0.41	-0.13	-0.20	0.12
HD 65907A	5995	4.62	1.05	-0.29	-0.24	0.12
HD 65982	5947	4.42	1.08	-0.10	-0.16	0.12
HD 66039	6149	4.52	1.14	0.17	0.16	0.12
HD 66040	5226	4.34	0.76	0.35	0.26	0.12
HD 66168	6198	4.69	1.18	-0.03	-0.01	0.12
HD 66221	5590	4.34	0.92	0.16	0.11	0.12
HD 66340	5284	4.36	0.75	0.03	-0.04	0.12
HD 66428	5671	4.30	0.96	0.23	0.22	0.12
HD 6673	4875	4.39	0.38	-0.28	-0.34	0.12
HD 66740	6666	4.49	1.70	0.04	0.03	0.13
HD 66838	5392	4.29	0.71	0.03	0.05	0.12
HD 67	5746	4.56	1.02	0.03	-0.07	0.12
HD 6718	5723	4.44	0.84	-0.07	-0.12	0.12
HD 67200	6105	4.44	1.19	0.32	0.31	0.12
HD 6735	6111	4.56	1.15	-0.04	-0.06	0.12
HD 67458	5903	4.54	1.04	-0.15	-0.26	0.11
HD 68089	5597	4.53	0.66	-0.77	-0.83	0.11
HD 68284	5933	4.08	1.40	-0.50	-0.53	0.11
HD 68287	6318	4.63	1.45	0.06	0.02	0.12

Continued on next page

Table D.1 – continued from previous page

Star	Teff	logg	Vtur	[Fe/H]	[C/H]	$\sigma_{[C/H]}$
HD 68607	5155	4.38	0.82	0.06	-0.14	0.12
HD 68978A	5967	4.48	1.09	0.05	0.05	0.11
HD 69611	5762	4.31	0.99	-0.58	-0.54	0.12
HD 69655	5977	4.49	1.15	-0.18	-0.20	0.12
HD 69830	5370	4.38	0.80	-0.07	-0.10	0.12
HD 70642	5659	4.43	0.82	0.17	0.16	0.11
HD 70889	6069	4.55	1.13	0.13	0.09	0.11
HD 70903	5118	4.52	0.63	-0.43	-0.50	0.13
HD 71334	5706	4.41	0.95	-0.08	-0.13	0.11
HD 7134	5979	4.49	1.17	-0.27	-0.26	0.12
HD 71479	5991	4.38	1.19	0.24	0.23	0.11
HD 71685	6038	4.58	1.09	-0.37	-0.40	0.12
HD 71835	5431	4.39	0.79	-0.04	-0.01	0.12
HD 7199	5292	4.21	1.01	0.25	0.16	0.11
HD 72374	5767	4.35	0.90	-0.09	-0.07	0.12
HD 72579	5419	4.28	0.84	0.18	0.16	0.12
HD 72659	5926	4.24	1.13	-0.02	-0.08	0.12
HD 72673	5230	4.43	0.67	-0.43	-0.48	0.12
HD 72769	5587	4.30	0.98	0.29	0.23	0.12
HD 73121	6083	4.27	1.34	0.09	0.09	0.11
HD 73256	5465	4.36	1.11	0.21	0.11	0.11
HD 73267	5373	4.37	0.66	0.05	0.01	0.12
HD 73524	6004	4.42	1.14	0.16	0.16	0.12
HD 73583	4695	4.50	0.71	-0.21	-0.46	0.13
HD 74014	5552	4.33	0.90	0.22	0.17	0.12
HD 7449	6040	4.53	1.11	-0.10	-0.15	0.12
HD 74698	5783	4.27	1.01	0.07	0.00	0.12
HD 74957	5915	4.54	0.95	-0.18	-0.19	0.13
HD 750	5069	4.33	0.66	-0.30	-0.41	0.12
HD 75289	6139	4.35	1.29	0.30	0.15	0.11
HD 75328	6003	4.46	1.05	-0.23	-0.25	0.12
HD 75530	5311	4.48	0.53	-0.54	-0.52	0.13
HD 75745	5885	4.29	1.34	-0.78	-0.76	0.11
HD 75881	6239	4.44	1.63	0.07	0.12	0.12
HD 76151	5781	4.44	0.96	0.12	0.14	0.11
HD 76188	5989	4.08	1.25	-0.44	-0.47	0.13
HD 76440	5764	4.43	0.89	-0.01	0.05	0.12
HD 77110	5717	4.48	0.86	-0.50	-0.51	0.12
HD 78429	5742	4.26	1.01	0.07	0.05	0.12
HD 78538	5790	4.50	0.98	-0.02	-0.17	0.11
HD 78558	5759	4.46	0.99	-0.42	-0.52	0.12
HD 78612	5838	4.30	1.14	-0.24	-0.27	0.12
HD 78747	5814	4.57	1.10	-0.65	-0.61	0.11
HD 78964B	5195	4.50	0.91	0.10	-0.12	0.12
HD 79601	5825	4.32	1.09	-0.59	-0.67	0.11
HD 8038	5694	4.45	0.88	0.15	0.11	0.12
HD 80883	5198	4.36	0.65	-0.27	-0.36	0.12
HD 81639	5516	4.39	0.79	-0.18	-0.30	0.11
HD 81700	5882	4.53	0.98	0.12	0.05	0.12
HD 81767	4978	4.46	0.68	0.05	-0.04	0.14
HD 82114	5912	4.20	1.28	0.01	-0.07	0.12
HD 82342	4470	4.60	0.10	-0.56	-0.38	0.14
HD 82516	5041	4.47	0.50	0.02	-0.08	0.12
HD 82783	5318	4.41	0.91	0.21	0.13	0.13
HD 82943	5992	4.42	1.10	0.28	0.30	0.11
HD 8326	4834	4.35	0.44	0.04	-0.13	0.11
HD 83443	5442	4.32	0.93	0.32	0.26	0.12
HD 83529	5909	4.36	1.11	-0.22	-0.27	0.11

Continued on next page

Table D.1 – continued from previous page

Star	Teff	logg	Vtur	[Fe/H]	[C/H]	$\sigma_{[C/H]}$
HD 8389A	5182	4.33	1.06	0.36	0.45	0.12
HD 8406	5731	4.52	0.87	-0.10	-0.09	0.11
HD 84305	5963	4.51	0.95	-0.23	-0.29	0.12
HD 84627B	6113	4.50	1.10	-0.28	-0.33	0.13
HD 85119	5413	4.50	0.88	-0.21	-0.36	0.12
HD 8535	6158	4.42	1.25	0.04	-0.02	0.12
HD 85390	5135	4.32	0.66	-0.09	-0.05	0.13
HD 85512	4400	4.36	0.02	-0.26	-0.46	0.17
HD 85725	5986	3.95	1.54	0.15	0.17	0.12
HD 86065	4863	4.27	0.38	-0.03	-0.24	0.12
HD 86140	4776	4.40	0.15	-0.28	-0.34	0.12
HD 86171	5394	4.45	0.76	-0.25	-0.33	0.12
HD 8638	5508	4.45	0.74	-0.40	-0.36	0.12
HD 86652	5934	4.47	1.01	0.13	0.05	0.12
HD 870	5360	4.40	0.79	-0.12	-0.23	0.12
HD 87320	5639	4.41	0.95	-0.17	-0.16	0.12
HD 87521	4770	4.31	0.47	-0.01	-0.17	0.12
HD 87838	6118	4.47	1.33	-0.40	-0.46	0.13
HD 88084	5765	4.45	0.96	-0.10	-0.12	0.12
HD 88218	5872	4.14	1.23	-0.14	-0.12	0.11
HD 8828	5369	4.40	0.72	-0.18	-0.24	0.12
HD 88474	6122	3.91	1.91	-0.48	-0.45	0.12
HD 8859	5495	4.40	0.79	-0.09	-0.11	0.12
HD 88656	5099	4.35	0.69	-0.12	-0.25	0.11
HD 88725	5654	4.49	0.86	-0.64	-0.60	0.12
HD 88742	6004	4.52	1.07	0.00	-0.11	0.12
HD 88885	5361	4.46	0.77	-0.11	-0.18	0.12
HD 8912	5178	4.40	0.70	-0.09	-0.24	0.12
HD 89147	5310	4.45	0.76	-0.09	-0.17	0.12
HD 8930	5687	4.52	0.79	-0.23	-0.28	0.12
HD 89454	5708	4.45	0.96	0.11	-0.01	0.11
HD 89668	4811	4.45	0.63	-0.11	-0.31	0.15
HD 89749	5443	4.48	0.61	-0.29	-0.30	0.12
HD 89839	6314	4.49	1.35	0.04	0.02	0.12
HD 8985	6473	4.96	2.15	-0.01	0.03	0.13
HD 89920	4827	4.32	0.10	-0.03	-0.15	0.13
HD 89965	5039	4.48	0.72	-0.09	-0.23	0.12
HD 90081	5912	4.34	1.08	-0.20	-0.21	0.12
HD 90133	5064	4.42	0.37	-0.16	-0.31	0.14
HD 90156	5591	4.45	0.86	-0.25	-0.32	0.12
HD 90422	6085	4.14	1.67	-0.62	-0.53	0.12
HD 90702	5760	4.56	1.04	0.20	0.11	0.12
HD 90711	5396	4.33	0.92	0.21	0.17	0.12
HD 90722	5711	4.28	1.06	0.31	0.30	0.12
HD 90812	5118	4.35	0.50	-0.38	-0.39	0.11
HD 90926	5538	4.35	0.80	0.13	0.12	0.12
HD 90936	5928	4.48	1.04	0.03	0.00	0.12
HD 91267	4928	4.48	0.26	-0.06	-0.14	0.13
HD 91345	5658	4.53	0.71	-1.04	-1.10	0.12
HD 91379	6164	4.41	0.98	-0.29	-0.41	0.13
HD 9246	4976	4.52	0.33	-0.56	-0.47	0.12
HD 92547	6020	4.45	1.14	-0.37	-0.41	0.12
HD 92588	5105	3.60	0.94	-0.02	-0.12	0.12
HD 92719	5812	4.47	0.96	-0.11	-0.18	0.11
HD 92788	5729	4.35	0.95	0.27	0.24	0.12
HD 93083	5048	4.32	0.81	0.08	-0.04	0.12
HD 93351	5408	4.41	0.57	-0.23	-0.32	0.12
HD 93380	4512	4.61	0.05	-0.68	-0.65	0.20

Continued on next page

Table D.1 – continued from previous page

Star	Teff	logg	Vtur	[Fe/H]	[C/H]	$\sigma_{[C/H]}$
HD 93385	5989	4.46	1.14	0.03	-0.01	0.12
HD 93745	6065	4.34	1.33	0.12	0.10	0.12
HD 93932	5950	4.30	1.16	0.05	0.07	0.12
HD 94151	5581	4.40	0.83	0.04	-0.02	0.12
HD 94444	5998	4.34	1.29	-0.62	-0.63	0.11
HD 94771	5631	4.03	1.10	0.22	0.19	0.12
HD 94964	6139	4.55	1.26	-0.07	-0.21	0.13
HD 95456	6311	4.38	1.40	0.18	0.17	0.12
HD 95521	5762	4.46	0.96	-0.15	-0.21	0.12
HD 95533	5366	4.36	0.63	0.16	0.04	0.12
HD 95542	5984	4.52	1.01	-0.04	-0.15	0.12
HD 9578	6055	4.52	1.07	0.11	0.03	0.12
HD 95860	6054	4.48	1.25	-0.31	-0.38	0.12
HD 95922	6293	4.63	1.23	-0.06	-0.09	0.12
HD 9608	5954	4.43	0.98	-0.26	-0.30	0.12
HD 96116	5832	4.52	0.96	-0.01	-0.08	0.12
HD 96276	6080	4.49	1.12	-0.02	-0.04	0.12
HD 96290	6219	4.56	1.21	0.03	0.03	0.12
HD 96423	5701	4.35	0.98	0.10	0.05	0.12
HD 96673	4788	4.38	0.55	-0.13	-0.24	0.13
HD 967	5595	4.59	0.77	-0.66	-0.70	0.12
HD 96700	5854	4.39	1.04	-0.18	-0.17	0.11
HD 97037	5890	4.32	1.13	-0.07	-0.08	0.11
HD 97320	6165	4.57	1.50	-1.05	-0.93	0.12
HD 97343	5385	4.31	0.82	-0.08	-0.10	0.12
HD 97783	5682	4.50	0.88	-0.73	-0.78	0.12
HD 9782	6013	4.38	1.09	0.09	0.09	0.12
HD 9796	5139	4.34	0.49	-0.25	-0.31	0.12
HD 97998	5725	4.53	0.94	-0.42	-0.42	0.12
HD 98281	5389	4.39	0.64	-0.27	-0.33	0.12
HD 98284	5913	4.52	1.18	-0.84	-0.80	0.12
HD 98356	5274	4.35	0.75	0.09	-0.02	0.12
HIP102025	4684	4.32	0.53	-0.28	-0.43	0.13
HIP102964	4797	4.43	0.72	-0.23	-0.34	0.12
HIP103867	4559	4.14	0.77	-0.45	-0.58	0.27
HIP104856	5023	4.43	0.22	-0.24	-0.30	0.12
HIP105506	4840	4.37	0.22	-0.01	-0.17	0.14
HIP10741	4859	4.40	0.51	-0.15	-0.23	0.13
HIP108216	4830	4.53	0.66	-0.51	-0.59	0.18
HIP109149	4960	4.43	0.32	-0.12	-0.24	0.12
HIP109421	4576	4.42	0.32	-0.27	-0.62	0.18
HIP113596	4580	4.25	0.67	-0.21	-0.44	0.24
HIP116374	4626	4.31	0.42	0.01	-0.31	0.22
HIP116939	4984	4.35	0.56	-0.07	-0.13	0.14
HIP12147	5050	4.50	0.43	-0.32	-0.40	0.13
HIP15587	5239	4.46	0.66	-0.12	-0.21	0.12
HIP16094	4877	4.44	0.39	-0.04	-0.18	0.13
HIP17346	4699	4.32	0.66	-0.16	-0.36	0.14
HIP1745	5416	4.39	0.47	-0.44	-0.44	0.12
HIP18918	4572	4.28	0.45	-0.20	-0.45	0.21
HIP20444	4907	4.41	0.54	-0.12	-0.20	0.13
HIP21539	4496	4.23	0.43	-0.32	-0.44	0.17
HIP21934	4674	4.19	0.62	0.03	-0.29	0.18
HIP22059	4672	4.33	0.47	-0.28	-0.47	0.13
HIP25612	4571	4.35	0.56	-0.50	-0.64	0.23
HIP26013	4891	4.41	0.90	0.02	-0.14	0.13
HIP26542	4598	4.38	0.10	-0.53	-0.46	0.17
HIP31639	5400	4.53	0.31	-0.54	-0.53	0.12

Continued on next page

Table D.1 – continued from previous page

Star	Teff	logg	Vtur	[Fe/H]	[C/H]	$\sigma_{[C/H]}$
HIP32127	5302	4.44	0.58	-0.64	-0.60	0.13
HIP32812	4977	4.41	0.56	-0.02	-0.09	0.13
HIP33392	4986	4.54	0.97	-0.09	-0.25	0.12
HIP35992	4939	4.25	0.62	-0.02	-0.15	0.12
HIP36347	4719	4.38	0.84	-0.05	-0.30	0.15
HIP38324	4615	4.39	0.48	-0.30	-0.71	0.18
HIP39470	4571	4.40	0.61	-0.39	-0.63	0.15
HIP41659	5197	4.38	0.42	-0.53	-0.53	0.13
HIP45301	4788	4.46	0.10	-0.12	-0.26	0.16
HIP46933	4487	4.22	0.22	-0.24	-0.47	0.24
HIP5114	4846	4.39	0.74	-0.69	-0.52	0.17
HIP5158	4813	4.32	0.54	0.17	0.03	0.16
HIP54446	4992	4.51	0.74	-0.18	-0.31	0.12
HIP54597	4799	4.43	0.52	-0.22	-0.33	0.13
HIP57688	4712	4.32	0.37	-0.14	-0.29	0.13
HIP58348	4828	4.34	0.43	0.00	-0.16	0.13
HIP59925	4590	4.40	0.43	-0.26	-0.50	0.19
HIP61406	4855	4.42	0.68	0.03	-0.14	0.14
HIP64965	4888	4.78	0.00	-1.03	-0.90	0.12
HIP67126	4681	4.20	0.27	-0.19	-0.31	0.13
HIP69224	5005	4.30	0.32	-0.14	-0.24	0.12
HIP7058	4749	4.55	0.41	-0.10	-0.33	0.16
HIP7743	4692	4.39	0.74	-0.17	-0.45	0.15
HIP78242	5244	4.40	0.73	-0.01	-0.06	0.12
HIP80083	4800	4.78	0.31	-0.80	-0.99	0.20
HIP88316	5159	4.38	0.35	-0.01	-0.08	0.13
HIP9398	4734	4.49	0.62	-0.43	-0.71	0.18
HIP96240	4849	4.47	0.70	-0.15	-0.30	0.13
HIP98764	4811	4.33	0.42	-0.32	-0.43	0.12
HIP99606B	5764	4.19	0.98	-0.41	-0.41	0.12

E

C/O vs Mg/Si

Table E.1: [C/O] and $[C/O]_{corr}$ abundances

Star	Teff	logg	[Fe/H]	ξ_t	[C/O]	$[C/O]_{corr}$	$\sigma_{[C/O]}$
HD 62364	6255	4.47	-0.11	1.42	-0.19	-0.06	0.03
HD 161555	5850	4.15	0.12	1.23	-0.02	0.02	0.17
HD 66428	5671	4.30	0.23	0.96	-0.02	-0.01	0.29
HD 3229	6583	4.14	-0.09	1.80	-0.08	0.04	0.04
HD 33081	6399	4.56	-0.16	2.47	-0.33	-0.18	0.02
HD 225297	6181	4.55	-0.09	1.24	-0.17	-0.05	0.04
HD 70642	5659	4.43	0.17	0.82	-0.10	-0.07	0.21
HD 142022A	5482	4.35	0.18	0.83	-0.05	-0.02	0.04
HD 24633	5276	4.36	-0.04	0.59	-0.095	0.01	0.32
HD 202209	6009	4.68	-0.01	1.19	-0.16	-0.08	0.29
HD 66838	5392	4.29	0.03	0.71	-0.005	0.07	0.49
HD 203335	6306	4.56	-0.04	1.44	0.01	0.11	0.13
HD 33822	5726	4.29	0.26	0.98	-0.045	-0.03	0.39
HD 93932	5950	4.30	0.05	1.16	0.015	0.08	0.26
HD 139879	6203	4.61	0.30	1.25	-0.035	-0.03	0.04
HD 223854	6080	4.08	-0.54	1.60	-0.49	-0.08	0.01
HD 151772	6631	4.81	-0.36	2.27	-0.25	0.02	0.02
HD 21161	5923	4.24	0.09	1.14	-0.095	-0.04	0.18
HD 77110	5717	4.48	-0.50	0.86	-0.43	-0.05	0.09
HD 224817	5894	4.36	-0.53	1.13	-0.43	-0.02	0.02
HD 55693	5908	4.38	0.35	1.07	-0.06	-0.06	0.10
HD 82783	5318	4.41	0.21	0.91	0.055	0.08	0.44
HD 19994	6315	4.44	0.27	1.72	0.05	0.06	0.18
HD 144880	6152	4.38	-0.30	1.33	-0.26	-0.03	0.17
HD 83443	5442	4.32	0.32	0.93	0.02	0.03	0.09
HD 220367	6116	4.45	-0.23	1.34	-0.18	0.02	0.03
HD 29263	5780	4.35	0.03	0.94	0.00	0.07	0.38
HD 217786	5966	4.35	-0.14	1.12	-0.04	0.10	0.31
HD 161566	6230	4.20	-0.28	1.67	-0.25	-0.03	0.04
HD 212231	5762	4.20	-0.30	1.01	-0.31	-0.07	0.22
HD 177758	5933	4.51	-0.54	1.11	-0.45	-0.03	0.04
HD 20807	5875	4.50	-0.23	1.04	-0.11	0.09	0.08
HD 114729	5865	4.20	-0.26	1.23	-0.23	-0.02	0.06
HD 81639	5516	4.39	-0.18	0.79	-0.13	0.03	0.28
HD 44447	6004	4.41	-0.22	1.26	-0.17	0.02	0.07

Continued on next page

Table E.1 – continued from previous page

Star	Teff	logg	[Fe/H]	ξ_t	[C/O]	$[C/O]_{corr}$	$\sigma_{[C/O]}$
HD 196761	5414	4.46	-0.31	0.76	-0.18	0.06	0.12
HD 20794	5398	4.41	-0.41	0.67	-0.35	-0.04	0.04
HD 143114	5811	4.46	-0.41	0.92	-0.31	0.00	0.11
HD 221356	6100	4.51	-0.20	1.12	-0.20	-0.03	0.06
HD 5388	6311	4.24	-0.28	1.65	-0.22	0.00	0.07
HD 69611	5762	4.31	-0.58	0.99	-0.67	-0.22	0.01
HD 109098	5888	4.14	0.06	1.24	-0.095	-0.04	0.06
HD 224347	6092	4.27	-0.42	1.31	-0.37	-0.05	0.02
HD 90702	5760	4.56	0.20	1.04	-0.05	-0.03	0.42
HD 18386	5446	4.37	0.14	0.92	0.005	0.04	0.04
HD 107148	5744	4.30	0.28	0.93	0.04	0.05	0.32
HD 90936	5928	4.48	0.03	1.04	-0.055	0.02	0.31
HD 8638	5508	4.45	-0.40	0.74	-0.37	-0.06	0.16
HD 181428	6151	4.45	0.06	1.29	-0.08	-0.02	0.04
HD 88218	5872	4.14	-0.14	1.23	-0.075	0.07	0.12
HD 20407	5885	4.52	-0.43	1.09	-0.28	0.05	0.02
HD 197300	6022	4.69	0.02	1.21	-0.13	-0.06	0.25
HD 52449	6362	4.55	0.12	1.29	-0.02	0.02	0.04
HD 124785	5867	4.20	-0.56	1.29	-0.42	0.01	0.02
HD 24892	5360	3.99	-0.33	0.88	-0.29	-0.04	0.16
HD 14747	5547	4.46	-0.37	0.72	-0.40	-0.12	0.05
HD 61383	5716	4.20	-0.49	1.12	-0.46	-0.08	0.04
HD 65907A	5995	4.62	-0.29	1.05	-0.37	-0.14	0.05
HD 68287	6318	4.63	0.06	1.45	-0.07	-0.01	0.08
HD 16382	5953	4.50	0.03	1.04	-0.08	-0.01	0.26
HD 199086	6149	4.65	0.18	1.21	-0.095	-0.07	0.17
HD 100777	5530	4.31	0.25	0.81	-0.035	-0.02	0.04
HD 210272	5713	4.13	-0.22	1.16	-0.085	0.10	0.36
HD 208487	6172	4.54	0.10	1.24	-0.075	-0.03	0.09
HD 79601	5825	4.32	-0.59	1.09	-0.58	-0.12	0.01
HD 150433	5680	4.48	-0.36	0.88	-0.35	-0.08	0.02
HD 167300	5837	4.30	-0.45	1.05	-0.36	-0.02	0.10
HD 198075	5842	4.55	-0.24	0.95	-0.26	-0.07	0.15
HD 224433	5527	4.42	0.09	0.72	-0.045	0.01	0.43
HD 115773	6312	4.23	-0.08	1.57	-0.13	-0.02	0.03
HD 106290	6012	4.55	0.13	1.03	0.05	0.09	0.53
HD 70889	6069	4.55	0.13	1.13	-0.03	0.01	0.09
HD 213575	5676	4.22	-0.15	1.02	-0.24	-0.09	0.03
HD 216770	5351	4.31	0.20	0.91	0.015	0.04	0.04
HD 181720	5792	4.25	-0.53	1.16	-0.45	-0.04	0.03
HD 111232	5482	4.46	-0.43	0.62	-0.40	-0.07	0.05
HD 21019	5468	3.93	-0.45	1.05	-0.30	0.05	0.09
HD 2768	5548	4.40	-0.03	0.81	-0.02	0.07	0.51
HD 38277	5882	4.35	-0.06	1.10	-0.10	0.01	0.04
HD 11505	5757	4.39	-0.22	0.99	-0.28	-0.10	0.02
HD 24062	6107	4.62	0.28	1.34	-0.05	-0.04	0.08
HD 150139	5968	4.29	-0.51	1.29	-0.23	0.16	0.21
HD 28969	6255	4.68	-0.01	1.47	-0.16	-0.07	0.16
HD 195633	6154	4.25	-0.51	1.47	-0.25	0.13	0.18
HD 213941	5565	4.45	-0.44	0.72	-0.36	-0.03	0.17
HD 870	5360	4.40	-0.12	0.79	-0.05	0.08	0.39
HD 1581	5990	4.49	-0.18	1.12	-0.18	-0.02	0.05
HD 90711	5396	4.33	0.21	0.92	-0.01	0.01	0.04
HD 51754	5848	4.49	-0.55	1.05	-0.68	-0.26	0.01
HD 117105	5912	4.44	-0.28	1.13	-0.26	-0.04	0.02
HD 160089	6312	4.78	0.11	1.60	-0.07	-0.03	0.09
HD 4308	5662	4.44	-0.32	0.90	-0.40	-0.15	0.05
HD 199847	5763	4.22	-0.54	1.04	-0.52	-0.10	0.06

Continued on next page

Table E.1 – continued from previous page

Star	Teff	logg	[Fe/H]	ξ_t	[C/O]	$[C/O]_{corr}$	$\sigma_{[C/O]}$
HD 29137	5768	4.28	0.30	1.10	-0.025	-0.02	0.04
HD 25587	6258	4.61	-0.12	1.78	-0.14	-0.01	0.26
HD 34327	5883	4.20	-0.06	1.19	-0.005	0.10	0.41
HD 78558	5759	4.46	-0.42	0.99	-0.66	-0.34	0.01
HD 27471	5871	4.25	0.11	1.13	-0.15	-0.10	0.13
HD 4915	5660	4.50	-0.21	0.90	-0.18	0.00	0.03
HD 218504	5962	4.34	-0.55	1.21	-0.61	-0.18	0.02
HD 136352	5659	4.40	-0.35	0.90	-0.39	-0.12	0.03
HD 41248	5713	4.49	-0.37	0.84	-0.16	0.12	0.09
HD 17548	6011	4.44	-0.53	1.18	-0.18	0.23	0.18
HD 207832	5718	4.45	0.15	0.86	-0.07	-0.04	0.33
HD 96700	5854	4.39	-0.18	1.04	-0.07	0.09	0.07
HD 196384	6611	4.79	-0.13	1.78	-0.11	0.03	0.07
HD 190647	5636	4.18	0.23	0.99	-0.04	-0.02	0.04
HD 179346	6229	4.76	-0.03	1.35	0.03	0.12	0.29
HD 203432	5591	4.29	0.27	0.98	0.07	0.08	0.14
HD 95521	5762	4.46	-0.15	0.96	-0.075	0.07	0.04
HD 75289	6139	4.35	0.30	1.29	-0.05	-0.04	0.10
HD 130989	6414	4.27	-0.23	1.85	-0.21	-0.01	0.04
HD 220894	6282	4.60	0.02	1.35	-0.16	-0.08	0.04
HD 221420	5838	3.98	0.34	1.28	0.055	0.06	0.13
HD 72769	5587	4.30	0.29	0.98	0.055	0.07	0.05
HD 221343	5848	4.54	0.11	0.99	0.05	0.10	0.39
HD 119949	6359	4.47	-0.41	1.65	-0.10	0.21	0.03
HD 114853	5698	4.43	-0.23	0.92	-0.24	-0.04	0.03
HD 17439	5721	4.44	0.08	0.87	-0.07	-0.02	0.09
HD 3823	6054	4.37	-0.26	1.39	-0.25	-0.05	0.05
HD 54521	5973	4.54	-0.01	1.02	-0.16	-0.08	0.18
HD 201496	5974	4.44	-0.04	1.12	-0.11	-0.01	0.31
HD 73524	6004	4.42	0.16	1.14	-0.03	0.01	0.09
HD 172643	5645	4.50	-0.15	0.73	-0.28	-0.13	0.31
HD 30278	5374	4.37	-0.19	0.72	-0.21	-0.04	0.04
HD 4307	5840	4.13	-0.21	1.22	-0.20	-0.02	0.06
HD 16548	5690	3.96	0.15	1.15	-0.06	-0.03	0.04
HD 16008	5712	4.42	-0.09	0.78	-0.35	-0.23	0.19
HD 123265	5311	4.31	0.18	0.85	-0.06	-0.03	0.06
HD 129229	5872	3.89	-0.42	1.37	-0.29	0.03	0.12
HD 28701	5718	4.47	-0.32	0.95	-0.29	-0.04	0.02
HD 224063	5591	4.27	0.14	0.84	-0.24	-0.20	0.11
HD 39091	5991	4.40	0.09	1.12	0.025	0.08	0.11
HD 154195A	5961	4.48	-0.19	1.01	-0.19	-0.02	0.14
HD 139590	6200	4.49	0.13	1.31	-0.11	-0.07	0.05
HD 37226	6178	4.16	-0.12	1.61	-0.17	-0.03	0.04
HD 38382	6110	4.46	0.04	1.18	0.005	0.07	0.04
HD 124364	5601	4.49	-0.27	0.83	-0.22	0.00	0.11
HD 222582	5781	4.37	-0.01	1.00	-0.01	0.08	0.06
HD 95860	6054	4.48	-0.31	1.25	-0.38	-0.14	0.07
HD 96290	6219	4.56	0.03	1.21	-0.10	-0.03	0.033
HD 66740	6666	4.49	0.04	1.70	-0.12	-0.05	0.06
HD 220507	5676	4.30	0.00	1.01	-0.14	-0.06	0.08
HD 28185	5621	4.36	0.19	0.94	-0.045	-0.02	0.07
HD 97343	5385	4.31	-0.08	0.82	-0.085	0.03	0.17
HD 83529	5909	4.36	-0.22	1.11	-0.14	0.05	0.03
HD 102438	5562	4.43	-0.29	0.84	-0.11	0.12	0.05
HD 49035	5640	4.35	0.24	1.01	0.07	0.09	0.16
HD 28807	6602	4.67	0.06	1.89	-0.14	-0.08	0.04
HD 26729	5718	4.17	0.31	1.13	-0.02	-0.01	0.07
HD 21938	5800	4.41	-0.47	0.99	-0.49	-0.13	0.02

Continued on next page

Table E.1 – continued from previous page

Star	Teff	logg	[Fe/H]	ξ_t	[C/O]	$[C/O]_{corr}$	$\sigma_{[C/O]}$
HD 82114	5912	4.20	0.01	1.28	-0.14	-0.06	0.19
HD 141937	5892	4.46	0.13	1.00	0.11	0.14	0.05
HD 210320	5597	4.31	0.11	0.87	-0.15	-0.10	0.49
HD 221638	6360	4.53	-0.21	1.43	-0.16	0.02	0.03
HD 45184	5869	4.47	0.05	1.03	-0.025	0.04	0.11
HD 564	5902	4.53	-0.20	0.95	-0.14	0.03	0.04
HD 98281	5389	4.39	-0.27	0.64	-0.10	0.11	0.03
HD 196800	6007	4.40	0.18	1.17	-0.065	-0.04	0.04
HD 102300	5987	4.23	-0.31	1.14	-0.27	-0.04	0.20
HD 210752	5970	4.52	-0.55	1.20	-0.24	0.18	0.05
CD-436810	6011	4.41	-0.44	1.09	-0.55	-0.21	0.03
HD 68284	5933	4.08	-0.50	1.40	-0.41	-0.03	0.02
HD 209449	5854	4.16	0.41	1.19	-0.015	-0.01	0.06
HD 223171	5830	4.16	0.11	1.12	0.01	0.06	0.12
HD 124292	5426	4.37	-0.14	0.77	-0.085	0.06	0.03
HD 197536	6105	4.39	-0.41	1.34	-0.30	0.01	0.13
HD 63765	5445	4.41	-0.15	0.82	-0.055	0.09	0.04
HD 93745	6065	4.34	0.12	1.33	0.015	0.06	0.10
HD 66168	6198	4.69	-0.03	1.18	0.05	0.14	0.21
HD 143790	6557	4.11	-0.06	2.05	-0.16	-0.06	0.12
HD 88474	6122	3.91	-0.48	1.91	-0.20	0.16	0.19
HD 3220	5846	4.51	-0.22	0.87	-0.14	0.05	0.14
BD-131161	5389	4.37	0.09	0.68	-0.24	-0.18	0.29
HD 59711A	5741	4.44	-0.12	0.86	-0.01	0.12	0.37
HD 32804	5910	4.53	0.06	1.08	-0.04	0.02	0.14
HD 31532	5896	4.07	-0.08	1.33	-0.22	-0.11	0.13
HD 122474	5716	4.37	0.13	0.88	-0.16	-0.12	0.31
HD 197083	5735	4.50	-0.45	0.90	-0.32	0.02	0.15
HD 2567	6038	4.44	0.22	1.19	-0.055	-0.04	0.07
HD 12387	5704	4.42	-0.25	0.93	-0.32	-0.12	0.04
HD 196050	5871	4.26	0.23	1.21	-0.09	-0.07	0.10
HD 168746	5561	4.31	-0.11	0.81	-0.15	-0.02	0.34
HD 197197	5812	4.20	-0.46	1.25	-0.46	-0.11	0.02
HD 11397	5564	4.46	-0.54	0.75	-0.16	0.25	0.03
HD 208	5914	4.47	-0.31	1.05	-0.11	0.14	0.03
HD 76188	5989	4.08	-0.44	1.25	-0.37	-0.03	0.22
HD 90926	5538	4.35	0.13	0.80	0.00	0.04	0.49
HD 44420	5772	4.30	0.28	1.06	0.025	0.04	0.10
HD 7134	5979	4.49	-0.27	1.17	-0.20	0.03	0.03
HD 48115	5825	4.48	-0.19	0.89	-0.14	0.03	0.10
HD 36051	6118	4.63	-0.08	1.21	-0.15	-0.03	0.08
HD 216435	6034	4.21	0.27	1.34	0.00	0.01	0.11
HD 148577	5713	4.29	-0.09	0.95	-0.23	-0.11	0.08
HD 117207	5649	4.31	0.21	1.01	0.01	0.03	0.04
HD 157172	5419	4.32	0.09	0.77	-0.09	-0.04	0.05
HD 144585	5880	4.32	0.32	1.15	-0.06	-0.05	0.08
HD 73256	5465	4.36	0.21	1.11	-0.09	-0.07	0.06
HD 108768	5633	4.45	0.14	0.86	0.025	0.06	0.47
HD 189567	5718	4.39	-0.25	0.95	-0.075	0.13	0.09
HD 177122	6021	4.52	-0.10	1.03	0.18	0.30	0.66
HD 72579	5419	4.28	0.18	0.84	-0.025	0.00	0.04
HD 75881	6239	4.44	0.07	1.63	0.005	0.06	0.09
HD 203384	5564	4.42	0.26	0.90	-0.04	-0.03	0.04
HD 180409	6031	4.51	-0.15	1.16	-0.10	0.05	0.19
HD 152433	6144	4.49	-0.10	1.19	-0.24	-0.11	0.15
HD 212708	5644	4.31	0.26	0.99	-0.05	-0.04	0.09
HD 108063	6081	4.11	0.55	1.54	-0.05	-0.04	0.08
HD 111564	6004	4.37	0.07	1.13	-0.05	0.00	0.04

Continued on next page

Table E.1 – continued from previous page

Star	Teff	logg	[Fe/H]	ξ_t	[C/O]	$[C/O]_{corr}$	$\sigma_{[C/O]}$
HD 33811	5554	4.39	0.30	0.78	-0.02	-0.01	0.44
HD 45364	5428	4.37	-0.18	0.71	-0.07	0.10	0.04
HD 90722	5711	4.28	0.31	1.06	0.11	0.12	0.33
HD 131664	5901	4.50	0.31	1.04	0.08	0.08	0.07
HD 16417	5843	4.16	0.14	1.18	-0.01	0.03	0.09
HD 62128	5828	4.22	0.33	1.16	-0.05	-0.04	0.08
HD 78429	5742	4.26	0.07	1.01	-0.04	0.02	0.11
HD 224578	6158	4.67	-0.01	1.13	-0.05	0.04	0.42
HD 205294	6370	4.30	-0.25	1.71	-0.17	0.04	0.08
HD 207129	5946	4.48	0.01	1.06	-0.07	0.01	0.08
HD 104263	5456	4.35	0.01	0.81	-0.04	0.04	0.05
HD 191033	6206	4.47	-0.19	1.35	-0.29	-0.12	0.17
HD 174153	6196	4.49	-0.08	1.34	0.00	0.11	0.11
HD 96423	5701	4.35	0.10	0.98	-0.09	-0.04	0.03
HD 162396	6121	4.33	-0.34	1.43	-0.20	0.07	0.06
HD 114613	5712	3.94	0.18	1.18	0.05	0.08	0.14
HD 211317	5965	4.30	0.27	1.21	0.01	0.02	0.04
HD 190984	6007	4.02	-0.49	1.58	-0.24	0.13	0.03
HD 222669	5898	4.44	0.06	1.01	0.025	0.09	0.10
HD 8535	6158	4.42	0.04	1.25	-0.18	-0.11	0.06
HD 105837	5932	4.60	-0.50	1.14	-0.18	0.21	0.27
HD 38772	6106	4.37	-0.23	1.16	-0.16	0.04	0.27
HD 135468	6417	4.25	-0.02	1.82	-0.14	-0.05	0.09
HD 214094	6288	4.28	-0.01	1.46	0.00	0.09	0.05
HD 56274	5734	4.51	-0.54	0.94	-0.28	0.13	0.04
HD 361	5888	4.54	-0.13	1.00	-0.15	-0.01	0.04
HD 142	6431	4.82	0.05	1.74	-0.095	-0.03	0.13
HD 69655	5977	4.49	-0.18	1.15	-0.06	0.10	0.07
HD 78612	5838	4.30	-0.24	1.14	-0.20	-0.01	0.03
HD 30306	5520	4.32	0.18	0.89	0.00	0.03	0.04
HD 24112	6175	4.35	0.16	1.26	-0.05	-0.02	0.07
HD 149200	6416	4.64	0.15	1.74	-0.15	-0.11	0.05
HD 104982	5682	4.42	-0.20	0.91	-0.14	0.03	0.15
HD 20782	5770	4.35	-0.06	1.00	-0.14	-0.03	0.05
HD 63754	6200	4.21	0.21	1.57	0.01	0.03	0.08
HD 31527	5917	4.47	-0.17	1.09	-0.045	0.11	0.04
HD 16141	5786	4.17	0.15	1.11	-0.045	-0.01	0.04
HD 36379	6039	4.35	-0.18	1.29	-0.12	0.04	0.07
HD 136894	5402	4.37	-0.11	0.75	-0.14	-0.01	0.03
HD 154962	5778	4.12	0.30	1.22	0.025	0.03	0.11
HD 119629	6250	4.17	-0.17	1.73	-0.12	0.04	0.03
HD 123651	5926	4.55	-0.48	1.05	-0.30	0.07	0.25
HD 21693	5418	4.38	0.00	0.76	-0.08	0.00	0.04
HD 125184	5660	4.11	0.27	1.13	0.17	0.18	0.06
HD 215906	6259	4.56	-0.28	1.55	-0.25	-0.03	0.16
HD 207970	5524	4.36	0.05	0.80	0.12	0.18	0.39
HD 101367	5615	4.38	0.29	0.91	-0.06	-0.05	0.38
HD 145666	5984	4.56	-0.02	1.04	-0.035	0.05	0.08
HD 204287	5743	4.15	-0.04	1.10	-0.16	-0.06	0.03
HD 37986	5479	4.29	0.24	0.92	-0.03	-0.01	0.04
HD 67200	6105	4.44	0.32	1.19	0.07	0.08	0.05
HD 10180	5898	4.39	0.08	1.11	-0.03	0.02	0.09
HD 76151	5781	4.44	0.12	0.96	0.085	0.13	0.05
HD 207190	6178	4.33	-0.42	1.51	-0.50	-0.18	0.02
HD 188748	5616	4.45	-0.13	0.83	-0.11	0.03	0.08
HD 78538	5790	4.50	-0.02	0.98	-0.19	-0.10	0.05
HD 34449	5861	4.45	-0.09	0.92	-0.14	-0.02	0.06
HD 87838	6118	4.47	-0.40	1.33	-0.34	-0.03	0.04

Continued on next page

Table E.1 – continued from previous page

Star	Teff	logg	[Fe/H]	ξ_t	[C/O]	$[C/O]_{corr}$	$\sigma_{[C/O]}$
HD 38858	5719	4.49	-0.23	0.94	-0.065	0.13	0.04
HD 206163	5506	4.42	0.02	0.94	-0.18	-0.10	0.34
HD 36108	5924	4.36	-0.20	1.21	-0.22	-0.04	0.03
HD 162236	5336	4.42	-0.12	0.82	-0.11	0.02	0.20
HD 199190	5937	4.27	0.15	1.14	-0.01	0.03	0.11
HD 8406	5731	4.52	-0.10	0.87	-0.065	0.06	0.09
HD 85725	5986	3.95	0.15	1.54	-0.01	0.03	0.10
HD 44219	5766	4.20	0.04	1.06	-0.085	-0.02	0.04
HD 195564	5663	4.02	0.05	1.11	-0.07	-0.01	0.05
HD 176666	6103	4.63	-0.37	1.18	-0.36	-0.07	0.17
HD 11964A	5285	3.81	0.06	0.99	-0.025	0.04	0.07
HD 2071	5729	4.49	-0.08	0.95	-0.08	0.03	0.03
HD 211415	5864	4.42	-0.21	0.99	-0.08	0.10	0.17
HD 171990	6048	4.15	0.06	1.40	-0.025	0.04	0.11
HD 67458	5903	4.54	-0.15	1.04	-0.20	-0.06	0.04
HD 215625	6282	4.58	0.10	1.35	-0.18	-0.13	0.03
HD 17865	5877	4.32	-0.57	1.16	-0.38	0.06	0.02
HD 109409	5833	4.11	0.31	1.24	0.045	0.05	0.12
HD 200538	6042	4.38	0.10	1.22	-0.11	-0.06	0.05
HD 30177	5601	4.34	0.37	0.89	0.04	0.04	0.07
HD 76440	5764	4.43	-0.01	0.89	0.065	0.15	0.07
HD 197823	5344	4.37	0.10	0.82	-0.025	0.02	0.04
HD 129191	5832	4.39	0.24	0.99	-0.09	-0.07	0.03
HD 69830	5370	4.38	-0.07	0.80	-0.035	0.07	0.09
HD 160691	5750	4.19	0.29	1.09	0.025	0.04	0.13
HD 125881	6046	4.49	0.07	1.10	-0.02	0.04	0.08
HD 68978A	5967	4.48	0.05	1.09	0.025	0.09	0.11
HD 31822	6061	4.61	-0.19	1.15	-0.15	0.02	0.03
HD 89454	5708	4.45	0.11	0.96	0.00	0.05	0.08
HD 108147	6318	4.53	0.21	1.30	-0.01	0.01	0.12
HD 161256	5652	4.27	0.14	0.93	-0.19	-0.15	0.07
HD 190248	5566	4.24	0.32	0.99	0.015	0.02	0.12
HD 21132	6243	4.60	-0.37	1.44	-0.25	0.03	0.04
HD 126525	5645	4.40	-0.09	0.90	-0.13	-0.01	0.03
HD 146233	5810	4.46	0.05	1.00	-0.085	-0.02	0.09
HD 117618	6003	4.45	0.03	1.13	-0.10	-0.03	0.07
HD 25912	5900	4.52	0.12	0.99	0.025	0.07	0.49
HD 31103	6078	4.49	0.09	1.08	0.085	0.14	0.06
HD 82943	5992	4.42	0.28	1.10	0.04	0.05	0.13
HD 71479	5991	4.38	0.24	1.19	-0.01	0.01	0.09
HD 40865	5719	4.50	-0.38	0.87	-0.20	0.09	0.08
HD 199960	5928	4.42	0.27	1.13	-0.10	-0.09	0.07
HD 71334	5706	4.41	-0.08	0.95	-0.16	-0.04	0.03
HD 214385	5679	4.47	-0.33	0.81	-0.16	0.09	0.32
HD 103197	5250	4.45	0.22	0.84	-0.025	-0.01	0.17
HD 220456	5887	4.50	-0.02	1.01	-0.17	-0.08	0.16
HD 150437	5826	4.29	0.30	1.09	0.15	0.16	0.49
HD 52265	6167	4.44	0.24	1.32	-0.03	-0.01	0.08
HD 63685	5497	4.05	0.00	0.94	-0.045	0.04	0.47
HD 90081	5912	4.34	-0.20	1.08	-0.16	0.02	0.37
HD 40483	6371	4.39	-0.06	1.80	-0.19	-0.09	0.03
HD 149724	5747	4.24	0.37	1.08	-0.01	-0.01	0.10
HD 141597	6285	4.38	-0.40	1.23	-0.28	0.02	0.08
HD 84627B	6113	4.50	-0.28	1.10	-0.30	-0.08	0.16
HD 196397	5378	4.33	0.29	0.68	-0.07	-0.06	0.47
HD 190613	5776	4.33	0.00	0.95	-0.15	-0.07	0.31
HD 156079	5892	4.24	0.28	1.16	-0.12	-0.10	0.03
HD 116259	5700	4.21	0.11	0.99	-0.11	-0.06	0.10

Continued on next page

Table E.1 – continued from previous page

Star	Teff	logg	[Fe/H]	ξ_t	[C/O]	$[C/O]_{corr}$	$\sigma_{[C/O]}$
HD 74014	5552	4.33	0.22	0.90	-0.10	-0.08	0.03
HD 148156	6251	4.51	0.25	1.36	-0.055	-0.04	0.10
HD 156098	6517	4.20	0.18	2.06	-0.19	-0.16	0.09
HD 37990	6215	4.56	0.00	1.15	-0.20	-0.11	0.05
HD 216008	5773	4.38	-0.04	0.91	-0.21	-0.11	0.23
HD 26887	6016	4.46	-0.35	1.00	-0.44	-0.17	0.11
HD 41323	5756	4.56	-0.31	0.84	-0.13	0.12	0.25
HD 109684	5992	4.38	-0.34	1.22	-0.31	-0.05	0.07
HD 144589	6372	4.28	-0.05	1.72	-0.12	-0.02	0.07
HD 43197	5449	4.30	0.36	0.83	-0.10	-0.10	0.03
HD 151504	5431	4.35	0.06	0.87	-0.25	-0.20	0.03
HD 151933	5849	4.29	-0.21	1.03	-0.28	-0.10	0.16
HD 179949	6312	4.56	0.23	1.36	0.005	0.02	0.11
HD 24085	6065	4.47	0.17	1.22	0.05	0.08	0.17
HD 17051	6237	4.46	0.20	1.29	0.035	0.06	0.13
HD 141598	5593	4.37	-0.10	0.75	-0.16	-0.03	0.36
HD 32724	5834	4.28	-0.16	1.14	-0.21	-0.05	0.03
HD 67	5746	4.56	0.03	1.02	0.09	0.16	0.53
HD 6718	5723	4.44	-0.07	0.84	-0.07	0.04	0.14
HD 177565	5614	4.39	0.08	0.91	-0.02	0.03	0.10
HD 20619	5716	4.51	-0.21	0.92	-0.05	0.13	0.04
HD 217395	5916	4.52	-0.13	0.95	-0.05	0.09	0.10
HD 195200	6201	4.44	-0.08	1.25	-0.21	-0.09	0.11
HD 165131	5870	4.45	0.06	0.99	-0.11	-0.05	0.05
HD 13724	5824	4.42	0.21	1.02	0.01	0.03	0.08
HD 9578	6055	4.52	0.11	1.07	-0.085	-0.04	0.07
HD 161612	5594	4.42	0.16	0.88	-0.035	-0.01	0.06
HD 202605	5637	4.47	0.18	1.02	0.085	0.11	0.12
HD 204313	5732	4.33	0.16	1.00	-0.005	0.03	0.09
HD 172513	5487	4.46	-0.07	0.79	-0.13	-0.02	0.04
HD 290327	5505	4.41	-0.14	0.73	-0.12	0.02	0.35
HD 44594	5828	4.37	0.15	1.06	-0.005	0.03	0.08
HD 188815	6217	4.34	-0.53	1.31	-0.41	-0.00	0.10
HD 30669	5400	4.37	0.13	0.55	-0.02	0.02	0.37
HD 47186	5643	4.34	0.22	0.93	0.02	0.04	0.11
HD 202871	6055	4.54	-0.09	1.04	-0.18	-0.06	0.03
HD 22177	5666	4.26	0.20	1.02	-0.07	-0.05	0.06
HD 173885	6264	4.37	-0.20	1.61	-0.21	-0.03	0.03
HD 10647	6222	4.63	0.01	1.22	-0.12	-0.04	0.10
HD 94151	5581	4.40	0.04	0.83	0.08	0.15	0.11
HD 185615	5555	4.33	0.08	0.84	-0.11	-0.05	0.04
HD 221146	5899	4.36	0.10	1.09	0.015	0.06	0.09
HD 135625	6003	4.32	0.12	1.16	-0.065	-0.02	0.07
HD 109271	5783	4.28	0.10	0.97	0.00	0.05	0.04
HD 86652	5934	4.47	0.13	1.01	-0.085	-0.05	0.25
HD 103891	6072	4.05	-0.19	1.50	-0.11	0.06	0.05
HD 27063	5759	4.44	0.05	0.94	0.11	0.17	0.12
HD 45289	5731	4.34	0.00	0.99	-0.26	-0.18	0.05
HD 73121	6083	4.27	0.09	1.34	-0.05	0.00	0.07
HD 115617	5537	4.38	-0.03	0.81	-0.045	0.05	0.12
HD 134664	5823	4.46	0.07	0.99	-0.12	-0.06	0.03
HD 11226	6112	4.35	0.05	1.28	-0.035	0.03	0.10
HD 215456	5798	4.14	-0.08	1.19	-0.11	0.01	0.09
HD 125612	5913	4.43	0.24	1.02	0.035	0.05	0.07
HD 71835	5431	4.39	-0.04	0.79	0.08	0.18	0.19
HD 25171	6160	4.43	-0.11	1.22	-0.16	-0.03	0.03
HD 28821	5663	4.37	-0.12	0.88	-0.075	0.06	0.04
HD 18083	6144	4.70	0.03	1.33	-0.13	-0.06	0.21

Continued on next page

Table E.1 – continued from previous page

Star	Teff	logg	[Fe/H]	ξ_t	[C/O]	$[C/O]_{corr}$	$\sigma_{[C/O]}$
HD 200633	5853	4.51	0.05	1.01	-0.16	-0.10	0.34
HD 7199	5292	4.21	0.25	1.01	-0.02	0.00	0.06
HD 123517	6082	4.08	0.09	1.53	0.02	0.07	0.04
HD 134060	5940	4.42	0.12	1.10	-0.08	-0.03	0.10
HD 33473A	5740	3.97	-0.13	1.20	-0.08	0.06	0.05
HD 40397	5498	4.35	-0.14	0.83	-0.27	-0.13	0.07
HD 115585	5683	4.19	0.36	1.14	0.01	0.01	0.06
HD 143638	5954	4.48	-0.27	1.04	-0.15	0.07	0.14
HD 21977	5930	4.45	0.10	1.03	-0.14	-0.09	0.14
HD 202206	5708	4.38	0.28	1.01	0.03	0.04	0.11
HD 166745	5621	4.31	0.25	0.98	-0.11	-0.09	0.20
HD 104760A	5953	4.43	0.12	1.02	0.05	0.09	0.44
HD 153950	6074	4.39	-0.01	1.23	-0.17	-0.08	0.07
HD 214759	5397	4.27	0.15	0.85	-0.10	-0.06	0.03
HD 111031	5749	4.30	0.26	1.05	0.06	0.07	0.12
HD 74698	5783	4.27	0.07	1.01	-0.18	-0.12	0.03
HD 59468	5582	4.36	0.01	0.88	0.01	0.08	0.12
HD 88084	5765	4.45	-0.10	0.96	0.01	0.13	0.37
HD 154088	5337	4.35	0.26	0.85	-0.03	-0.02	0.04
HD 92719	5812	4.47	-0.11	0.96	-0.08	0.05	0.04
HD 140901	5584	4.40	0.08	0.90	0.01	0.05	0.06
HD 208704	5835	4.38	-0.08	1.04	-0.11	0.01	0.03
HD 1461	5740	4.36	0.18	0.97	-0.04	-0.01	0.10
HD 176354	5271	3.84	0.27	1.07	-0.13	-0.12	0.04
HD 221287	6417	4.60	0.06	1.29	-0.20	-0.14	0.06
HD 207700	5660	4.26	0.04	0.98	-0.12	-0.05	0.08
HD 9782	6013	4.38	0.09	1.09	0.01	0.06	0.06
HD 44120	6059	4.25	0.14	1.31	-0.06	-0.02	0.09
HD 205591	6575	4.75	-0.08	1.85	-0.04	0.07	0.07
HD 224619	5425	4.40	-0.20	0.79	-0.12	0.05	0.22
HD 147512	5515	4.40	-0.09	0.81	-0.07	0.05	0.04
HD 171028	5671	3.84	-0.48	1.24	-0.23	0.14	0.03
HD 171665	5652	4.44	-0.05	0.89	-0.10	0.01	0.04
HD 96276	6080	4.49	-0.02	1.12	-0.09	0.01	0.20
HD 138549	5552	4.40	-0.01	0.87	-0.01	0.08	0.04
HD 50806	5598	4.10	0.01	1.03	-0.12	-0.04	0.10
HD 66039	6149	4.52	0.17	1.14	-0.06	-0.03	0.04
HD 6735	6111	4.56	-0.04	1.15	-0.10	-0.01	0.06
HD 210918	5747	4.35	-0.10	0.99	-0.19	-0.07	0.07
HD 115902	5705	4.39	-0.01	0.86	-0.24	-0.15	0.34
HD 134702	5782	4.50	-0.04	0.74	-0.05	0.05	0.42
HD 7449	6040	4.53	-0.10	1.11	-0.14	-0.02	0.07
HD 169830	6370	4.20	0.18	1.56	-0.04	-0.01	0.12
HD 14745	6290	4.72	-0.14	1.46	-0.12	0.03	0.03
HD 28471	5727	4.36	-0.07	0.95	-0.16	-0.05	0.03
HD 168871	5986	4.44	-0.09	1.17	-0.08	0.04	0.07
HD 72659	5926	4.24	-0.02	1.13	-0.13	-0.04	0.03
HD 13578	5842	4.18	-0.03	1.12	-0.07	0.03	0.25
HD 157347	5667	4.38	0.01	0.91	-0.13	-0.05	0.03
HD 177409	5896	4.51	-0.04	0.99	-0.11	-0.01	0.04
HD 122862	6009	4.25	-0.10	1.29	-0.13	0.00	0.08
HD 204385	6048	4.45	0.08	1.15	-0.06	0.00	0.04
HD 119638	6111	4.48	-0.13	1.22	-0.18	-0.04	0.06
HD 92788	5729	4.35	0.27	0.95	0.04	0.05	0.10
HD 165920	5286	4.36	0.27	0.79	-0.14	-0.13	0.03
HD 95456	6311	4.38	0.18	1.40	-0.04	-0.01	0.13
HD 116410	5939	4.43	0.23	1.07	0.01	0.03	0.18
HD 89839	6314	4.49	0.04	1.35	-0.12	-0.05	0.05

Continued on next page

Table E.1 – continued from previous page

Star	Teff	logg	[Fe/H]	ξ_t	[C/O]	$[C/O]_{corr}$	$\sigma_{[C/O]}$
HD 210277	5470	4.26	0.15	0.86	0.01	0.05	0.11
HD 128340	6259	4.64	-0.55	1.42	-0.50	-0.07	0.04
HD 213240	5967	4.28	0.13	1.25	-0.09	-0.05	0.04
HD 178904	5727	4.41	0.09	0.98	0.00	0.05	0.35
HD 105938	6208	4.27	0.03	1.60	-0.14	-0.07	0.03
HD 192865	6307	4.44	0.13	1.59	-0.06	-0.02	0.06
HD 150177	6216	4.18	-0.58	1.76	-0.21	0.24	0.06
HD 212301	6299	4.58	0.20	1.29	-0.06	-0.03	0.08
HD 145927	5819	4.41	-0.03	0.93	-0.14	-0.05	0.29
HD 94771	5631	4.03	0.22	1.10	-0.02	0.00	0.06
HD 209566	5500	4.38	0.12	0.75	-0.07	-0.02	0.19
HD 20003	5465	4.37	0.03	0.83	-0.08	-0.01	0.10
HD 140785	5756	4.12	-0.05	1.09	-0.11	-0.01	0.27
HD 222595	5618	4.43	-0.01	0.88	-0.12	-0.03	0.04
HD 156411	5910	3.99	-0.11	1.31	-0.02	0.11	0.08
HD 23079	6009	4.50	-0.11	1.12	-0.09	0.04	0.07
HD 134987	5700	4.22	0.23	1.08	0.03	0.05	0.13
HD 93385	5989	4.46	0.03	1.14	-0.11	-0.04	0.07
HD 95542	5984	4.52	-0.04	1.01	-0.13	-0.03	0.03
HD 88742	6004	4.52	0.00	1.07	-0.19	-0.10	0.07
HD 23456	6190	4.61	-0.31	1.38	-0.30	-0.06	0.05
HD 101612	6281	4.41	-0.36	1.17	-0.29	-0.02	0.13
HD 131183	5670	4.24	0.09	0.97	-0.18	-0.13	0.04
HD 19423	5752	4.23	-0.09	0.96	-0.18	-0.06	0.34
HD 66221	5590	4.34	0.16	0.92	-0.01	0.03	0.07
HD 144846	6102	4.52	0.13	1.11	-0.01	0.04	0.41
HD 108309	5781	4.24	0.13	1.08	-0.09	-0.05	0.09
HD 1388	5970	4.42	0.00	1.13	-0.13	-0.05	0.07
HD 102117	5620	4.28	0.26	0.99	-0.08	-0.07	0.09
HD 193193	5979	4.40	-0.05	1.15	-0.18	-0.07	0.06
HD 134606	5614	4.30	0.27	1.00	-0.03	-0.01	0.07
HD 212036	5687	4.41	-0.01	0.80	-0.02	0.07	0.48
HD 115341	6058	4.55	-0.01	1.10	-0.05	0.04	0.42
HD 149396	5657	4.47	0.19	0.91	-0.03	0.00	0.04
HD 100508	5384	4.39	0.35	0.86	-0.03	-0.03	0.09
HD 206116	6231	4.57	0.24	1.36	-0.18	-0.16	0.10
HD 145809	5778	4.15	-0.25	1.14	-0.25	-0.05	0.02
HD 18001	5772	4.44	-0.07	0.80	-0.23	-0.12	0.07
HD 100289	5483	4.42	0.03	0.70	0.04	0.10	0.56
HD 115674	5633	4.43	-0.18	0.85	0.01	0.17	0.47
HD 195145	5625	4.41	0.17	0.82	-0.05	-0.02	0.06
HD 189625	5848	4.43	0.19	1.03	0.05	0.08	0.11
HD 183658	5809	4.40	0.03	1.00	0.06	0.13	0.05
HD 65982	5947	4.42	-0.10	1.08	-0.03	0.10	0.40
HD 102365	5616	4.40	-0.28	0.91	-0.23	-0.01	0.06
HD 218379	5938	4.11	0.15	1.24	0.03	0.07	0.05
HD 199868	6152	4.45	-0.13	1.26	-0.14	0.00	0.18
HD 38973	6015	4.43	0.05	1.14	-0.02	0.04	0.10
HD 121504	6022	4.52	0.14	1.12	-0.10	-0.06	0.07
HD 145377	6054	4.53	0.12	1.11	0.05	0.09	0.10
HD 97037	5890	4.32	-0.07	1.13	-0.10	0.01	0.03
HD 28254	5653	4.15	0.36	1.08	0.11	0.11	0.07
HD 19641	5806	4.39	-0.01	0.94	-0.03	0.06	0.04
HD 457	6089	4.43	0.34	1.17	0.05	0.06	0.06
HD 163102	6433	4.64	0.00	1.94	-0.10	-0.02	0.06
HD 106116	5656	4.35	0.13	0.91	-0.06	-0.02	0.08
HD 92547	6020	4.45	-0.37	1.14	-0.35	-0.07	0.18
HD 157338	6037	4.49	-0.07	1.17	-0.07	0.04	0.09

Table E.2: C/O and Mg/Si abundances

Star	Teff	logg	[Fe/H]	ξ_t	C/O	$\sigma_{C/O}$	Mg/Si	$\sigma_{Mg/Si}$
HD 62364	6255	4.47	-0.11	1.42	0.38	0.50	2.04	0.16
HD 161555	5850	4.15	0.12	1.23	0.55	0.30	1.75	0.26
HD 66428	5671	4.30	0.23	0.96	0.55	0.40	1.88	0.34
HD 3229	6583	4.14	-0.09	1.80	0.48	0.40	1.25	0.11
HD 33081	6399	4.56	-0.16	2.47	0.27	0.40	1.18	0.18
HD 225297	6181	4.55	-0.09	1.24	0.39	0.30	1.60	0.17
HD 70642	5659	4.43	0.17	0.82	0.46	0.20	1.49	0.28
HD 142022A	5482	4.35	0.18	0.83	0.51	0.20	1.67	0.17
HD 24633	5276	4.36	-0.04	0.59	0.46	0.20	1.60	0.38
HD 202209	6009	4.68	-0.01	1.19	0.40	0.30	1.24	0.39
HD 66838	5392	4.29	0.03	0.71	0.57	0.20	1.48	0.44
HD 203335	6306	4.56	-0.04	1.44	0.59	0.20	1.44	0.22
HD 33822	5726	4.29	0.26	0.98	0.52	0.30	1.27	0.40
HD 93932	5950	4.30	0.05	1.16	0.60	0.20	1.60	0.28
HD 139879	6203	4.61	0.30	1.25	0.53	0.30	1.49	0.13
HD 223854	6080	4.08	-0.54	1.60	0.19	0.30	0.71	0.12
HD 151772	6631	4.81	-0.36	2.27	0.32	0.20	1.29	0.13
HD 21161	5923	4.24	0.09	1.14	0.46	0.20	0.93	0.28
HD 77110	5717	4.48	-0.50	0.86	0.21	0.10	1.38	0.29
HD 224817	5894	4.36	-0.53	1.13	0.21	0.10	1.38	0.11
HD 55693	5908	4.38	0.35	1.07	0.50	0.20	1.10	0.07
HD 82783	5318	4.41	0.21	0.91	0.65	0.20	1.28	0.38
HD 19994	6315	4.44	0.27	1.72	0.65	0.20	0.59	0.08
HD 144880	6152	4.38	-0.30	1.33	0.32	0.10	1.26	0.32
HD 83443	5442	4.32	0.32	0.93	0.60	0.20	1.03	0.07
HD 220367	6116	4.45	-0.23	1.34	0.38	0.10	1.23	0.14
HD 29263	5780	4.35	0.03	0.94	0.58	0.10	1.11	0.37
HD 217786	5966	4.35	-0.14	1.12	0.52	0.10	1.21	0.36
HD 161566	6230	4.20	-0.28	1.67	0.32	0.20	0.73	0.08
HD 212231	5762	4.20	-0.30	1.01	0.29	0.10	1.36	0.41
HD 177758	5933	4.51	-0.54	1.11	0.21	0.10	1.27	0.20
HD 20807	5875	4.50	-0.23	1.04	0.45	0.09	1.24	0.08
HD 114729	5865	4.20	-0.26	1.23	0.34	0.10	1.31	0.07
HD 81639	5516	4.39	-0.18	0.79	0.43	0.10	1.27	0.36
HD 44447	6004	4.41	-0.22	1.26	0.39	0.09	1.20	0.08
HD 196761	5414	4.46	-0.31	0.76	0.38	0.09	1.21	0.26
HD 20794	5398	4.41	-0.41	0.67	0.26	0.09	1.31	0.09
HD 143114	5811	4.46	-0.41	0.92	0.28	0.08	1.39	0.29
HD 221356	6100	4.51	-0.20	1.12	0.36	0.09	1.20	0.08
HD 5388	6311	4.24	-0.28	1.65	0.35	0.10	0.78	0.07
HD 69611	5762	4.31	-0.58	0.99	0.12	0.09	1.37	0.17
HD 109098	5888	4.14	0.06	1.24	0.46	0.10	1.08	0.17
HD 224347	6092	4.27	-0.42	1.31	0.25	0.10	1.14	0.13
HD 90702	5760	4.56	0.20	1.04	0.51	0.10	1.06	0.42
HD 18386	5446	4.37	0.14	0.92	0.58	0.10	0.88	0.15
HD 107148	5744	4.30	0.28	0.93	0.63	0.10	1.10	0.30
HD 90936	5928	4.48	0.03	1.04	0.51	0.10	0.93	0.34
HD 8638	5508	4.45	-0.40	0.74	0.25	0.07	1.37	0.36
HD 181428	6151	4.45	0.06	1.29	0.48	0.09	1.05	0.11
HD 88218	5872	4.14	-0.14	1.23	0.48	0.09	1.19	0.22
HD 20407	5885	4.52	-0.43	1.09	0.30	0.09	1.21	0.13
HD 197300	6022	4.69	0.02	1.21	0.43	0.20	0.80	0.34
HD 52449	6362	4.55	0.12	1.29	0.55	0.09	0.88	0.11
HD 124785	5867	4.20	-0.56	1.29	0.22	0.08	1.29	0.16
HD 24892	5360	3.99	-0.33	0.88	0.30	0.08	1.18	0.35
HD 14747	5547	4.46	-0.37	0.72	0.23	0.07	1.30	0.23
HD 61383	5716	4.20	-0.49	1.12	0.20	0.07	1.28	0.20

Continued on next page

Table E.2 – continued from previous page

Star	Teff	logg	[Fe/H]	ξ_t	C/O	$\sigma_{C/O}$	Mg/Si	$\sigma_{Mg/Si}$
HD 65907A	5995	4.62	-0.29	1.05	0.25	0.08	1.29	0.07
HD 68287	6318	4.63	0.06	1.45	0.49	0.10	0.91	0.19
HD 16382	5953	4.50	0.03	1.04	0.48	0.10	0.97	0.32
HD 199086	6149	4.65	0.18	1.21	0.46	0.10	0.75	0.25
HD 100777	5530	4.31	0.25	0.81	0.53	0.10	0.96	0.11
HD 210272	5713	4.13	-0.22	1.16	0.47	0.08	1.21	0.40
HD 208487	6172	4.54	0.10	1.24	0.48	0.08	1.06	0.07
HD 79601	5825	4.32	-0.59	1.09	0.15	0.07	1.30	0.13
HD 150433	5680	4.48	-0.36	0.88	0.26	0.07	1.32	0.11
HD 167300	5837	4.30	-0.45	1.05	0.25	0.08	1.25	0.26
HD 198075	5842	4.55	-0.24	0.95	0.31	0.07	1.20	0.31
HD 224433	5527	4.42	0.09	0.72	0.52	0.09	1.18	0.43
HD 115773	6312	4.23	-0.08	1.57	0.43	0.09	1.03	0.09
HD 106290	6012	4.55	0.13	1.03	0.65	0.09	0.86	0.42
HD 70889	6069	4.55	0.13	1.13	0.54	0.08	1.09	0.06
HD 213575	5676	4.22	-0.15	1.02	0.33	0.06	1.32	0.10
HD 216770	5351	4.31	0.20	0.91	0.60	0.10	1.00	0.099
HD 181720	5792	4.25	-0.53	1.16	0.20	0.07	1.27	0.11
HD 111232	5482	4.46	-0.43	0.62	0.23	0.07	1.32	0.21
HD 21019	5468	3.93	-0.45	1.05	0.29	0.07	1.24	0.25
HD 2768	5548	4.40	-0.03	0.81	0.55	0.10	1.09	0.46
HD 38277	5882	4.35	-0.06	1.10	0.46	0.07	1.17	0.10
HD 11505	5757	4.39	-0.22	0.99	0.30	0.07	1.28	0.11
HD 24062	6107	4.62	0.28	1.34	0.51	0.20	0.81	0.18
HD 150139	5968	4.29	-0.51	1.29	0.34	0.08	1.18	0.34
HD 28969	6255	4.68	-0.01	1.47	0.40	0.20	1.23	0.27
HD 195633	6154	4.25	-0.51	1.47	0.32	0.09	1.13	0.36
HD 213941	5565	4.45	-0.44	0.72	0.25	0.07	1.29	0.38
HD 870	5360	4.40	-0.12	0.79	0.51	0.07	1.19	0.41
HD 1581	5990	4.49	-0.18	1.12	0.38	0.07	1.11	0.07
HD 90711	5396	4.33	0.21	0.92	0.56	0.09	1.00	0.11
HD 51754	5848	4.49	-0.55	1.05	0.12	0.07	1.30	0.12
HD 117105	5912	4.44	-0.28	1.13	0.31	0.07	1.24	0.13
HD 160089	6312	4.78	0.11	1.60	0.49	0.10	0.85	0.21
HD 4308	5662	4.44	-0.32	0.90	0.23	0.06	1.30	0.08
HD 199847	5763	4.22	-0.54	1.04	0.18	0.07	1.31	0.27
HD 29137	5768	4.28	0.30	1.10	0.54	0.10	1.08	0.14
HD 25587	6258	4.61	-0.12	1.78	0.42	0.20	0.79	0.35
HD 34327	5883	4.20	-0.06	1.19	0.57	0.06	1.03	0.39
HD 78558	5759	4.46	-0.42	0.99	0.13	0.06	1.28	0.12
HD 27471	5871	4.25	0.11	1.13	0.41	0.08	1.00	0.23
HD 4915	5660	4.50	-0.21	0.90	0.38	0.07	1.15	0.11
HD 218504	5962	4.34	-0.55	1.21	0.14	0.08	1.24	0.11
HD 136352	5659	4.40	-0.35	0.90	0.23	0.06	1.27	0.081
HD 41248	5713	4.49	-0.37	0.84	0.40	0.08	1.16	0.26
HD 17548	6011	4.44	-0.53	1.18	0.38	0.08	1.19	0.31
HD 207832	5718	4.45	0.15	0.86	0.49	0.07	1.01	0.37
HD 96700	5854	4.39	-0.18	1.04	0.49	0.06	1.18	0.08
HD 196384	6611	4.79	-0.13	1.78	0.45	0.20	1.18	0.21
HD 190647	5636	4.18	0.23	0.99	0.52	0.08	1.10	0.11
HD 179346	6229	4.76	-0.03	1.35	0.62	0.10	1.03	0.30
HD 203432	5591	4.29	0.27	0.98	0.68	0.08	1.00	0.08
HD 95521	5762	4.46	-0.15	0.96	0.48	0.07	1.00	0.16
HD 75289	6139	4.35	0.30	1.29	0.51	0.08	0.92	0.056
HD 130989	6414	4.27	-0.23	1.85	0.36	0.10	0.87	0.10
HD 220894	6282	4.60	0.02	1.35	0.40	0.10	0.78	0.10
HD 221420	5838	3.98	0.34	1.28	0.65	0.07	1.17	0.06
HD 72769	5587	4.30	0.29	0.98	0.65	0.10	1.04	0.11

Continued on next page

Table E.2 – **continued from previous page**

Star	Teff	logg	[Fe/H]	ξ_t	C/O	$\sigma_{C/O}$	Mg/Si	$\sigma_{Mg/Si}$
HD 221343	5848	4.54	0.11	0.99	0.65	0.09	1.08	0.34
HD 119949	6359	4.47	-0.41	1.65	0.46	0.10	1.21	0.14
HD 114853	5698	4.43	-0.23	0.92	0.33	0.06	1.20	0.09
HD 17439	5721	4.44	0.08	0.87	0.49	0.06	1.14	0.20
HD 3823	6054	4.37	-0.26	1.39	0.32	0.06	1.14	0.07
HD 54521	5973	4.54	-0.01	1.02	0.40	0.09	1.14	0.28
HD 201496	5974	4.44	-0.04	1.12	0.45	0.06	1.05	0.37
HD 73524	6004	4.42	0.16	1.14	0.54	0.07	1.16	0.08
HD 172643	5645	4.50	-0.15	0.73	0.30	0.09	0.97	0.48
HD 30278	5374	4.37	-0.19	0.72	0.36	0.06	1.13	0.18
HD 4307	5840	4.13	-0.21	1.22	0.37	0.06	1.21	0.08
HD 16548	5690	3.96	0.15	1.15	0.50	0.06	1.16	0.11
HD 16008	5712	4.42	-0.09	0.78	0.26	0.08	1.11	0.41
HD 123265	5311	4.31	0.18	0.85	0.50	0.10	1.16	0.18
HD 129229	5872	3.89	-0.42	1.37	0.30	0.06	1.13	0.26
HD 28701	5718	4.47	-0.32	0.95	0.30	0.05	1.27	0.11
HD 224063	5591	4.27	0.14	0.84	0.33	0.08	1.17	0.25
HD 39091	5991	4.40	0.09	1.12	0.61	0.06	1.11	0.07
HD 154195A	5961	4.48	-0.19	1.01	0.37	0.07	1.07	0.29
HD 139590	6200	4.49	0.13	1.31	0.45	0.06	0.91	0.09
HD 37226	6178	4.16	-0.12	1.61	0.39	0.07	1.04	0.08
HD 38382	6110	4.46	0.04	1.18	0.58	0.06	1.12	0.11
HD 124364	5601	4.49	-0.27	0.83	0.35	0.06	1.15	0.25
HD 222582	5781	4.37	-0.01	1.00	0.56	0.05	1.14	0.08
HD 95860	6054	4.48	-0.31	1.25	0.24	0.07	1.14	0.24
HD 96290	6219	4.56	0.03	1.21	0.46	0.06	0.94	0.14
HD 66740	6666	4.49	0.04	1.70	0.44	0.10	0.72	0.11
HD 220507	5676	4.30	0.00	1.01	0.42	0.05	1.24	0.09
HD 28185	5621	4.36	0.19	0.94	0.52	0.07	1.00	0.08
HD 97343	5385	4.31	-0.08	0.82	0.47	0.06	1.23	0.29
HD 83529	5909	4.36	-0.22	1.11	0.42	0.05	1.19	0.10
HD 102438	5562	4.43	-0.29	0.84	0.45	0.05	1.18	0.10
HD 49035	5640	4.35	0.24	1.01	0.68	0.08	1.18	0.22
HD 28807	6602	4.67	0.06	1.89	0.42	0.10	0.94	0.17
HD 26729	5718	4.17	0.31	1.13	0.55	0.08	1.06	0.18
HD 21938	5800	4.41	-0.47	0.99	0.19	0.07	1.30	0.18
HD 82114	5912	4.20	0.01	1.28	0.42	0.09	0.82	0.29
HD 141937	5892	4.46	0.13	1.00	0.73	0.05	1.02	0.14
HD 210320	5597	4.31	0.11	0.87	0.41	0.10	1.24	0.52
HD 221638	6360	4.53	-0.21	1.43	0.40	0.10	0.92	0.11
HD 45184	5869	4.47	0.05	1.03	0.54	0.06	1.15	0.07
HD 564	5902	4.53	-0.20	0.95	0.42	0.05	1.12	0.16
HD 98281	5389	4.39	-0.27	0.64	0.46	0.06	1.18	0.16
HD 196800	6007	4.40	0.18	1.17	0.50	0.06	1.08	0.10
HD 102300	5987	4.23	-0.31	1.14	0.31	0.06	1.14	0.38
HD 210752	5970	4.52	-0.55	1.20	0.33	0.06	1.13	0.19
CD-436810	6011	4.41	-0.44	1.09	0.16	0.08	1.28	0.20
HD 68284	5933	4.08	-0.50	1.40	0.22	0.06	1.12	0.14
HD 209449	5854	4.16	0.41	1.19	0.56	0.10	1.00	0.09
HD 223171	5830	4.16	0.11	1.12	0.59	0.05	1.14	0.062
HD 124292	5426	4.37	-0.14	0.77	0.47	0.04	1.17	0.11
HD 197536	6105	4.39	-0.41	1.34	0.29	0.07	1.17	0.28
HD 63765	5445	4.41	-0.15	0.82	0.51	0.05	1.14	0.16
HD 93745	6065	4.34	0.12	1.33	0.60	0.07	1.04	0.19
HD 66168	6198	4.69	-0.03	1.18	0.65	0.10	0.83	0.26
HD 143790	6557	4.11	-0.06	2.05	0.40	0.10	0.79	0.094
HD 88474	6122	3.91	-0.48	1.91	0.36	0.10	0.82	0.32
HD 3220	5846	4.51	-0.22	0.87	0.42	0.05	1.12	0.24

Continued on next page

Table E.2 – **continued from previous page**

Star	Teff	logg	[Fe/H]	ξ_t	C/O	$\sigma_{C/O}$	Mg/Si	$\sigma_{Mg/Si}$
BD-131161	5389	4.37	0.09	0.68	0.33	0.06	1.26	0.44
HD 59711A	5741	4.44	-0.12	0.86	0.56	0.04	1.13	0.37
HD 32804	5910	4.53	0.06	1.08	0.52	0.05	1.16	0.23
HD 31532	5896	4.07	-0.08	1.33	0.35	0.09	1.16	0.28
HD 122474	5716	4.37	0.13	0.88	0.40	0.05	1.11	0.41
HD 197083	5735	4.50	-0.45	0.90	0.28	0.06	1.17	0.32
HD 2567	6038	4.44	0.22	1.19	0.51	0.05	1.06	0.11
HD 12387	5704	4.42	-0.25	0.93	0.28	0.04	1.24	0.07
HD 196050	5871	4.26	0.23	1.21	0.47	0.05	1.08	0.06
HD 168746	5561	4.31	-0.11	0.81	0.41	0.05	1.26	0.42
HD 197197	5812	4.20	-0.46	1.25	0.20	0.05	1.22	0.14
HD 11397	5564	4.46	-0.54	0.75	0.40	0.06	1.36	0.19
HD 208	5914	4.47	-0.31	1.05	0.45	0.06	1.17	0.14
HD 76188	5989	4.08	-0.44	1.25	0.25	0.08	1.06	0.45
HD 90926	5538	4.35	0.13	0.80	0.58	0.03	1.05	0.43
HD 44420	5772	4.30	0.28	1.06	0.61	0.06	1.01	0.071
HD 7134	5979	4.49	-0.27	1.17	0.36	0.05	1.15	0.12
HD 48115	5825	4.48	-0.19	0.89	0.42	0.05	1.10	0.21
HD 36051	6118	4.63	-0.08	1.21	0.41	0.06	1.03	0.20
HD 216435	6034	4.21	0.27	1.34	0.58	0.07	0.87	0.07
HD 148577	5713	4.29	-0.09	0.95	0.34	0.05	1.22	0.22
HD 117207	5649	4.31	0.21	1.01	0.59	0.06	1.05	0.12
HD 157172	5419	4.32	0.09	0.77	0.47	0.05	1.05	0.10
HD 144585	5880	4.32	0.32	1.15	0.50	0.06	1.21	0.06
HD 73256	5465	4.36	0.21	1.11	0.47	0.05	1.00	0.07
HD 108768	5633	4.45	0.14	0.86	0.61	0.03	1.03	0.40
HD 189567	5718	4.39	-0.25	0.95	0.48	0.04	1.22	0.08
HD 177122	6021	4.52	-0.10	1.03	0.87	0.08	1.09	0.40
HD 72579	5419	4.28	0.18	0.84	0.54	0.07	1.22	0.15
HD 75881	6239	4.44	0.07	1.63	0.58	0.10	0.97	0.19
HD 203384	5564	4.42	0.26	0.90	0.52	0.07	1.04	0.11
HD 180409	6031	4.51	-0.15	1.16	0.46	0.06	1.11	0.29
HD 152433	6144	4.49	-0.10	1.19	0.33	0.05	1.04	0.31
HD 212708	5644	4.31	0.26	0.99	0.51	0.08	1.06	0.07
HD 108063	6081	4.11	0.55	1.54	0.51	0.07	0.96	0.09
HD 111564	6004	4.37	0.07	1.13	0.51	0.05	1.12	0.11
HD 33811	5554	4.39	0.30	0.78	0.55	0.20	1.08	0.41
HD 45364	5428	4.37	-0.18	0.71	0.50	0.04	1.16	0.11
HD 90722	5711	4.28	0.31	1.06	0.74	0.07	1.04	0.30
HD 131664	5901	4.50	0.31	1.04	0.68	0.06	1.02	0.07
HD 16417	5843	4.16	0.14	1.18	0.57	0.05	1.17	0.06
HD 62128	5828	4.22	0.33	1.16	0.51	0.07	1.08	0.08
HD 78429	5742	4.26	0.07	1.01	0.52	0.07	1.04	0.08
HD 224578	6158	4.67	-0.01	1.13	0.51	0.10	1.07	0.42
HD 205294	6370	4.30	-0.25	1.71	0.39	0.08	0.90	0.09
HD 207129	5946	4.48	0.01	1.06	0.49	0.04	1.10	0.06
HD 104263	5456	4.35	0.01	0.81	0.53	0.04	1.25	0.10
HD 191033	6206	4.47	-0.19	1.35	0.30	0.20	1.15	0.34
HD 174153	6196	4.49	-0.08	1.34	0.58	0.05	1.02	0.20
HD 96423	5701	4.35	0.10	0.98	0.47	0.04	1.14	0.12
HD 162396	6121	4.33	-0.34	1.43	0.37	0.05	1.09	0.08
HD 114613	5712	3.94	0.18	1.18	0.65	0.06	1.05	0.06
HD 211317	5965	4.30	0.27	1.21	0.59	0.07	0.97	0.15
HD 190984	6007	4.02	-0.49	1.58	0.33	0.06	1.04	0.09
HD 222669	5898	4.44	0.06	1.01	0.61	0.05	1.12	0.07
HD 8535	6158	4.42	0.04	1.25	0.38	0.04	1.06	0.07
HD 105837	5932	4.60	-0.50	1.14	0.38	0.06	1.10	0.38
HD 38772	6106	4.37	-0.23	1.16	0.40	0.10	1.14	0.37

Continued on next page

Table E.2 – **continued from previous page**

Star	Teff	logg	[Fe/H]	ξ_t	C/O	$\sigma_{C/O}$	Mg/Si	$\sigma_{Mg/Si}$
HD 135468	6417	4.25	-0.02	1.82	0.42	0.10	0.96	0.09
HD 214094	6288	4.28	-0.01	1.46	0.58	0.05	1.04	0.07
HD 56274	5734	4.51	-0.54	0.94	0.30	0.05	1.12	0.18
HD 361	5888	4.54	-0.13	1.00	0.41	0.04	1.07	0.09
HD 142	6431	4.82	0.05	1.74	0.46	0.10	0.79	0.09
HD 69655	5977	4.49	-0.18	1.15	0.50	0.06	1.03	0.08
HD 78612	5838	4.30	-0.24	1.14	0.36	0.04	1.21	0.10
HD 30306	5520	4.32	0.18	0.89	0.58	0.05	1.15	0.12
HD 24112	6175	4.35	0.16	1.26	0.51	0.03	0.94	0.07
HD 149200	6416	4.64	0.15	1.74	0.41	0.10	0.80	0.11
HD 104982	5682	4.42	-0.20	0.91	0.42	0.04	1.20	0.27
HD 20782	5770	4.35	-0.06	1.00	0.42	0.03	1.14	0.08
HD 63754	6200	4.21	0.21	1.57	0.59	0.10	1.04	0.08
HD 31527	5917	4.47	-0.17	1.09	0.52	0.04	1.11	0.13
HD 16141	5786	4.17	0.15	1.11	0.52	0.04	1.16	0.11
HD 36379	6039	4.35	-0.18	1.29	0.44	0.04	1.06	0.07
HD 136894	5402	4.37	-0.11	0.75	0.42	0.04	1.16	0.12
HD 154962	5778	4.12	0.30	1.22	0.61	0.06	1.10	0.07
HD 119629	6250	4.17	-0.17	1.73	0.44	0.20	0.74	0.12
HD 123651	5926	4.55	-0.48	1.05	0.29	0.09	1.20	0.44
HD 21693	5418	4.38	0.00	0.76	0.48	0.03	1.09	0.12
HD 125184	5660	4.11	0.27	1.13	0.85	0.06	1.14	0.16
HD 215906	6259	4.56	-0.28	1.55	0.32	0.08	0.89	0.33
HD 207970	5524	4.36	0.05	0.80	0.76	0.07	1.18	0.33
HD 101367	5615	4.38	0.29	0.91	0.50	0.08	1.02	0.40
HD 145666	5984	4.56	-0.02	1.04	0.53	0.04	1.05	0.09
HD 204287	5743	4.15	-0.04	1.10	0.40	0.03	1.21	0.16
HD 37986	5479	4.29	0.24	0.92	0.54	0.07	1.15	0.12
HD 67200	6105	4.44	0.32	1.19	0.68	0.20	0.69	0.12
HD 10180	5898	4.39	0.08	1.11	0.54	0.04	1.09	0.06
HD 76151	5781	4.44	0.12	0.96	0.70	0.05	1.09	0.14
HD 207190	6178	4.33	-0.42	1.51	0.18	0.06	1.04	0.10
HD 188748	5616	4.45	-0.13	0.83	0.45	0.04	1.14	0.20
HD 78538	5790	4.50	-0.02	0.98	0.38	0.04	1.11	0.17
HD 34449	5861	4.45	-0.09	0.92	0.42	0.04	1.10	0.18
HD 87838	6118	4.47	-0.40	1.33	0.27	0.08	1.21	0.10
HD 38858	5719	4.49	-0.23	0.94	0.50	0.04	1.09	0.09
HD 206163	5506	4.42	0.02	0.94	0.38	0.03	1.04	0.43
HD 36108	5924	4.36	-0.20	1.21	0.35	0.04	1.13	0.11
HD 162236	5336	4.42	-0.12	0.82	0.45	0.05	0.94	0.31
HD 199190	5937	4.27	0.15	1.14	0.56	0.04	1.12	0.07
HD 8406	5731	4.52	-0.10	0.87	0.50	0.04	1.11	0.19
HD 85725	5986	3.95	0.15	1.54	0.56	0.03	0.89	0.07
HD 44219	5766	4.20	0.04	1.06	0.47	0.03	1.17	0.10
HD 195564	5663	4.02	0.05	1.11	0.49	0.03	1.17	0.07
HD 176666	6103	4.63	-0.37	1.18	0.25	0.10	1.10	0.37
HD 11964A	5285	3.81	0.06	0.99	0.54	0.06	1.20	0.08
HD 2071	5729	4.49	-0.08	0.95	0.48	0.03	1.07	0.14
HD 211415	5864	4.42	-0.21	0.99	0.48	0.04	1.13	0.27
HD 171990	6048	4.15	0.06	1.40	0.54	0.03	1.07	0.07
HD 67458	5903	4.54	-0.15	1.04	0.36	0.04	1.07	0.08
HD 215625	6282	4.58	0.10	1.35	0.38	0.08	0.97	0.12
HD 17865	5877	4.32	-0.57	1.16	0.24	0.06	1.25	0.11
HD 109409	5833	4.11	0.31	1.24	0.64	0.09	1.03	0.07
HD 200538	6042	4.38	0.10	1.22	0.45	0.04	1.03	0.09
HD 30177	5601	4.34	0.37	0.89	0.63	0.09	1.20	0.17
HD 76440	5764	4.43	-0.01	0.89	0.67	0.06	1.13	0.48
HD 197823	5344	4.37	0.10	0.82	0.54	0.03	1.00	0.12

Continued on next page

Table E.2 – continued from previous page

Star	Teff	logg	[Fe/H]	ξ_t	C/O	$\sigma_{C/O}$	Mg/Si	$\sigma_{Mg/Si}$
HD 129191	5832	4.39	0.24	0.99	0.47	0.04	1.04	0.14
HD 69830	5370	4.38	-0.07	0.80	0.53	0.04	1.09	0.08
HD 160691	5750	4.19	0.29	1.09	0.61	0.05	1.09	0.07
HD 125881	6046	4.49	0.07	1.10	0.55	0.03	0.97	0.07
HD 68978A	5967	4.48	0.05	1.09	0.61	0.04	1.00	0.07
HD 31822	6061	4.61	-0.19	1.15	0.41	0.04	1.05	0.15
HD 89454	5708	4.45	0.11	0.96	0.58	0.03	1.05	0.07
HD 108147	6318	4.53	0.21	1.30	0.56	0.05	0.90	0.07
HD 161256	5652	4.27	0.14	0.93	0.37	0.05	1.17	0.21
HD 190248	5566	4.24	0.32	0.99	0.60	0.20	0.88	0.07
HD 21132	6243	4.60	-0.37	1.44	0.32	0.05	1.01	0.08
HD 126525	5645	4.40	-0.09	0.90	0.43	0.03	1.13	0.15
HD 146233	5810	4.46	0.05	1.00	0.47	0.05	1.13	0.07
HD 117618	6003	4.45	0.03	1.13	0.46	0.03	1.06	0.07
HD 25912	5900	4.52	0.12	0.99	0.61	0.10	1.20	0.42
HD 31103	6078	4.49	0.09	1.08	0.70	0.02	0.99	0.10
HD 82943	5992	4.42	0.28	1.10	0.63	0.03	0.99	0.06
HD 71479	5991	4.38	0.24	1.19	0.56	0.03	1.04	0.06
HD 40865	5719	4.50	-0.38	0.87	0.36	0.04	1.17	0.21
HD 199960	5928	4.42	0.27	1.13	0.46	0.05	1.03	0.08
HD 71334	5706	4.41	-0.08	0.95	0.40	0.03	1.16	0.14
HD 214385	5679	4.47	-0.33	0.81	0.40	0.04	1.15	0.42
HD 103197	5250	4.45	0.22	0.84	0.54	0.07	1.08	0.25
HD 220456	5887	4.50	-0.02	1.01	0.39	0.04	1.07	0.29
HD 150437	5826	4.29	0.30	1.09	0.81	0.07	1.06	0.34
HD 52265	6167	4.44	0.24	1.32	0.54	0.04	0.97	0.09
HD 63685	5497	4.05	0.00	0.94	0.52	0.04	1.18	0.45
HD 90081	5912	4.34	-0.20	1.08	0.40	0.08	1.18	0.45
HD 40483	6371	4.39	-0.06	1.80	0.37	0.06	1.03	0.13
HD 149724	5747	4.24	0.37	1.08	0.56	0.06	1.09	0.20
HD 141597	6285	4.38	-0.40	1.23	0.30	0.10	1.35	0.24
HD 84627B	6113	4.50	-0.28	1.10	0.29	0.07	1.07	0.35
HD 196397	5378	4.33	0.29	0.68	0.49	0.05	1.00	0.46
HD 190613	5776	4.33	0.00	0.95	0.41	0.05	1.04	0.39
HD 156079	5892	4.24	0.28	1.16	0.44	0.03	1.04	0.11
HD 116259	5700	4.21	0.11	0.99	0.45	0.03	1.29	0.21
HD 74014	5552	4.33	0.22	0.90	0.46	0.07	1.03	0.12
HD 148156	6251	4.51	0.25	1.36	0.51	0.05	0.86	0.07
HD 156098	6517	4.20	0.18	2.06	0.37	0.10	0.76	0.072
HD 37990	6215	4.56	0.00	1.15	0.37	0.08	0.90	0.17
HD 216008	5773	4.38	-0.04	0.91	0.35	0.05	1.09	0.37
HD 26887	6016	4.46	-0.35	1.00	0.21	0.06	1.09	0.33
HD 41323	5756	4.56	-0.31	0.84	0.43	0.04	1.06	0.34
HD 109684	5992	4.38	-0.34	1.22	0.28	0.05	0.99	0.22
HD 144589	6372	4.28	-0.05	1.72	0.44	0.10	0.74	0.09
HD 43197	5449	4.30	0.36	0.83	0.46	0.08	1.05	0.11
HD 151504	5431	4.35	0.06	0.87	0.32	0.04	1.22	0.12
HD 151933	5849	4.29	-0.21	1.03	0.30	0.03	1.12	0.32
HD 179949	6312	4.56	0.23	1.36	0.58	0.06	0.80	0.07
HD 24085	6065	4.47	0.17	1.22	0.65	0.08	1.03	0.21
HD 17051	6237	4.46	0.20	1.29	0.62	0.10	0.95	0.08
HD 141598	5593	4.37	-0.10	0.75	0.40	0.07	1.29	0.45
HD 32724	5834	4.28	-0.16	1.14	0.36	0.03	1.17	0.11
HD 67	5746	4.56	0.03	1.02	0.71	0.05	1.08	0.39
HD 6718	5723	4.44	-0.07	0.84	0.49	0.03	1.08	0.24
HD 177565	5614	4.39	0.08	0.91	0.55	0.02	1.07	0.07
HD 20619	5716	4.51	-0.21	0.92	0.51	0.05	1.16	0.16
HD 217395	5916	4.52	-0.13	0.95	0.51	0.05	1.06	0.20

Continued on next page

Table E.2 – continued from previous page

Star	Teff	logg	[Fe/H]	ξ_t	C/O	$\sigma_{C/O}$	Mg/Si	$\sigma_{Mg/Si}$
HD 195200	6201	4.44	-0.08	1.25	0.36	0.08	0.98	0.25
HD 165131	5870	4.45	0.06	0.99	0.45	0.04	1.05	0.17
HD 13724	5824	4.42	0.21	1.02	0.59	0.03	1.04	0.07
HD 9578	6055	4.52	0.11	1.07	0.47	0.03	1.04	0.07
HD 161612	5594	4.42	0.16	0.88	0.53	0.03	1.12	0.09
HD 202605	5637	4.47	0.18	1.02	0.70	0.03	1.03	0.20
HD 204313	5732	4.33	0.16	1.00	0.57	0.03	1.09	0.07
HD 172513	5487	4.46	-0.07	0.79	0.43	0.03	1.08	0.10
HD 290327	5505	4.41	-0.14	0.73	0.44	0.05	1.08	0.42
HD 44594	5828	4.37	0.15	1.06	0.57	0.03	1.08	0.07
HD 188815	6217	4.34	-0.53	1.31	0.22	0.10	0.98	0.33
HD 30669	5400	4.37	0.13	0.55	0.55	0.02	1.14	0.37
HD 47186	5643	4.34	0.22	0.93	0.60	0.06	1.14	0.07
HD 202871	6055	4.54	-0.09	1.04	0.38	0.03	1.04	0.12
HD 22177	5666	4.26	0.20	1.02	0.49	0.05	1.13	0.18
HD 173885	6264	4.37	-0.20	1.61	0.36	0.05	1.03	0.11
HD 10647	6222	4.63	0.01	1.22	0.44	0.04	0.95	0.07
HD 94151	5581	4.40	0.04	0.83	0.69	0.03	1.11	0.20
HD 185615	5555	4.33	0.08	0.84	0.45	0.04	1.20	0.10
HD 221146	5899	4.36	0.10	1.09	0.60	0.02	1.09	0.07
HD 135625	6003	4.32	0.12	1.16	0.50	0.02	0.99	0.08
HD 109271	5783	4.28	0.10	0.97	0.58	0.02	1.13	0.11
HD 86652	5934	4.47	0.13	1.01	0.47	0.04	1.02	0.32
HD 103891	6072	4.05	-0.19	1.50	0.45	0.04	1.01	0.10
HD 27063	5759	4.44	0.05	0.94	0.73	0.03	1.10	0.08
HD 45289	5731	4.34	0.00	0.99	0.31	0.02	1.20	0.08
HD 73121	6083	4.27	0.09	1.34	0.51	0.02	1.07	0.07
HD 115617	5537	4.38	-0.03	0.81	0.52	0.03	1.18	0.08
HD 134664	5823	4.46	0.07	0.99	0.44	0.03	1.05	0.10
HD 11226	6112	4.35	0.05	1.28	0.53	0.02	1.04	0.07
HD 215456	5798	4.14	-0.08	1.19	0.45	0.02	1.14	0.07
HD 125612	5913	4.43	0.24	1.02	0.62	0.03	1.02	0.08
HD 71835	5431	4.39	-0.04	0.79	0.69	0.02	1.08	0.24
HD 25171	6160	4.43	-0.11	1.22	0.40	0.05	1.08	0.13
HD 28821	5663	4.37	-0.12	0.88	0.48	0.02	1.19	0.14
HD 18083	6144	4.70	0.03	1.33	0.43	0.10	1.04	0.32
HD 200633	5853	4.51	0.05	1.01	0.40	0.05	1.04	0.43
HD 7199	5292	4.21	0.25	1.01	0.56	0.09	1.02	0.07
HD 123517	6082	4.08	0.09	1.53	0.60	0.20	1.00	0.12
HD 134060	5940	4.42	0.12	1.10	0.48	0.04	1.12	0.07
HD 33473A	5740	3.97	-0.13	1.20	0.48	0.02	1.11	0.16
HD 40397	5498	4.35	-0.14	0.83	0.31	0.05	1.27	0.22
HD 115585	5683	4.19	0.36	1.14	0.58	0.07	1.11	0.09
HD 143638	5954	4.48	-0.27	1.04	0.41	0.07	1.10	0.24
HD 21977	5930	4.45	0.10	1.03	0.42	0.03	0.98	0.25
HD 202206	5708	4.38	0.28	1.01	0.61	0.04	0.97	0.07
HD 166745	5621	4.31	0.25	0.98	0.45	0.03	1.24	0.30
HD 104760A	5953	4.43	0.12	1.02	0.65	0.06	1.08	0.37
HD 153950	6074	4.39	-0.01	1.23	0.39	0.02	1.06	0.08
HD 214759	5397	4.27	0.15	0.85	0.46	0.07	1.19	0.15
HD 111031	5749	4.30	0.26	1.05	0.66	0.04	1.04	0.07
HD 74698	5783	4.27	0.07	1.01	0.38	0.05	1.16	0.10
HD 59468	5582	4.36	0.01	0.88	0.58	0.03	1.16	0.08
HD 88084	5765	4.45	-0.10	0.96	0.59	0.03	1.14	0.36
HD 154088	5337	4.35	0.26	0.85	0.54	0.10	1.14	0.09
HD 92719	5812	4.47	-0.11	0.96	0.48	0.03	1.12	0.10
HD 140901	5584	4.40	0.08	0.90	0.58	0.04	1.11	0.09
HD 208704	5835	4.38	-0.08	1.04	0.45	0.03	1.09	0.13

Continued on next page

Table E.2 – continued from previous page

Star	Teff	logg	[Fe/H]	ξ_t	C/O	$\sigma_{C/O}$	Mg/Si	$\sigma_{Mg/Si}$
HD 1461	5740	4.36	0.18	0.97	0.53	0.03	1.08	0.05
HD 176354	5271	3.84	0.27	1.07	0.43	0.08	1.07	0.11
HD 221287	6417	4.60	0.06	1.29	0.37	0.04	0.94	0.09
HD 207700	5660	4.26	0.04	0.98	0.44	0.04	1.24	0.10
HD 9782	6013	4.38	0.09	1.09	0.58	0.02	1.04	0.10
HD 44120	6059	4.25	0.14	1.31	0.50	0.02	1.01	0.06
HD 205591	6575	4.75	-0.08	1.85	0.52	0.09	0.88	0.08
HD 224619	5425	4.40	-0.20	0.79	0.44	0.06	1.15	0.33
HD 147512	5515	4.40	-0.09	0.81	0.49	0.04	1.14	0.16
HD 171028	5671	3.84	-0.48	1.24	0.34	0.03	1.12	0.13
HD 171665	5652	4.44	-0.05	0.89	0.46	0.01	1.10	0.16
HD 96276	6080	4.49	-0.02	1.12	0.47	0.07	1.07	0.29
HD 138549	5552	4.40	-0.01	0.87	0.57	0.03	1.07	0.12
HD 50806	5598	4.10	0.01	1.03	0.44	0.02	1.27	0.07
HD 66039	6149	4.52	0.17	1.14	0.50	0.04	1.03	0.11
HD 6735	6111	4.56	-0.04	1.15	0.46	0.02	1.01	0.08
HD 210918	5747	4.35	-0.10	0.99	0.37	0.01	1.21	0.07
HD 115902	5705	4.39	-0.01	0.86	0.33	0.10	1.20	0.48
HD 134702	5782	4.50	-0.04	0.74	0.51	0.05	0.99	0.45
HD 7449	6040	4.53	-0.10	1.11	0.42	0.01	0.98	0.08
HD 169830	6370	4.20	0.18	1.56	0.52	0.02	0.95	0.06
HD 14745	6290	4.72	-0.14	1.46	0.44	0.07	0.95	0.16
HD 28471	5727	4.36	-0.07	0.95	0.40	0.02	1.12	0.11
HD 168871	5986	4.44	-0.09	1.17	0.48	0.05	1.12	0.07
HD 72659	5926	4.24	-0.02	1.13	0.43	0.02	1.10	0.10
HD 13578	5842	4.18	-0.03	1.12	0.50	0.03	1.09	0.30
HD 157347	5667	4.38	0.01	0.91	0.43	0.01	1.09	0.10
HD 177409	5896	4.51	-0.04	0.99	0.45	0.03	1.09	0.10
HD 122862	6009	4.25	-0.10	1.29	0.43	0.01	1.04	0.07
HD 204385	6048	4.45	0.08	1.15	0.51	0.02	1.04	0.11
HD 119638	6111	4.48	-0.13	1.22	0.38	0.02	1.02	0.06
HD 92788	5729	4.35	0.27	0.95	0.62	0.05	1.02	0.08
HD 165920	5286	4.36	0.27	0.79	0.42	0.05	1.00	0.15
HD 95456	6311	4.38	0.18	1.40	0.52	0.02	0.98	0.06
HD 116410	5939	4.43	0.23	1.07	0.59	0.06	0.98	0.24
HD 89839	6314	4.49	0.04	1.35	0.44	0.07	0.97	0.06
HD 210277	5470	4.26	0.15	0.86	0.59	0.03	1.17	0.07
HD 128340	6259	4.64	-0.55	1.42	0.18	0.08	1.10	0.22
HD 213240	5967	4.28	0.13	1.25	0.47	0.03	1.08	0.08
HD 178904	5727	4.41	0.09	0.98	0.58	0.03	1.08	0.35
HD 105938	6208	4.27	0.03	1.60	0.42	0.07	0.99	0.10
HD 192865	6307	4.44	0.13	1.59	0.51	0.04	0.94	0.09
HD 150177	6216	4.18	-0.58	1.76	0.36	0.06	0.93	0.07
HD 212301	6299	4.58	0.20	1.29	0.51	0.05	0.86	0.09
HD 145927	5819	4.41	-0.03	0.93	0.42	0.06	1.13	0.37
HD 94771	5631	4.03	0.22	1.10	0.55	0.05	1.12	0.09
HD 209566	5500	4.38	0.12	0.75	0.50	0.03	1.11	0.28
HD 20003	5465	4.37	0.03	0.83	0.48	0.02	1.09	0.22
HD 140785	5756	4.12	-0.05	1.09	0.45	0.03	1.08	0.36
HD 222595	5618	4.43	-0.01	0.88	0.44	0.03	1.08	0.10
HD 156411	5910	3.99	-0.11	1.31	0.55	0.02	1.07	0.08
HD 23079	6009	4.50	-0.11	1.12	0.47	0.02	1.06	0.07
HD 134987	5700	4.22	0.23	1.08	0.62	0.06	1.05	0.06
HD 93385	5989	4.46	0.03	1.14	0.45	0.02	1.04	0.08
HD 95542	5984	4.52	-0.04	1.01	0.43	0.02	1.04	0.13
HD 88742	6004	4.52	0.00	1.07	0.38	0.02	1.02	0.07
HD 23456	6190	4.61	-0.31	1.38	0.29	0.04	1.00	0.07
HD 101612	6281	4.41	-0.36	1.17	0.30	0.08	0.99	0.33

Continued on next page

Table E.2 – **continued from previous page**

Star	Teff	logg	[Fe/H]	ξ_t	C/O	$\sigma_{C/O}$	Mg/Si	$\sigma_{Mg/Si}$
HD 131183	5670	4.24	0.09	0.97	0.38	0.03	1.23	0.17
HD 19423	5752	4.23	-0.09	0.96	0.38	0.05	1.19	0.44
HD 66221	5590	4.34	0.16	0.92	0.57	0.03	1.11	0.09
HD 144846	6102	4.52	0.13	1.11	0.57	0.05	1.10	0.37
HD 108309	5781	4.24	0.13	1.08	0.47	0.02	1.09	0.08
HD 1388	5970	4.42	0.00	1.13	0.43	0.02	1.09	0.08
HD 102117	5620	4.28	0.26	0.99	0.48	0.07	1.07	0.07
HD 193193	5979	4.40	-0.05	1.15	0.38	0.01	1.06	0.08
HD 134606	5614	4.30	0.27	1.00	0.54	0.06	1.05	0.08
HD 212036	5687	4.41	-0.01	0.80	0.55	0.02	1.04	0.44
HD 115341	6058	4.55	-0.01	1.10	0.52	0.07	1.02	0.41
HD 149396	5657	4.47	0.19	0.91	0.54	0.03	0.98	0.11
HD 100508	5384	4.39	0.35	0.86	0.54	0.09	0.91	0.07
HD 206116	6231	4.57	0.24	1.36	0.38	0.10	0.73	0.22
HD 145809	5778	4.15	-0.25	1.14	0.32	0.02	1.19	0.11
HD 18001	5772	4.44	-0.07	0.80	0.34	0.03	1.10	0.20
HD 100289	5483	4.42	0.03	0.70	0.62	0.04	1.10	0.45
HD 115674	5633	4.43	-0.18	0.85	0.59	0.04	1.08	0.41
HD 195145	5625	4.41	0.17	0.82	0.52	0.03	1.07	0.17
HD 189625	5848	4.43	0.19	1.03	0.65	0.03	1.07	0.08
HD 183658	5809	4.40	0.03	1.00	0.66	0.02	1.07	0.14
HD 65982	5947	4.42	-0.10	1.08	0.54	0.04	1.06	0.39
HD 102365	5616	4.40	-0.28	0.91	0.34	0.07	1.06	0.08
HD 218379	5938	4.11	0.15	1.24	0.62	0.05	1.06	0.11
HD 199868	6152	4.45	-0.13	1.26	0.42	0.04	1.06	0.28
HD 38973	6015	4.43	0.05	1.14	0.55	0.01	1.00	0.07
HD 121504	6022	4.52	0.14	1.12	0.46	0.01	1.00	0.07
HD 145377	6054	4.53	0.12	1.11	0.64	0.01	0.98	0.07
HD 97037	5890	4.32	-0.07	1.13	0.46	0.03	1.14	0.14
HD 28254	5653	4.15	0.36	1.08	0.73	0.08	1.09	0.09
HD 19641	5806	4.39	-0.01	0.94	0.54	0.01	1.09	0.14
HD 457	6089	4.43	0.34	1.17	0.65	0.04	0.97	0.08
HD 163102	6433	4.64	0.00	1.94	0.46	0.10	1.26	0.18
HD 106116	5656	4.35	0.13	0.91	0.50	0.02	1.10	0.07
HD 92547	6020	4.45	-0.37	1.14	0.26	0.08	1.08	0.38
HD 157338	6037	4.49	-0.07	1.17	0.49	0.02	1.03	0.07

F

Refractory-elements abundances

Table F.1: Refractory-elements abundances

Star	T_{eff}	log$g$	[Fe/H]	ξ_t	[Na/Fe]	[Mg/Fe]	[Al/Fe]	[Si/Fe]	[Ca/Fe]
HD 37124	5460 ± 35	4.24 ± 0.04	-0.42 ± 0.03	0.61 ± 0.07	0.12 ± 0.04	0.24 ± 0.06	0.27 ± 0.09	0.20 ± 0.07	0.14 ± 0.08
WASP-37	5917 ± 72	4.25 ± 0.15	-0.23 ± 0.05	0.59 ± 0.13	0.12 ± 0.06	0.01 ± 0.11	0.06 ± 0.06	0.06 ± 0.07	0.22 ± 0.16
HIP 109384	5236 ± 43	4.40 ± 0.08	-0.24 ± 0.03	0.60 ± 0.10	0.20 ± 0.10	0.30 ± 0.04	0.33 ± 0.05	0.20 ± 0.07	0.25 ± 0.07
Kepler 37	5378 ± 53	4.47 ± 0.12	-0.23 ± 0.04	0.58 ± 0.13	0.05 ± 0.14	0.12 ± 0.06	0.10 ± 0.04	0.12 ± 0.05	0.21 ± 0.11
Kepler 444	5111 ± 43	4.50 ± 0.13	-0.51 ± 0.03	0.37 ± 0.15	0.22 ± 0.11	0.28 ± 0.11	0.35 ± 0.07	0.26 ± 0.04	0.26 ± 0.09
HD 13445	5114 ± 61	4.55 ± 0.13	-0.29 ± 0.04	0.66 ± 0.15	0.17 ± 0.09	0.21 ± 0.11	0.22 ± 0.04	0.18 ± 0.06	0.18 ± 0.11
BD-11 4672	4553 ± 75	4.87 ± 0.51	-0.30 ± 0.02	0.14 ± 0.07	0.11 ± 0.17	0.22 ± 0.12	0.26 ± 0.19	-0.04 ± 0.20	0.30 ± 0.22
HD 155358	5906 ± 33	4.04 ± 0.03	-0.61 ± 0.02	1.30 ± 0.05	0.15 ± 0.13	0.16 ± 0.14	–	0.14 ± 0.03	0.14 ± 0.07
KELT-6	6246 ± 88	3.89 ± 0.09	-0.22 ± 0.06	1.66 ± 0.13	0.05 ± 0.15	0.02 ± 0.11	–	0.06 ± 0.09	0.05 ± 0.12
WASP-61	6265 ± 169	4.21 ± 0.21	-0.38 ± 0.11	1.44 ± 0.02	0.56 ± 0.23	0.32 ± 0.23	–	–	0.34 ± 0.22
HD 197037	6233 ± 45	4.22 ± 0.04	-0.12 ± 0.03	1.22 ± 0.06	-0.08 ± 0.06	-0.06 ± 0.12	-0.22 ± 0.07	-0.04 ± 0.05	0.06 ± 0.07
HD 220842	5999 ± 39	4.30 ± 0.06	-0.08 ± 0.03	1.21 ± 0.05	-0.01 ± 0.05	0.10 ± 0.06	0.02 ± 0.13	0.04 ± 0.09	0.12 ± 0.09
HD 154857	5584 ± 23	3.90 ± 0.04	-0.23 ± 0.02	1.18 ± 0.03	0.04 ± 0.03	0.00 ± 0.05	0.01 ± 0.02	0.04 ± 0.04	0.04 ± 0.07
WASP-100	6853 ± 55	4.15 ± 0.10	-0.30 ± 0.04	1.87 ± 0.02	-0.12 ± 0.12	-0.12 ± 0.12	–	0.02 ± 0.11	0.27 ± 0.12
HD 97658	5219 ± 54	4.60 ± 0.10	-0.28 ± 0.04	0.78 ± 0.11	0.08 ± 0.08	0.13 ± 0.08	0.13 ± 0.05	0.08 ± 0.06	0.17 ± 0.10
WASP-58	6039 ± 55	4.23 ± 0.10	-0.09 ± 0.04	1.12 ± 0.08	0.00 ± 0.07	-0.02 ± 0.09	0.01 ± 0.10	0.00 ± 0.09	0.11 ± 0.09
HD 6434	5704 ± 38	4.23 ± 0.06	-0.54 ± 0.03	0.80 ± 0.06	0.12 ± 0.06	0.22 ± 0.06	0.14 ± 0.06	0.22 ± 0.08	0.28 ± 0.09
HD 70573	5889 ± 186	4.32 ± 0.27	-0.42 ± 0.13	1.14 ± 0.01	0.41 ± 0.10	0.31 ± 0.15	–	0.36 ± 0.10	0.38 ± 0.18
HD 114762	5879 ± 35	4.40 ± 0.04	-0.66 ± 0.03	1.16 ± 0.07	0.05 ± 0.07	0.12 ± 0.06	-0.03 ± 0.03	0.16 ± 0.06	0.20 ± 0.09
WASP-21	5959 ± 49	4.43 ± 0.08	-0.23 ± 0.04	1.13 ± 0.07	0.16 ± 0.12	0.08 ± 0.03	0.06 ± 0.09	0.08 ± 0.07	0.16 ± 0.09
HAT-P-24	6470 ± 55	4.75 ± 0.10	-0.41 ± 0.04	1.40 ± 0.03	0.42 ± 0.12	0.22 ± 0.12	–	0.30 ± 0.11	0.04 ± 0.12
HAT-P-39	6745 ± 55	4.91 ± 0.10	-0.21 ± 0.04	1.53 ± 0.04	0.30 ± 0.12	0.40 ± 0.12	–	0.02 ± 0.11	0.08 ± 0.12

Star	[ScI/Fe]	[ScII/Fe]	[TiI/Fe]	[TiII/Fe]	[V/Fe]	[CrI/Fe]	[CrII/Fe]
HD 37124	0.10 ± 0.09	0.11 ± 0.10	0.21 ± 0.10	0.16 ± 0.12	0.06 ± 0.15	-0.04 ± 0.06	0.04 ± 0.09
WASP-37	–	0.12 ± 0.09	0.05 ± 0.05	-0.11 ± 0.11	–	-0.04 ± 0.11	0.04 ± 0.07
HIP 109384	0.29 ± 0.06	0.19 ± 0.05	0.34 ± 0.06	-0.01 ± 0.08	0.37 ± 0.10	0.09 ± 0.07	-0.02 ± 0.06
Kepler 37	0.16 ± 0.16	0.06 ± 0.06	0.13 ± 0.09	0.07 ± 0.10	0.12 ± 0.11	0.10 ± 0.12	0.24 ± 0.06
Kepler 444	0.26 ± 0.10	0.22 ± 0.07	0.41 ± 0.06	0.22 ± 0.14	–	0.10 ± 0.06	0.10 ± 0.05
HD 13445	0.08 ± 0.10	0.06 ± 0.07	0.17 ± 0.07	0.10 ± 0.14	0.18 ± 0.09	0.05 ± 0.08	0.14 ± 0.07
HD 155358	–	0.00 ± 0.04	0.14 ± 0.03	0.06 ± 0.04	–	-0.09 ± 0.08	-0.07 ± 0.06
KELT-6	–	-0.08 ± 0.07	0.02 ± 0.18	-0.04 ± 0.09	–	-0.04 ± 0.12	-0.06 ± 0.06
WASP-61	–	0.24 ± 0.13	0.27 ± 0.34	0.26 ± 0.17	–	0.30 ± 0.24	–
HD 197037	–	-0.15 ± 0.03	-0.06 ± 0.11	-0.14 ± 0.06	–	-0.08 ± 0.08	-0.08 ± 0.03
HD 220842	–	-0.05 ± 0.04	-0.01 ± 0.09	-0.06 ± 0.07	–	-0.03 ± 0.07	0.05 ± 0.06
HD 154857	–	0.03 ± 0.03	0.01 ± 0.04	-0.01 ± 0.06	-0.02 ± 0.04	-0.05 ± 0.04	0.00 ± 0.10
WASP-100	–	0.40 ± 0.11	–	-0.09 ± 0.11	–	–	–
HD 97658	0.13 ± 0.08	-0.03 ± 0.03	0.19 ± 0.08	-0.01 ± 0.11	-0.03 ± 0.10	0.09 ± 0.09	-0.08 ± 0.12
WASP-58	–	-0.09 ± 0.06	0.04 ± 0.13	0.00 ± 0.09	–	0.09 ± 0.15	0.00 ± 0.06
HD 6434	–	0.16 ± 0.04	0.03 ± 0.06	0.23 ± 0.07	–	-0.03 ± 0.09	0.10 ± 0.05
HD 70573	–	0.10 ± 0.09	0.38 ± 0.13	0.14 ± 0.20	–	–	–
HD 114762	–	0.12 ± 0.04	0.16 ± 0.05	0.20 ± 0.06	–	-0.07 ± 0.07	0.07 ± 0.05
WASP-21	0.23 ± 0.07	0.09 ± 0.05	0.15 ± 0.06	0.13 ± 0.08	0.13 ± 0.07	-0.01 ± 0.11	0.05 ± 0.05
HAT-P-24	–	-0.02 ± 0.11	–	-0.05 ± 0.11	–	–	–
HAT-P-39	–	0.60 ± 0.11	–	-0.09 ± 0.11	–	–	–

Star	[Mn/Fe]	[Co/Fe]	[Ni/Fe]
HD 37124	-0.06 ± 0.14	0.04 ± 0.08	0.02 ± 0.09
WASP-37	0.00 ± 0.11	0.08 ± 0.11	0.02 ± 0.08
HIP 109384	-0.08 ± 0.06	0.20 ± 0.06	0.03 ± 0.05
Kepler 37	0.01 ± 0.11	0.12 ± 0.04	0.04 ± 0.08
Kepler 444	-0.08 ± 0.09	0.16 ± 0.07	0.04 ± 0.04
HD 13445	0.04 ± 0.08	0.04 ± 0.07	0.02 ± 0.06
HD 155358	-0.18 ± 0.05	-0.10 ± 0.03	-0.06 ± 0.06
KELT-6	0.02 ± 0.15	–	-0.03 ± 0.10
WASP-61	–	0.14 ± 0.18	–
HD 197037	-0.11 ± 0.08	–	-0.10 ± 0.07
HD 220842	-0.22 ± 0.21	-0.07 ± 0.07	-0.10 ± 0.05
HD 154857	0.00 ± 0.10	-0.02 ± 0.04	-0.06 ± 0.05
WASP-100	–	–	–
HD 97658	0.02 ± 0.10	0.05 ± 0.06	0.00 ± 0.08
WASP-58	-0.14 ± 0.11	0.01 ± 0.09	0.00 ± 0.09
HD 6434	-0.30 ± 0.14	–	-0.01 ± 0.10
HD 70573	–	0.18 ± 0.10	–
HD 114762	-0.19 ± 0.08	-0.03 ± 0.07	-0.08 ± 0.06
WASP-21	-0.08 ± 0.17	0.04 ± 0.11	-0.04 ± 0.06
HAT-P-24	–	–	-0.06 ± 0.11
HAT-P-39	–	–	–

Table F.4: Galactic space velocities and membership to stellar population probabilities. Bensby et al. (2003) and Reddy et al. (2006) criteria were followed to obtain membership.

				Bensby et al. (2003)				Reddy et al. (2006)			
Star	U	V	W	Pop_{thin}	Pop_{thick}	Pop_{halo}	group	Pop_{thin}	Pop_{thick}	Pop_{halo}	group
WASP-100	7	24	40	0.90	0.10	0.00	thin	0.93	0.07	0.00	thin
HAT-P-24	24	-5	23	0.99	0.01	0.00	thin	0.98	0.02	0.00	thin
HD 70573	10	4	-10	0.99	0.01	0.00	thin	0.99	0.01	0.00	thin
HD 155358	1	-21	39	0.93	0.07	0.00	thin	0.91	0.09	0.00	thin
HD 37124	44	-34	-36	0.87	0.13	0.00	thin	0.88	0.12	0.00	thin
WASP-61	-7	6	-2	0.99	0.01	0.00	thin	0.99	0.01	0.00	thin
HD 97658	0	13	2	0.99	0.01	0.00	thin	0.99	0.01	0.00	thin
HD 154857	31	4	-29	0.98	0.02	0.00	thin	0.97	0.03	0.00	thin
KELT-6	-4	24	8	0.99	0.01	0.00	thin	0.99	0.01	0.00	thin
HD 197037	46	16	-6	0.99	0.01	0.00	thin	0.99	0.01	0.00	thin
HD 114762	-68	-54	64	0.01	0.99	0.00	thick	0.03	0.97	0.00	thick
HD 6434	101	-58	6	0.38	0.62	0.00	trans	0.80	0.20	0.00	thin
Kepler-444	66	-114	-79	0.00	1.00	0.00	thick	0.00	1.00	0.00	thick
HD 13445	-89	-64	-22	0.23	0.77	0.00	thick	0.66	0.34	0.00	trans
HIP 109384	-7	-48	-63	0.07	0.93	0.00	thick	0.11	0.89	0.00	thick
HD 220842	29	-1	59	0.42	0.58	0.00	trans	0.44	0.56	0.00	trans

Bibliography

Adibekyan, V. Z., Santos, N. C., Sousa, S. G., Israelian, G. 2011, A&A, 535, L11

Adibekyan, V. Z., Santos, N. C., Sousa, S. G., et al. 2012, A&A, 543, A89

Adibekyan, V. Z., Sousa, S. G., Santos, N. C., et al. 2012, A&A, 545, A32

Adibekyan, V. Z., Delgado Mena, E., Sousa, S. G., et al. 2012, A&A, 547, A36

Adibekyan, V. Z., Figueira, P., Santos, N. C., et al. 2013, A&A, 554, A44

Adibekyan, V. Z., González Hernández, J. I., Delgado Mena, E., et al. 2014, A&A, 564, L15

Adibekyan, V., Santos, N. C., Figueira, P., et al. 2015a, A&A, 581, L2

Adibekyan, V. Z., Benamati, L., Santos, N. C., et al. 2015b, MNRAS, 450, 1900

Adibekyan, V., Gonçalves da Silva, H. M., et al. 2017, submitted

Ali-Dib, M., Mousis, O., Pettit, J.-M., & Lunine, J. I. 2014, ApJ, 785, 125

Aller, L. H., & Greenstein, J. L. 1960, ApJS, 5, 139

Anders, E., & Grevesse, N. 1989, Geochim. Cosmochim. Acta, 53, 197

Andreasen,D.T., et al. 2017, A&A, http://www.aanda.org/articles/aa/pdf/forth/aa29967-16.pdf

Asplund, M. 2005, ARA&A, 43, 481

Backer, D., Sallmen, S., & Foster, R. 1992, Nature, 358, 24

Barbieri, M., & Gratton, R. G. 2002, A&A, 384, 879

Bensby T., Feltzing S., Lundström I. 2003, A&A, 410, 527

Bertran de Lis, S., Delgado Mena, E., Adibekyan, V. Z., Santos, N. C., & Sousa, S. G. 2015, A&A, 576, A89

Bessell, M. S., & Norris, J. 1982, ApJ, 263, L29

Bond, I. A., Udalski, A., Jaroszyński, M., et al. 2004, ApJ, 606, L155

Bond, J. C., O'Brien, D. P., & Lauretta, D. S. 2010, ApJ, 715, 1050

Bond, J. C., Lauretta, D. S., & O'Brien, D. P. 2010, Icarus, 205, 321

Bressan, A., Marigo, P., Girardi, L., et al. 2012, MNRAS, 427, 127

Brewer, J. M., & Fischer, D. A. 2016, ApJ, 831, 20

Brewer, J. M., Fischer, D. A., & Madhusudhan, N. 2016, arXiv:1612.04372

Buchhave, L. A., Latham, D. W., Johansen, A., et al. 2012, Nature, 486, 375

Buchhave, L. A., & Latham, D. W. 2015, ApJ, 808, 187

Bodaghee, A., Santos, N. C., Israelian, G., & Mayor, M. 2003, A&A, 404, 715

Caffau, E., Ludwig, H.-G., Steffen, M., et al. 2008, A&A, 488, 1031

Caffau, E., Ludwig, H.-G., Bonifacio, P., et al. 2010, A&A, 514, A92

Caffau, E., Ludwig, H.-G., Steffen, M., Freytag, B., & Bonifacio, P. 2011, Sol. Phys., 268, 255

Campante, T. L., Barclay, T., Swift, J. J., et al. 2015, ApJ, 799, 170

Carbon, D. F., Barbuy, B., Kraft, R. P., Friel, E. D., & Suntzeff, N. B. 1987, PAGP, 99, 335

Carigi, L. 2000, Rev. Mexicana Astron. Astrofis., 36, 171

Carter-Bond, J. C., O'Brien, D. P., & Raymond, S. N. 2012, ApJ, 760, 44

Chavero, C., de La Reza, R., Domingos, R. C., et al. 2010, A&A, 517, AA40

Clegg, R. E. S, Tomkin, J.,& Lambert, D. L. 1981, ApJ, 250, 262

Barbieri, M., & Gratton, R. G. 2002, A&A, 384, 879

Da Silva, R., Milone, A. C., & Reddy, B. E. 2011, A&A, 526, A71

Da Silva, R., Milone, A. d. C., & Rocha-Pinto, H. J. 2015, A&A, 580, A24

Damasso, M., Esposito, M., Nascimbeni, V., et al. 2015, A&A, 581, L6

Delgado Mena, E., Israelian, G., González Hernández, J. I., et al. 2010, ApJ, 725, 2349

Delgado Mena, E., Israelian, G., González Hernández, J. I., Santos, N. C., & Rebolo, R. 2012, ApJ, 746, 47

Díaz, R. F., Santerne, A., Sahlmann, J., et al. 2012, A&A, 538, A113

Dorn, C., Khan, A., Heng, K., et al. 2015, A&A, 577, A83

Ecuvillon, A., Israelian, G., Santos, N. C., et al. 2004, A&A, 418, 703

Ecuvillon, A., Israelian, G., Santos, N. C., et al. 2004, A&A, 426, 619

Ecuvillon, A., Israelian, G., Santos, N. C., et al. 2006, A&A, 445, 633

Ecuvillon, A., Israelian, G., Santos, N. C., Mayor, M., & Gilli, G. 2006, A&A, 449, 809

Edvardsson, B., Andersen, J., Gustafsson, B., et al. 1993, A&A, 275, 101

Elser, S., Meyer, M. R., & Moore, B. 2012, Icarus, 221, 859

Figueira, P., Santos, N. C., Pepe, F., Lovis, C., & Nardetto, N. 2013, A&A, 557, A93

Fischer, D. A., & Valenti, J. 2005, ApJ, 622, 2

Frandsen S., Lindberg B., 1999, in H. Karttunen, V. Piirola, eds, Astrophysics with the NOT. p. 71

Ghezzi, L., Cunha, K., Smith, V. V., et al. 2009, ApJ, 698, 451

Gonzalez, G. 1997, MNRAS, 285, 403

Gonzalez, G., 1999, MNRAS, 308, 447

Gonzalez, G., & Laws, C. 2000, AJ, 119, 390

Gonzalez, G., Laws, C., Tyagi, S., & Reddy, B. E. 2001, AJ, 121, 432

Gonzalez, G., Brownlee, D., & Ward, P. 2001, Icarus, 152, 185

Gonzalez, G. 2006, PAGP, 118, 1494

González Hernández, J. I., Israelian, G., Santos, N. C., et al. 2010, ApJ, 720, 1592

González Hernández, J. I., Casares, J., Rebolo, R., et al. 2011, ApJ, 738, 95

González Hernández, J. I., Delgado-Mena, E., Sousa, S. G., et al. 2013, A&A, 552, A6

Gray, D. F. 1992, Camb. Astrophys. Ser., Vol. 20,, 20,

Grevesse, N., Lambert, D. L., Sauval, A. J., et al. 1990, A&A, 232, 225

Haywood, M. 2008, A&A, 482, 673

Haywood, M. 2009, ApJ, 698, L1

Hébrard, G., Arnold, L., Forveille, T., et al. 2016, A&A, 588, A145

Hellier, C., Anderson, D. R., Collier Cameron, A., et al. 2012, MNRAS, 426, 739

Hellier, C., Anderson, D. R., Cameron, A. C., et al. 2014, MNRAS, 440, 1982

Henry, R. B. C., Edmunds, M. G., Kppen, J. 2000, ApJ, 541, 660

Hog, E., Kuzmin, A., Bastian, U., et al. 1998, A&A, 335, L65

Holmberg, J., Nordström, B., & Andersen, J. 2009, A&A, 501, 941

Howard, A. W., Johnson, J. A., Marcy, G. W., et al. 2011, ApJ, 730, 10

Ida, S., & Lin, D. N. C. 2004, ApJ, 604, 388

Israelian, G., Santos, N. C., Mayor, M., & Rebolo, R. 2001, Nature, 411, 163

Israelian, G., Santos, N. C., Mayor, M., & Rebolo, R. 2003, A&A, 405, 753

Israelian, G., Ecuvillon, A., Rebolo, R., et al. 2004, A&A, 421, 649

Kipping, D. M., Bakos, G. Á., Hartman, J., et al. 2010, ApJ, 725, 2017

Kirkman, T.W., 1996, Statistics to use: College of Saint Benedict and Saint John's University, Collegeville, Minnesota, 'http://www.physics.csbsju.edu/stats/', 1996,

Konopacky, Q. M., Barman, T. S., Macintosh, B. A., & Marois, C. 2013, Science, 339, 1398

Kreidberg, L., Line, M. R., Bean, J. L., et al. 2015, ApJ, 814, 66

Kurucz, R. L., Furenlid, I., Brault, J., & Testerman, L. 1984, National Solar Observatory Atlas, Sunspot, New Mexico: National Solar Observatory, 1984,

Kurucz, R. 1993, in ATLAS9 Stellar Atmosphere Programs and 2 km s^{-2} grid, Kurucz CD-ROM(Cambridge, Mass.: Smithsonian Astrophysical Observatory), 13

Laws, C., Gonzalez, G., Walker, K.M. et al. 2003, AJ, 125, 2664

Liang, Y. C., Zhao, G., & Shi, J. R. 2001, A&A, 374, 936

Lindegren, L., Lammers, U., Bastian, U., et al. 2016, A&A, 595, A4

Mayor, M., & Queloz, D. 1995, Nature, 378, 355

Lo Curto, G., Mayor, M., Benz, W., et al. 2010, A&A, 512, A48

Lodders, K. 2003, ApJ, 591, 1220

Madhusudhan, N., Lee, K. K. M., & Mousis, O. 2012, ApJ, 759, L40

Maeder, A. 1992, A&A, 264, 105

Maeder, A., & Meynet, G. 2000, ARA&A, 38, 143

Maeder, A. 2009, Physics, Formation and Evolution of Rotating Stars: , Astronomy and Astrophysics Library. ISBN 978-3-540-76948-4. Springer Berlin Heidelberg, 2009, Mandell, A. M., Ge, J., & Murray, N. 2004, AJ, 127, 1147

Marboeuf, U., Thiabaud, A., Alibert, Y., Cabral, N., & Benz, W. 2014, A&A, 570, A36

Marigo, P. 2001, A&A, 370, 194

Mata Sánchez, D., González Hernández, J. I., Israelian, G., et al. 2014, A&A, 566, A83

Mayor, M., & Queloz, D. 1995, Nature, 378, 355

Mayor, M., Pepe, F., Queloz, D., et al. 2003, The Messenger, 114, 20

Mayor, M., Marmier, M., Lovis, C., et al. 2011, arXiv:9.2497

Meynet, G., & Maeder, A. 2002, A&A, 390, 561

Minchev, I., Chiappini, C., & Martig, M. 2013, A&A, 558, A9

Mordasini, C., Alibert, Y., Klahr, H., & Henning, T. 2012, A&A, 547, A111

Morgan, J. W., & Anders, E. 1980, Proceedings of the National Academy of Science, 77, 6973

Mortier, A., Santos, N. C., Sousa, S. G., et al. 2013, A&A, 551, A112

Mortier, A., Sousa, S. G., Adibekyan, V. Z., Brandão, I. M., & Santos, N. C. 2014, A&A, 572, A95

Moses, J. I., Madhusudhan, N., Visscher, C., & Freedman, R. S. 2013, ApJ, 763, 25

Moutou, C., Lo Curto, G., Mayor, M., et al. 2015, A&A, 576, A48

Navarro J. F., Abadi M. G., Venn K. A., Freeman K. C., Anguiano B. 2011, MNRAS, 412, 1203

Neves, V., Santos, N. C., Sousa, S. G., Correia, A. C. M., & Israelian, G. 2009, A&A, 497, 563

Niedzielski, A., Nowak, G., Adamów, M., & Wolszczan, A. 2009, ApJ, 707, 768

Nissen, P. E., & Schuster, W. J. 2010, A&A, 511, L10

Nissen, P. E., & Schuster, W. J. 2011, A&A, 530, A15

Nissen, P. E. 2013, A&A, 552, A73

Nissen, P. E., Chen, Y. Q., Carigi, L., Schuster, W. J., & Zhao, G. 2014, A&A, 568, A25

Nissen, P. E. 2015, A&A, 579, A52

Öberg, K. I., Murray-Clay, R., & Bergin, E. A. 2011, ApJ, 743, L16

Pagel, B. E. J., & Edmunds, M. G. 1981, ARA&A, 19, 77

Pettini, M., Ellison, S. L., Bergeron, J., & Petitjean, P. 2002, A&A, 391, 21

Petigura, E. A., & Marcy, G. W. 2011, ApJ, 735, 41

Pollack, J.B., Hubickyj, O., Bodenheimer, P., et al. 1996, Icarus, 124, 62

Portinari, L., Chiosi, C., & Bressan, A. 1998, A&A, 334, 505

Press, W. H., Teukolsky, S. A., Vetterling, W. T., & Flannery, B. P. 1992, Cambridge: University Press, 1992, 2nd ed.,

Recio-Blanco, A., de Laverny, P., Kordopatis, G., et al. 2014, A&A, 567, A5

Reddy B. E., Lambert D. L., Allende Prieto C. 2006, MNRAS, 367, 1329

Reid, I. N., & Cruz, K. L. 2002, AJ, 123, 2806

Ryabchikova, T., Piskunov, N., Kurucz, R. L., et al. 2015, Phys. Scr, 90, 054005

Sadakane, K., Ohkubo, M., Takeda, Y., et al. 2002, PASJ, 54, 911

Santos, N. C., Israelian, G., & Mayor, M. 2000, A&A, 363, 228

Santos, N. C., Israelian, G., & Mayor, M. 2001, A&A, 373, 1019

Santos, N. C., García Lpez, R. J., Israelian, G., et al. 2002, A&A, 386, 1028

Santos, N. C., Israelian, G., Mayor, M., Rebolo, R., & Udry, S. 2003, A&A, 398, 363

Santos, N. C., Israelian, G., & Mayor, M. 2004, A&A, 415, 1153

Santos, N. C., Israelian, G., Mayor, M., et al. 2005, A&A, 437, 1127

Santos, N. C., Mayor, M., Bonfils, X., et al. 2011, A&A, 526, A112

Santos, N. C., Sousa, S. G., Mortier, A., et al. 2013, A&A, 556, A150

Santos, N. C., Adibekyan, V., Mordasini, C., et al. 2015, A&A, 580, L13

Schönrich, R., Binney, J., & Dehnen, W. 2010, MNRAS, 403, 1829

Schuler, S. C., Margheim, S. J, Sivarani, T., et al. 2008, AJ, 136, 2244

Sneden, C. A. 1973, Ph.D. Thesis,

Sousa, S. G., Santos, N. C., Israelian, G., Mayor, M. & Monteiro, M. J. P. F. G. 2007, A&A, 469, 783

Sousa, S. G., Santos, N. C., Mayor, M., et al. 2008, A&A, 487, 373

Sousa, S. G., Santos, N. C., Israelian, G., et al. 2011a, A&A, 526, AA99

Sousa, S. G., Santos, N. C., Israelian, G., Mayor, M., & Udry, S. 2011b, A&A, 533, AA141

Sousa, S. G., Santos, N. C., Mortier, A., et al. 2015, A&A, 576, A94

Sousa, S. G., Santos, N. C., Adibekyan, V., Delgado-Mena, E., & Israelian, G. 2015, A&A, 577, A67

Suárez-Andrés, L., Israelian, G., González Hernández, J. I., et al. , 2016, A&A, 591, A69

Suárez-Andrés, L., Israelian, G., González Hernández, J. I., et al. 2017, A&A, 599, A96

Takeda, Y., Sato, B., Kambe, E., et al. 2001, PASJ, 53, 1211

Takeda, Y., & Honda, S. 2005, PASJ, 57, 65

Telting, J. H., Avila, G., Buchhave, L., et al. 2014, Astronomische Nachrichten, 335, 41

Teske, J. K., Cunha, K., Smith, V. V., Schuler, S. C., & Griffith, C. A. 2014, ApJ, 788, 39

Théado & Vauclair, ApJ, 744, 2

Thiabaud, A., Marboeuf, U., Alibert, Y., et al. 2014, A&A, 562, A27

Thiabaud, A., Marboeuf, U., Alibert, Y., Leya, I., & Mezger, K. 201a5, A&A, 574, A138

Thiabaud, A., Marboeuf, U., Alibert, Y., Leya, I., & Mezger, K. 2015b, A&A, 580, A30

Tsantaki, M., Sousa, S. G., Adibekyan, V. Z., et al. 2013, A&A, 555, A150

Valencia, D., Ikoma, M., Guillot, T., & Nettelmann, N. 2010, A&A, 516, A20

Valencia, D., Guillot, T., Parmentier, V., & Freedman, R. S. 2013, ApJ, 775, 10

Valenti, J. A., & Fischer, D. A. 2005, ApJS, 159, 141

Vanderburg, A., Montet, B. T., Johnson, J. A., et al. 2015, ApJ, 800, 59

van den Hoek, L. B., & Groenewegen, M. A. T. 1997, A&AS, 123, 305

van Leeuwen, F. 2007, A&A, 474, 653

Vogt, S. S., Butler, R. P., Marcy, G. W., et al. 2005, ApJ, 632, 638

Wallerstein, G. 1962, ApJS, 6, 407

Wang, J., Fischer, D. A., Barclay, T., et al. 2013, ApJ, 776, 10

Wenger, M., Ochsenbein, F., Egret, D., et al. 2000, A&AS, 143, 9

Wolszczan, A., & Frail, D. A. 1992, Nature, 355, 145

Zhao, G. & Gehren, T. 2000a, A&A, 362, 1077

Zhao, G. & Gehren, T. 2000b, Liege International Astrophysical Colloquia, 35, 277